Charge Generation and Transport Studies in Fullerene-free Bulk Heterojunction Polymer Solar Cells

A Thesis Submitted in Partial Fulfillment for the Requirements of the degree of

Doctor of Philosophy

by

Ravichandran Shivanna

Chemistry and Physics of Materials Unit,
Jawaharlal Nehru Centre for Advanced Scientific Research
(Deemed University)
Bangalore - 560 064,
India.

JULY 2015

Declaration

I hereby declare that the matter embodied in the thesis entitled "***Charge Generation and Transport Studies in Fullerene-free Bulk Heterojunction Polymer Solar Cells***" is the result of investigations carried out by me at the Chemistry and Physics of Materials Unit, Jawaharlal Nehru Centre for Advanced Scientific Research, Bangalore, India under the supervision of Prof. K. S. Narayan and that it has not been submitted elsewhere for the award of any degree or diploma.

In keeping with the general practice in reporting scientific observations, due acknowledgment has been made whenever the work described is based on the findings of other investigators.

Ravichandran Shivanna

JAWAHARLAL NEHRU CENTRE FOR ADVANCED SCIENTIFIC RESEARCH
Jakkur, Bangalore 560064, India

K. S. NARAYAN
Professor and Dean (R&D)
PHONE: 91 80 22082822
FAX: 91 80 22082766
e-mail: narayan@jncasr.ac.in URL: www.jncasr.ac.in/narayan

July 6th, 2015

Certificate

I hereby certify that the matter embodied in this thesis entitled "***Charge Generation and Transport Studies in Fullerene-free Bulk Heterojunction Polymer Solar Cells***" has been carried out by Mr. Ravichandran Shivanna at the Chemistry and Physics of Materials Unit, Jawaharlal Nehru Centre for Advanced Scientific Research, Bangalore, India under my supervision and that it has not been submitted elsewhere for the award of any degree or diploma.

Prof. K. S. Narayan
(Research Supervisor)

Dedicated to my Family...

Acknowledgement

First and foremost I would like to express my sincere thanks to my research supervisor Prof. K. S. Narayan for providing me an opportunity to work in the vastly equipped Molecular Electronics lab, JNCASR. I would like to acknowledge him for providing all the freedom for research, abundant scientific inputs and surplus funding during my PhD. His enthusiastic approach to research is infectious and motivational for me to solve harder scientific problems. I also like to thank him for his constant support and guidance which has enormously impacted my professional and personality development.

I would like to extend my special thanks to Prof. C.N.R. Rao for his constant source of inspiration.

I thank all the faculty members in CPMU, TSU, NCU and ICMS for various course-works and scientific interactions. My special thanks to Prof. Balasubramanian Sundaram, Prof. Chandrabhas Narayan, Prof. S.M.Shivaprasad and Dr. Vidyadhiraja for all the things I learnt.

My sincere thanks to Dr. Sridhar Rajaram, ICMS, JNCASR, for providing the wonderful 'Twisted Perylene' molecules. I am also grateful for many scientific discussions with him where I learnt a lot about perylenes. Special thanks to Sunil Kumar who synthesized twisted perylenes.

I am thankful to Dr. Subi George, NCU, JNCASR, for providing interesting molecules to study upon. I also acknowledge his group for many discussions which immensely helped me to understand the different aspects of supra-molecular chemistry.

I thank Prof. M. K. Mathew and his group at NCBS, Bangalore, for teaching me the art and tricks related to the patch-clamp technique. I also thank Prof. Prabal Maiti and his group at IISC, Bangalore, for molecular dynamics simulation and fruitful discussions on nanopore related work.

I would like to express my heartfelt gratitude to Prof. James Durrant and his group at Imperial College London, UK, for a fruitful collaboration on the transient absorption measurements and hosting me wonderfully in UK. Special thanks to Dr. Safa Shoaee for introducing me to transient spectroscopy and being a great colleague.

I also thank Prof. Neil Robertson and his group at University of Edinburgh, UK for a productive collaboration. My sincere thanks to Dr. Akshay Rao and Aditya for an informative and wonderful time I had during my visit to University of Cambridge, UK.

I would like to acknowledge Department of Science and Technology for the funding support in terms of fellowships and travel grants.

I would like to acknowledge INDO-UK APEX project jointly funded by DST, government of India and EPSRC, UK for providing fellowship and travel grants during my student exchange visit to Imperial College London and also to attend several workshops and conferences. Special thanks to Prof. Hari Upadhyaya, Brunel University, UK and Dr. Suresh Chand, NPL, India for constant support and encouragement.

I acknowledge the support from staffs at Library, Workshop, Academic section, Administrative section, Purchase section and Computer lab. I thank Dr. A. N. Jayachandra, Sr. administrative officer and his staff for all the timely help and support. I also thank the doctors and staffs at Dhanvantari, Hostel Office, Hostel mess and Utility stores for making my life pleasant and comfortable.

I would like to acknowledge all my lab colleagues who made my stay enjoyable and memorable. I was fortunate to work with many people and exchange ideas and perspectives in both academic and non-academic issues. I thank my lab seniors who taught me a lot : Drs. Dinesh, Dhritiman, Arun, Shruti, Manohar, Monojit, Sachi, Anshuman, Balaraju, Kishore, Srinidhi, Poonam and Murthy. I specially thank Satya and Vini for all the fun and memorable moments along with the healthy and constructive scientific environment and temper created by them. I further thank my current lab mates Prashant, Ashar, Raaghesh, Swathi, Vikas, Rishav, Apoorv. I specially thank Swathi for complete proof-read of the thesis. I also thank Dhruv, Madhu, Nishit, Vijay, Arun D, Ranbir, Matthew, Krishna and Nisha for their company. I thank Manjunath M N for all his assistance during my PhD.

I would like to thank all my friends those who are in JNCASR as well as outside for their well wishes. Special thanks to Avinash, Mohit, Ankit, Pawan, Chidambar, Pandu, Malli's, Varun, Vijay J and Jayaram for all the fun we had together at JNC. I also thank Darshana, Arpit, Rajesh and Croor for the wonderful time we had during our student representative tenure.

I also acknowledge Abhijith T N and C V Vinod, my childhood friends, for all the memorable time and ever growing encouragement.

I thank all my teachers from the school and college days who inspired and mentored me. A special thanks to all my Integrated M.Sc friends who played a key role in my choice for research.

Most importantly, I thank my mother, father and my brother for their unconditional love and faith on me. Their constant support and encouragement has made me what I am today. I also thank my sister-in-law for her encouragement. My Special thanks to my brother Ravi for all the joy and liveliness he has brought to my life. I also thank all my other family members for being around with their love and encouragement.

Finally, I am thankful to the Almighty for everything.

July, 2015

Ravichandran Shivanna JNCASR, Bangalore

Synopsis

Organic photovoltaic technology is a promising and cost-effective alternative to other solar energy technologies due to roll-to-roll processing and easy installation. Significant advances have been made in terms of increasing power conversion efficiency of bulk heterojunction (BHJ) organic solar cells (OSCs) thereby reaching over 10 %. The common component of high efficiency devices is use of low band gap donor-acceptor co-polymers as electron donors and a fullerene based derivative as the electron acceptor. The success of fullerene based materials as electron acceptors is due to a variety of factors with particular emphasis on favorable nano-scale morphology. However, there are important limiting factors for fullerenes besides practical constraints and elaborate purification procedures. This includes relatively low absorption of fullerene acceptors in the visible region and limited tunability of fullerene energy levels. In this regard, perylenes with good electron mobility are potential alternatives to fullerenes as electron acceptors in BHJ OSCs, due to their flexibility of functionalization, increased visible absorption and high photo-stability.

The first part of this thesis deals with perylene based electron acceptors as options for the fabrication of efficient fullerene-free BHJ OSCs. Several studies exploring perylene as electron transporters revealed that the large scale phase separation of perylene molecules in the blend leads to inefficient photocharge generation. This suggests that reducing the co-facial stacking of perylene molecules without adversely impacting their charge-transport properties may be an important design principle. Following up on this, two PDI molecules are brought together in which the units are oriented perpendicular to each other forming a twisted structure between them. In combination with a hole transporting polymer (PBDTTT-CT) and the 'Twisted Perylene', a device efficiency of 2.77% has been achieved. A 10-fold increase in short circuit current density (J_{sc}) is observed in comparison with a planar PDI, resulting in one of the highest J_{sc} values for a solution processed device featuring a PDI. The increase in J_{sc} is attributed to three plausible factors: (1) Reduction in the formation of micrometer-size crystals of the acceptor in the active blend layer, (2) Increased separation distance between the donor and acceptor at the interface leading to a loosely bound charge transfer state and (3) Increasing the dimensionality of the perylene from one to two which increased the anisotropy of charge transport.

The second part of the thesis probes the charge generation and transport dynamics in the above mentioned blends using transient absorption spectroscopy (TAS). Strong PL

quenching of both the donor and acceptor emissions indicates efficient electron and hole transfer processes at the PBDTTT-CT:TP interface. The near-IR pump–probe experiments and IPCE measurements demonstrate that polarons are generated from both the polymer and TP excitons. It is observed that in these blends, electron and hole transfer processes occur on a similar time scale of a few picoseconds. In the microsecond time scale, the magnitude of polaron yield of PBDTTT-CT:TP blends is comparable to that of fullerene blends and exhibits similar decay dynamics.

The third part of the thesis focuses on the relaxed charge transfer (CT) states in these fullerene-free BHJ OSCs. Photo-thermal deflection spectroscopy (PDS) in combination with lock-in based sensitive photocurrent measurement method is utilized to probe the CT states. The existence of red shifted CT absorption for several combinations of donor molecules indicates the formation of CT-state with TP acceptor. To understand the energetics of CT state in these efficient blend systems, electroluminescence (EL) of BHJ in forward bias conditions is obtained. The comparative studies of twisted perylene (TP) acceptor based BHJs with that of PCBM systems reveal the role of molecular structure-order correlation on charge generation processes. The inference drawn from these results points to lower recombination-losses at the TP-donor interface and possibility of higher efficiencies in such non-fullerene systems compared to PCBM based systems.

The final part of the thesis deals with interfacial engineering of electrode active layer interface for efficient charge extraction. In this regard, we have utilized the property of wrinkling in the sol gel based ZnO buffer layer. The patterning of buffer layer increases the optical length and hence increased light absorption in the active layer. However, this nano-patterning induces inhomogeneity in the current extraction at the interface. To reduce this loss, a TP interlayer between ZnO and the active BHJ layer is introduced. Along with increase in current homogeneity, the reduced work function and selective transport of electrons prevents the accumulation of charges and decreases the electron-hole recombination at the interface. This resulted in an overall increase of efficiency to 4.6 %, which is among the highest efficient fullerene-free organic solar cells.

In summary, the thesis reports realization of high efficient fullerene-free bulk heterojunction polymer solar cells. Optical and electrical characterization provides novel insight onto charge photogeneration, transport and recombination processes in fullerene-free cells. ‘Twisted Perylene’ is utilized as a model electron acceptor system to understand the photo-physics and develop strategies for enhancing the efficiency of BHJ solar cells.

List of Publications

- **Ravichandran Shivanna**, Sridhar Rajaram, K S Narayan, "*Role of charge transfer states in fullerene-free organic solar cells*", **manuscript submitted**.

- **Ravichandran Shivanna**, Sridhar Rajaram and K. S. Narayan, "*Interface engineering for efficient fullerene-free organic solar cells*", **Applied Physics Letters, 2015**, 106, (12), 123301.

- **Ravichandran Shivanna**, Safa S, Stoichko D, Sunil K K, Sridhar R, James R D and K S Narayan, "*Charge generation and transport in efficient organic bulk heterojunction solar cells with a perylene acceptor*", **Energy and Environmental Science, 2014**, 7, 435-441.

- **Ravichandran Shivanna**, Debabrata P, Hemant K, K V Rao, Subi J G, Prabal K M, K S Narayan, "*Confinement Induced Stochastic Sensing of Charged Coronene and Perylene Aggregates in α–Hemolysin Nanochannel*", **Soft Matter**, **2013**, 9, 10196-10202.

- Sridhar Rajaram, **Ravichandran Shivanna**, Sunil Kumar Kandappa, KS Narayan, "*Non-planar Perylene Diimides as Potential Alternatives to Fullerenes in Organic Solar Cells*", **Journal of Physical Chemistry letters**, **2012**, 3, 17.

- Dhruv J, **Ravichandran Shivanna**, K S Narayan, "*Organic photovoltaics: key photophysical, device and design aspects*", **Journal of Modern Optics**, **2014**, 61, 1703.

- Anshuman J D, **Ravichandran Shivanna**, K.S. Narayan, "*Photoconductive NSOM for mapping optoelectronic phases in nanostructures*", **Nanophotonics, 2014**, 3, 19-31.

- K S Narayan, B N Madhushankar, Vini G, Satyaprasad P S, **Ravichandran Shivanna**, "*Water-Gated Phospholipid-Monolayer Organic Field Effect Transistor Through Modified Mueller–Montal Method*", **Electron Device Letters-IEEE**, **2013,** 99, 1-3.

- Safa S, Florent D, Pabitra S T, **Ravichandran Shivanna**, K S Narayan, Sridhar R, James R D, "*A Comparison of Charge Separation Dynamics in Organic Blend Films Employing Fullerene and Perylene Diimide Electron Acceptors*", **Journal of Physical Chemistry letters**, **2015**, *6 (1), 201-205.*

- Miquel P, Efthymios K, Martina C, **Ravichandran Shivanna**, K V Rao, Oleg C, Anita C J, Bryce S R, Subi J G, KS Narayan, Neil R, "*Luminescent Polymer Films from Simple Processing of Coronene and Europium Precursors in Water*", **European Journal of Inorganic Chemistry, 2014**, 19, 3095

- Ranbir S, **Ravichandran Shivanna**, K. S. Narayan, Panagiotis E. Keivanidis, "Energy Transfer Effects on the Excimer Dissociation Efficiency of High-performance Perylene-diimide Photovoltaic Blend Films", **manuscript submitted**.

Table of Contents

List of Figures

Abbreviations

PV	Photovoltaic
OPV	Organic Photovoltaic
OSC	Organic Solar Cells
BHJ	Bulk Heterojunction
J_{sc}	Short Circuit Current
V_{oc}	Open Circuit Voltage
FF	Fill Factor
HOMO	Highest Occupied Molecular Orbital
LUMO	Lowest Unoccupied Molecular Orbital
J-V	Current density- Voltage
C-V	Capacitance –Voltage
EQE	External Quantum Efficiency
IQE	Internal Quantum Efficiency
IPCE	Incident Photon to Current Conversion Efficiency
TAS	Transient Absorption Spectroscopy
PP	Planar Perylene
TP	Twisted Perylene
D-A	Donor-acceptor

Chapter 1:

Introduction

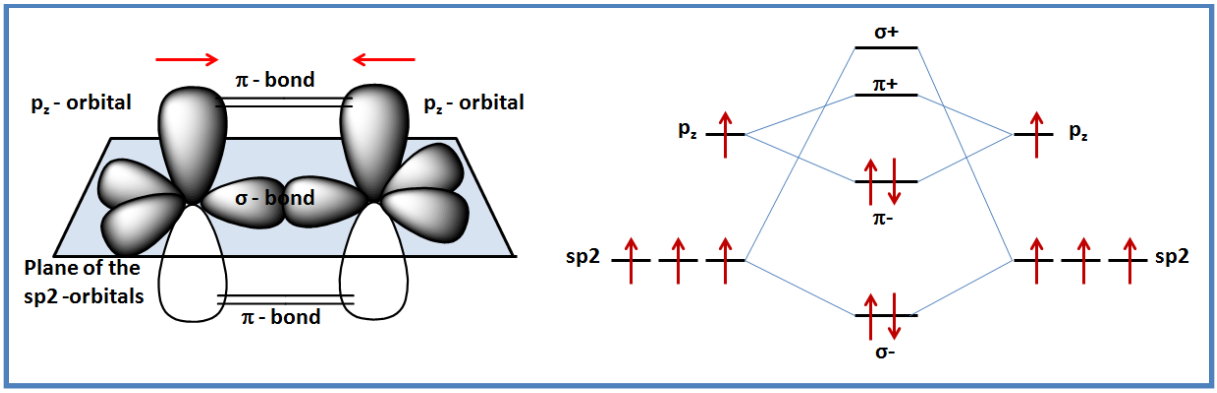

1 Introduction

Rapid growth in the global energy requirement coupled with rapid depletion of non-renewable fossil fuel necessitates alternative sources of energy. Alternative sources need to be efficient, inexpensive and environmentally sustainable to mitigate the future global energy challenges. Solar energy is the ultimate source of energy for almost all life on Earth either directly or indirectly. Photosynthesis is the direct way of harvesting solar energy whereas, fossil fuels are a product of photosynthesis over millions of years. If it is possible to mimic nature, solar energy can be directly harvested in the form of photovoltaic (PV) technology for the global energy landscape in the cleanest possible manner.

Dramatic improvements in photovoltaic technology in terms of performance (*1*) and cost effectiveness (*2*) have taken place over the last few decades. The PV segment is presently dominated by silicon (Si) technology, which accounted for ~ 89% of total PV-technology in 2013 (*3*). This well established technology provides the highest commercially available device efficiency (Figure 1.1). The 'second generation' technologies (*4*) make use of thin films (*5*) of amorphous silicon (a-Si:H) and more optimally designed direct band gap semiconducting materials such as CdTe (Cadmium-Telluride)(*6*) and CIGS (Copper Indium Gallium Selenide-sulphide)(*7*) in solar cells. They have shown impressive efficiencies and are in close competition with first generation PV. Their present market share is about ~11%, and is limited by the energy and cost intensive manufacturing besides utilizing scarce and toxic materials in certain cases, calling to question their environmental impact and sustainability.

Third generation PV technologies (*8, 9*) introduces a paradigm shift in fabrication of devices by utilizing non-conventional semiconductors as photoactive materials. One of their strong points is the possibility to overcome the Shockley-Queisser efficiency limit (*10*) through various light harvesting strategies. Organic Photovoltaic (OPV) belongs to this class of solar cell technologies and makes use of semiconducting polymers or small-molecule organic compounds as photoactive materials. The fabrication of devices in this technology utilizes potentially low-cost and high-throughput techniques such as spincoating, spray-coating (*11*), inkjet printing (*12*), screen-printing, flexo printing (*13*), slot-die coating and other printing methodologies.(*14*) The use of these low-cost 'roll-to-roll' processes on

lightweight, flexible substrates imparts new possibilities for the form factor of photovoltaic modules and make them inherently suited for large-area applications.(*15, 16*)

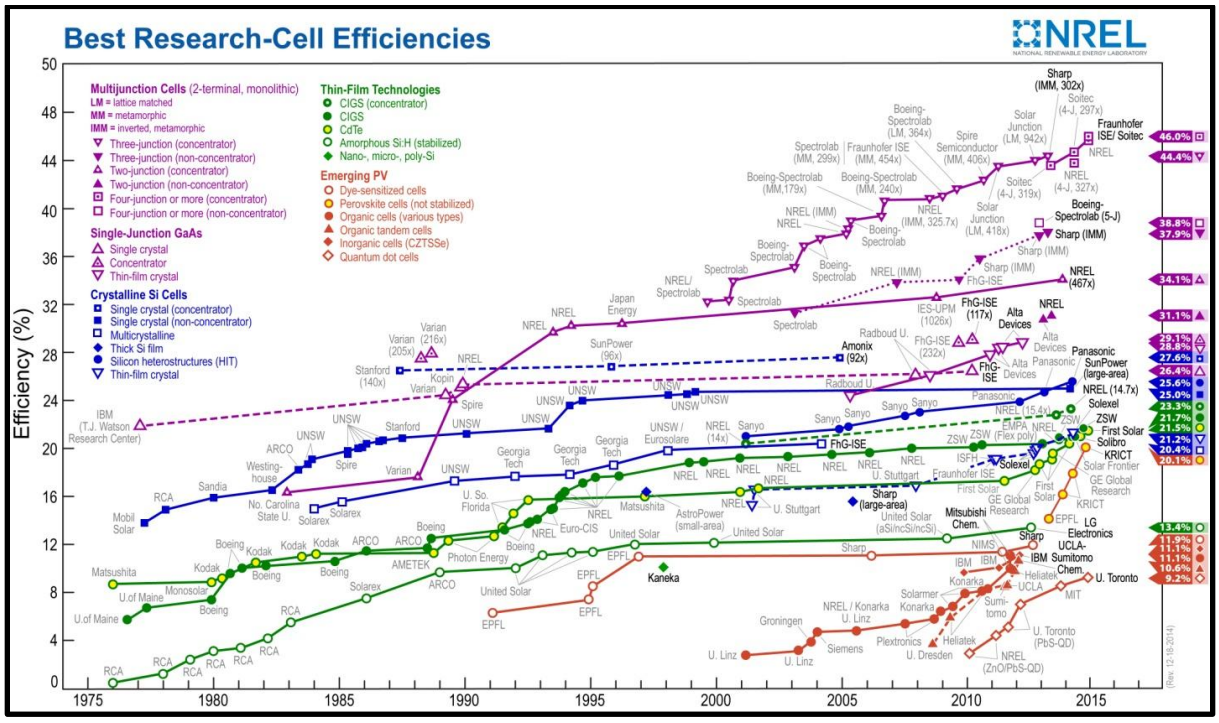

Figure 1.1: NREL efficiency chart depicting the growth of different PV technology over time. The steep rise in the solution processable organic –inorganic hybrid solar cells efficiency can be observed in the chart.(NREL)

In addition, these photoactive semiconducting molecules can be custom synthesized with the right combination of physical, optical and electrical properties. This thesis focuses on optimizing these properties required for organic solar cells by combination of strategies including rational material design and optimized device architectures. The next few sections provide the necessary introduction to the scientific principles and models in OPV systems. The relevant background in the context of problems addressed and the methodology adopted is documented in the subsequent sections.

1.1 Organic semiconductors:

The essential aspects of organic semiconducting molecules are the carbon atoms which are sp^2-hybridized having the sp^2-orbitals in a trigonal planar configuration with the p_z-orbitals perpendicular to the plane. This forms a conjugated system with delocalized π electrons due to resonating alternate double ($\sigma + \pi$) and single bonds (σ) in the molecule. As

a result of this conjugation, *p*-orbitals split into two energy levels: bonding orbitals (π-orbital; low energy) and antibonding orbitals (π*-orbital; high energy). In the ground state of the molecule, the π-orbital is occupied and is termed as highest occupied molecular orbital (HOMO). The π*-orbital is unoccupied and is termed as lowest unoccupied molecular orbital (LUMO). The electronic characteristics of organic semiconductors are dictated by the interaction of these π-electrons (Figure 1.2).

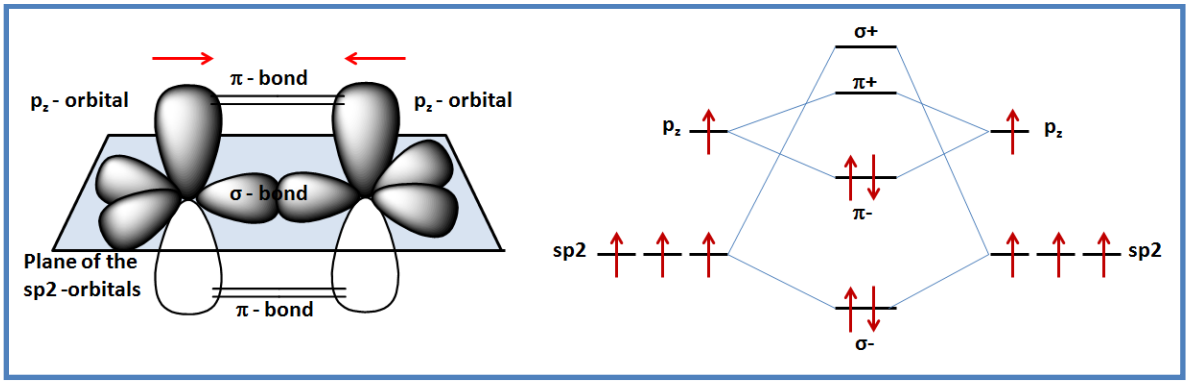

Figure 1.2: Scheme of the orbitals and bonds for two sp_2-hybridised carbon atoms.

Organic semiconductors can either be in the form of long polymers with an extended conjugated backbone or oligomers or in form of molecular assembly. As the delocalization length of π–electrons increases, the energy levels become closely spaced forming a band structure nearly similar to inorganic semiconductors. In general, polymers are structurally and electronically disordered materials. Any disturbance along the conjugation of the polymer backbone will change the HOMO and LUMO levels locally. The density of states available for charge transport is often approximated by Gaussian distribution. Hence, charge transport in polymer materials is significantly lower than in inorganic materials. The mechanism of conductivity/mobility in these molecules is based on the motion of charged defects within the conjugated framework.(*17-20*) The general requirements which are considered while designing these molecules are solution-processibility, stability (thermal, photo and environmental), and wide visible spectral coverage of absorption.

1.2 Evolution of organic solar cells:

Before describing the concepts and principles of organic solar cells a brief summary of typical solar cell characteristics is presented. The performance parameters obtained from basic characterization of solar cells directly reflects on the microscopic factors and the

electronic levels of the different constituents in the system. Typically, the device structure of organic solar cells consists of organic semiconductors as photoactive materials sandwiched between two electrodes of different work functions. A hallmark of PV cell is the current-voltage response under illumination. The general characteristics of Current density (J) – Voltage (V) in solar cells give the output parameters to determine the power conversion efficiency of the solar cells (Figure 1.3). The measurements are carried out in the dark and under illumination by simulated sunlight. When the devices are measured in dark conditions, the J-V curve generally follows the p-n junction diode characteristics. Under illumination, the characteristics of J-V curve exhibits the combination of dark current and additional reverse photogenerated current. The standard illumination intensity is AM 1.5 Global, 1 Sun units (100 mW/cm^2).(*21*) The most important parameters obtained from light J-V characteristics of solar cells are the open-circuit voltage (V_{oc}), short-circuit current density (J_{sc}), fill factor (*FF*) and power conversion efficiency (η).

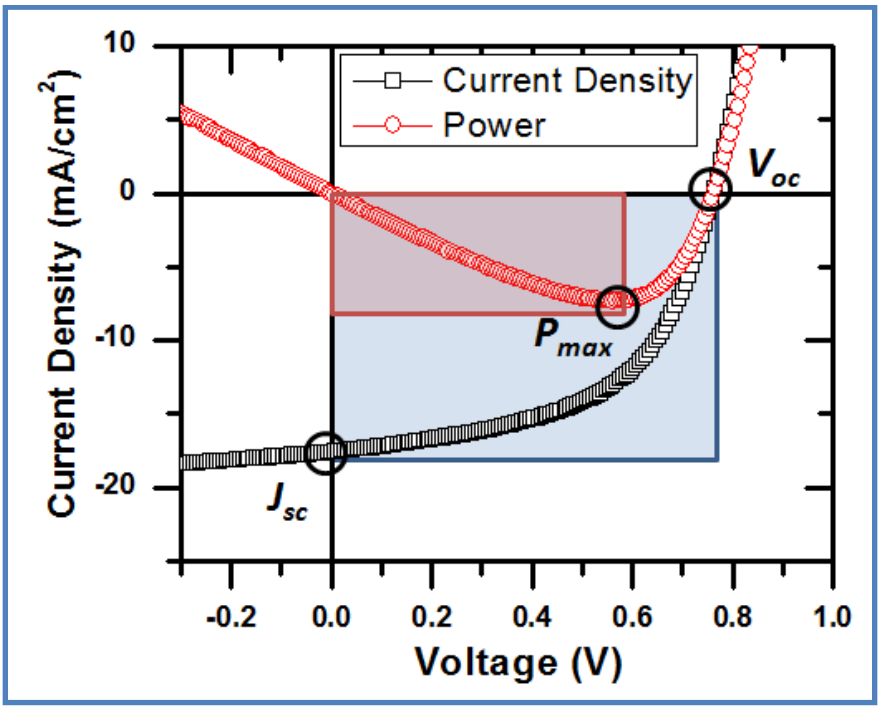

Figure 1.3: Typical J-V and P-V characteristics of solar cells. The circles represent the V_{oc}, J_{sc} and P_{max} of the device.

The open circuit voltage (V_{oc}) is the voltage at which the net current through the solar cells becomes zero, which is equivalent to open circuit. At this point, the applied bias in forward direction cancels the built-in reverse field of the solar cells. The V_{oc} is directly related to the effective band gap of the photoactive material, and modified by loss term

associated in charge dissociation and transport.(*22-25*); $eV_{OC} = E_g - E_{loss}$ where, E_g = effective band gap of the semiconductor, E_{loss} = energy loss associated with the charge dissociation and transport. *The short circuit current density* (J_{sc}) is the current density through the cell when no external bias is applied to the cell (V = 0), i.e. the device is shorted between the two electrodes. In ideal devices, the magnitude of J_{sc} should be same as the photocurrent density J_{ph}. However, the J_{sc} will be lower than the J_{ph} due to parasitic resistance associated with the device. In general, J_{sc} (*26, 27*) directly quantifies the extent of carrier generation and collection in the solar cells. At both the V_{oc} and J_{sc}, the output power is zero and hence cannot be used as operating point. The maximum power output will be at a point where the product of '*V'* and '*J'* becomes maxima. *The fill factor (FF)* of the device can be defined as $FF = \frac{(V_{max} \cdot J_{max})}{(V_{oc} \cdot J_{sc})}$ which represents the fraction of maximum power output from the solar cells. The fill factor (*28-30*) relates to recombination pathways via the shunt resistance, series resistance and diode characteristics of the cell. The most important performance parameter of the solar cells is the power conversion efficiency which is defined as the percentage of input solar power converted to electrical power. Hence the power conversion efficiency (η) can be obtained by the following relation,

$$\eta = \frac{P_{out}}{P_{in}} = \frac{V_{max} \cdot J_{max}}{P_{in}} = \frac{FF \cdot V_{oc} \cdot J_{sc}}{P_{in}}$$

where P_{in} is the incident solar power. To standardize the measurement of the efficiency of the cells, the input flux is calibrated to AM 1.5 G, 1 sun unit.

Application of semiconducting molecules as photo-active materials in solar cells underwent gradual improvement in terms of device architecture and device performances. Next section discusses the evolution of device architectures in the process of developing efficient organic solar cells.

The primary photoexcitations in typical organic conjugated semiconductors are excitonic in nature.(*31*) An absorbed photon excites an electron from the HOMO to the LUMO level leaving behind a hole. This neutral quasiparticle consisting of the bound electron-hole pair in the singlet state represents an exciton. In organic systems, excitons are Frenkel type with high binding energy in the range of 0.3 - 0.5 eV.(*32*) This is largely due to the low dielectric constant and high electron-lattice interactions.(*33*) Since the binding energy of excitons is larger than the thermal energy at room temperature (k_BT~25 meV), the excitons undergo radiative and/or nonradiative decay to the ground state. The typical lifetime of an exciton is in the range of 100 ps to 10 ns.(*31*) In addition, the diffusion length of

excitons are in the range of 10-20 nm due to lack of crystallinity and high disorder in organic semiconductors.(*34*)

Efficient dissociation of excitons into free charges forms the basic vital challenge for the realization of organic photovoltaic devices. The device architecture for organic solar cells has evolved from a single component, single layer structure forming a schottky-type electrode interface. The single active layer Schottky diode structures exhibited low photoresponse and power conversion efficiency.(*35-37*) Introduction of an additional layer consisting of molecules with appropriate electron affinities was first employed by Tang.(*38*) The utilization of vacuum-deposited CuPc and perylene based bilayer in the device structure exhibited relatively higher efficiency in photocurrent generation and power conversion efficiency to about 1 %. This concept of bilayer structure was further extended to solution processed macromolecular active layers (Figure 1.4). In these devices, the driving force for the dissociation of exciton was created by the energy offset between LUMO levels of donor/acceptor molecules at the interface.(*39*) However, the typical optical absorption depths of organic molecules are in the range of ~100 nm, hence these planar bilayer junction devices were severely limited by exciton diffusion length (~10 nm) and interfacial area.

1.3 The Bulk heterojunction (BHJ)

The concept of bulk heterojunction was introduced to circumvent the problem of short diffusion length of excitons existing in donor polymer.(*40*) The active layer of bulk heterojunctions consists of a binary mixture of the electron donor and acceptor (typically fullerene (*41, 42*)) materials (Figure 1.4). This interpenetrating bicontinuous network of donor/acceptor molecules enhances the interfacial area available for exciton dissociation. If the inter-mixed D/A microphase lengths are in the range of 10-20 nm, then most of the excitons reach the D/A interface to dissociate into free charges. Hence the efficiency of charge generation in these bulk heterojunction films is governed by the crystallinity and phase-separation property of the individual components.(*43, 44*) Initial reports on BHJ devices showed promising results in which the donor polymers were blended with fullerene derivatives acceptors.(*40*) The donor polymer poly-[3-hexylthiophene] (P3HT) and acceptor molecule [6, 6]-phenyl C61-butyric acid methyl ester ($PC_{60}BM$) has been a model BHJ system for decades.

The generation of photo-carriers in a polymer: fullerene BHJ can be explained in the following sequential steps: Incident photons of energy higher than the band-gap of the donor

(acceptor) molecule are absorbed to create excitons. The exciton generated inside the donor (acceptor) domain subsequently diffuses to the donor:acceptor interface, where it is quenched by electron (hole) transfer to the acceptor (donor) molecule. This electron (hole) transfer process does not necessarily generate dissociated free charge carriers. At this point, the electron and hole are located on different materials but can be bound by the Coulomb attraction (~ of 0.1 - 0.5 eV) forming an interfacial bound electron-hole pair which is more commonly referred as charge transfer (CT) states. The dissociation of these bound electron−hole pairs into free charge carriers is the most important step in the overall process from absorption of photons to free charge generation. Upon overcoming their binding energy, the exciton dissociates and free charges are transported through the bulk and finally extracted at the device electrodes.

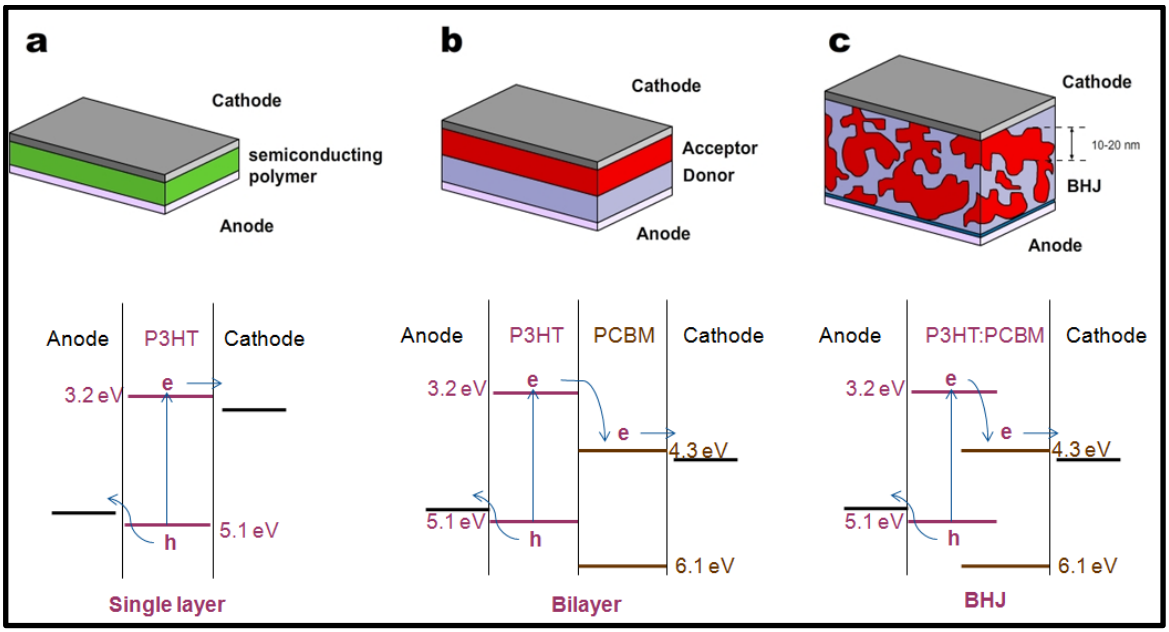

Figure 1.4: Evolution of organic solar cells: (a) single layer of organic semiconductor sandwiched between two electrodes of different workfunction, (b) device of donor and acceptor molecular bilayer sandwiched between two electrodes, where the acceptor molecules assist in quenching of donor singlet excitons at the bilayer interface, (c) spinodal decomposition of binary mixture to form intimate mix of donor and acceptor molecular blend film spun coated between two electrodes, adapted with permission from the reference (45).

Most of the understanding on photo-physical processes is based on BHJ consisting of polymer as electron donor and fullerene derivatives as electron acceptor. The very common fullerene derivatives are [6,6]- phenyl C_{61}-butyric acid methyl ester (PCBM) and [6,6]-phenyl C71-butyric acid methyl ester (C_{71}-PCBM). The success of these electron acceptors is

due to number of reasons, particularly its ability to form BHJ nano-morphology with donor polymers. Despite all the advantage of fullerenes as electron acceptor, there are important limitation needs to be addressed besides its elaborate purification procedures. Importantly, relatively low absorption of fullerenes in visible region along with limited tunability of energy levels. In this regard, the development of new electron acceptor materials is of utmost importance which posses and exhibits all the required optical and electrical properties efficiently. To address these issues, rational design of n-type perylene molecules along with device engineering strategies are implemented in this thesis. Many photo-physical processes for the generation of charges and its association with the morphology of the active layer are studied. It should be noted that, the current understanding of charge photogeneration is mostly followed by electron transfer from polymer donor to fullerene acceptors. However, the counter path of hole transfer from acceptor excitons are highly neglected. Thesis also addresses the efficient charge generation from hole transfer path.

The subsequent sections briefly discuss studies carried out to identify and quantify the various photo-physical processes involved in charge photogeneration consisting of polymer donor and fullerene derivative acceptors based BHJs.

1.4 Photogeneration of charges in organic solar cells:

The conversion of solar energy to electrical charges is governed by the dissociation efficiency of electron-hole pairs (excitons) into long-lived free charges. The dissociation should be accompanied by high quantum yield and minimum energy loss for high efficient devices. The dissociation of excitons is dictated by the coulomb attraction between electron-hole pair, the potential between them is given by *V*, $V = \frac{e^2}{4\pi\varepsilon_r\varepsilon_o r}$, where 'e' is electronic charge, 'ε_0' is the permittivity of free-space, ε_r is the dielectric constant of the surrounding medium, and 'r' is the electron−hole separation distance. In inorganic materials this Coulomb potential can be easily overcome due to high dielectric constant ($\varepsilon_r \sim 12$ for silicon) and highly delocalized transport bands. This is similar in the case of dye-sensitized solar cells, where the electron is transferred to the nanoparticles of TiO_2 having dielectric constant ~ 80. However, for organic bulk heterojunction solar cells, the low dielectric constant ($\varepsilon_r \sim 2-4$) and localized nature of charges pose a key challenge for efficient dissociation of the excitons. The most sophisticated organic based photo-conversion is in the natural photosynthetic systems. In photosynthesis, the absorbed photon energy follows the charge transfer process

with relay of redox reactions (cascaded energy levels).(*46*) However, the photogeneration of charges in this natural photosynthesis system is energy demanding with low quantum yield. In organic BHJs, the interfaces are formed with single donor and acceptor materials and the percolation of charges occurs due to the interconnected network of donor and acceptor domains. The detailed understanding of charge transfer process in dilute solution of donor-acceptor systems is studied from non-adiabatic electron transfer theory.(*47-50*) These organic materials typically exhibit localized electronic states and weak electron−lattice interactions. However, several reports show near unity quantum yield of molecular donor-acceptor systems. This makes the of mechanism for dissociation of electron-hole pair overcoming Coulomb attraction central to understanding of molecular processes in organic semiconducting materials for the development of high efficient devices.

1.5 Exciton dissociation in organic semiconductors

The initial photoexcitation in the organic molecules typically undergo a quantum mechanically allowed transition of electron from HOMO to LUMO level forming a singlet excitonic state. Typically, the binding energy (E_B^{exc}) of this singlet state is large compared to thermal energy (k_BT) in these systems. In pristine molecules, this excitonic singlet state can recombine back radiatively or non-radiatively to ground state or can dissociates into free charges by interacting with impurities, defect sites and even under the influence of external electric field. In the concept of "bulk heterojunction" the exciton dissociates at the donor-acceptor interface. The important characteristics of excitons are its binding energy, diffusion length and life time. All these properties of excitons are highly dependent on the electronic structure of the organic semiconducting materials and, are crucial in efficient generation of charges in the bulk heterojunction.(*51-54*) The singlet excitons are spatially more localized on the back bone of the conjugation. Electronic transitions are accompanied with local relaxation of the neighboring molecular structure. This is due to the strong electron-phonon coupling in the organic semiconductors.(*33*) In polythiophene (P3HT), the singlet exciton induces a structural relaxation accompanied by reversal of the C-C bond length. The magnitude of bond length reversal is maximum at the center of the exciton and gradually decreases away from the center. The bond reversal in excited state makes the P3HT more rigid and planar. This is evident from photoluminescence spectra with more vibronic features as compared to ground state absorption spectra of P3HT solutions.(*55, 56*) P3HT is a stiff polymer with flexible side chains, which promotes the solubility. In the melt phase this class

of polymers generally exhibits a microphase separation between the stiff main chain and the alkyl side chains leading to a layered, liquid crystalline structure. Upon crystallization the layered structure is preserved and the main chains as well as the side chains order onto a common crystalline lattice. In this respect, aspects of side chain crystallization, as they are observed in comb-like polymers consisting of an amorphous main chain and crystallizable alkyl side chains, are combined with aspects of the usual main chain crystallization as it occurs for polymers consisting of chemically regular, flexible chains. Apart from the features introduced by the side groups, the 3-hexyl substituent in a thiophene ring of P3HT can also result in two different regioregularities. If the 3-hexyl chain is attached to thiophene ring in a head-to-tail regioregularity(RR-P3HT), then P3HT chains self assemble in two-dimensional (2D) lamella nanostructure with interchain distance of ~ 3.8 Å, resulting in strong interchain interactions. In contrast, regio- randomly substituted P3HT (RRa-P3HT) forms disordered amorphous films having unfavorable HH coupling causing a sterically driven twist of the thipohene rings. This results in shorter conjugation of RRa-P3HT chains.(*57, 58*) The steady state spectroscopic measurements show red shifted absorption and PL band of RR-P3HT as compared to RRa-P3HT. This is due to the fact that the superior planar lamellae ordered RR-P3HT chains lead to longer conjugation lengths with fewer defects. However, the PL quantum yield of RR-P3HT (8%) is an order of magnitude less than RRa-P3HT (< 0.5 %).(*59*) The extent of the spatial deformation depends on the electronic and chemical structure of the molecules. In polyphenylenevinlylenes (PPV) molecules, it was shown that the singlet excitons extends over six monomer units where as the triplet excitons extends over one to two monomer units.(*52, 60*) It is also known that, the polarons are coupled with the structural deformation in the organic materials.(*61, 62*) Due to their electrical neutrality, the excitons diffuse randomly following Brownian motion without any drift from the external electric field. The excitons can diffuse intermolecularly or intramolecularly through incoherent energy transfer process (Froster energy transfer). The process of diffusion occurs through an energy downhill pathway in the inhomogeneous density of states.(*54*) During migration, the exciton often gets trapped and detrapped at the defect sites. The probability of detrapping depends on the thermal fluctuations.

Generally, the initial excitation from high energy photons creates vibrationally excited excitons which have been referred as hot-excitons. The hot-exciton can vibrationally relax by an internal conversion process within a sub-picosecond time scale (*63-65*). This is followed by intramolecular and intermolecular diffusion processes in which, if it successfully reaches

the donor-acceptor interface it dissociates into free charges. Hence the diffusion length of excitons is an important parameter in deciding the efficiency of free charge generation. If the excitons are generated at the defects or at the interface of donor and acceptor molecules, then the hot-excitons directly dissociates with extra free energy following Franck-Condon principle.(*66-68*) Hence BHJ films having adequate donor-acceptor interfacial area along with optimum domain sizes for efficient diffusion of excitons and charges is a guideline prerequisite to observe reasonable efficiency . The size and density of the different phases in the organic BHJ highly depends on the processing conditions during the fabrication. The reported value of diffusion lengths for PPV and P3HT are 5-14 nm and 6-9 nm respectively.(*69, 70*)

It should be mentioned that there is no clear single description for the film morphology formed by BHJs. For instance, the phase separation length scales, phase-purity and demixing features are quite different in amorphous donor polymer based BHJs compared to crystalline donor-polymer based BHJs

Theoretical approaches to the exciton formation and dissociation in organic semiconductors have developed significantly. Mott-Wannier and Frenkle type exciton models are applied to understand the exciton formation in inorganic crystals and molecular crystals respectively. These models are used to estimate the exciton characteristics like radius, binding energy etc. The Marcus model has provided a basic framework to understand the key intermediate steps in photocarrier generation.

1.5.1 Marcus theory of electron transfer:

The Marcus theory was initially developed to explain the electron transfer process in many chemical reactions(*71*) and further was successfully extended to photoinduced electron transfer in semiconducting polymer blends.(*72, 73*) In this theory, the potential energy surfaces of reactant and product are considered as two intersecting harmonic oscillators plotted with respect to reaction coordinates (Figure 1.5).

The electron transfer process must satisfy both energy conservation and the Franck-Condon (F-C) Principle. During electron transfer, the F-C principle assumes that the effective change in the nuclear coordinates is negligible. Therefore, the intersection point of reactant and product potential surfaces represents the energy level and nuclear coordinates for the iso-energetic electron transfer during reaction.

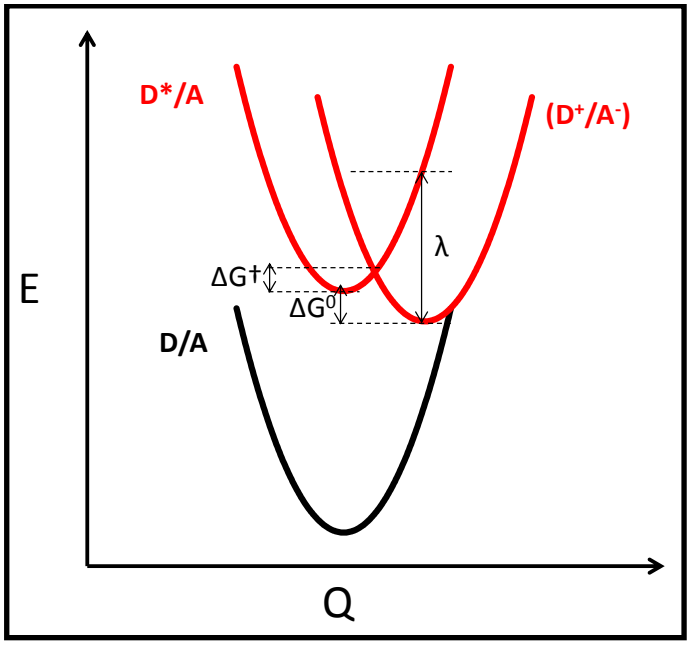

Figure 1.5: Potential energy surfaces for a donor/acceptor(D/A) system, where photoexcitation generates excited-donor/acceptor(D/A) and subsequent electron transfer generates D^+/A^-. ΔG° is the energy difference between the two surfaces' minima; the energy barrier for the reaction, ΔG†, is the energy difference between the reactant's minimum and the point of intersection between the two surfaces, and λ is the reorganization energy.(Adapted with permission from the reference (31))*

The activated process of electron transfer should overcome the activation energy barrier, $\Delta G^{\dagger}$. The Marcus theory considers the relation between activation energy barrier with Gibbs free energy (ΔG^0) and reorganizational energy (λ) by the following relation:

$$\Delta G^{\dagger} = \frac{\lambda + \Delta G^0}{4\lambda}$$

The Gibbs free energy (ΔG^0) corresponds to the difference between energy minima of reactant and product potential surface. The reorganization energy (λ) is associated with energy loss during geometrical equilibrium of reactant and product state.

The reorganization losses can have two contributions: vibrational losses within the molecule and external stabilization of surrounding medium. Typically, the vibrational losses can be determined from the vibrational force constants of the reactant and product, and the external losses using the dielectric continuum model of the solvent.(*49*) The Fermi's Golden rule analysis gives the electron transfer rate (k_{ET}) equation as given below:

$$k_{ET} = \frac{2\pi}{\hbar} V^2 FC = \frac{2\pi}{\hbar\sqrt{4\pi\lambda kT}} V^2 \exp\left(-\frac{(\lambda + \Delta G^0)^2}{4\lambda kT}\right)$$

The electronic coupling between reactant and product states is represented by the matrix term V, which depends on electron wave function overlap between donor and

acceptor molecules. In the case of weak electronic coupling, the two potential energy surfaces splits smaller compared to k_{BT}, hence the electron transfer process occurs non-adiabatically. This is a semiclassical analysis in which the electronic coupling is treated quantum mechanically and nuclear motion classically. The nuclear motion can also be treated quantum mechanically by considering the nuclear tunneling approach. In equation (3), the term inside exponential corresponds to F-C factor. This factor predicts that, as -ΔG° increases the electron transfer rate also increases. At $\lambda = -\Delta G°$, the reaction proceeds without any activation barrier. Further increase in $-\Delta G°$ which corresponds to the Marcus inverted regime ($-\Delta G° > \lambda$), decreases the electron transfer rate.(*74, 75*)

In the case of solid state BHJ films, the acceptor energy levels which generally belong to fullerene derivatives are considered to be in the form of a band. Hence the above equation will be integrated over density of available states.(*76*) If the excitons are generated directly at the interface, then the process of excitons dissociation occurs at ultrafast time scales.

After the electron transfer from the donor to acceptor molecule at the interface, the electron on the acceptor LUMO is still bound to the hole on the donor HOMO due to Coulomb attraction. Efficient generation of free charges depends on the probability of dissociation of this charge transfer exciton within their lifetime otherwise this CT state undergoes geminate recombination back to the ground state, either radiatively or non-radiatively, which is a significant loss in terms of device performance. Since the identification and the role of CT state in a non-fullerene BHJ form one of the highlights of this thesis, a required background in this direction is provided. The next section discusses the theoretical model applied on this aspect of dissociation and recombination of CT states.

1.5.2 Onsager theory of charge pair dissociation:

The concept of geminate recombination was first quantitatively described by Onsager.(*77*) Initially, this model was employed to study dissociation probability of Coulombically bound positive and negative ions undergoing Brownian motion in a weak electrolyte solution. Later this model was modified to study the dissociation probability of photo-induced electron transfer between donor and acceptor molecule where electron and hole of the bound charge transfer state dissociate into free charges. In this model, photon absorption creates a localized-hole and a hot-electron with excess thermal energy. This excess thermal energy assists the motion of hot-electron away from the Coulombically bound localized-hole (Figure 1.6). The distance between hole and electron is quantified by the

Coulomb capture radius, r_c , defined as the distance at which the Coulomb attraction energy equals the thermal energy(k_{BT}). The relation for the Coulomb capture radius is given by:

$$r_c = \frac{e^2}{4\pi\varepsilon_r\varepsilon_0 k_b T}$$

Where, e is the electronic charge, ε_r is the dielectric constant of the medium, ε_0 is the permittivity of free space, k_B is Boltzmann's constant, and T is temperature.

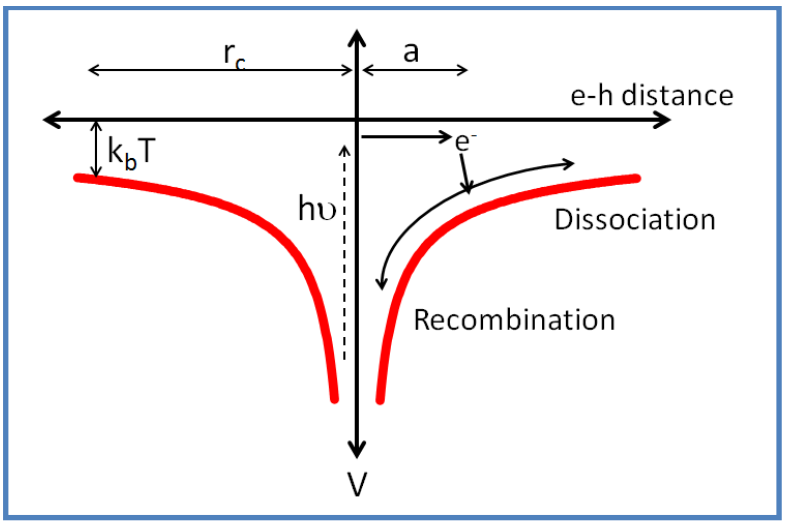

Figure 1.6: Potential energy diagram summarizing Onsager theory for autoionization. The red curve illustrates the potential energy resulting from Coulomb attraction as a function of electron–hole separation. Photoexcitation results in generation of a hot, mobile electron. This electron subsequently thermalizes at a particular distance from the hole (the thermalization length, a). If 'a' is less than the Coulomb capture radius, rc (as is typical for single-component organic systems), then the charge transfer state can either undergo geminate recombination or dissociate into free charges. Adapted with permission from the reference (31).

In inorganic semiconductors, the dielectric constants are relatively high (ε_r > 10 reducing the Coulomb capture radius leading to efficient dissociation of excitons into free charges. However in organic semiconductors, the low dielectric (ε_r > 4) constant results in large Coulomb capture radius and reduced escape probability of the hot-electron.

Under the external electric field 'E', if the thermalization length 'a' is greater than r_c, the electron and hole is considered to be fully dissociated. If, a < r_c, the dissociation of the bound state into free charges occurs with an escape probability of P(E) while the geminate recombination probability to the ground state occurs as 1 − P(E). The escape probability P(E) of the electron depends on thermalization length 'a', temperature 'T' and any applied external electric field, E. If the external field is absent then the escape probability is proportional to the negative reciprocal of thermalization length 'a'. In the presence of an external field, the magnitude of Coulomb barrier is reduced and enhances the escape probability.(*78*) For low magnitude of external field, the P(E) is given by:

$$P(E) = \exp\left(-\frac{r_c}{a}\right)\left(1 + \frac{er_c}{2k_BT}E\right)$$

Where, 'a' is the initial thermalization length.

At low magnitude of 'E', the P(E) varies linearly. A plot of P(E) versus E under such low field conditions gives a slope to intercept ratio of $e^3/2\varepsilon_r k_B^2 T^2$ and is thus independent of 'a'. The parameters in the ratio are directly measureable and hence Onsager theory can be successfully applied to several systems.(*79-81*)

In the case of BHJs with the presence of CT state formation process, the life-time of CT needs to be considered for estimating the escape probability within this framework. In addition, the Onsager theory considers the boundary condition that, if the separation distance between the opposite charges reached zero, then the charge pair recombine irreversibly. Due to this limitation of the theory, Braun(*82*) revised the model by invoking rate dependent terms; electric-field dependent rate constant ($k_d(E)$) and rate of geminate recombination (k_f): The revised equation is given by:

$$P(E) = \frac{k_d(E)}{k_f + k_d(E)} = k_d(E)\,\tau(E)$$

Where, P(E) is the escape probability and τ(E) is the lifetime of the CT state. In this modified model the dissociation of CT is a reversible process. During the lifetime of CT state, the free charges can be generated with a rate constant k_r from the CT state. Applying this to original Onsager work, the dissociation rate can be defined as(*83*):

$$k_d(E) = \frac{3\langle\mu\rangle e}{4\pi\langle\varepsilon_r\rangle\varepsilon_0 a^3}\exp\left(-\frac{\Delta E}{k_BT}\right)\left[1 + b + \frac{b^2}{3} + \frac{b^3}{18} + \ \ldots\right]$$

Where, ⟨μ⟩ is the spatially averaged sum of the electron and hole mobilities, $\langle\varepsilon_r\rangle$ is the spatially averaged dielectric constant, 'ΔE' is the Coulomb attraction of the initial generated ion pair after thermalization given by,

$$\Delta E = \frac{e^2}{4\pi\langle\varepsilon_r\rangle\varepsilon_0 a}$$

and

$$b = \frac{e^3 E}{8\pi\langle\varepsilon_r\rangle\varepsilon_0 k_b^2 T^2}$$

and the summation is a first-order Bessel function. Although, the fitting of this function with experimental parameters exhibited increased dissociation yield with increased thermalization length, the significant photogeneration was predicted only at high electric field of the order of ~ 10^7 Vcm^{-1}. In polymer: fullerene BHJ blends, the CT-state separation

distance is distributed over a range of values and hence the probability equation can be integrated over the distribution(*80, 82*):

$$P(T,E) = N_F \int_0^\infty P(r,T,E)F(r)dr$$

where, P(r, T, E) is the escape probability function of CT state generated at distance 'r' apart with external field 'E' at temperature 'T'. F(r) is the charge pair separation distance distribution function, and N_F is a normalization function. It is to be noted that the modified Braun model also exhibit the same slope to intercept ratio as that of the original Onsager model. However, now the charge generation is described by including nearest neighbor interactions also.

In addition to this, several modifications were proposed to the original Onsager's model to explain the experimental observations. For example, very high electron mobility systems implies large mean free path of the electron. Tachiya proposed a new model(*78*) by incorporating the effect of electron mobility and calculating the effect of electron's trajectory to the Coulomb potential. This model agreed well with the experimental observation in high electron mobility systems. Barth and Bassler(*84*) proposed that the presence of energetic disorder at the donor-acceptor interface assists in increasing the CT state separation distance. This is due to the nonequilibirium energetic state at the interface during the formation of CT state. The outcome of this model was utilized in the thesis in designing the acceptor molecule having higher energetic disorder with respect to donor polymers. Further, Arkhipov et al.,(*85*) suggested the importance of donor-acceptor interface ordering. In their model, the dipolar layer of donor and acceptor formed induced partial dipoles upon formation of CT states. The generated repulsive potential barrier from the partial dipoles separated electron and hole by suppressing the geminate recombination. Another model considering the interfacial effect was from Peumans et al.,(*86*) where kinetic Monte Carlo modeling was employed to the Onsager model with additional considerations. They suggested that the dissociation of e-h pair occur perpendicular to the interface surface. Their model also suggested that if the electron mobility exceed by two orders of magnitude than the hole mobility, the dissociation probability increases. Recently, the quantum mechanical picture of charge dissociation was considered for two high efficient BHJ blend systems, one consisting of small molecule electron donor p-DTS(FBTTh$_2$)$_2$, ((7,7'-(4,4-bis(2-ethylhexyl)-4H-silolo[3,2-b:4,5-b']dithiophene-2,6-diyl)bis(6-fluoro-4-(5′-hexyl-[2,2'-bithiophen]-5-yl)benzo[c][1,2,5] thiadiazole))) and PC71BM acceptor blend and second consisting of donor

polymer PCDTBT, (poly[N-11W–henicosanyl-2,7-carbazole-alt-5,5-(40, 70- di-2-thienyl-20, 10, 30-benzothiadiazole)]) and PC61BM acceptor blend system, in which it was experimentally shown that the electron coherently diffused over several fullerene molecules after the charge transfer, resulting in efficient dissociation of CT state.(*87*)

Currently, the Onsager theory does not includes the effects due to lattice distortion (reorganization energy) and the presence of a dynamic interfacial electric field during the charge transfer process as discussed above in Marcus theory. This leads to an overestimation of the Coulomb capture radius for organic BHJ systems (~ 16 nm). However, the Onsager theory has proven effective for homogeneous systems in predicting experimentally observed charge generation probability.

Subsequent section discusses the experimental approaches to identify CT states, particularly experimental observation and energetics associated with dissociation of CT states in organic BHJ blends.

1.6 Charge separation at the interface:

It is important to identify energetics and associated dynamics of CT state. The performance parameters of the BHJ organic solar cells highly depend on these factors of CT state. The existence of CT state was experimentally demonstrated using both absorption and emission measurements. Since the energy level of CT state lies below the band gap of the individual components in the blend, it is expected to show a red shifted band in both absorption and emission spectra.

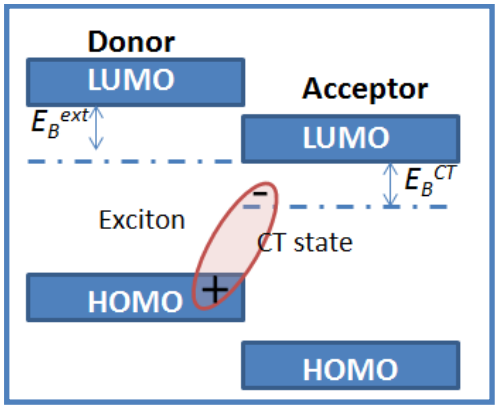

Figure 1.7: Schematic of charge transfer state. After electron transfer process at the interface, the electron on the acceptor molecule is still bound to the hole on the donor molecule due to their Coulomb attraction forming charge transfer state. E_B^{ext} and E_B^{CT} are binding energies of singlet exciton and charge transfer state respectively.

1.6.1 Absorption of the CT state:

The CT state is formed by transfer of electron from donor to acceptor molecule resulting in the formation of hybrid orbitals between donor HOMO and acceptor LUMO levels (Figure 1.7).(*88*) Since, the hybridization is due to the electronic wavefunction overlap between two different materials at the interface, the absorption coefficient of CT state is relatively small. Typically, absorption co-efficient 'α' of the CT state is in the range of 10^3 - 10^2 cm^{-1} organic BHJ blends. Hence, sensitive absorption techniques like Photo-thermal deflection methods are employed to detect the CT band in the BHJ blends.(*89*) In Photo-thermal deflection spectroscopy (PDS), local temperature difference on the sample due to the absorption of particular photons is measured as a change in the refractive index with respect to surrounding. Comparing absorption of pristine components with donor-acceptor blends shows the presence of an extra red-shifted absorption band. This was observed for several donor polymer and fullerene acceptor systems (Figure 1.8a, 1.8b).(*89-91*)

In addition, the CT state band can be detected using photocurrent measurements, and quantified using external and internal quantum efficiency measurements. The external quantum efficiency (EQE) of organic BHJ solar cells is typically quantified using Fourier-transform photocurrent spectroscopy (FTPS) or sensitive lock-in based photocurrent technique.(*25, 91-95*) In the former method organic solar cells are utilized as the external detector in the Fourier-transform infrared spectrometer, in the latter method the monochrome light will be modulated with a particular frequency while lock-in amplifier measures the photocurrent as a function of wavelength. The presence of sub-gap band-tail photocurrent response is observed in this thesis using both the techniques (Figure 1.8a).

1.6.2 Photoluminescence (PL) of the CT state:

Generally, the PL of pristine donor and acceptor excitons are expected to quench completely in BHJ films. However, the photoexcitation of donor molecule transfers the electron to the acceptor molecule, where the electron can dissociate into free charge or radiatively recombine back with the hole left on the donor. Since recombination occurs from the thermally relaxed CT state, a red shifted emission band is observed in the spectra compared to its pristine PL spectra. In initial measurements, this extra CT state emission band was observed in the solution containing donor and acceptor materials. Later the presence of this additional band was monitored in several polymer: fullerene blend films PL spectra.(*96-98*) Although the PL of individual molecules PL is quenched significantly in the blend, the residual emission from pristine molecule overlaps with the CT state emission.

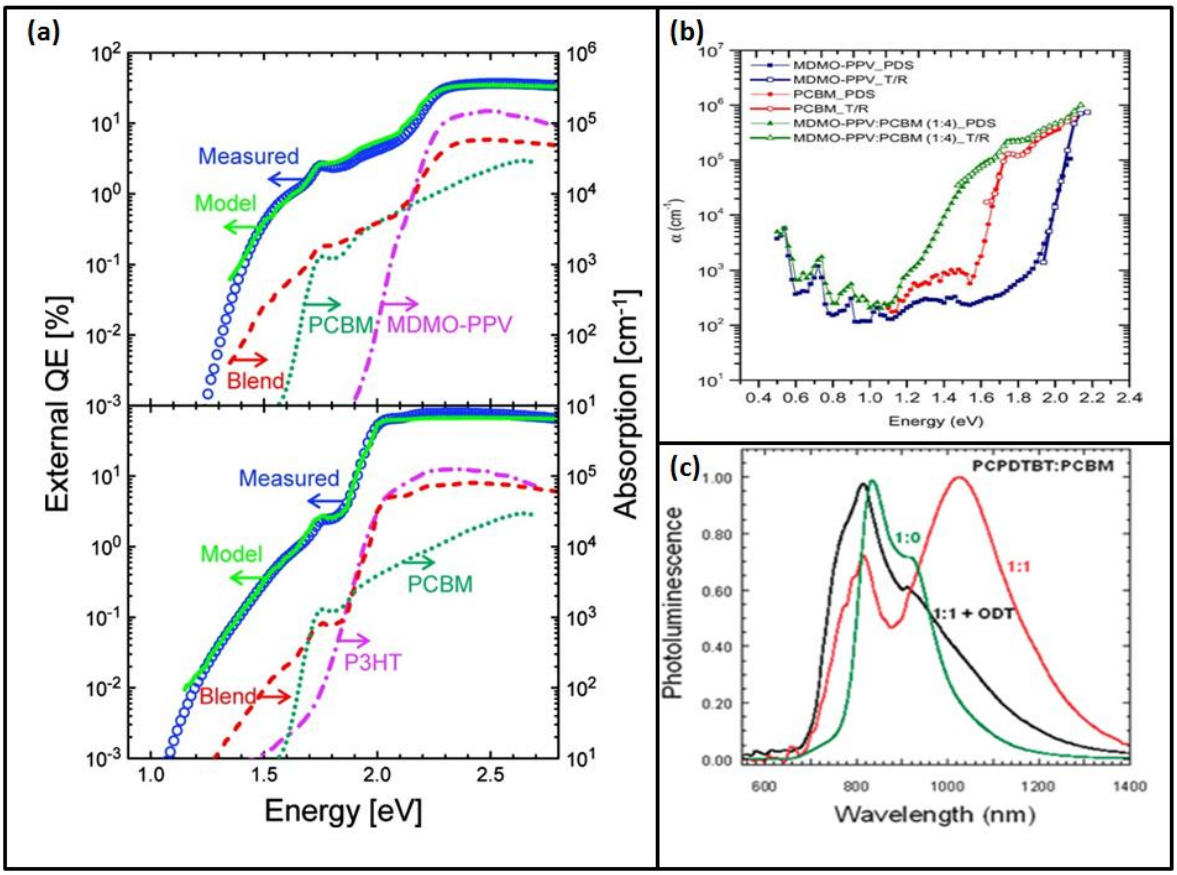

Figure 1.8: (a) The external quantum efficiency (EQE) spectrum (circles) under short-circuit conditions compared to the absorption spectrum of an MDMO-PPV:PCBM device. The absorption coefficients of MDMO-PPV (dash-dotted line), PCBM (dotted line), and blends (dashed line) are shown.(ref) (b) Absorption spectra of MDMO-PPV, PCBM and MDMOPPV:PCBM blend measured through PDS and transmission techniques.(ref) (c) Normalized photoluminescence spectra of the pristine polymer thin film and of the 1:1 BHJ with and without ODT.(ref)(figure a,b and c are reproduced with permission from the reference (95), (89), and (96) respectively)

Typical emission spectrum from the blend shows contribution from pristine donor and acceptor molecule along with the extra CT band (Figure 1.8). The intensity of pristine emission acts as an indicator for mixing of blend components. In some cases, in which the PL quantum yields of pristine molecules are high, the CT emission band is merged by the pristine emission (*99*, *100*) and is difficult to extract as a separate band.

1.6.3 Electroluminescence (EL) of the CT state:

Electroluminescence from the CT state was also observed in the organic BHJ solar cells operating in forward bias conditions (Figure 1.9). The solar cell device structure can be readily used for (EL) studies. The injected electron and hole from the external electrodes in the forward bias conditions recombines radiatively at the donor:acceptor interface.(*101*)

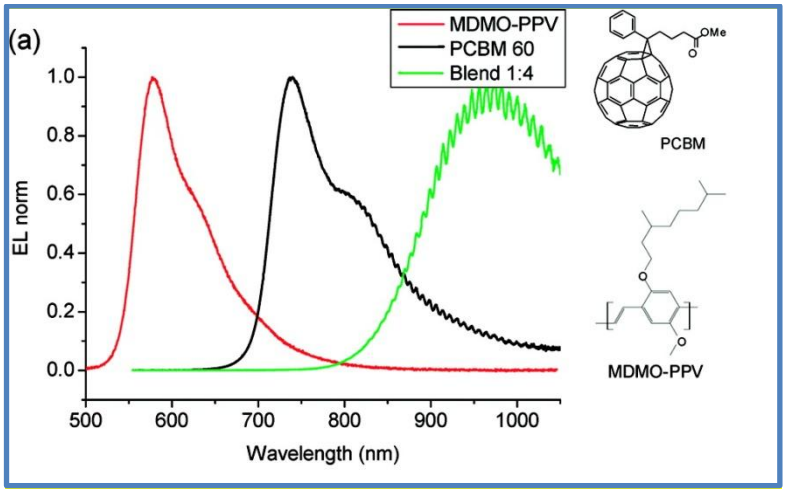

Figure 1.9: Electroluminescence (EL) spectra of MDMO-PPV, P_{60}CBM and MDMO-PPV: PC_{60}BM blend. The EL of the blend clearly shows the red shifted emission corresponds to CT state formed at MDMO-PPV and PC_{60}BM interface. The chosen stoichiometries corresponded to the best PV performance. (Reproduced with permission from the reference (99))

It is interesting to note that the EL is expected from the same CT state formed between donor and acceptor molecule, the spectra is usually slightly red-shifted than the PL of the CT state.(*102*) One of the explanation is attributed to the fact that the EL from the CT state is from the more ordered donor:acceptor interface of the BHJ, in which the electron and hole recombine from the lower most energy levels. In addition, the EL spectra exhibit new bands appearing in the higher wavelength regions. The formation of new bands is attributed to the pristine molecule emission, in which the recombination zone of electron and hole shift from interface to pristine domains.(*99*, *100*, *103*)

Previous sections discussed the observation of CT state using steady state techniques, next section discusses the formation and dissociation dynamics of CT states at ultrafast time scales.

1.6.4 Charge transfer states in ultrafast time scales:

Time resolved transient absorption spectroscopic measurements are generally employed to study the charge generation and recombination dynamics in the donor-acceptor systems. Transient absorption spectroscopy is a pump-probe technique, in which the pump laser pulse excites the sample from ground state to excited state and the probe pulse monitors the excited state dynamics. After exciting the sample using pump pulse, the excited species can be re-excited to higher lying energy levels by absorbing the probe pulse. The delay between pump and probe pulse assists in monitoring the dynamics of the excited species.

Along with radiative species like singlet excitons, the non-radiative excited species like polarons and triplet excitons can also be monitored using this technique. The key challenge of this technique is to resolve and assign all the bands observed in the transient spectra. Although, quasi-steady state spectra is utilized in assigning basic bands, the combination of quantum chemical calculation and global fitting of transient spectra has proved to be more useful in recent analysis.

Charge transfer from polymer donor to fullerene derivative was first observed using ultrafast (~45 fs) pump-probe spectroscopy by Brabec et al.(*104*) However, they could not resolve the charge transfer process and formation of bound CT state or free charge carriers. Later on, Hwang et al.(*105, 106*) showed the formation of free charge carriers within few picoseconds in P3HT :$PC_{61}BM$ blends. This result were subsequently observed by other groups in varied donor-acceptor BHJs.(*107-114*) Very recently, Grancini et al.(*115*) utilized sub-20 fs transient absorption spectroscopy on the high efficient PCPDTT:$PC_{61}BM$ blends and showed that bound CT state and as well as free charge carriers are generated promptly within ~50 fs of photoexcitation. Apart from transient optical pump-probe measurements, the free charge generation in ultrafast timescales was confirmed by other techniques. Optical-pump and terahertz-probe measurements were employed to investigate time-resolved conductivity of photogenerated free charges. Their results confirmed the formation of free charges within 100 fs in several donor-acceptor BHJs.(*116*)

1.7 Dissociation of the CT state into free charge carriers:

The presence of bound CT state and formation of free charge carriers in ultrafast timescales were discussed in the previous sections. The important and highly debated topic is the dissociation of this CT state into free charge carriers. As mentioned earlier, the CT state will be formed by transfer of electron from donor to acceptors (leaving hole behind on donor molecule) at the donor-acceptor interface. Considering the energy diagram of photocharge generation, the CT state possesses excess thermal energy (ΔG_{CS}) initially due to the difference in energy between donor singlet exciton and CT state. The dissociation of this hot-CT state occurs through two possible pathways: (1) formation of free charges from hot-CT state, or (2) thermal relaxation of CT state to its ground state followed by dissociation into free charges. We will discuss both the theories of free charge generation with experimental evidences and conflicting arguments in the following section:

1.7.1 Charge generation from hot-CT state:

In this theory, the excess energy associated with hot-CT state will assist in dissociation of CT state into free charges before relaxing to its ground state. Thermalization is an internal conversion process, which occurs at an ultrafast timescale of the order of hundreds of femtosecond.(*117*) To kinetically compete with this process, the dissociation of hot-CT state should also occur in similar time scales. Several ultrafast measurements confirmed the formation of free charges within the time limit of hot-CT state (~50 fs).(*115*) In addition, in this theory, the thermally relaxed CT state usually undergoes geminate recombination due to the lack of driving energy for dissociation. A series of polythiophene and fullerene blends having different $LUMO_D$-$LUMO_A$ offset were investigated using transient absorption measurements to obtain a relation between excess driving energy and yield of photogenerated charges.(*117*) They found that the yield of polarons varied by an order of magnitude with different polythiophenes and exhibited strong dependence with the driving energy. Based on these results, they suggested that the excess energy during charge transfer provides extra kinetic energy for the CT state dissociation. These results were subsequently supported by measurements on several other polymer:fullerene and polymer:perylene blends.(*118*) Vardeny and group(*119*) employed a set of measurements comparing sub-gap and above-gap excitation to probe the dependence of yield of polarons with excess energy. They found that the above -gap excitation produces more photocurrent, which was in support of hot-CT state dissociation.

Recently, transient absorption measurements with sub-20 fs pulses were employed on PCPDTBT:PC_{61}BM BHJs to address the concept of ultrafast charge generation. In their experiment, depending on the excess energy, they found the formation of CT state and free charges within 50 fs (Figure 1.10). Excitation with higher energy photons led to the occupation of high lying singlet energy states, which was then followed by formation of hot CT-state. This was due to strong coupling between high-energy singlets and hot-CT states.(*115*) They suggested that the thermally relaxed CT states are basically loss channel with decreased yield of free charges. In addition, they found that the internal quantum efficiency (IQE) measurements on optimized devices (based on PCPDTBT:PC_{60}BM BHJ) exhibited wavelength dependent charge generation. The charge generation efficiency increased for higher energy photons and supported the theory of hot-CT state dissociation. However, accuracy in the IQE measurements on the transverse geometry of solar cells was questioned by Scharber and Armin et al. For this, Grancini et al. constructed transverse

geometry photovoltaic devices and re-demonstrated the wavelength dependent IQE measurements.(*115*)

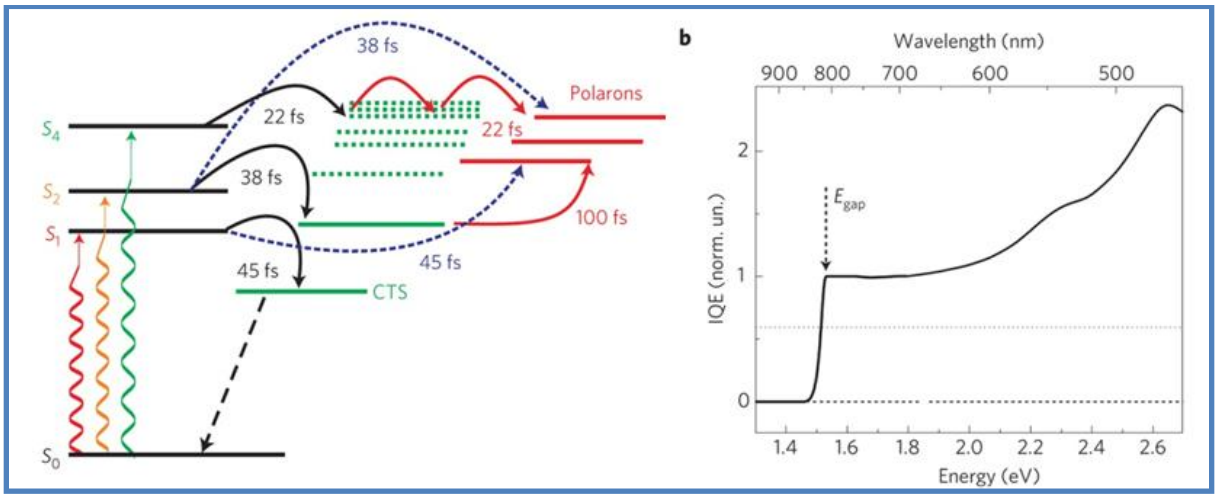

*Figure 1.10: (a) Schematic of the hot electron transfer mechanism and excited states involved: singlet exciton states (represented by the black lines), interfacial CTSs (green-coloured levels) and free polarons (red-coloured levels). The solid black arrows represent exciton dissociation into the CTS manifold; blue dashed arrows indicate exciton quenching into free polarons and solid red arrows represent CTS dissociation into free polarons. The time constants for each process are included. (**b**) IQE obtained from the measured external quantum efficiency on a PCPDTBT: $PC_{60}BM$-based device in a standard bulk heterojunction architecture normalized by the blend absorption. (reproduced with permission from the ref (115))*

1.7.2 Charge generation from relaxed-CT state:

Although, the most direct way of proving the concept of hot-CT state dissociation is through IQE measurements, the inaccuracy in the measurements of absolute IQE lead to controversy in wavelength dependent charge generation. To this point, the IQE measurements were extended to sub-gap CT-state absorption regime, to directly probe the charge generation efficiency from the relaxed CT state. Surprisingly, the IQE measurements were wavelength independent even at CT-state absorption region, suggesting generation of equal amount of charges as compared to pristine molecular absorption.(*120*) This indicated that CT-state was the sole precursor in the formation of free charges.

Investigation of IQE on polymer:fullerene blends by Lee et al.(*95*) showed that the charge generation efficiency was almost constant extending to sub-gap CT state absorption. They also demonstrated the temperature independence on photocurrent generation in comparison with pristine and CT state absorption region. They further showed that, at similar intensities of above-gap and below-gap excitations, the devices exhibited similar current-voltage characteristics. In addition, the field independent normalized EQE measurements

from another group (extending upto sub-gap region) was consistent with the previous results, suggesting that excess thermal energy plays negligible role in dissociation of CT state.

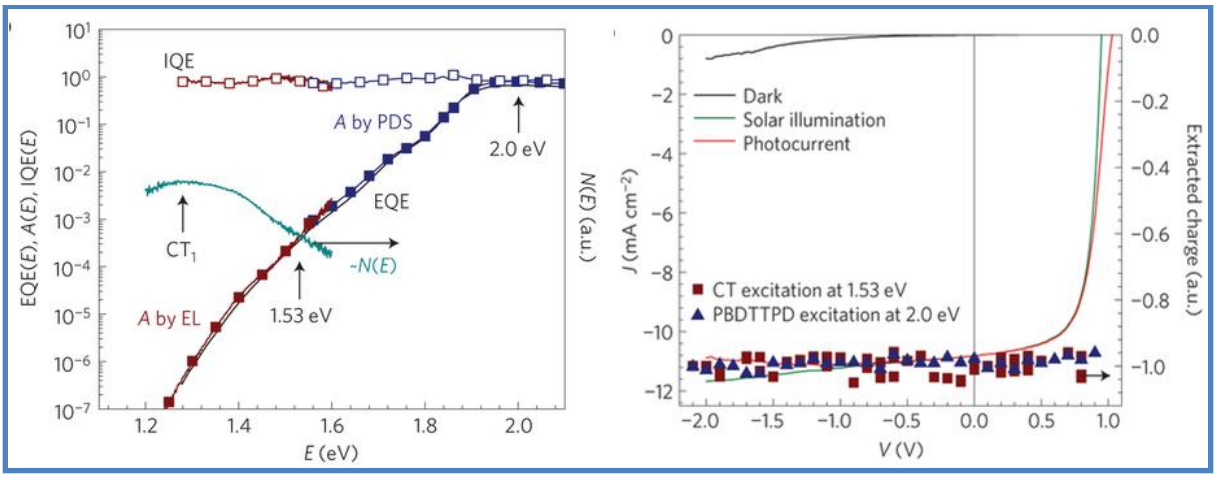

Figure 1.11: (a) EQE(E) (black line), electroluminescence (EL) emission spectra N(E) (cyan line) and the high energy part of the A(E) spectra (blue line filled squares) are measured directly on photovoltaic devices and active layers PBDTTPD:$PC_{61}BM$ blend. In the very weakly absorbing region, the A(E) spectra are reconstructed using N(E) as described in the main text, and are matched to the A(E) spectra measured by PDS in the overlapping region (red line, filled squares). (b) J–V curves in the dark and under solar illumination for a solution-processed for a PBDTTPD:$PC_{61}BM$ device. The relative number of generated charge carriers, extracted in the TDCF experiment as a function of applied bias, is shown on the right axis, for dominant excitations of D^*, A^* and those directly into the CT band. (reproduced with permission from the reference (114))

In 2014, Vandewal et al.(*120*) carried out time-delayed –collection-field (TDFC) measurements on several combination of polymer:fullerene BHJ devices. In their measurements, optical pump was followed by electrical probe (reverse bias, ~ -3 V) of particular time delay (~ 10 ns) to extract the photogenerated charges. The important observation is that the charge extraction was independent of incident photon energies (even at sub-gap regime). They concluded that, the relaxed CT states can produce similar quantity of charges as that of pristine singlet excitation in organic BHJs.

All the above experimental evidences support the dissociation of thermally relaxed CT-state from below gap excitation measurements. However, the below-gap excitation need not exclusively probe the thermally relaxed lowest CT-state at given temperature, since the photo-absorption of CT state can produce vibrationally excited CT state before dissociation. To access the lowest CT state, Vandewal et al.(*25*, *113*) reconstructed absorption spectra from EL of CT state. IQE spectrum estimated from the reconstructed absorption spectrum exhibited similar wavelength independence (figure 1.11). From the above results, they

concluded that the thermally relaxed CT-states are the exclusive precursor for the photogeneration of charges at the donor: acceptor interface in organic BHJ devices.

After dissociation of CT state, the free charges generally compete with the recombination losses. The next section discusses these loss processes prevailed in the BHJ systems.

1.8 Geminate and non-geminate recombination

As mentioned earlier, the process of recombination of charges carriers (electron and hole pair) generated from same excitons is known as geminate or monomolecular recombination. There are two possible ways of geminate recombination; a) the Coulombically bound electron-hole pair (CT state) recombines back to ground state before dissociation and b) the dissociated electron and hole in their respective domains find original pairs to recombine at the interface. Non-geminate recombination involves recombination of free charges which are produced from completely different excitons. Depending on the mechanism of recombination, there are three kinds of non-geminate recombination: trap-assisted recombination, bimolecular recombination and auger recombination.(*121*) The important efficiency limiting recombination in organics BHJ devices is bimolecular recombination. Bimolecular recombination in disordered semiconductors is limited by the rate of capturing opposite charges. The high mobile charges encounter faster opposite charges to recombine, as a result the rate of bimolecular recombination is directly proportional to charge carrier mobilities. For organic semiconductors, the rate of bimolecular recombination is described by the Langevin expression:(*122*)

$$R_L = \frac{q}{\varepsilon}(\mu_e + \mu_h)(np - n_i^2)$$

Where, q is the electronic charge, ε is the dielectric constant, μ_e mobility of the electrons, μ_h mobility of the holes, n and p represent the electron and hole charge density respectively and n_i is the intrinsic carrier concentration. The above relation describes the recombination rates of two mobile carriers having opposite charges which recombine due to their attractive Coulomb field. This kind of recombination is effective in organic materials, in which the mean free path of charges is less than the Coulomb capture radius r_c. From the above expression, one may expect that higher mobilities increase recombination rates. However, the simulation results showed that, at higher carrier mobility the bimolecular recombination rate decreases in BHJ blends.(*123*) This is due to decreased charge carrier density with improved charge extraction. In contrast, if the charge carrier mobilities are too

low then the recombination rate increases due to increased charge density resulting from inefficient extraction of charges. Although the above equation was successfully applied to many organic semiconductors, the simulated recombination rates for organic BHJ devices were overestimated than the experimentally observed values. Hence the above equation was modified by introducing the Langevin-reduction factor, ξ.(*121, 124*) Assuming the density of electrons and holes to be same (n = p) and also neglecting n_i,

$$R_{BI} = \gamma_{BMR} n^2$$

where,

$$\gamma_{BMR} = \xi \frac{1}{\varepsilon} (\mu_e + \mu_h)$$

is known as the bimolecular recombination coefficient. The estimated value of 'ξ' for many polymer:fullerene BHJ blends is between 0.01 to 1. The reduced Langevin recombination was employed by several groups.(*121, 124*) Further, the correlation between phase separation and recombination were studied, where increased phase separation reduced Langevin recombination rates. In addition, a combination of effect of domain size, energetic disorder at the interface, and balanced electron-hole mobility were also considered to accurately estimate reduced recombination rates as observed experimentally for several organic BHJs.

In addition to bimolecular recombination, monomolecular trap-assisted recombination also decides the photocurrent generation efficiency in organic BHJ devices. In trap-assisted recombination, a single carrier gets localized first by an energetic trap followed by recombination of opposite charge with the localized charge. In this case, the recombination rate depends on density of traps and rate of trapping and detrapping of mobile charges from the localized traps. The Shockley-Read-Hall recombination was employed for several organic molecules,(*125*) where the rate of trap-assisted recombination is described by the relation:

$$R_{SRH} = C_e C_h N_{tr} \frac{(np - n_i^2)}{[C_e(n + n_1) C_h (p - p_1)]}$$

where, C_n represents the probability per unit time that an electron in the conduction band will be captured by an empty trap. Correspondingly, C_h represents the probability per unit time that a hole will be captured by the electron in the trap. N_{tr} indicates the density of traps, n_i denotes the intrinsic carrier concentration. For organic solar cells, where n = p and $np \gg n_1 p_1$ for the case of electron traps, the SRH equation can be expressed as:

$$R_{SRH} = C_h(N_{tr}p)$$

where, thermally activated capture coefficient is expressed as:

$$C_h = \left(\frac{q}{\varepsilon}\right)\mu_h$$

The above equation implies that trap-assisted recombination in organic semiconductors is decided by the diffusion of free charges towards the trapped charges. Similar to Langevin recombination, trap-assisted recombination is also shown to be thermally activated and dictated by the free carrier transport. In spite of the presence of traps in organic BHJ devices, the majority of high efficient solar cells exhibit near unity quantum yield indicating that the devices are not exclusively limited by trap-assisted recombination. However, for low efficient devices, the trap-assisted recombination seems to be an important limiting factor for charge transport.

Bimolecular recombination differs from geminate recombination due to the time scale involved in diffusion of charges within the Coulomb capture radius of each other before recombination. Hence, bimolecular recombination is expected to be slower than geminate recombination. The typical timescale for geminate recombination is reported to be in the range of 100 ps – 100 ns, where as the bimolecular recombination can extend up to several milliseconds.(*106, 126, 127*) The dynamics of geminate recombination are expected to be independent of excitation density and should follow mono-exponential decay kinetics. In contrast, the bimolecular recombination depends on charge density and thus follows second-order kinetics. Due to this, bimolecular recombination exhibits excitation density dependence with power-law decay dynamics.

After avoiding all the recombination loss processes, the free charges can then be extracted from their respective electrodes. Next section discusses the current understanding of all the photo-physical processes exist in the organic BHJ solar cells.

1.9 Kinetics and dynamics of charge photogeneration in BHJ:

The current understanding of complete charge photogeneration processes in organic BHJ (*31, 128*) is summarized in the figure (1.12). Initial photoexcitation of donor molecule creates singlet S_1 exciton in which the electron is promoted from HOMO into the LUMO level. Successively, the singlet exciton is quenched by electron transfer to the acceptor LUMO level. The electron on acceptor LUMO and hole on donor HOMO level can still experience the Coulomb force and forms interfacial charge-transfer state.

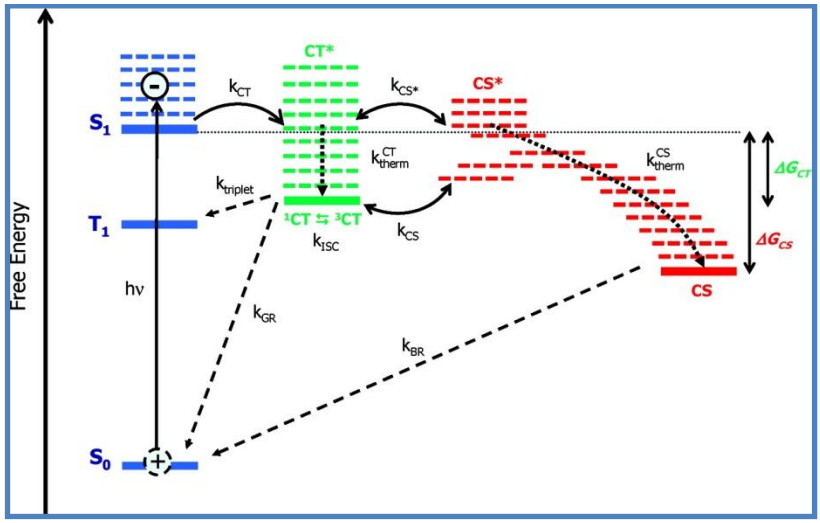

Figure 1.12: Energy level diagram summarizing the main processes involved in charge photogeneration. hv: Photoexcitation to singlet exciton (S_1). k_{CT}: Exciton dissociation to form the hot charge-transfer (CT) state. k^{CT}_{therm}: Thermal relaxation of the CT state. k_{ISC}: Spin mixing of the ^1CT and ^3CT states. $k_{triplet}$: Geminate recombination of the ^3CT to the triplet exciton, T_1. k_{GR}: Geminate recombination of the ^1CT state back to the ground state, S_0. k_{CS*}: Dissociation of the hot CT state into a fully charge-separated (CS) state. k_{CS}: Dissociation of the thermally relaxed CT state into the CS state. k^{CS}_{therm}: Thermal relaxation of the CS state and migration away from the donor/acceptor interface, resulting in an increase in state degeneracy (entropy) and charge localization on lower energy sites (traps etc.). k_{BR}: Bimolecular recombination of the CS state. This diffusion-limited bimolecular process may result from either direct recombination or, more probably, reformation of interfacial charge-transfer states (shown as reversible arrows in processes k_{CS*} and k_{CS} and subsequent geminate recombination (k_{GR})). (Adapted with permission from ref (31).)

Initially this CT sate is relatively hot due to excess thermal energy but subsequently relaxes to the thermalization length of electron hole pair. During thermal relaxation the spin state of electron-hole pair can also interchange from singlet S_1 to triplet state T_1. At this point of time, the electron and hole can geminately recombine back to ground state or dissociate into free charges which can percolate through the interconnected network of donor and acceptor domains to their respective electrodes competing with bimolecular recombination. The figure (1.12) depicts the importance of kinetic competition between charge recombination and dissociation during the process of photocharge generation. In the case of charge generation from hot CT state, the kinetic competition is between thermalization of electron (k^{CT}_{therm}) and the dissociation of hot charge pair (k_{CS*}). If the electron on acceptor LUMO level thermalizes, then the kinetic competition will be between geminate recombination (k_{GR} for recombining to singlet ground state or k_{trip} for electron back transfer from acceptor LUMO to donor triplet level) and charge separation (k_{CS}). It should be noted that the spin of the CT states (^{1}CT and ^{3}CT) plays a crucial role in deciding its dissociation

efficiency at donor-acceptor interfaces. Increased charge separation distance potentially reduces exchange splitting between singlet and triplet CT states. When the two states are almost degenerate in energy, intersystem crossing rate between the two states becomes significant. Dissociation probability of initially photogenerated singlet excitons is higher for formation of ^{1}CT states (spin conservation). However, due to spin statistics, bimolecular recombination of charges leads to formation of ^{1}CT and ^{3}CT in 1:3 ratio. Singlet CT states can recombine back to ground state either radiatively (slow because of intermolecular in nature) or non-radiatively. Decay of triplet CT states to ground state is a spin forbidden transition and hence both radiative and non-radiative processes are very slow. A general criterion to maximize the open circuit voltage of OPV is by increasing the CT state energy. This pushes the energy of CT states above energy of triplet exciton on the donor or acceptor molecule. This leads to crucial loss pathway for CT states to local triplet states 'k_{trip}' or 'triplet drain'. Once the electron fully separates from the hole, the kinetic competition is between charge trapping (k_{therm}^{CS}) and bimolecular recombination (k_{BR}). ΔG_{CS} is the energy difference between singlet exciton and completely separated charge, which represents the free energy loss associated during overall charge generation process. The energy of completely dissociated charge is defined as difference between ionization potential of donor (IP_D) and electron affinity of acceptor (EA_A). ΔG_{CS} correlates with LUMO-LUMO offset between donor and acceptor along with exciton binding energy (E_B^{exc}). The driving energy (ΔG_{CT}) is defined as energy difference between singlet exciton and charge transfer state. Efficient photo generation of charges depends on balance between ΔG_{CT} and ΔG_{CS}, in which ΔG_{CT} should be large to increase dissociation efficiency and ΔG_{CS} should be small in order to conserve overall energy. Hence this interfacial energetics during the process of charge dissociation is of significant importance and utmost care should be taken in designing the donor and acceptor molecular combination in organic BHJ solar cells.

1.10 Quantum efficiency of photocharge generation:

As mentioned earlier, the process of conversion of photons to electrical current in organic BHJ solar cells is mainly accomplished by four consecutive steps (Figure 1.13). Efficiency of each step is crucial for overall power conversion efficiency of the devices. The four important steps occur in the following sequence:(*31, 128*)

1. *Absorption of photons from donor and acceptor materials to create singlet excitons.*

The fraction of absorbed to incident photons gives the quantum efficiency of absorption, *'η_{Abs}'*. This fraction mainly depends on absorption coefficient, absorption spectra, and active layer thickness.

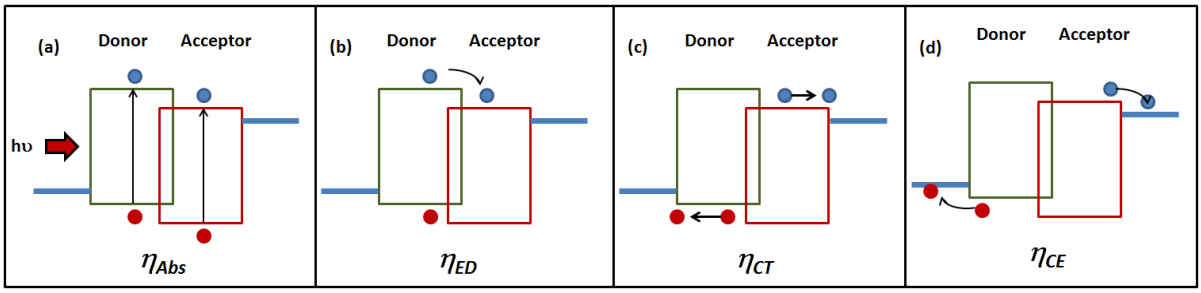

Figure 1.13: Quantum efficiency of photocharge generation. Schematic of four important sequential steps involved in generation of free charges. The quantum efficiency of each step decides the overall efficiency of solar cells.

2. *Dissociation of Singlet excitons into free charges at the donor and acceptor interface.*

The quantum efficiency of exciton dissociation, *'η_{ED}',* is defined as fraction of excitons dissociated into free charges over generated excitons throughout the bulk. This quantum efficiency involves two sub processes: diffusion of excitons from bulk of the domain to the donor-acceptor interface followed by dissociation of excitons by electron (hole) transfer process. The exciton diffusion depends on structural order and purity of the domain. Generally the exciton diffusion length in organic semiconductors is estimated to be ~ 10-20 nm. Hence the domain size should be ~ 10-20 nm. The electron (hole) transfer process is governed by the energy offset ($LUMO_D$-$LUMO_A$) between donor and acceptor molecules. In addition, the interfacial energetic disorder and bulk mobility of donor and acceptor molecules is crucial in reducing geminate recombination.

3. *Transport of dissociated charges towards respective electrode under built-in/external electric field.*

After the successful dissociation of CT state, the free charges have to reach their respective electrode. The fraction of charges transported to the electrode over charges generated at the donor-acceptor interface determines the quantum efficiency of charge transport, *'η_{CT}'*. This fraction is governed by the rate of bimolecular recombination which depends on bulk mobility, density of traps etc.

4. *Extraction of charges at the electrode: active layer interface.*

An ohmic contact is expected between electrode and active material to ensure efficient extraction of dissociated charges. Hence, the quantum efficiency of charge extraction

depends on the fraction of charges that reach the electrode to the number that are extracted from the electrode, *'η_{CE}'*. The important factor which influences this fraction is the work function of the electrodes.

The overall quantum efficiency of the device 'η' is given by the following equation:

$$\eta = \eta_{Abs} \cdot \eta_{ED} \cdot \eta_{CT} \cdot \eta_{CE}$$

Optimizing each of these factors by rational design of photoactive material along with careful fabrication processes is necessary for obtaining high efficient organic BHJ solar cells. The predictive understanding of the relationship between molecular structure and device performance is an important aspect in the development of organic bulk heterojunction solar cells.(*124, 129, 130*) To mention a few, the molecular structure and size defines and regulates the photoactivity and device parameters. The position of the HOMO and LUMO levels of the donor and acceptor molecules govern the charge transfer processes at the interface.(*131*) . The energy levels alignment of the donor and acceptor molecules is also critical for efficient exciton quenching coupled with electron and hole transfer processes. The bandgap between these levels defines the optical activity of the organic semiconductor.(*132*) The structural order in the solid state of these molecules influences charge carrier mobilities and the charge extraction efficiency.(*133*) The photocurrent generation efficiency is directly influenced by several factors such as, amount of light absorbed by the photoactive materials i.e., absorption spectra, extinction coefficient and thickness of the absorbing layer. Further, the nanomorphology of the BHJ formed by the binary mixture of donor:acceptor materials is crucial for efficient exciton diffusion to the interface as well as for efficient charge transport through the interconnected pathways competing with recombination losses.

In this thesis, we focus on overcoming the above mentioned limitations by correlating a relationship between structure-size and device performance featuring a non-fullerene acceptor based donor-acceptor BHJ system specifically. In particular, we concentrate on electron and hole transfer processes occurring at the donor-acceptor interface, the dissociation efficiency of a bound charge transfer state and improvment of charge extraction efficiency. The understanding of these processes in a non-fullerene based BHJ is of great significance and can assist in rational design of high performing organic materials for photovoltaic devices.

1.11 Thesis Outline and Structure:

Fast growth in the global energy demand and near depletion of non-renewable fossil fuel urges for alternative sources of sustainable energy to minimize the global energy challenges. In this regard, the third generation organic photovoltaic technology is a promising and cost-effective alternative to other solar energy technologies due to roll-to-roll processing and easy logistics. The power conversion efficiency of this technology is reaching over 10 %. The active layer in most of the high efficiency devices consists of low bandgap donor–acceptor co-polymers as electron donors and a fullerene based derivative as the electron acceptor. The monopoly of fullerene based materials as successful electron acceptors is due to its ability to form favorable nanoscale morphology. In spite of these promising properties, fullerene derivatives are limited by elaborate synthesis and purification procedures. In addition, the relatively low absorption in the visible region and limited tunability of fullerene energy levels urges for design of new n-type molecules. In this regard, perylenes with good electron mobility are potential alternatives to fullerenes as electron acceptors in BHJ OSCs, due to their flexibility of functionalization, increased visible absorption and high photostability.

Chapter 2 of the thesis provides the detailed description of materials utilized in the study. It also gives an overview of advanced characterization methods used to probe photo-physical processes prevailing in the BHJ devices.

Chapter 3 deals with evaluation of non-fullerene electron acceptor based organic BHJ solar cells. In particular, perylene based electron acceptors are used as alternatives to fullerene derivatives in fabrication of BHJ OSCs. The rational design of non-planar perylene (*Twisted Perylene (TP)*) is utilized to disrupt the co-facial stacking of perylene molecules without adversely impacting their charge-transport properties.(*134*) This results in reduced large scale phase separation of perylene molecules in the blends. Inverted devices fabricated using low band-gap donor polymer PBDTTT-CT and TP acceptor BHJ exhibit power conversion efficiency > 2.7 %. The control experiments show order of magnitude increase in J_{sc} in TP blend when compare to planar perylene blends. The increase in J_{sc} is attributed to reduction in the formation of micrometer-size crystals, reduction in geminate recombination losses and increase in the anisotropy of charge transport.(*134*)

Chapter 4 addresses the origin of the high J_{sc} in TP acceptor based BHJ system. Both steady-state and transient absorption spectroscopy techniques are employed to probe the charge generation and transport dynamics in these blend systems. Photoluminescence

quenching of both the donor and acceptor excitons indicates efficient electron and hole transfer processes at the PBDTTT-CT:TP interface.(*135*) Incident photons to current conversion efficiency (IPCE) spectra confirms the generation of charges from both the polymer and TP excitons. Transient measurements reveal balanced charge transfer dynamics at the interface ($\tau_e \approx 1.6$ ps, $\tau_h \approx 1.8$ ps). Optimization of blend concentration ratio yielded devices with power conversion efficiency > 3.2 %. Although, the magnitude of polaron yield of PBDTTT-CT:TP blends is comparable to that of fullerene blends, the limitation in the overall efficiency is attributed to charge transport properties.(*135*)

Chapter 5 of the thesis focuses on the energetics and kinetics of relaxed charge transfer (CT) states in this fullerene-free BHJs. Combination of photo-thermal deflection spectroscopy (PDS) and lock-in based sensitive photocurrent measurement methods is utilized to probe the CT states. The formation of ground CT-state with several combinations of donors and TP acceptors is observed by the enhanced absorption spectra in the tail states.(*136*) Electroluminescence (EL) of an efficient BHJ in forward bias conditions is obtained in order to understand the energetics of these CT states. The comparative studies of twisted perylene (TP) acceptor based BHJs with that of $PC_{71}BM$ systems reveal the role of molecular structure-order correlation on charge generation processes. The trends in the CT characteristics indicate the possibility of sizable charge dissociation which can be achieved in these non-fullerene devices, which may surpass overall efficiency of fullerene based devices.(*136*)

Chapter 6 deals with optimization of device efficiency by combination of interfacial engineering strategies to increase the charge extraction efficiency at the active layer and electrode interface. The spontaneous formation of ZnO wrinkles is utilized to increase the light absorption in the active layer by increasing the optical path length. Along with nano-structured ZnO buffer layer, an additional TP interlayer is utilized to reduce the work function difference and increase the current homogeneity at the electron extraction interface.(*137*) The reduction in electron-hole recombination enabled an overall increase of efficiency to 4.6%, which is one of the highest efficiencies for devices featuring a non-fullerene as the electron transporter.(*137*)

In summary, the thesis addresses the fundamental process of charge generation and transport dynamics in fullerene-free bulk heterojunction polymer solar cells. The rational design of twisted perylene along with various device engineering strategies has enabled to enhance the power conversion efficiency of the solar cells.

References:

(1) Green, M.A.; Emery, K.; Hishikawa, Y.; Warta, W.; Dunlop, E.D., Solar cell efficiency tables (version 42). *Progress in Photovoltaics: Research and Applications* **2013,** *21*, (5), 827-837.

(2) Feldman, D.; Barbose, G.; Margolis, R.; Darghouth, N.; James, T.; Weaver, S.; Goodrich, A.; Wiser, R., Photovoltaic System Pricing Trends: Historical, Recent, and Near-Term Projections–2013 Edition. *Golden, CO: National Renewable Energy Laboratory, PR-6A20-60207. Accessed December* **2013,** *9*, 2013.

(3) Gillingham, K.; Deng, H.; Wiser, R.; Darghouth, N.; Barbose, G.; Nemet, G.; Rai, V.; Dong, C. *Deconstructing Solar Photovoltaic Pricing: The Role of Market Structure, Technology, and Policy*; Ernest Orlando Lawrence Berkeley National Laboratory, Berkeley, CA (US): 2014.

(4) Green, M.A., Recent developments in photovoltaics. *Solar Energy* **2004,** *76*, (1–3), 3-8.

(5) Green, M., Thin-film solar cells: review of materials, technologies and commercial status. *Journal of Materials Science: Materials in Electronics* **2007,** *18*, (1), 15-19.

(6) Gessert, T., Review of photovoltaic energy production using CdTe thin film modules. *Workshop on physics and chemistry of II-VI materials, Las Vegas, US* **2008**.

(7) Reinhard, P.; Chirila, A.; Blosch, P.; Pianezzi, F.; Nishiwaki, S.; Buechelers, S.; Tiwari, A.N., Review of progress toward 20% efficiency flexible CIGS solar cells and manufacturing issues of solar modules. *Photovoltaics, IEEE Journal of* **2013,** *3*, (1), 572-580.

(8) Green, M.A., Third generation photovoltaics: solar cells for 2020 and beyond. *Physica E: Low-dimensional Systems and Nanostructures* **2002,** *14*, (1–2), 65-70.

(9) Conibeer, G., Third-generation photovoltaics. *Materials Today* **2007,** *10*, (11), 42-50.

(10) Shockley, W.; Queisser, H.J., Detailed Balance Limit of Efficiency of p-n Junction Solar Cells. *Journal of Applied Physics* **1961,** *32*, (3), 510-519.

(11) Girotto, C.; Moia, D.; Rand, B.P.; Heremans, P., High-Performance Organic Solar Cells with Spray-Coated Hole-Transport and Active Layers. *Advanced Functional Materials* **2011,** *21*, (1), 64-72.

(12) Hoth, C.N.; Choulis, S.A.; Schilinsky, P.; Brabec, C.J., High photovoltaic performance of inkjet printed polymer: fullerene blends. *Advanced Materials* **2007,** *19*, (22), 3973-3978.

(13) Sommer-Larsen, P.; Jørgensen, M.; Søndergaard, R.R.; Hösel, M.; Krebs, F.C., It is all in the Pattern—High-Efficiency Power Extraction from Polymer Solar Cells through High-Voltage Serial Connection. *Energy Technology* **2013,** *1*, (1), 15-19.

(14) Krebs, F.C., Fabrication and processing of polymer solar cells: A review of printing and coating techniques. *Solar Energy Materials and Solar Cells* **2009,** *93*, (4), 394-412.

(15) Kalowekamo, J.; Baker, E., Estimating the manufacturing cost of purely organic solar cells. *Solar Energy* **2009,** *83*, (8), 1224-1231.

(16) Krebs, F.C.; Espinosa, N.; Hösel, M.; Søndergaard, R.R.; Jørgensen, M., 25th Anniversary Article: Rise to Power – OPV-Based Solar Parks. *Advanced Materials* **2014,** *26*, (1), 29-39.

(17) Shirakawa, H.; Louis, E.J.; MacDiarmid, A.G.; Chiang, C.K.; Heeger, A.J., Synthesis of electrically conducting organic polymers: halogen derivatives of polyacetylene, (CH). *Journal of the Chemical Society, Chemical Communications* **1977**, (16), 578-580.

(18) Chiang, C.K.; Fincher, C.R.; Park, Y.W.; Heeger, A.J.; Shirakawa, H.; Louis, E.J.; Gau, S.C.; MacDiarmid, A.G., Electrical Conductivity in Doped Polyacetylene. *Physical Review Letters* **1977,** *39*, (17), 1098-1101.

(19) Coropceanu, V.; Li, H.; Winget, P.; Zhu, L.; Brédas, J.-L., Electronic-Structure Theory of Organic Semiconductors: Charge-Transport Parameters and Metal/Organic Interfaces. *Annual Review of Materials Research* **2013,** *43*, (1), 63-87.

(20) Roncali, J., Conjugated poly(thiophenes): synthesis, functionalization, and applications. *Chemical Reviews* **1992,** *92*, (4), 711-738.

(21) Smestad, G.P.; Krebs, F.C.; Lampert, C.M.; Granqvist, C.G.; Chopra, K.; Mathew, X.; Takakura, H., Reporting solar cell efficiencies in solar energy materials and solar cells. *Solar Energy Materials and Solar Cells* **2008,** *92*, (4), 371-373.

(22) Brabec, C.J.; Cravino, A.; Meissner, D.; Sariciftci, N.S.; Fromherz, T.; Rispens, M.T.; Sanchez, L.; Hummelen, J.C., Origin of the open circuit voltage of plastic solar cells. *Advanced Functional Materials* **2001,** *11*, (5), 374-380.

(23) Scharber, M.C.; Mühlbacher, D.; Koppe, M.; Denk, P.; Waldauf, C.; Heeger, A.J.; Brabec, C.J., Design rules for donors in bulk-heterojunction solar cells—Towards 10% energy-conversion efficiency. *Advanced Materials* **2006,** *18*, (6), 789-794.

(24) Veldman, D.; Meskers, S.C.J.; Janssen, R.A.J., The Energy of Charge-Transfer States in Electron Donor–Acceptor Blends: Insight into the Energy Losses in Organic Solar Cells. *Advanced Functional Materials* **2009,** *19*, (12), 1939-1948.

(25) Vandewal, K.; Tvingstedt, K.; Gadisa, A.; Inganas, O.; Manca, J.V., On the origin of the open-circuit voltage of polymer-fullerene solar cells. *Nat Mater* **2009,** *8*, (11), 904-909.

(26) Monestier, F.; Simon, J.-J.; Torchio, P.; Escoubas, L.; Flory, F.; Bailly, S.; de Bettignies, R.; Guillerez, S.; Defranoux, C., Modeling the short-circuit current density of polymer solar cells based on P3HT:PCBM blend. *Solar Energy Materials and Solar Cells* **2007,** *91*, (5), 405-410.

(27) Nelson, J.; Choulis, S.A.; Durrant, J.R., Charge recombination in polymer/fullerene photovoltaic devices. *Thin Solid Films* **2004,** *451–452*, (0), 508-514.

(28) Gupta, D.; Bag, M.; Narayan, K., Correlating reduced fill factor in polymer solar cells to contact effects. *Applied Physics Letters* **2008,** *92*, (9), 093301.

(29) Gupta, D.; Mukhopadhyay, S.; Narayan, K.S., Fill factor in organic solar cells. *Solar Energy Materials and Solar Cells* **2010,** *94*, (8), 1309-1313.

(30) Qi, B.; Wang, J., Fill factor in organic solar cells. *Physical Chemistry Chemical Physics* **2013,** *15*, (23), 8972-8982.

(31) Clarke, T.M.; Durrant, J.R., Charge Photogeneration in Organic Solar Cells. *Chemical Reviews* **2010,** *110*, (11), 6736-6767.

(32) Nunzi, J.-M., Organic photovoltaic materials and devices. *Comptes Rendus Physique* **2002,** *3*, (4), 523-542.

(33) Brédas, J.-L.; Cornil, J.; Heeger, A.J., The exciton binding energy in luminescent conjugated polymers. *Advanced Materials* **1996,** *8*, (5), 447-452.

(34) Forrest, S.R., The Limits to Organic Photovoltaic Cell Efficiency. *MRS Bulletin* **2005,** *30*, (01), 28-32.

(35) Antoniadis, H.; Hsieh, B.R.; Abkowitz, M.A.; Jenekhe, S.A.; Stolka, M., Photovoltaic and photoconductive properties of aluminum/poly(p-phenylene vinylene) interfaces. *Synthetic Metals* **1994,** *62*, (3), 265-271.

(36) Rieβ, W.; Karg, S.; Dyakonov, V.; Meier, M.; Schwoerer, M., Electroluminescence and photovoltaic effect in PPV Schottky diodes. *Journal of Luminescence* **1994,** *60–61*, (0), 906-911.

(37) Hoppe, H.; Sariciftci, N.S., Organic solar cells: An overview. *Journal of Materials Research* **2004,** *19*, (07), 1924-1945.

(38) Tang, C.W., Two-layer organic photovoltaic cell. *Applied Physics Letters* **1986,** *48*, (2), 183-185.

(39) Manoj, A.G.; Alagiriswamy, A.A.; Narayan, K.S., Photogenerated charge carrier transport in p-polymer n-polymer bilayer structures. *Journal of Applied Physics* **2003,** *94*, (6), 4088-4095.

(40) Yu, G.; Gao, J.; Hummelen, J.C.; Wudl, F.; Heeger, A.J., Polymer Photovoltaic Cells: Enhanced Efficiencies via a Network of Internal Donor-Acceptor Heterojunctions. *Science* **1995,** *270*, (5243), 1789-1791.

(41) Sariciftci, N.S.; Smilowitz, L.; Heeger, A.J.; Wudl, F., Photoinduced Electron Transfer from a Conducting Polymer to Buckminsterfullerene. *Science* **1992,** *258*, (5087), 1474-1476.

(42) Kraabel, B.; Lee, C.H.; McBranch, D.; Moses, D.; Sariciftci, N.S.; Heeger, A.J., Ultrafast photoinduced electron transfer in conducting polymer—buckminsterfullerene composites. *Chemical Physics Letters* **1993,** *213*, (3–4), 389-394.

(43) Mukhopadhyay, S.; Das, A.J.; Narayan, K., High Resolution Photocurrent Imaging of Bulk Heterojunction Solar Cells. *The Journal of Physical Chemistry Letters* **2013,** *4*, (1), 161-169.

(44) Mukhopadhyay, S.; Ramachandra, S.; Narayan, K., Direct observation of charge generating regions and transport pathways in bulk heterojunction solar cells with asymmetric electrodes using near field photocurrent microscopy. *The Journal of Physical Chemistry C* **2011,** *115*, (34), 17184-17189.

(45) Joshi, D.; Shivanna, R.; Narayan, K., Organic photovoltaics: key photophysical, device and design aspects. *Journal of Modern Optics* **2014,** *61*, (21), 1703-1713.

(46) Iwata, S.; Barber, J., Structure of photosystem II and molecular architecture of the oxygen-evolving centre. *Current Opinion in Structural Biology* **2004,** *14*, (4), 447-453.

(47) Gust, D.; Moore, T.A.; Moore, A.L., Mimicking Photosynthetic Solar Energy Transduction. *Accounts of Chemical Research* **2001,** *34*, (1), 40-48.

(48) Harriman, A., Unusually Slow Charge Recombination in Molecular Dyads. *Angewandte Chemie International Edition* **2004,** *43*, (38), 4985-4987.

(49) Wasielewski, M.R., Photoinduced electron transfer in supramolecular systems for artificial photosynthesis. *Chemical Reviews* **1992,** *92*, (3), 435-461.

(50) Wasielewski, M.R., Energy, Charge, and Spin Transport in Molecules and Self-Assembled Nanostructures Inspired by Photosynthesis. *The Journal of Organic Chemistry* **2006,** *71*, (14), 5051-5066.

(51) Markov, D.E.; Amsterdam, E.; Blom, P.W.M.; Sieval, A.B.; Hummelen, J.C., Accurate Measurement of the Exciton Diffusion Length in a Conjugated Polymer Using a Heterostructure with a Side-Chain Cross-Linked Fullerene Layer. *The Journal of Physical Chemistry A* **2005,** *109*, (24), 5266-5274.

(52) Österbacka, R.; Wohlgenannt, M.; Shkunov, M.; Chinn, D.; Vardeny, Z.V., Excitons, polarons, and laser action in poly(p-phenylene vinylene) films. *The Journal of Chemical Physics* **2003,** *118*, (19), 8905-8916.

(53) Scully, S.R.; McGehee, M.D., Effects of optical interference and energy transfer on exciton diffusion length measurements in organic semiconductors. *Journal of Applied Physics* **2006,** *100*, (3), 034907.

(54) Scheblykin, I.G.; Yartsev, A.; Pullerits, T.; Gulbinas, V.; Sundström, V., Excited State and Charge Photogeneration Dynamics in Conjugated Polymers. *The Journal of Physical Chemistry B* **2007,** *111*, (23), 6303-6321.

(55) Janssen, R.A.J.; Smilowitz, L.; Sariciftci, N.S.; Moses, D., Triplet-state photoexcitations of oligothiophene films and solutions. *The Journal of Chemical Physics* **1994,** *101*, (3), 1787-1798.

(56) Chosrovian, H.; Rentsch, S.; Grebner, D.; Dahm, D.U.; Birckner, E.; Naarmann, H., Time-resolved fluorescence studies on thiophene oligomers in solution. *Synthetic Metals* **1993,** *60*, (1), 23-26.

(57) Sirringhaus, H.; Brown, P.J.; Friend, R.H.; Nielsen, M.M.; Bechgaard, K.; Langeveld-Voss, B.M.W.; Spiering, A.J.H.; Janssen, R.A.J.; Meijer, E.W.; Herwig, P., et al., Two-dimensional charge transport in self-organized, high-mobility conjugated polymers. *Nature* **1999,** *401*, (6754), 685-688.

(58) Chen, T.-A.; Wu, X.; Rieke, R.D., Regiocontrolled Synthesis of Poly(3-alkylthiophenes) Mediated by Rieke Zinc: Their Characterization and Solid-State Properties. *Journal of the American Chemical Society* **1995,** *117*, (1), 233-244.

(59) Jiang, X.M.; Österbacka, R.; Korovyanko, O.; An, C.P.; Horovitz, B.; Janssen, R.A.J.; Vardeny, Z.V., Spectroscopic Studies of Photoexcitations in Regioregular and Regiorandom Polythiophene Films. *Advanced Functional Materials* **2002,** *12*, (9), 587-597.

(60) Graham, S.C.; Bradley, D.D.C.; Friend, R.H.; Spangler, C., Raman and photoluminescence spectra of PPV oligomers. *Synthetic Metals* **1991,** *41*, (3), 1277-1280.

(61) Kohler, A.; dos Santos, D.A.; Beljonne, D.; Shuai, Z.; Bredas, J.L.; Holmes, A.B.; Kraus, A.; Mullen, K.; Friend, R.H., Charge separation in localized and delocalized electronic states in polymeric semiconductors. *Nature* **1998,** *392*, (6679), 903-906.

(62) Clarke, T.M.; Gordon, K.C.; Officer, D.L.; Grant, D.K., The effect of oxidation on the structure of styryl-substituted sexithiophenes: A resonance Raman

spectroscopy and density functional theory study. *The Journal of Chemical Physics* **2006,** *124*, (16), 164501.

(63) Banerji, N.; Cowan, S.; Vauthey, E.; Heeger, A.J., Ultrafast Relaxation of the Poly(3-hexylthiophene) Emission Spectrum. *The Journal of Physical Chemistry C* **2011,** *115*, (19), 9726-9739.

(64) Kee, T.W., Femtosecond Pump–Push–Probe and Pump–Dump–Probe Spectroscopy of Conjugated Polymers: New Insight and Opportunities. *The Journal of Physical Chemistry Letters* **2014,** *5*, (18), 3231-3240.

(65) Dai, D.C.; Monkman, A.P., Femtosecond hot-exciton emission in a ladder-type $\ensuremath{\pi}$-conjugated rigid-polymer nanowire. *Physical Review B* **2013,** *87*, (4), 045308.

(66) Arkhipov, V.I.; Emelianova, E.V.; Bässler, H., Hot Exciton Dissociation in a Conjugated Polymer. *Physical Review Letters* **1999,** *82*, (6), 1321-1324.

(67) Arkhipov, V.I.; Emelianova, E.V.; Barth, S.; Bässler, H., Ultrafast on-chain dissociation of hot excitons in conjugated polymers. *Physical Review B* **2000,** *61*, (12), 8207-8214.

(68) Basko, D.M.; Conwell, E.M., Hot exciton dissociation in conjugated polymers. *Physical Review B* **2002,** *66*, (15), 155210.

(69) Lüer, L.; Egelhaaf, H.J.; Oelkrug, D.; Cerullo, G.; Lanzani, G.; Huisman, B.H.; de Leeuw, D., Oxygen-induced quenching of photoexcited states in polythiophene films. *Organic Electronics* **2004,** *5*, (1–3), 83-89.

(70) Kroeze, J.E.; Savenije, T.J.; Vermeulen, M.J.W.; Warman, J.M., Contactless Determination of the Photoconductivity Action Spectrum, Exciton Diffusion Length, and Charge Separation Efficiency in Polythiophene-Sensitized TiO2 Bilayers. *The Journal of Physical Chemistry B* **2003,** *107*, (31), 7696-7705.

(71) Marcus, R.A., On the Theory of Oxidation-Reduction Reactions Involving Electron Transfer. I. *The Journal of Chemical Physics* **1956,** *24*, (5), 966-978.

(72) Brédas, J.L.; Beljonne, D.; Cornil, J.; Calbert, J.P.; Shuai, Z.; Silbey, R., Electronic structure of π-conjugated oligomers and polymers: a quantum–chemical approach to transport properties. *Synthetic Metals* **2001,** *125*, (1), 107-116.

(73) Petrella, A.; Cremer, J.; De Cola, L.; Bäuerle, P.; Williams, R.M., Charge Transfer Processes in Conjugated Triarylamine−Oligothiophene−Perylenemonoimide Dendrimers. *The Journal of Physical Chemistry A* **2005,** *109*, (51), 11687-11695.

(74) Piotrowiak, P., Photoinduced electron transfer in molecular systems: recent developments. *Chemical Society Reviews* **1999,** *28*, (2), 143-150.

(75) Closs, G.L.; Calcaterra, L.T.; Green, N.J.; Penfield, K.W.; Miller, J.R., Distance, stereoelectronic effects, and the Marcus inverted region in intramolecular electron transfer in organic radical anions. *The Journal of Physical Chemistry* **1986,** *90*, (16), 3673-3683.

(76) Schmickler, W., *Interfacial Electrochemistry*; Editor Ed.^Eds.; Oxford University Press: Oxford, 1996.

(77) Onsager, L., Initial Recombination of Ions. *Physical Review* **1938,** *54*, (8), 554-557.

(78) Tachiya, M., Breakdown of the Onsager theory of geminate ion recombination. *The Journal of Chemical Physics* **1988,** *89*, (11), 6929-6935.

(79) Mihailetchi, V.D.; Koster, L.J.A.; Blom, P.W.M.; Melzer, C.; de Boer, B.; van Duren, J.K.J.; Janssen, R.A.J., Compositional Dependence of the Performance of Poly(p-phenylene vinylene):Methanofullerene Bulk-Heterojunction Solar Cells. *Advanced Functional Materials* **2005,** *15*, (5), 795-801.

(80) Mihailetchi, V.D.; Koster, L.J.A.; Hummelen, J.C.; Blom, P.W.M., Photocurrent Generation in Polymer-Fullerene Bulk Heterojunctions. *Physical Review Letters* **2004,** *93*, (21), 216601.

(81) Singh, J.; Baessler, H., Solution of the Onsager Ion Recombination Model in One Dimension. *physica status solidi (b)* **1974,** *63*, (1), 425-430.

(82) Braun, C.L., Electric field assisted dissociation of charge transfer states as a mechanism of photocarrier production. *The Journal of Chemical Physics* **1984,** *80*, (9), 4157-4161.

(83) Onsager, L., Deviations from Ohm's Law in Weak Electrolytes. *The Journal of Chemical Physics* **1934,** *2*, (9), 599-615.

(84) Barth, S.; Hertel, D.; Tak, Y.H.; Bässler, H.; Hörhold, H.H., Geminate pair dissociation in random organic systems. *Chemical Physics Letters* **1997,** *274*, (1–3), 165-170.

(85) Arkhipov, V.I.; Heremans, P.; Bässler, H., Why is exciton dissociation so efficient at the interface between a conjugated polymer and an electron acceptor? *Applied Physics Letters* **2003,** *82*, (25), 4605-4607.

(86) Peumans, P.; Forrest, S.R., Separation of geminate charge-pairs at donor–acceptor interfaces in disordered solids. *Chemical Physics Letters* **2004,** *398*, (1–3), 27-31.

(87) Gélinas, S.; Rao, A.; Kumar, A.; Smith, S.L.; Chin, A.W.; Clark, J.; van der Poll, T.S.; Bazan, G.C.; Friend, R.H., Ultrafast Long-Range Charge Separation in Organic Semiconductor Photovoltaic Diodes. *Science* **2014,** *343*, (6170), 512-516.

(88) Méndez, H.; Heimel, G.; Opitz, A.; Sauer, K.; Barkowski, P.; Oehzelt, M.; Soeda, J.; Okamoto, T.; Takeya, J.; Arlin, J.-B., et al., Doping of Organic Semiconductors: Impact of Dopant Strength and Electronic Coupling. *Angewandte Chemie International Edition* **2013,** *52*, (30), 7751-7755.

(89) Goris, L.; Haenen, K.; Nesládek, M.; Wagner, P.; Vanderzande, D.; De Schepper, L.; D'haen, J.; Lutsen, L.; Manca, J.V., Absorption phenomena in organic thin films for solar cell applications investigated by photothermal deflection spectroscopy. *Journal of Materials Science* **2005,** *40*, (6), 1413-1418.

(90) Benson-Smith, J.J.; Goris, L.; Vandewal, K.; Haenen, K.; Manca, J.V.; Vanderzande, D.; Bradley, D.D.C.; Nelson, J., Formation of a Ground-State Charge-Transfer Complex in Polyfluorene//[6,6]-Phenyl-C61 Butyric Acid Methyl Ester (PCBM) Blend Films and Its Role in the Function of Polymer/PCBM Solar Cells. *Advanced Functional Materials* **2007,** *17*, (3), 451-457.

(91) Goris, L.; Poruba, A.; Hod'ákova, L.; Vaněček, M.; Haenen, K.; Nesládek, M.; Wagner, P.; Vanderzande, D.; De Schepper, L.; Manca, J.V., Observation of the subgap optical absorption in polymer-fullerene blend solar cells. *Applied Physics Letters* **2006,** *88*, (5), 052113.

(92) Ko, S.; Hoke, E.T.; Pandey, L.; Hong, S.; Mondal, R.; Risko, C.; Yi, Y.; Noriega, R.; McGehee, M.D.; Brédas, J.-L., et al., Controlled Conjugated Backbone Twisting for an Increased Open-Circuit Voltage while Having a High Short-Circuit Current in Poly(hexylthiophene) Derivatives. *Journal of the American Chemical Society* **2012,** *134*, (11), 5222-5232.

(93) Vandewal, K.; Gadisa, A.; Oosterbaan, W.D.; Bertho, S.; Banishoeib, F.; Van Severen, I.; Lutsen, L.; Cleij, T.J.; Vanderzande, D.; Manca, J.V., The Relation Between Open-Circuit Voltage and the Onset of Photocurrent Generation by Charge-Transfer Absorption in Polymer : Fullerene Bulk Heterojunction Solar Cells. *Advanced Functional Materials* **2008,** *18*, (14), 2064-2070.

(94) Hoke, E.T.; Vandewal, K.; Bartelt, J.A.; Mateker, W.R.; Douglas, J.D.; Noriega, R.; Graham, K.R.; Fréchet, J.M.J.; Salleo, A.; McGehee, M.D., Recombination in Polymer:Fullerene Solar Cells with Open-Circuit Voltages Approaching and Exceeding 1.0 V. *Advanced Energy Materials* **2013,** *3*, (2), 220-230.

(95) Lee, J.; Vandewal, K.; Yost, S.R.; Bahlke, M.E.; Goris, L.; Baldo, M.A.; Manca, J.V.; Voorhis, T.V., Charge transfer state versus hot exciton dissociation in polymer−fullerene blended solar cells. *Journal of the American Chemical Society* **2010,** *132*, (34), 11878-11880.

(96) Scharber, M.C.; Lungenschmied, C.; Egelhaaf, H.-J.; Matt, G.; Bednorz, M.; Fromherz, T.; Gao, J.; Jarzab, D.; Loi, M.A., Charge transfer excitons in low band gap polymer based solar cells and the role of processing additives. *Energy & Environmental Science* **2011,** *4*, (12), 5077-5083.

(97) Loi, M.A.; Toffanin, S.; Muccini, M.; Forster, M.; Scherf, U.; Scharber, M., Charge Transfer Excitons in Bulk Heterojunctions of a Polyfluorene Copolymer and a Fullerene Derivative. *Advanced Functional Materials* **2007,** *17*, (13), 2111-2116.

(98) Zhou, Y.; Tvingstedt, K.; Zhang, F.; Du, C.; Ni, W.-X.; Andersson, M.R.; Inganäs, O., Observation of a Charge Transfer State in Low-Bandgap Polymer/Fullerene Blend Systems by Photoluminescence and Electroluminescence Studies. *Advanced Functional Materials* **2009,** *19*, (20), 3293-3299.

(99) Tvingstedt, K.; Vandewal, K.; Gadisa, A.; Zhang, F.; Manca, J.; Inganäs, O., Electroluminescence from Charge Transfer States in Polymer Solar Cells. *Journal of the American Chemical Society* **2009,** *131*, (33), 11819-11824.

(100) Veldman, D.; İpek, Ö.; Meskers, S.C.J.; Sweelssen, J.; Koetse, M.M.; Veenstra, S.C.; Kroon, J.M.; Bavel, S.S.v.; Loos, J.; Janssen, R.A.J., Compositional and Electric Field Dependence of the Dissociation of Charge Transfer Excitons in Alternating Polyfluorene Copolymer/Fullerene Blends. *Journal of the American Chemical Society* **2008,** *130*, (24), 7721-7735.

(101) Kim, H.; Kim, J.Y.; Park, S.H.; Lee, K.; Jin, Y.; Kim, J.; Suh, H., Electroluminescence in polymer-fullerene photovoltaic cells. *Applied Physics Letters* **2005,** *86*, (18), 183502.

(102) Tvingstedt, K.; Vandewal, K.; Zhang, F.; Inganäs, O., On the Dissociation Efficiency of Charge Transfer Excitons and Frenkel Excitons in Organic Solar Cells: A Luminescence Quenching Study. *The Journal of Physical Chemistry C* **2010,** *114*, (49), 21824-21832.

(103) Faist, M.A.; Kirchartz, T.; Gong, W.; Ashraf, R.S.; McCulloch, I.; de Mello, J.C.; Ekins-Daukes, N.J.; Bradley, D.D.C.; Nelson, J., Competition between the Charge Transfer State and the Singlet States of Donor or Acceptor Limiting the Efficiency in Polymer:Fullerene Solar Cells. *Journal of the American Chemical Society* **2012,** *134*, (1), 685-692.

(104) Brabec, C.J.; Zerza, G.; Cerullo, G.; De Silvestri, S.; Luzzati, S.; Hummelen, J.C.; Sariciftci, S., Tracing photoinduced electron transfer process in conjugated polymer/fullerene bulk heterojunctions in real time. *Chemical Physics Letters* **2001,** *340*, (3–4), 232-236.

(105) Hwang, I.W.; Soci, C.; Moses, D.; Zhu, Z.; Waller, D.; Gaudiana, R.; Brabec, C.J.; Heeger, A.J., Ultrafast Electron Transfer and Decay Dynamics in a Small Band Gap Bulk Heterojunction Material. *Advanced Materials* **2007,** *19*, (17), 2307-2312.

(106) Hwang, I.-W.; Moses, D.; Heeger, A.J., Photoinduced Carrier Generation in P3HT/PCBM Bulk Heterojunction Materials. *The Journal of Physical Chemistry C* **2008,** *112*, (11), 4350-4354.

(107) Tong, M.; Coates, N.E.; Moses, D.; Heeger, A.J.; Beaupré, S.; Leclerc, M., Charge carrier photogeneration and decay dynamics in the poly(2,7-carbazole) copolymer PCDTBT and in bulk heterojunction composites with ${\text{PC}}_{70}\text{BM}$. *Physical Review B* **2010,** *81*, (12), 125210.

(108) Guo, J.; Ohkita, H.; Benten, H.; Ito, S., Charge Generation and Recombination Dynamics in Poly(3-hexylthiophene)/Fullerene Blend Films with Different Regioregularities and Morphologies. *Journal of the American Chemical Society* **2010,** *132*, (17), 6154-6164.

(109) Guo, J.; Ohkita, H.; Benten, H.; Ito, S., Near-IR Femtosecond Transient Absorption Spectroscopy of Ultrafast Polaron and Triplet Exciton Formation in Polythiophene Films with Different Regioregularities. *Journal of the American Chemical Society* **2009,** *131*, (46), 16869-16880.

(110) Marsh, R.A.; Hodgkiss, J.M.; Albert-Seifried, S.; Friend, R.H., Effect of Annealing on P3HT:PCBM Charge Transfer and Nanoscale Morphology Probed by Ultrafast Spectroscopy. *Nano Letters* **2010,** *10*, (3), 923-930.

(111) De, S.; Kesti, T.; Maiti, M.; Zhang, F.; Inganäs, O.; Yartsev, A.; Pascher, T.; Sundström, V., Exciton dynamics in alternating polyfluorene/fullerene blends. *Chemical Physics* **2008,** *350*, (1–3), 14-22.

(112) Pal, S.K.; Kesti, T.; Maiti, M.; Zhang, F.; Inganäs, O.; Hellström, S.; Andersson, M.R.; Oswald, F.; Langa, F.; Österman, T., et al., Geminate Charge Recombination in Polymer/Fullerene Bulk Heterojunction Films and Implications for Solar Cell Function. *Journal of the American Chemical Society* **2010,** *132*, (35), 12440-12451.

(113) Howard, I.A.; Mauer, R.; Meister, M.; Laquai, F., Effect of Morphology on Ultrafast Free Carrier Generation in Polythiophene:Fullerene Organic Solar Cells. *Journal of the American Chemical Society* **2010,** *132*, (42), 14866-14876.

(114) Howard, I.A.; Laquai, F., Optical Probes of Charge Generation and Recombination in Bulk Heterojunction Organic Solar Cells. *Macromolecular Chemistry and Physics* **2010,** *211*, (19), 2063-2070.

(115) Grancini, G.; Maiuri, M.; Fazzi, D.; Petrozza, A.; Egelhaaf, H.J.; Brida, D.; Cerullo, G.; Lanzani, G., Hot exciton dissociation in polymer solar cells. *Nat Mater* **2013,** *12*, (1), 29-33.

(116) Parkinson, P.; Lloyd-Hughes, J.; Johnston, M.B.; Herz, L.M., Efficient generation of charges via below-gap photoexcitation of polymer-fullerene blend films investigated by terahertz spectroscopy. *Physical Review B* **2008,** *78*, (11), 115321.

(117) Ohkita, H.; Cook, S.; Astuti, Y.; Duffy, W.; Tierney, S.; Zhang, W.; Heeney, M.; McCulloch, I.; Nelson, J.; Bradley, D.D.C., et al., Charge Carrier Formation in Polythiophene/Fullerene Blend Films Studied by Transient Absorption Spectroscopy. *Journal of the American Chemical Society* **2008,** *130*, (10), 3030-3042.

(118) Shoaee, S.; An, Z.; Zhang, X.; Barlow, S.; Marder, S.R.; Duffy, W.; Heeney, M.; McCulloch, I.; Durrant, J.R., Charge photogeneration in polythiophene-perylene diimide blend films. *Chemical Communications* **2009**, (36), 5445-5447.

(119) Drori, T.; Sheng, C.X.; Ndobe, A.; Singh, S.; Holt, J.; Vardeny, Z.V., Below-Gap Excitation of $$\pi${}$-Conjugated Polymer-Fullerene Blends: Implications for Bulk Organic Heterojunction Solar Cells. *Physical Review Letters* **2008,** *101*, (3), 037401.

(120) Vandewal, K.; Albrecht, S.; Hoke, E.T.; Graham, K.R.; Widmer, J.; Douglas, J.D.; Schubert, M.; Mateker, W.R.; Bloking, J.T.; Burkhard, G.F., et al., Efficient charge generation by relaxed charge-transfer states at organic interfaces. *Nat Mater* **2014,** *13*, (1), 63-68.

(121) Proctor, C.M.; Kuik, M.; Nguyen, T.-Q., Charge carrier recombination in organic solar cells. *Progress in Polymer Science* **2013,** *38*, (12), 1941-1960.

(122) Cowan, S.R.; Banerji, N.; Leong, W.L.; Heeger, A.J., Charge Formation, Recombination, and Sweep-Out Dynamics in Organic Solar Cells. *Advanced Functional Materials* **2012,** *22*, (6), 1116-1128.

(123) Deibel, C.; Wagenpfahl, A.; Dyakonov, V., Influence of charge carrier mobility on the performance of organic solar cells. *physica status solidi (RRL) – Rapid Research Letters* **2008,** *2*, (4), 175-177.

(124) Pivrikas, A.; Sariciftci, N.S.; Juška, G.; Österbacka, R., A review of charge transport and recombination in polymer/fullerene organic solar cells. *Progress in Photovoltaics: Research and Applications* **2007,** *15*, (8), 677-696.

(125) Shockley, W.; Read, W.T., Statistics of the recombinations of holes and electrons. *Physical Review* **1952,** *87*, (5), 835-842.

(126) Meskers, S.C.J.; van Hal, P.A.; Spiering, A.J.H.; Hummelen, J.C.; van der Meer, A.F.G.; Janssen, R.A.J., Time-resolved infrared-absorption study of photoinduced charge transfer in a polythiophene-methanofullerene composite film. *Physical Review B* **2000,** *61*, (15), 9917-9920.

(127) Gulbinas, V.; Hertel, D.; Yartsev, A.; Sundström, V., Charge carrier photogeneration and recombination in ladder-type poly(\textit{para} -phenylene): Interplay between impurities and external electric field. *Physical Review B* **2007,** *76*, (23), 235203.

(128) Brédas, J.-L.; Norton, J.E.; Cornil, J.; Coropceanu, V., Molecular Understanding of Organic Solar Cells: The Challenges. *Accounts of Chemical Research* **2009,** *42*, (11), 1691-1699.

(129) Thompson, B.C.; Fréchet, J.M.J., Polymer–Fullerene Composite Solar Cells. *Angewandte Chemie International Edition* **2008,** *47*, (1), 58-77.

(130) Dennler, G.; Scharber, M.C.; Brabec, C.J., Polymer-Fullerene Bulk-Heterojunction Solar Cells. *Advanced Materials* **2009,** *21*, (13), 1323-1338.

(131) Kroon, R.; Lenes, M.; Hummelen, J.C.; Blom, P.W.M.; de Boer, B., Small Bandgap Polymers for Organic Solar Cells (Polymer Material Development in the Last 5 Years). *Polymer Reviews* **2008,** *48*, (3), 531-582.

(132) Brédas, J.-L.; Beljonne, D.; Coropceanu, V.; Cornil, J., Charge-Transfer and Energy-Transfer Processes in π-Conjugated Oligomers and Polymers: A Molecular Picture. *Chemical Reviews* **2004,** *104*, (11), 4971-5004.

(133) Hoppe, H.; Sariciftci, N.S., Morphology of polymer/fullerene bulk heterojunction solar cells. *Journal of Materials Chemistry* **2006,** *16*, (1), 45-61.

(134) Rajaram, S.; Shivanna, R.; Kandappa, S.K.; Narayan, K.S., Nonplanar Perylene Diimides as Potential Alternatives to Fullerenes in Organic Solar Cells. *The Journal of Physical Chemistry Letters* **2012,** *3*, (17), 2405-2408.

(135) Shivanna, R.; Shoaee, S.; Dimitrov, S.; Kandappa, S.K.; Rajaram, S.; Durrant, J.R.; Narayan, K., Charge generation and transport in efficient organic bulk heterojunction solar cells with a perylene acceptor. *Energy & Environmental Science* **2014,** *7*, (1), 435-441.

(136) Ravichandran Shivanna, S.R., K S Narayan, Role of Charge transfer state in fullerene free organic solar cells. *submitted* **2015**.

(137) Shivanna, R.; Rajaram, S.; Narayan, K., Interface engineering for efficient fullerene-free organic solar cells. *Applied Physics Letters* **2015,** *106*, (12), 123301.

Chapter 2:

Materials and Methods

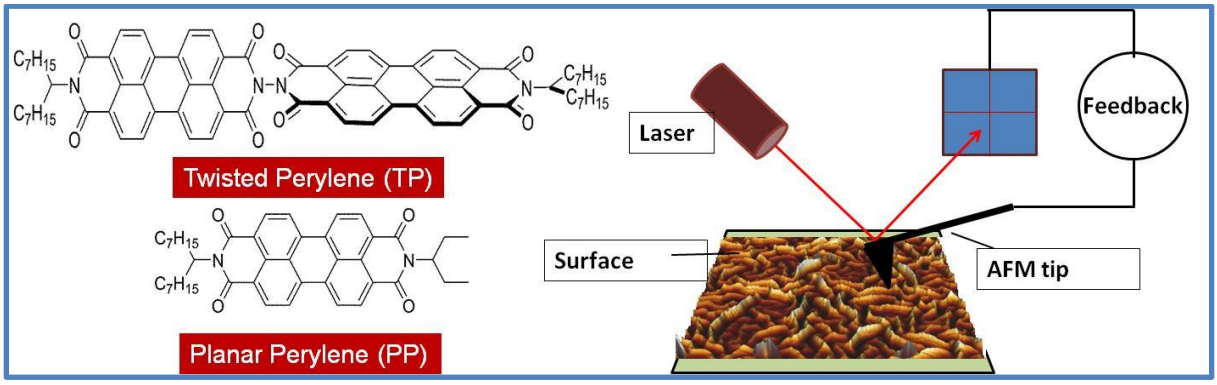

2 Materials and Methods

The power conversion efficiency of organic bulk heterojunction solar cells highly depends on selective choice of donor and acceptor molecules and their optimal processing conditions. Device architectures and fabrication procedures have huge impact on the performance parameters. The very high absorption coefficient (~10^3 times higher than Si (*1*, *2*)) and lower density (~ 2 times lower than Si (*3*, *4*)) of organic semiconductors ensure the least amount of materials is used in the devices. The solution processability of photo-active materials enables easy fabrication procedures in this technology.(*5-7*) First section of this chapter overviews the materials and device fabrication techniques used in the thesis. Subsequent sections discuss advanced characterization techniques utilized to probe the optoelectronic processes in these organic solar cells.

2.1 Materials - Organic Bulk heterojunction solar cells:

Organic bulk heterojunction solar cells typically consist of photo-active layer, charge selective interlayers (or buffer layers) and electrodes to extract photo-generated charges.(*8*) The photo-active layer is a heterojunction of donor and acceptor molecules formed by single-solution processing step. The sustained efforts in understanding and co-relating performance parameters to the molecular levels, have assisted chemists in designing and synthesizing materials specifically to achieve tailored interfaces and controlled morphology. These efforts have led to internal quantum efficiencies (IQEs) approaching 100% and fill factors exceeding 80 % (*9*, *10*). The structure, size, solubility and electronic levels of photo-active components are needed to optimize in order to enhance the efficacy of charge-generation, separation and extraction processes simultaneously.(*11*)

2.1.1 Donor and Acceptor Materials

The spectral overlap between the solar photon flux and absorption of organic semiconductors determines the charge generation efficiency. The most common donors of organic solar cells are polymers with an extended delocalized π-electron system, which is responsible for their semiconducting nature.(*12*) The widely used donor polymer is poly-3-hexylthiophene (P3HT, regioregular).(*13*) It has a bandgap of 2.1 eV, making it as a visible-range absorber (~300-600 nm).(*14*) Only 20 % of the solar photons is absorbed by the P3HT

based devices due to the poor matching of the absorption spectrum with the solar emission spectrum.(*15*) (In the thesis, P3HT is utilized as control polymer to compare with many photo-physical processes.) Therefore, to enhance the matching of the solar spectrum, the ideal situation is to design conjugated polymers with lower bandgaps. The two common approaches used for synthesizing lower band gap polymers are: conversion of aromatic moieties into quinoid structure along the polymer backbone (*16*, *17*) and alternating donor-acceptor copolymerization (*18-20*).

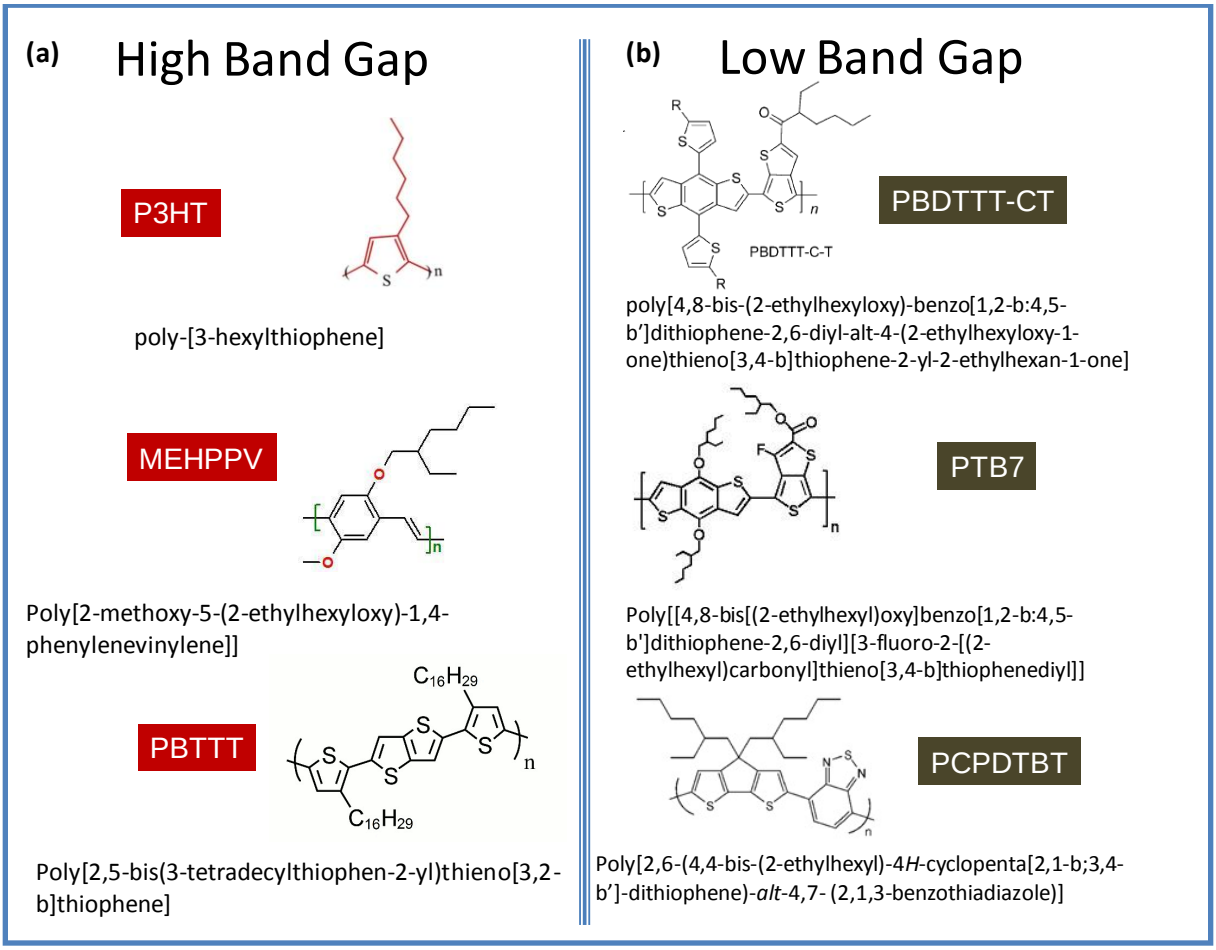

Figure 2.1: Structures of donor molecules. (a) High band gap molecules having the band gap above 2 eV. (b) low band gap molecules having band gap below 2 eV.

In the donor-acceptor co-polymer approach, the electron-rich monomers and electron-deficient monomers are fused alternately along the backbone of the polymer. The quinodal form is stabilized along the alternating structure of monomers due to the charge-separated resonance structure. This approach offers to tune individually the HOMO and LUMO level of the polymer because of their different locations on the polymer-backbone. It was shown that, the LUMO level is observed to be exclusively on the acceptor unit whereas the HOMO

level is more delocalized but predominantly observed on the donor unit.(*21*, *22*) The donor-acceptor co-polymer approach is the principal way to obtain efficient low bandgap polymers. In this thesis, the commercially available benzodithiophene co-polymer with thienothiophene polymer known as poly[4,8-bis-(2-ethylhexyloxy)-benzo[1,2-b:4,5-b']dithiophene-2,6-diyl-alt-4-(2-ethylhexyloxy-1-one)thieno[3,4-b]thiophene-2-yl)-2-ethylhexan-1-one] (PBDTTT-CT)(*23*) is used extensively to enhance the device efficiency of the fullerene-free organic solar cells. The absorption of this polymer extends to NIR (~800 nm).(*24-27*) The high band gap donor polymers (E_g > 2.0 eV) like P3HT, MEHPPV and PBTTT, and the low band gap donor polymers (E_g < 2.0 eV) are also utilized to study the photophysical processes in BHJ featuring fullerene-free acceptors.

Table 1: Electronic levels and band gap of the donor molecules.

Material	HOMO (eV)	LUMO (eV)	Band gap (E_g) (eV)
P3HT (*28*)	- 5.0	- 3.0	~2.0
PBTTT (*29*)	- 5.1	-3.1	~2.0
MEHPPV (*30*)	- 5.02	- 2.7	~2.3
PBDTTT-CT (*31*)	- 5.11	- 3.25	~1.58
PTB7 (*32*)	- 5.15	- 3.31	~1.65
PCPDTBT (*33*)	- 4.9	- 3.5	~1.46

Fullerene derivatives have been used as electron acceptors since the earliest reports on organic photovoltaics. Among these, [6, 6]-phenyl C61-butyric acid methyl ester ($PC_{60}BM$) (*34*) has been the used most widely, with its variant [6, 6]-phenyl C71-butyric acid methyl ester ($PC_{70}BM$) (*35*) showing enhanced optical absorption and device characteristics. Fullerene multiadducts such as indene-C_{60} bisadduct (ICBA) (*36*) have also yielded excellent results as electron acceptors. These materials show greater V_{oc} compared to conventional $PC_{60}BM$ and $PC_{70}BM$ due to higher LUMO level, resulting in high PCEs (*37*).

The monopoly of fullerene based materials as successful electron acceptors in BHJ organic solar cells are due to variety of reasons, importantly:

1. Ability to form a favorable nanoscale morphology forming continuous network with the donor polymers in the films.(*38*, *39*) Efficient charge transport directly depends on the interconnected network of donor:acceptor domains leading to an overall increased J_{sc} of the device.

2. Low-lying LUMO levels (typically ~ 3.8−4.2 eV) provide large driving energy for dissociation of donor singlet excitons during electron transfer process from $HOMO_D$ to $LUMO_A$ at the interface.(*19, 40*)
3. Ability to accept upto six electrons because of the spherical symmetry.(*41*) It is shown that the PCBM has 6 reduction potentials. This assists in multiple electron transfer from surrounding donor molecules to fullerene simultaneously at the interface.
4. Reversible reduction of fullerene molecules helps in the regeneration of fullerene back to ground state. This is critical in the longevity of the device under illumination.(*41*)
5. Ultra-fast three-dimensional charge transfer in femtosecond time scale.(*42, 43*)
6. High electron mobility, which is a prerequisite for efficient charge transport after the dissociation of bound charges.(*41*)

Despite the above advantages of fullerene derivative, there are important limitations such as low absorption coefficient and elaborate purification procedure.

Table 2: Electronic levels and band gap of the acceptor molecules.

Material	HOMO (eV)	LUMO (eV)	Band gap (E_g) (eV)
TP (*44*)	- 6.02	- 4.1	~2.0
PP (*45*)	- 6.0	- 4.1	~2.1
$PC_{60}BM$ (*46*)	- 6.1	- 4.3	~1.8
$PC_{70}BM$ (*46*)	- 6.1	- 4.3	~1.7

In this thesis, we introduced the soluble perylene based electron acceptors as potential alternatives to fullerenes.(*25*, *26*) These simple molecules could be fabricated at a fraction of the cost of fullerene-based acceptors. Perylenes have been used as highly fluorescent and stable dyes in industries for long time. The structures of electron donor polymers (both high band gap and low band gap) and electron acceptors used in this thesis are represented in Figure 2.1 and 2.2, also corresponding energy levels and the band-gaps are tabulated in the table 1 and 2.

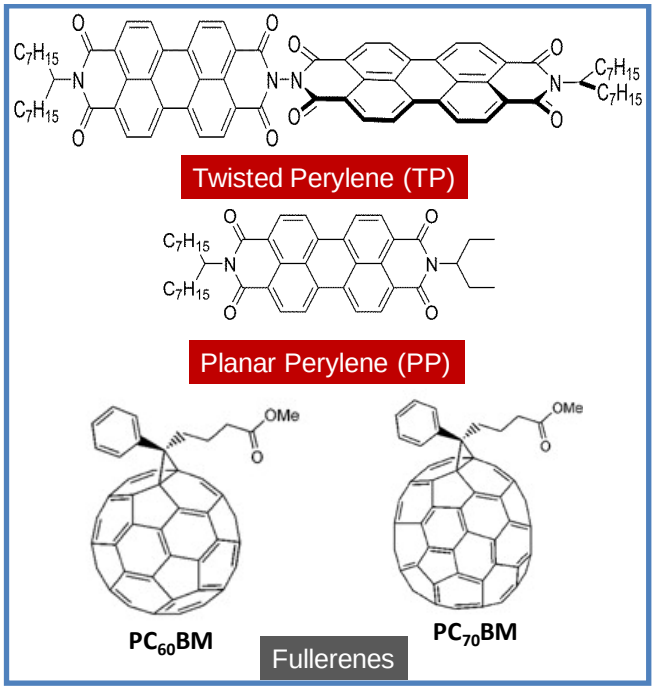

Figure 2.2: Structures of acceptor molecules.

2.1.2 Conducting electrodes and buffer layer materials

The photoactive materials are sandwiched between two metal electrodes of different work functions (ϕ_m). The intrinsic electric field is generated due to the offset in the work-function of the electrodes. This offset generates the potential gradient across the active layer. The generated external field drifts the photogenerated charges towards respective electrodes. The charges are then extracted at the active-layer: electrode interface. The power dissipation to the external load now depends only on the sheet resistance of these electrodes. In organic solar cells, one of the metal electrodes, either cathode or anode, should be transparent to light. Commonly used Transparent Conducting Oxides (TCO) in solar cell applications are Indium Tin Oxide (ITO) and Fluorine doped Tin Oxide (FTO) due to high electrical conductivity. The work function and conductivity of these TCOs mainly depends on the doping concentrations.(*47*) The choice of counter metal electrode depends upon the type of the charge needs to extract at the interface. To extract electrons, low work function electrodes like Al ($\phi_m \approx 4.3$ eV), Mg ($\phi_m \approx 3.7$ eV), Ca ($\phi_m \approx 2.8$ eV) or combination of them are used to match the LUMO level of the acceptor molecule. To extract holes, high work function electrodes like Au ($\phi_m \approx 5.1$ eV) or Ag ($\phi_m \approx 4.6$ eV) are used to match the HOMO level of the donor molecule. All these metal electrodes are thermally evaporated onto the photoactive layer using shadow mask technique at base pressure of 10^{-6} mbar.

Table 3: Work Functions of common electrodes.

Metal	Work function (ϕ_m) (*48*)
Al	≈ 4.1 eV
Mg	≈ 3.7 eV
Ca	≈ 2.8 eV
Au	≈ 5.1 eV
Ag	≈ 4.6 eV

The device geometric configurations of solar cells are classified based on the nature of TCO (cathode or anode) or light illumination direction. In the 'conventional or normal' configuration TCO acts as a hole extracting electrode (anode), and in the 'Inverted' configuration TCO acts as an electron extracting electrode (Figure 2.3). The inverted device geometry exhibit enhanced stability and solar cell performance and hence it is widely used in recent days.(*49*)

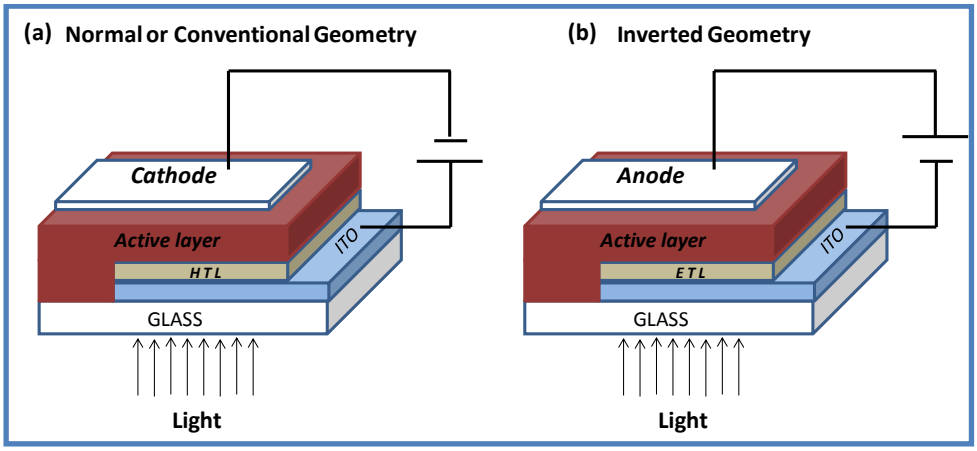

Figure 2.3: Normal and Inverted geometry of organic solar cells. In the normal geometry, light is illuminated from anode side, whereas in the inverted geometry light is illuminated from cathode side. Work functions of transparent conducting oxides are modified using additional buffer layers. Generally, ZnO, TiO2 etc were used to selectively extract electrons, and PEDOT:PSS, MoOx etc were used to selectively extract holes.

One of the important factors which determine the overall efficiency of solar cells is the efficiency of charge extraction at the active-layer: electrode interface. The charge extraction depends on the nature of contact (ohmic or non-ohmic) between the active layer and the electrode. In working devices, the interface is generally non-ohmic in nature due to the

surface roughness associated with the solution processing conditions of thin active layer, and mismatch in the work function of electrode and molecular electronic levels. The use of additional thin buffer layers (generally 1-10 nm for thermally evaporated and 10-50 nm for spin coated films) is shown to be effective in improving energy level alignment at the interface.(*50*) The commonly used electron buffer layers are TiO_2, ZnO, LiF etc.,(*51*) and hole buffer layers are PEDOT:PSS, MoO_x, V_2O_5 etc.(*51*) The sol gel based buffer layers (ZnO) often exhibit spontaneous nanostructures. We have utilized this property of sol-gel based ZnO to increase efficiency of electron extraction in the fullerene free solar cells.

2.2 Device fabrication:

The organic solar cells were fabricated in both normal and inverted geometries. The normal structure consists of heterojunction of ITO/PEDOT:PSS/Active-layer/LiF/Al. The PEDOT:PSS material acts as a hole transport layer and LiF was used as electron conducting layer. The patterned ITO-coated glass substrates were first cleaned with detergent, sonicated in water and a 1:1:1 mixture of acetone, chloroform, and isopropyl alcohol, and subsequently cleaned with RCA treatment; a mixture of hydrogen peroxide (H_2O_2), ammonium hydroxide (NH_4OH) and water (1:1:5 by volume) at 80 °C for 15 minutes. PEDOT:PSS was procured from Clevios™ or Byatron P and filtered using 0.4 µm Whatman™ filter paper before each coating. The filtered solution was spin coated on to cleaned ITO substrate at 2000 rpm for 60 s. The thin films of PEDOT:PSS were annealed at 100^0 C for 15 min. After cooling the substrate to room temperature, active layer was subsequently spin coated at 1000 rpm for 60 s inside the nitrogen filled glovebox. The concentration of active blend layer used was 12 mg/mL in anhydrous chlorobenzene solvent. Choice of the solvent is due to its high boiling point ~ 130 ^{0}C, which is suitable for spin coating technique. Annealing of active layer was selective with respect to donor:acceptor combination under study (which was carried out inside the glove box). For crystalline polymers like P3HT based BHJ, the annealing was carried out at 100 ^{0}C for 15 mins. Annealing enhanced the overall performance of these devices. For amorphous polymer like PBDTTT-CT based BHJ, the devices were fabricated without annealing. Annealing of these amorphous polymers lead to decreased device performance. The device fabrication was completed by thermal evaporation of electron transport layer LiF and then Al electrode sequentially at base pressure of 10^{-6} mbar. The area of the top electrodes depends on the mask used when evaporating metals. Generally devices with the area of 14 mm^2 were fabricated to calculate efficiency of solar cells.

The ZnO precursor containing zinc acetate dihydrate (314 mg), 2-methoxyethanol (3.14 mL), and ethanolamine (86 µL) was vigorously stirred at 50 °C for 8 h in air. It was then spin coated on to cleaned ITO substrates at 2000 rpm. The substrates were subsequently annealed at 250 °C for 30 min in air to obtain crystalline ZnO films. The ZnO layer thickness was in the ~ 20 - 30 nm range as measured using Dektak thickness profilometer.

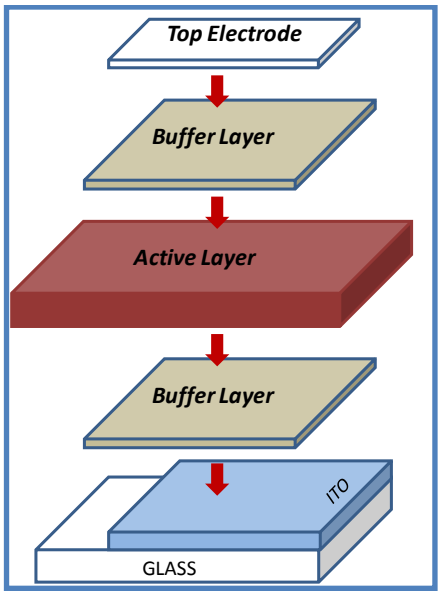

Figure 2.4: Fabrication of BHJ solar cells. Initially, selective buffer layers are coated on the ITO coated glass substrate. After annealing the buffer layer, the solution of active layer is spin coated on to the buffer layer coated ITO substrate in side nitrogen filled glove box. Finally, the counter buffer layer and electrode are thermally evaporated using shadow mask technique under base pressure of 10^{-6} mbar.

Similarly, the inverted geometry was fabricated with the heterojunction consist of ITO/ ZnO/Active layer/MoOx/Ag. Here, the sol-gel based ZnO films were deposited using spin coating method on top of ITO coated glass substrates. The ZnO precursor containing zinc acetate dihydrate (314 mg), 2-methoxyethanol (3.14 mL), and ethanolamine (86 µL) was vigorously stirred at 50 °C for 8 h in air. It was then spin coated on to cleaned ITO substrates at 2000 rpm. The substrates were subsequently annealed at 250 °C for 30 min in air to obtain crystalline ZnO films. The ZnO layer thickness was in the ~ 20 - 30 nm range as measured using Dektak thickness profilometer. After coating the active layer in inert atmosphere, device fabrication was completed by thermal evaporation of buffer layer MoOx and counter electrode Ag.([25](), [26]()) The schematic of the multilayer structure used in the fabrication of the device is depicted in the Figure 2.4. All the devices were fabricated using existing facility at JNCASR, Bangalore.

2.3 Characterization of organic solar cells:

2.3.1 J-V characteristics:

The performance parameters were determined using current density (J) – Voltage (V) characteristics of the solar cells. The measurements are carried out in the dark and under simulated sunlight illumination. To standardize the measurement of the power conversion efficiency of the cells, the input flux is calibrated to AM 1.5 G, 1 sun unit. This corresponds to air mass or atmosphere thickness of 1.5 and the sun is at the zenith angel of 48.2^0. The simulated light should also match spectrally with the described conditions. In the simulated light context, the photon flux of 100 mW/cm^2 from the xenon lamp with AM 1.5 filter at room temperature is considered to be standard 1 Sun illumination testing. The experimental setup used to measure J-V characteristics consists of Oriel SolAAA solar simulator with a uniform illumination across 2 x 2 inches area and external source meter Kiethley 2400 to measure J-V curve. LabVIEW^{TM} is used to automate instruments and acquire data remotely through the computer. During measurements, only active area is exposed to the light and all the other side of the devices were masked with the black tape. The active areas of the devices are measured by using calibrated optical microscope to avoid any inconsistency in measuring the accurate efficiency of the devices. All *J-V* characteristics were carried out using existing facility at JNCASR, Bangalore.

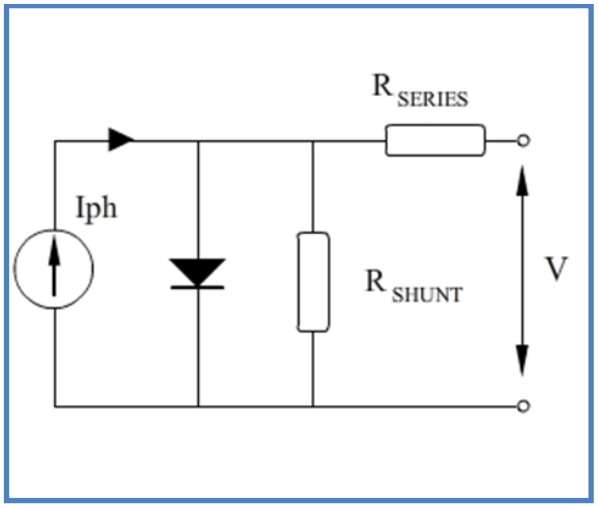

Figure 2.5: The Circuit model of the working solar cells is depicted in the right. The circuit consists of diode in parallel with additional current source, series resistance and parallel resistance (right).

The circuit model of working solar cells can be represented as the ideal diode with additional current source having parasitic resistances in series and parallel to the diode

(Figure 2.5).(*52*, *53*) The series resistance arises from the contact resistance between active layer and electrode interface, and the sheet resistance of the electrodes. The parallel resistance is due to the effect of shunt between the two electrodes. Under illumination, the current density relation can be obtained by modifying the Shockley diode equation as

$$J(V) = J_{ph} + J_0 \left[\exp\left(\frac{q(V - JR_s)}{nkT}\right) - 1\right] - \frac{V - JR_s}{R_p}$$

where, Jo is the reverse saturation current density, n is the ideality factor of the diode. Generally the 'n' value ranges between 1 and 2.

2.3.2 External quantum efficiency:

External Quantum Efficiency (EQE) also known as incident photon to current conversion efficiency (IPCE) is the ability of solar cells to convert incident photons to free charge carriers. It is defined as the fraction of photo-generated charges to incident photons. The wavelength dependence on the charge generation efficiency of the absorbing components of the BHJ can be quantified by this fraction as a function of wavelength. The relation between EQE and experimentally obtained parameters is given below.(*54*)

$$IPCE(\lambda) = EQE(\lambda) = \frac{n_{elec}}{n_{phot}} = \frac{I/e}{P/h\upsilon} = \frac{I}{P}\frac{hc}{e\lambda} = \frac{I}{P}\frac{1240}{\lambda(nm)}$$

where, n_{elec} and n_{phot} are the number of charges and photons respectively, '*I*' is externally measured current in A/m^2 and *P* is incident power in W/cm^2, λ is the wavelength, *h* is Planck's constant, *c* is the speed of light, and *e* is the elementary charge.

The short-circuit current density expected under a light source can be estimated from the EQE and the spectral irradiance of the light source by integrating the product of the EQE and the photon flux density. For the standard AM1.5 G spectrum, the calculation is given as,

$$J_{sc} = \int_0^\infty e \cdot EQE\,(\lambda) \cdot \left(\frac{\lambda}{hc}\right) \cdot E_\lambda^{AM1.5}(\lambda) \cdot d\lambda$$

where $E_\lambda^{AM1.5}(\lambda)$ is the AM 1.5 G spectrum. It is expected to have good correlation between the *Jsc* measured from J-V characteristics and J_{sc} estimated from the above equation. In organic solar cells, the J_{sc} typically vary non-linearly with the illumination intensity. This overestimate the J_{sc} value measured through EQE measurements. The main

cause for this overestimation is due to the low photon flux (≈ μW/cm^2) used in measuring EQE compare to 1 Sun (≈ 100 mw/cm^2) illumination when measuring light J-V.

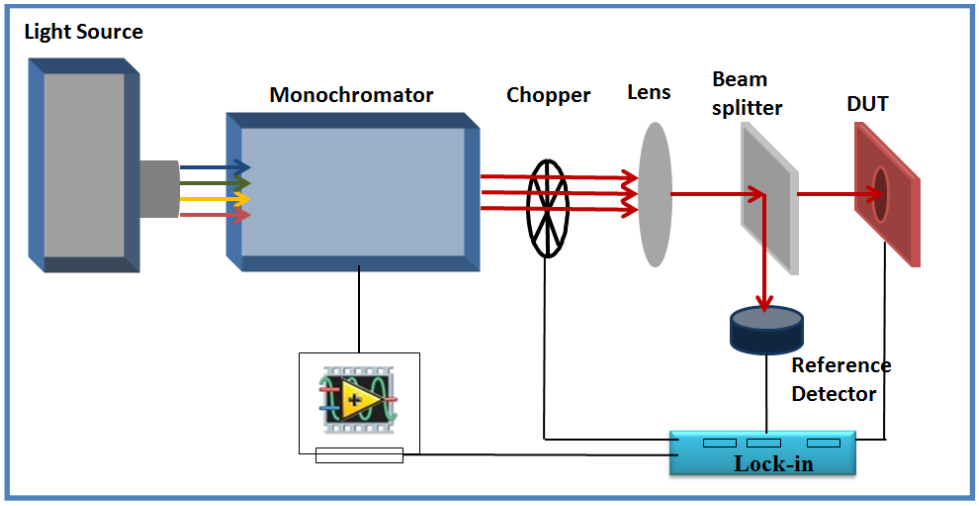

Figure 2.6: Schematic representation of EQE measurements setup. The light from tungsten-halogen bulb is passed through monochromator. The monochromatic light is modulated using optical chopper and then converged onto the sample using convex lens. A beam splitter and calibration detector is used to calculate the input power. The photoresponse from the solar cells is measured using lock-in amplifier as a function of wavelength.

The experimental setup used for EQE measurement is as shown in the figure 2.6. The broad white-light from the Tungsten-Halogen bulb (Zolix Instruments) was passed through the monochromator (Zolix Instruments). The monochrome light was modulated using optical chopper. The modulated light was then concentrated using convex lens to illuminate locally on to the device area. The photogenerated current from the devices was measured using Stanford Research System (SRS 830) lock-in amplifier. Calibrated Si solar cell From UDT Sensors was utilized to measure the absolute incident power (Figure 2.7 shows the responsivity of the Si detector). All the instruments were automated using LabVIEW^{TM} and the data were acquired remotely from the computer. Internal Quantum Efficiency (IQE) is defined as fraction of charges generated for absorbed photons, was measured by normalizing EQE with the absorption spectra of the donor acceptor blends.

For measuring CT-state photocurrent response, the intensity of illuminated monochrome light was increased by order of magnitude. For low-current measurements, the Current to voltage converting transimpedence pre-amplifier, Femto DLPCA 200, was connected in series with the device and the output was measured using SRS 830 lock-in amplifier. Both the EQE and CT-state photoresponse measurement setups were custom built at JNCASR, Bangalore.

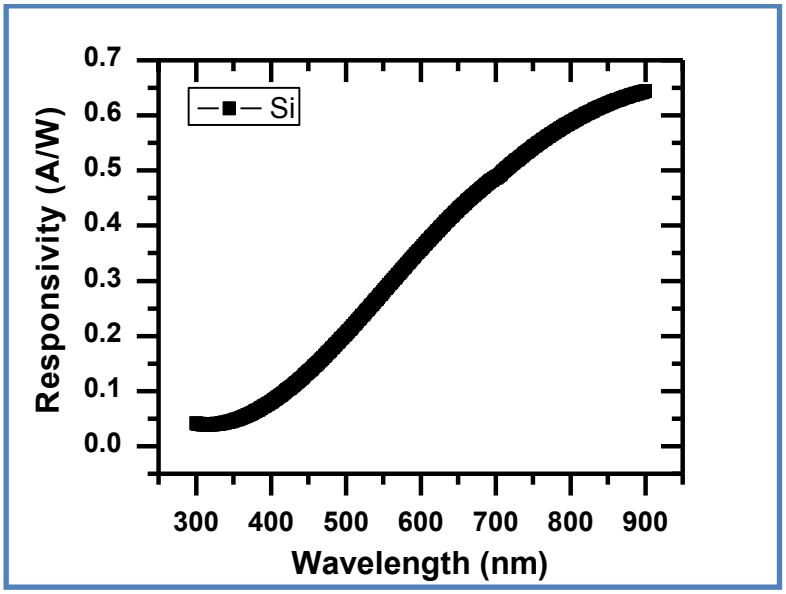

Figure 2.7: Responsivity of Si PIN detector (UDT sensors, Inc.) of device area 1 cm^2 is used to calibrate the input flux during EQE calculations.

2.4 Timescales involved in the organic bulk heterojunction solar cells:

Photophysical properties of donor:acceptor system are measured using both steady state and transient techniques. A series of photophysical processes is involved in ultimate generation of charges in the organic BHJ solar cells can be quantified utilizing transient techniques. Each of these processes is characterized by the life time of the quasi particles formed during the transitions. General picture of photo-generation of charges and their corresponding timescales are described in the following section (Figure 2.8).(*55*) At first, the photons are absorbed by the photoactive materials and form an excited state species. The absorption of light generally occurs at ultrafast timescales < 100 fs.(*56*) The excited –state species then vibrationally relaxes to singlet state exciton at a rapid timescale of < 100 fs.(*57, 58*) At this point of time, the singlet exciton can undergo two possible processes: fluorescence by radiative recombination with a typical life time in the range of ps-ns, or diffuse to the donor:acceptor interface to transfer the electron to the acceptor molecule. The exciton diffusion depends on molecular structure –order and phase purity of donor/acceptor domains in the BHJ. Hence time scale for exciton diffusion can be dispersive in nature (typically in the range of ps-100 ps). The diffusion lengths of the singlet excitons in the organic polymeric semiconductors are estimated to be 10-20 nm. The electron transfer

process at the donor: acceptor interface is quasi adiabatic in nature and occurs promptly at ultrafast time scales less than the experimental limits (< 100 fs).(*59*)

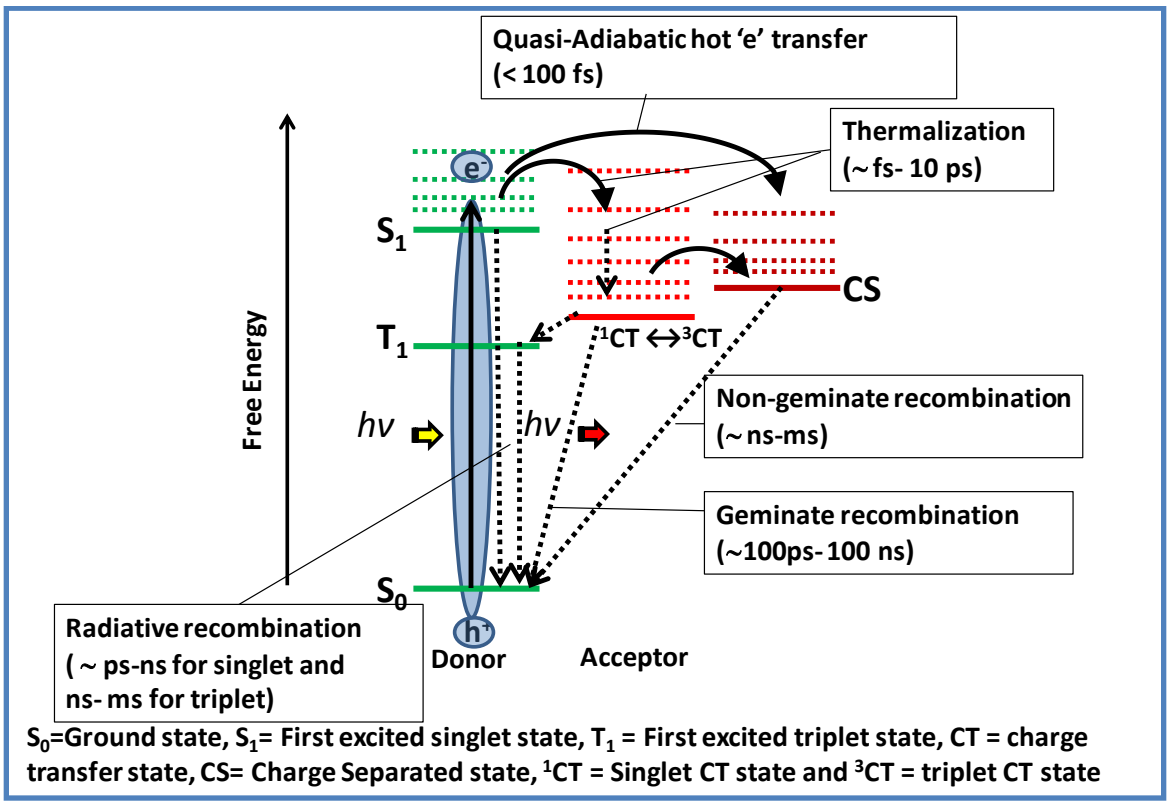

Figure 2.8: Timescales involved in the organic bulk heterojunction solar cells. Evolution of free charges from the photoexcitation occurs at various timescales. The figure depicts the different photophysical processes and associated transient lifetimes.

The electron transfer process creates bound electron-hole pair called as charge transfer (CT) state, in which electron is at acceptors' LUMO and hole is at donors' HOMO levels. The bound CT state can directly dissociate into free charges before thermally relaxing into CT –state manifolds. This process is known as hot electron transfer process which generally occurs at < 50 fs.(*60*) In hot electron transfer process, it is believed that the extra thermal energy assists in dissociation of bound CT state into free charges.(*60*) Otherwise the CT-state thermally relaxes into ground state CT at a time scale of fs-ps.(*61*) At this point, the thermally relaxed CT can undergo geminate recombination in which the electron on acceptors' LUMO combines with the original hole on the HOMO level of the donor molecules. The geminate recombination occurs in the range of ~ 100 ps- 100 ns time scale.(*59, 62, 63*) If the CT-state overcomes the geminate recombination process then it dissociates into free charges. The free charge then drifts towards the electrode through the intermixed network of donor and acceptor domain. During their motion, free charges

encounter opposite charges and it may bimolecularly recombine radiatively or non-radiatively. The bimolecular recombination is a trap limited process and hence the time scale involves a large range (ns-ms).(*59*) The efficient photo-generation of free charges sequence of above mentioned multiple steps. Hence the clear understanding of the dynamics of each process gives clear protocol for rational design of photoactive molecules.

2.5 Transient absorption spectroscopy (TAS):

As mentioned in the previous section, the photophysical processes in organic BHJ occur at various time and length scales. The dynamics of these processes can be probed using transient absorption spectroscopic techniques. The advent of ultrafast lasers opened new avenues to probe the dynamics in femtosecond timescales. In conjunction with steady state optical measurements, the transient techniques provide kinetics and energetics of the photo-physical processes such as exciton relaxation, charge generation, and recombination prevailing in the BHJ films. TAS technique involves radiating the sample with a short intense pulse of light (pump / excitation pulse) to excite the sample from ground state to excited state. Another pulse of light is passed through the sample with desired time delay to probe the generated excited species.(*64*) The experimental setup of TAS is shown in the Figure 2.9. The pump pulse will be monochromatic light for selective excitation of the sample and probe pulse will be supercontinuum white light to monitor the spectra of excited species. The delay between pump and probe pulses provide the dynamics of these excited species. In fs-TAS, the pump and probe pulses are produced from ultrafast laser (Ti:Sapphire) crystals with series of parametric amplifiers utilized to tune and shape the laser pulses. The delay between pump and probe pulses is generated by the translation stage with set of mirrors. In the case of µs-TAS, the ns laser pulses (generally produced from Nd:YAG lasers) are used. The time delay is obtained from the electronic circuits. In both the techniques, the transmission difference occurred with and without pump pulses are measured using external detectors. The data presented in the thesis were recorded from the existing fs-TAS and µs-TAS setup at Imperial College London, UK.

The experimental setup consist of a nanosecond response silicon photodiode (Fast optical transient preamplifier, ~5MW, Costronics Electronics) for $\lambda \approx$ 400- 1000 nm regime and InGaAs detector for $\lambda \approx$ 900- 1700 nm regime, a Nd-YAG laser (Ultra Nd:YAG BigSkyLaser Company) as the excitation source (532nm, FWHM < 6ns) and a 75W Xenon arc lamp (200-2000nm) or laser diode (Thorlabs TLCDM9, controlled by ITC502 laser diode

combi controller) as the probe source coupled to a single PTI model 101 monochromator after the sample. For tunable pumping, non-linear crystal coupled laser was utilized to pump in the range of 350 -700 nm. A photodetector with a fast response photodiode was used in order to obtain earlier time resolution transient decays (~50ns). The use of a fast photodiode allowed for an increase in the distance between the sample and photodiode so that scatter and emission noise were reduced. This required the use of a probe beam that was more coherent over long distances and so a laser diode was used with a probe wavelength of 980nm (~50mW, 24°C, 106mA). The system response was typically 50ns with a threshold RC high pass coupling of 10 microseconds. Long pass filters between 680 - 1000nm were used throughout the system to reduce the laser scatter and noise. The signal was collected using an oscilloscope (Tektronix, TDS220) and the data collected on to the computer using Tekave acquisition software.

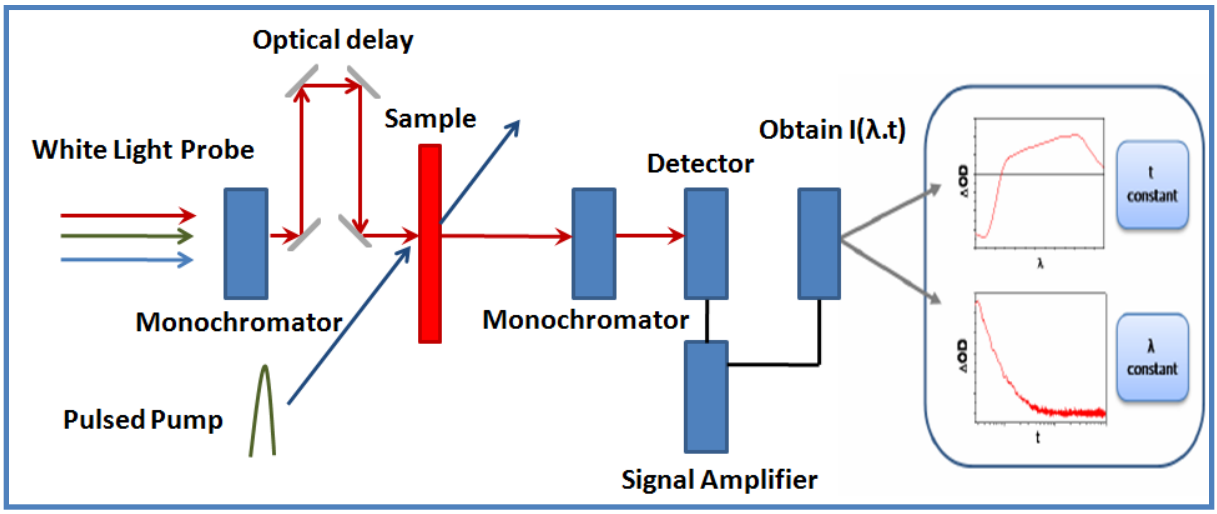

Figure 2.9: Schematic of Transient absorption spectroscopy (TAS). The system consists of two optical pulses, pump and probe pulse. Initially, pump excites the sample and the probe pulse with appropriate time delay monitors the decay dynamics of the transient species. The delay between pump and probe can be obtained from the translation stage and set of mirrors. The probe pulse transmission difference between with and without pump is acquired through detectors.

The measured output from the detector is a voltage difference with and without pump. The calculation of fractional change in the optical density (ΔOD) is given by:

$$\frac{V(t) - V(0)}{V(0)} = \frac{10^{-OD(t)} - 10^{-OD(0)}}{10^{-OD(0)}} = 10^{-OD(t)+OD(0)} - 1$$

Where, *V(0)* is the detector voltage before pump, *V(t)* is the detector voltage after pump at particular time '*t*'. Considering the approximation that, for small value of x, $10^{-x} \approx 1-x\ln 10$, we have,

$$\frac{\Delta V(t)}{V(0)} = 1 - \Delta OD \ln(10) - 1 = \Delta OD \ln(10)$$

Or,

$$\Delta OD = \frac{1}{2.303}\left(\frac{\Delta V(t)}{V(0)}\right)$$

Hence, the change in detector voltage is linearly proportional to ΔOD for small changes in optical density. The data represented in the thesis corresponds to this change in the voltage output from the detectors.

2.6 Electroluminescence measurements:

Electroluminescence from the organic BHJ solar cells is studied in the forward bias conditions.(*65*) Electrons and holes injected from the external electrode undergo bimolecular recombination at the donor acceptor interface.

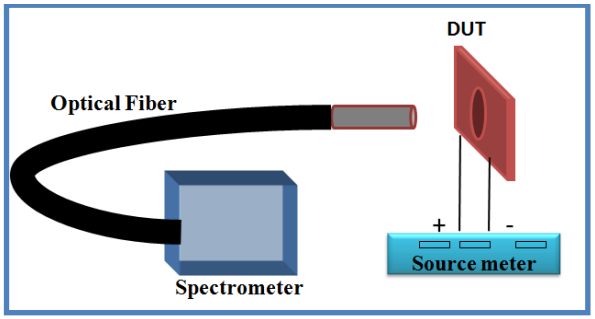

Figure 2.10: Schematic of electroluminescence setup. The optical fiber coupled spectrometer is used to acquire the EL spectrum from devices. The organic BHJ were forward bias using Kiethley 2400 source meter externally.

The bimolecular recombination can be radiative in nature and the emission spectra provide insights to the energetics involved at the donor:acceptor interface. The electroluminescence measurement setup consists of optical fiber coupled with spectrometer, electronic source meter and device under test (DUT) as shown in the Figure 2.10. The EL-measurement setup was custom built at JNCASR, Bangalore. The highly efficient BHJ solar cells were forward biased using Kiethley 2400 source meter. Electroluminescence spectrum was acquired from the Hamamatsu mini spectrometer (Model: TM-VIS/NIR C10083CA) equipped with back-thinned CCD image sensor of 2048 pixels. The spectral response range is 320 nm – 1000 nm with spectral resolution of 8 nm (FWHM). The data was collected using SpecEvaluation^{TM} software.

2.7 AFM –morphological characterization:

The optimized morphology for the efficient working of organic BHJ solar cells depends on number of factors including molecular ordering, orientation and packing, mixing and phase-separation, and the vertical segregation of donors and acceptors within the active layer.(*38, 66*) Associated length scales with structure formed are in the range of nanometers. For example, polymer and fullerene phases have a typical length scale from < 1 nm to 10's of nm. Generally, AFM technique is used to probe the surface morphology and phase separation of the BHJ.

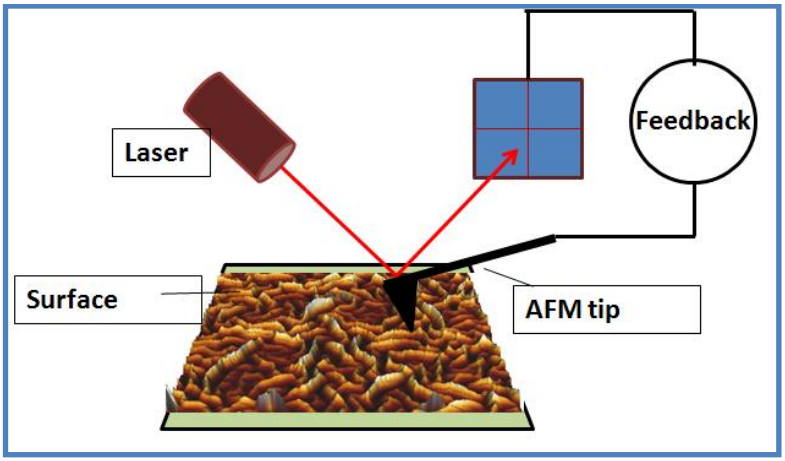

Figure 2.11: Schematic of AFM setup used to map the surface morphology.

Atomic force microscopy (AFM) is one of the most notable tools for imaging surface at the nanoscale and belongs to a subset of scanning probe microscopy (SPM). The atomically sharp tip is used to probe the surface with the aid of piezoelectric crystal. Depending on the inter-atomic forces between surface atoms and the tip atoms, the AFM cantilever gets deflected during the surface scan.(*67*) The deflection of this tip is monitored by means of laser and position sensitive detector arrangement. The information obtained is then fed to an electrical feedback loop which controls the piezoelectric crystal inside the AFM's scanner (Figure 2.11). The contact and non-contact modes are the general modes of operation in AFM. In the contact mode, the tip is allowed to be in contact with the surface and the interactive forces are mapped depending on the deflection of the cantilever. In the non-contact mode, the cantilever is kept slight away from the surface (~ few nm) oscillating at particular frequency and amplitude. In this thesis, the surface characterizations were carried out using Nanowizard 3 AFM system, JPK Instruments, Germany. The contact mode images were obtained using cantilever Multi-75E (Resonant frequency, ω_R ~ 75 kHz). The

amplitude and phase images were obtained using Al coated silicon nitride-cantilevers having force constant of 40 N/m and resonance frequency ω_R ~ 375 kHz) obtained from Budget Sensors. Advanced AFM techniques like conducting -AFM and Kelvin probe-AFM were also used in the thesis. All the image processing was carried out using JPK data processing software for perceptible representation. All AFM images were acquired from exsisting nano-facility at JNCASR, Bangalore.

2.8 Photothermal Deflection Spectroscopy (PDS):

The Photothermal Deflection Spectroscopy (PDS) is a highly sensitive surface averaged absorption measurement technique. Experimental setup includes pump-probe light beams, in which a monochromatic pump light beam produced by a combination of a Light Support MKII 100 W Xenon arc source and a CVI DK240 monochromator, is illuminated on the sample surface (film on Quartz substrate). It is incident perpendicular to the plane of the sample, which on absorption produces a thermal gradient near the sample surface via non-radiative relaxation induced heating. This results in a refractive index gradient in the area surrounding the sample surface. This refractive index gradient is further enhanced by immersing the sample in a deflection medium comprising of an inert liquid FC-72 Fluorinert® (3M Company) which has a high refractive index change per unit change in temperature. A fixed wavelength CW transverse laser probe beam, produced using a Qioptiq 670 nm fiber-coupled diode laser with temperature stabilizer for reduced beam pointing noise, passes through the thermal gradient in front of the sample producing a deflection proportional to the absorbed light at that particular wavelength, which is detected by a differentially amplified quadrant photodiode and a Stanford Research SR830 lock-in amplifier combination. Scanning through different wavelengths gives us the complete absorption spectra. The PDS-data presented in the thesis was obtained from the existing PDS facility at University of Cambridge, UK.

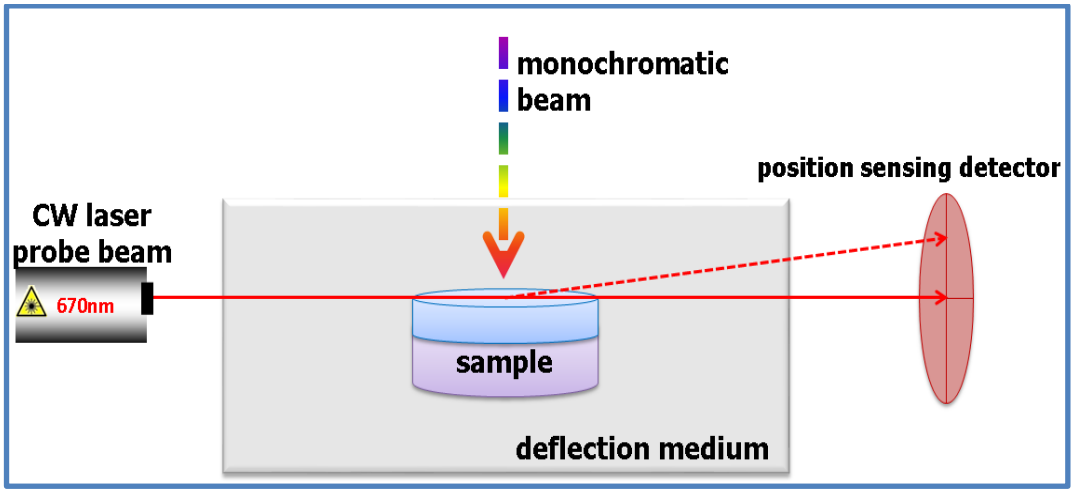

Figure 2.12: Schematic of Photothermal Deflection Spectroscopy (PDS) setup.

2.9 Summary:

Highly efficient organic BHJ solar cells can be fabricated by engineering the device heterojunction and appropriate choice of donor and acceptor molecules. Different combinations and ratio of donor and acceptor materials, electron and hole buffer layers and electrodes of different work functions were explored to optimize the efficiency of BHJ solar cells. Along with fundamental characterization of the solar cells, several advanced characterization techniques were utilized to understand the photo physical processes exist in these devices. Particularly, BHJ featuring perylene based acceptors were studied extensively in this thesis. The following chapters simultaneously discuss the optimization of device efficiency and novel insights into the optoelectronic processes prevailing in the fullerene-free organic solar cells.

References:

(1) Günes, S.; Neugebauer, H.; Sariciftci, N.S., Conjugated Polymer-Based Organic Solar Cells. *Chemical Reviews* **2007,** *107*, (4), 1324-1338.

(2) Walker, B.; Tamayo, A.B.; Dang, X.-D.; Zalar, P.; Seo, J.H.; Garcia, A.; Tantiwiwat, M.; Nguyen, T.-Q., Nanoscale Phase Separation and High Photovoltaic Efficiency in Solution-Processed, Small-Molecule Bulk Heterojunction Solar Cells. *Advanced Functional Materials* **2009,** *19*, (19), 3063-3069.

(3) Yang, X.; Loos, J.; Veenstra, S.C.; Verhees, W.J.H.; Wienk, M.M.; Kroon, J.M.; Michels, M.A.J.; Janssen, R.A.J., Nanoscale Morphology of High-Performance Polymer Solar Cells. *Nano Letters* **2005,** *5*, (4), 579-583.

(4) van Bavel, S.; Sourty, E.; de With, G.; Frolic, K.; Loos, J., Relation between Photoactive Layer Thickness, 3D Morphology, and Device Performance in P3HT/PCBM Bulk-Heterojunction Solar Cells. *Macromolecules* **2009,** *42*, (19), 7396-7403.

(5) Espinosa, N.; Hosel, M.; Angmo, D.; Krebs, F.C., Solar cells with one-day energy payback for the factories of the future. *Energy & Environmental Science* **2012,** *5*, (1), 5117-5132.

(6) Lunt, R.R.; Osedach, T.P.; Brown, P.R.; Rowehl, J.A.; Bulović, V., Practical Roadmap and Limits to Nanostructured Photovoltaics. *Advanced Materials* **2011,** *23*, (48), 5712-5727.

(7) Lizin, S.; Van Passel, S.; De Schepper, E.; Vranken, L., The future of organic photovoltaic solar cells as a direct power source for consumer electronics. *Solar Energy Materials and Solar Cells* **2012,** *103*, (0), 1-10.

(8) *ORGANIC SOLAR CELLS: Fundamentals, Devices, and Upscaling*; Editor Ed.^Eds.;CRC Press: Boca Raton, 2014.

(9) Park, S.H.; Roy, A.; Beaupre, S.; Cho, S.; Coates, N.; Moon, J.S.; Moses, D.; Leclerc, M.; Lee, K.; Heeger, A.J., Bulk heterojunction solar cells with internal quantum efficiency approaching 100%. *Nat Photon* **2009,** *3*, (5), 297-302.

(10) He, Z.; Zhong, C.; Su, S.; Xu, M.; Wu, H.; Cao, Y., Enhanced power-conversion efficiency in polymer solar cells using an inverted device structure. *Nat Photon* **2012,** *6*, (9), 591-595.

(11) Hoppe, H.; Sariciftci, N.S., Organic solar cells: An overview. *Journal of Materials Research* **2004,** *19*, (07), 1924-1945.

(12) Roncali, J., Synthetic Principles for Bandgap Control in Linear π-Conjugated Systems. *Chemical Reviews* **1997,** *97*, (1), 173-206.

(13) Osaka, I.; McCullough, R.D., Advances in Molecular Design and Synthesis of Regioregular Polythiophenes. *Accounts of Chemical Research* **2008,** *41*, (9), 1202-1214.

(14) I. F. Perepichka, D.F.P., *Handbook of Thiophene-Based Materials: Applications in Organic Electronics and Photonics; Synthesis and Theory*; Editor Ed.^Eds.;Wiley VCH: Weinheim, 2009.

(15) Christoph Brabec, V.D., Ullrich Scherf, *Organic Photovoltaics*; Editor Ed.^Eds.;Wiley-VCH Verlag GmbH & Co: 2009.

(16) Kularatne, R.S.; Magurudeniya, H.D.; Sista, P.; Biewer, M.C.; Stefan, M.C., Donor–acceptor semiconducting polymers for organic solar cells. *Journal of Polymer Science Part A: Polymer Chemistry* **2013,** *51*, (4), 743-768.

(17) van Mullekom, H.A.M.; Vekemans, J.A.J.M.; Havinga, E.E.; Meijer, E.W., Developments in the chemistry and band gap engineering of donor–acceptor substituted conjugated polymers. *Materials Science and Engineering: R: Reports* **2001,** *32*, (1), 1-40.

(18) Thompson, B.C.; Fréchet, J.M., Polymer–fullerene composite solar cells. *Angewandte Chemie International Edition* **2008,** *47*, (1), 58-77.

(19) Bundgaard, E.; Krebs, F.C., Low band gap polymers for organic photovoltaics. *Solar Energy Materials and Solar Cells* **2007,** *91*, (11), 954-985.

(20) Hou, J.; Chen, H.-Y.; Zhang, S.; Li, G.; Yang, Y., Synthesis, Characterization, and Photovoltaic Properties of a Low Band Gap Polymer Based on Silole-Containing Polythiophenes and 2,1,3-Benzothiadiazole. *Journal of the American Chemical Society* **2008,** *130*, (48), 16144-16145.

(21) Zhu, Z.; Waller, D.; Gaudiana, R.; Morana, M.; Mühlbacher, D.; Scharber, M.; Brabec, C., Panchromatic Conjugated Polymers Containing Alternating Donor/Acceptor Units for Photovoltaic Applications. *Macromolecules* **2007,** *40*, (6), 1981-1986.

(22) Zhou, H.; Yang, L.; Stoneking, S.; You, W., A Weak Donor−Strong Acceptor Strategy to Design Ideal Polymers for Organic Solar Cells. *ACS Applied Materials & Interfaces* **2010,** *2*, (5), 1377-1383.

(23) Huo, L.; Zhang, S.; Guo, X.; Xu, F.; Li, Y.; Hou, J., Replacing Alkoxy Groups with Alkylthienyl Groups: A Feasible Approach To Improve the Properties of Photovoltaic Polymers. *Angewandte Chemie International Edition* **2011,** *50*, (41), 9697-9702.

(24) Guo, X.; Zhang, M.; Ma, W.; Ye, L.; Zhang, S.; Liu, S.; Ade, H.; Huang, F.; Hou, J., Enhanced Photovoltaic Performance by Modulating Surface Composition in Bulk Heterojunction Polymer Solar Cells Based on PBDTTT-C-T/PC71BM. *Advanced Materials* **2014,** *26*, (24), 4043-4049.

(25) Rajaram, S.; Shivanna, R.; Kandappa, S.K.; Narayan, K., Nonplanar perylene diimides as potential alternatives to fullerenes in organic solar cells. *The Journal of Physical Chemistry Letters* **2012,** *3*, (17), 2405-2408.

(26) Shivanna, R.; Shoaee, S.; Dimitrov, S.; Kandappa, S.K.; Rajaram, S.; Durrant, J.R.; Narayan, K., Charge generation and transport in efficient organic bulk heterojunction solar cells with a perylene acceptor. *Energy & Environmental Science* **2014,** *7*, (1), 435-441.

(27) Shoaee, S.; Deledalle, F.; Shakya Tuladhar, P.; Shivanna, R.; Narayan, K.; Rajaram, S.; Durrant, J.R., A Comparison of Charge Separation Dynamics in Organic Blend Films Employing Fullerene and Perylene Diimide Electron Acceptors. *The Journal of Physical Chemistry Letters* **2014**.

(28) http://www.sigmaaldrich.com/catalog/product/aldrich/698997?lang=en&region=IN.

(29) http://www.sigmaaldrich.com/catalog/product/aldrich/l753971?lang=en&region=IN.

(30) Wu, C.-S.; Chen, Y., Copolyfluorenes containing pendant bipolar groups: Synthesis, optoelectronic properties and applications. *Journal of Materials Chemistry* **2010,** *20*, (36), 7700-7709.

(31) Huo, L.; Zhang, S.; Guo, X.; Xu, F.; Li, Y.; Hou, J., Replacing Alkoxy Groups with Alkylthienyl Groups: A Feasible Approach To Improve the Properties of Photovoltaic Polymers. *Angewandte Chemie* **2011,** *123*, (41), 9871-9876.

(32) Lu, L.; Yu, L., Understanding Low Bandgap Polymer PTB7 and Optimizing Polymer Solar Cells Based on It. *Advanced Materials* **2014,** *26*, (26), 4413-4430.

(33) Peet, J.; Kim, J.Y.; Coates, N.E.; Ma, W.L.; Moses, D.; Heeger, A.J.; Bazan, G.C., Efficiency enhancement in low-bandgap polymer solar cells by processing with alkane dithiols. *Nat Mater* **2007,** *6*, (7), 497-500.

(34) Hummelen, J.C.; Knight, B.W.; LePeq, F.; Wudl, F.; Yao, J.; Wilkins, C.L., Preparation and Characterization of Fulleroid and Methanofullerene Derivatives. *The Journal of Organic Chemistry* **1995,** *60*, (3), 532-538.

(35) Wienk, M.M.; Kroon, J.M.; Verhees, W.J.H.; Knol, J.; Hummelen, J.C.; van Hal, P.A.; Janssen, R.A.J., Efficient Methano[70]fullerene/MDMO-PPV Bulk Heterojunction Photovoltaic Cells. *Angewandte Chemie International Edition* **2003,** *42*, (29), 3371-3375.

(36) Ameri, T.; Heumuller, T.; Min, J.; Li, N.; Matt, G.; Scherf, U.; Brabec, C.J., IR sensitization of an indene-C60 bisadduct (ICBA) in ternary organic solar cells. *Energy & Environmental Science* **2013,** *6*, (6), 1796-1801.

(37) Zhao, G.; He, Y.; Li, Y., 6.5% Efficiency of Polymer Solar Cells Based on poly(3-hexylthiophene) and Indene-C60 Bisadduct by Device Optimization. *Advanced Materials* **2010,** *22*, (39), 4355-4358.

(38) Mukhopadhyay, S.; Das, A.J.; Narayan, K., High Resolution Photocurrent Imaging of Bulk Heterojunction Solar Cells. *The Journal of Physical Chemistry Letters* **2013,** *4*, 161-169.

(39) Huang, Y.; Kramer, E.J.; Heeger, A.J.; Bazan, G.C., Bulk Heterojunction Solar Cells: Morphology and Performance Relationships. *Chemical Reviews* **2014,** *114*, (14), 7006-7043.

(40) Scharber, M.C.; Mühlbacher, D.; Koppe, M.; Denk, P.; Waldauf, C.; Heeger, A.J.; Brabec, C.J., Design Rules for Donors in Bulk-Heterojunction Solar Cells—Towards 10 % Energy-Conversion Efficiency. *Advanced Materials* **2006,** *18*, (6), 789-794.

(41) Kadish, K.M., Ruoff, Rodney S, *Fullerenes : chemistry, physics, and technology*; Editor Ed.^Eds.;Wiley-Interscience: New York, 2000.

(42) Sariciftci, N.S.; Smilowitz, L.; Heeger, A.J.; Wudl, F., Photoinduced Electron Transfer from a Conducting Polymer to Buckminsterfullerene. *Science* **1992,** *258*, (5087), 1474-1476.

(43) Kraabel, B.; Lee, C.H.; McBranch, D.; Moses, D.; Sariciftci, N.S.; Heeger, A.J., Ultrafast photoinduced electron transfer in conducting polymer—buckminsterfullerene composites. *Chemical Physics Letters* **1993,** *213*, (3–4), 389-394.

(44) Rajaram, S.; Shivanna, R.; Kandappa, S.K.; Narayan, K.S., Nonplanar Perylene Diimides as Potential Alternatives to Fullerenes in Organic Solar Cells. *The Journal of Physical Chemistry Letters* **2012,** *3*, (17), 2405-2408.

(45) Shoaee, S.; Deledalle, F.; Shakya Tuladhar, P.; Shivanna, R.; Rajaram, S.; Narayan, K.S.; Durrant, J.R., A Comparison of Charge Separation Dynamics in Organic Blend Films Employing Fullerene and Perylene Diimide Electron Acceptors. *The Journal of Physical Chemistry Letters* **2015,** *6*, (1), 201-205.

(46) Kim, J.Y.; Lee, K.; Coates, N.E.; Moses, D.; Nguyen, T.-Q.; Dante, M.; Heeger, A.J., Efficient Tandem Polymer Solar Cells Fabricated by All-Solution Processing. *Science* **2007,** *317*, (5835), 222-225.

(47) Gordon, R.G., Criteria for Choosing Transparent Conductors. *MRS Bulletin* **2000,** *25*, (08), 52-57.

(48) http://hyperphysics.phy-astr.gsu.edu/hbase/tables/photoelec.html.

(49) Han, D.; Yoo, S., The stability of normal vs. inverted organic solar cells under highly damp conditions: Comparison with the same interfacial layers. *Solar Energy Materials and Solar Cells* **2014,** *128*, (0), 41-47.

(50) Lattante, S., Electron and Hole Transport Layers: Their Use in Inverted Bulk Heterojunction Polymer Solar Cells. *Electronics* **2014,** *3*, (1), 132-164.

(51) Litzov, I.; Brabec, C., Development of Efficient and Stable Inverted Bulk Heterojunction (BHJ) Solar Cells Using Different Metal Oxide Interfaces. *Materials* **2013,** *6*, (12), 5796-5820.

(52) Mazhari, B., An improved solar cell circuit model for organic solar cells. *Solar Energy Materials and Solar Cells* **2006,** *90*, (7–8), 1021-1033.

(53) Cheknane, A.; Hilal, H.S.; Djeffal, F.; Benyoucef, B.; Charles, J.-P., An equivalent circuit approach to organic solar cell modelling. *Microelectronics Journal* **2008,** *39*, (10), 1173-1180.

(54) Armin, A.; Velusamy, M.; Wolfer, P.; Zhang, Y.; Burn, P.L.; Meredith, P.; Pivrikas, A., Quantum Efficiency of Organic Solar Cells: Electro-Optical Cavity Considerations. *ACS Photonics* **2014,** *1*, (3), 173-181.

(55) Clarke, T.M.; Durrant, J.R., Charge Photogeneration in Organic Solar Cells. *Chemical Reviews* **2010,** *110*, (11), 6736-6767.

(56) Banerji, N.; Cowan, S.; Vauthey, E.; Heeger, A.J., Ultrafast Relaxation of the Poly(3-hexylthiophene) Emission Spectrum. *The Journal of Physical Chemistry C* **2011,** *115*, (19), 9726-9739.

(57) Kee, T.W., Femtosecond Pump–Push–Probe and Pump–Dump–Probe Spectroscopy of Conjugated Polymers: New Insight and Opportunities. *The Journal of Physical Chemistry Letters* **2014,** *5*, (18), 3231-3240.

(58) Dai, D.C.; Monkman, A.P., Femtosecond hot-exciton emission in a ladder-type $\ensuremath{\pi}$-conjugated rigid-polymer nanowire. *Physical Review B* **2013,** *87*, (4), 045308.

(59) Bakulin, A.A.; Martyanov, D.S.; Paraschuk, D.Y.; Pshenichnikov, M.S.; van Loosdrecht, P.H.M., Ultrafast Charge Photogeneration Dynamics in Ground-State Charge-Transfer Complexes Based on Conjugated Polymers. *The Journal of Physical Chemistry B* **2008,** *112*, (44), 13730-13737.

(60) Grancini, G.; Maiuri, M.; Fazzi, D.; Petrozza, A.; Egelhaaf, H.J.; Brida, D.; Cerullo, G.; Lanzani, G., Hot exciton dissociation in polymer solar cells. *Nat Mater* **2013,** *12*, (1), 29-33.

(61) Bakulin, A.A.; Rao, A.; Pavelyev, V.G.; van Loosdrecht, P.H.; Pshenichnikov, M.S.; Niedzialek, D.; Cornil, J.; Beljonne, D.; Friend, R.H., The Role of Driving Energy and Delocalized States for Charge Separation in Organic Semiconductors. *Science* **2012**.

(62) Gulbinas, V.; Hertel, D.; Yartsev, A.; Sundström, V., Charge carrier photogeneration and recombination in ladder-type poly(\textit{para} -phenylene): Interplay between impurities and external electric field. *Physical Review B* **2007,** *76*, (23), 235203.

(63) De, S.; Pascher, T.; Maiti, M.; Jespersen, K.G.; Kesti, T.; Zhang, F.; Inganäs, O.; Yartsev, A.; Sundström, V., Geminate Charge Recombination in Alternating

Polyfluorene Copolymer/Fullerene Blends. *Journal of the American Chemical Society* **2007,** *129*, (27), 8466-8472.

(64) Berera, R.; van Grondelle, R.; Kennis, J.M., Ultrafast transient absorption spectroscopy: principles and application to photosynthetic systems. *Photosynthesis Research* **2009,** *101*, (2-3), 105-118.

(65) Tvingstedt, K.; Vandewal, K.; Gadisa, A.; Zhang, F.; Manca, J.; Inganäs, O., Electroluminescence from Charge Transfer States in Polymer Solar Cells. *Journal of the American Chemical Society* **2009,** *131*, (33), 11819-11824.

(66) Müller-Buschbaum, P., The Active Layer Morphology of Organic Solar Cells Probed with Grazing Incidence Scattering Techniques. *Advanced Materials* **2014,** *26*, (46), 7692-7709.

(67) Binnig, G.; Quate, C.F.; Gerber, C., Atomic force microscope. *Physical review letters* **1986,** *56*, (9), 930.

Chapter 3

Perylene Based Electron Acceptors in Organic Solar Cells

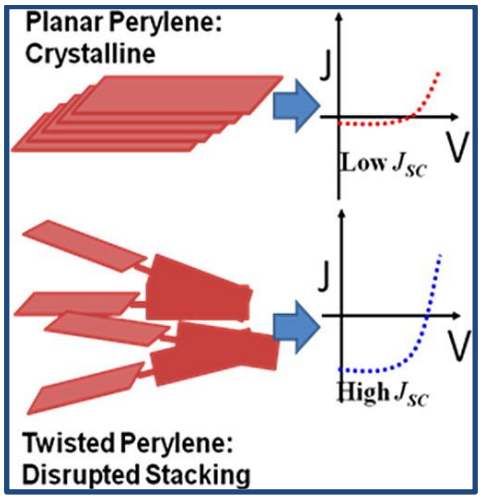

Perylene diimides (PDIs) based electron acceptor is used as an alternative to fullerenes in organic bulk heterojunction solar cells. The non-planar structure of perylene is utilized to disrupt the crystallinity without adversely impacting its charge-transport properties. In combination with a low band-gap hole transporting polymer, the device efficiency of 2.77% has been achieved. A 10-fold increase in J_{sc} is observed in comparison with a planar PDI, resulting in one of the highest J_{sc} values for a solution processed device featuring a PDI as electron transporter.

3 Perylene Based Electron Acceptors in Organic Solar Cells

Organic bulk heterojunction (BHJ) solar cell technology has exhibited continuous growth in terms of power conversion efficiency in the recent past. Intense research is being carried out in printing large area solar cells through roll-to-roll processing.(*1*) Significant efforts have also made to commercialize them, due to low cost, light weight, and their flexibility. The certified power conversion efficiency (PCE) was reported to reach ~ 10 % recently.(*2*, *3*) A start-up company, Heliatek Gmbh, claimed to have achieved a PCE of 12 % was achieved in their organic photovoltaic cells featuring patented absorbing molecules.(*4*) Simultaneous advances in understanding the fundamental processes, such as charge generation and transport, and optimization of device fabrication procedures led to continuous growth in the PCEs.(*5-7*) Particularly, the main focus is on the development of new material designs and properties.(*8*) Several low band-gap donor polymers were synthesized with improved properties such as solar-absorption sensitivity, enhanced hole mobilities, favorable nano-morphology and electronic levels matching with the acceptor molecules.(*9*) However, less attention was given towards synthesis of new n-type electron acceptor materials. The active layer in most of the high efficiency cells consists of a low band gap polymer as the electron donor and fullerene based derivatives as electron acceptors.(*10*) The most commonly employed fullerene based electron acceptor materials are [6,6]- phenyl C_{61}-butyric acid methyl ester (PCBM) and [6,6]-phenyl C71-butyric acid methyl ester (C_{71}-PCBM). The monopoly of fullerene based materials as successful electron acceptors in BHJ organic solar cells is due to variety of reasons, most importantly its ability to form nanoscale morphology.

3.1 Limitations of Fullerene acceptors

In spite of all the advantages of fullerene based electron acceptors, there are important limiting factors which need to be addressed.

1. Relatively less absorption of fullerene acceptors in the visible wavelength region limits the possibility of efficient hole transfer from fullerene to polymer. Extinction coefficient of $PC_{71}BM$ is several times less than the donor polymer. In addition, they

occupy more than 50 % by volume (since > 1:1 ratio of D/A) of the entire photoactive layer, and hence 50 % of the volume is devoid of high absorbing material.(11)

2. Fullerenes have an inherently low lying LUMO level compared with those of common donors,(12) which results in the thermalization loss during charge carrier generation. This results in decreased V_{oc} of the device.
3. The stability and longevity of the fabricated device depends upon the photo-stability of the molecular components.(13) Fullerenes have poor photochemical stability in air compared to many other n-type materials reported in the literature which leads to accelerated degradation of cells.
4. Elaborate synthesis and purification procedures lead to a high cost of production for these materials.(13, 14)

To address these issues, the urge for the development of new electron acceptor materials is of utmost importance in the field of organic BHJ photovoltaics. Many photo-physical processes for the generation of charges and the morphology of the active layer are decided by the choice of donor and acceptor combination. These factors determine the device characteristics like V_{oc}, J_{sc} and ultimately PCE.(15) Hence, the putative n-type acceptors should posses and exhibit all the required optical and electrical properties efficiently. In this regard, n-type perylene molecules are potential alternatives for fullerenes as electron transporters in BHJ solar cells.

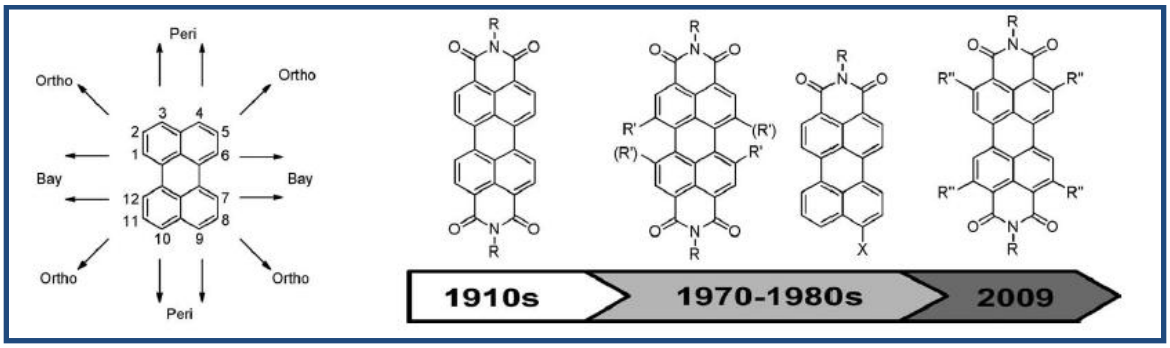

Figure 3.1: Evolution of perylene functionalization.(16) Core of the perylene molecule can be functionalized at 12 different positions, in which positions 3,4,9,10 are known as peri; 1,6,7,12 are known as bay; and 2,5,8,11 are known as ortho. The history of functionalization of perylene core is plotted in the time axis. (Reproduced with permission from the reference (16))

Perylene imides (Figure 3.1) are among the most stable organic compounds.(17, 18) These compounds have been known for centuries as an important class of pigments used widely in the coloring industry. They are used, for example, in the coloration of automotive paint, synthetic fiber and engineering resins are among the most applied industries of perylene based pigments.(19) The structure of the perylene core is shown in the Figure 3.1. The core of the perylene can be functionalized at 12 different positions. The position 3,4,9,10 are known as peri; 1,6,7,12 are known as bay; and 2,5,8,11 are known as ortho. Li and

Wonneberger (16) classified the development of perylene imides to different generations according to development of the functionalizing perylene at different positions. The first generation of development included substituting peri-positions in the perylene core. The second generation substituted bay-positions, while the third and most recent developments are involved in the functionalization of ortho positions. The choice of perylenes as alternatives for fullerenes in BHJ is multifold:

1. High extinction coefficient in the visible region,(17) which gives the possibility of hole transfer process from perylene to donor polymer.
2. Robustness in tuning the energy levels(20): The LUMO levels can be adjusted with respect to donor materials to simultaneously optimize large driving energy for electron transfer and along with high V_{oc} of the device.
3. Good photostability which could increase the lifetime of the organic solar cells under illumination.(21)
4. Good electron mobility which assists in efficient charge transport in the bulk.(22)
5. Tunable solubility in common solvents which gives control over aggregation properties which can be optimized for favorable nanoscale morphology.(23)

3.2 Evolution of perylene based electron acceptors

The first generation imide functionalized perylenes were used for bilayer organic photovoltaics. The second and third generation soluble perylenes with bay-substitutions were utilized in solution processed BHJ solar cells.(16) Despite such promising properties of perylene, BHJ solar cells with perylene diimide's (PDI) as acceptors often exhibited very low efficiencies. Tuning the molecular architecture of perylene provides a possible solution to this problem.(24) In this chapter, we address issues related to low efficiencies and demonstrate a specific PDI-based system, which exhibits good efficiency. This lays down a route to achieve high-efficiency fullerene-free BHJ-PSCs.

Several studies have explored reasons for the low efficiencies of PDI-based solar cells. PDIs tend to crystallize due to their π-π interactions leading to large-scale phase separation of polymer and PDI domains.(25) To reduce the formation of micrometer-sized crystals, Rajaram et al. reported the importance of a diblock copolymer as a compatibilizer.(26) The presence of compatibilizer enhanced the performance of the devices and an efficiency of 0.55 % was achieved when blended with P3HT, which was one of the highest efficient P3HT/PDI based BHJ solar cells till then.

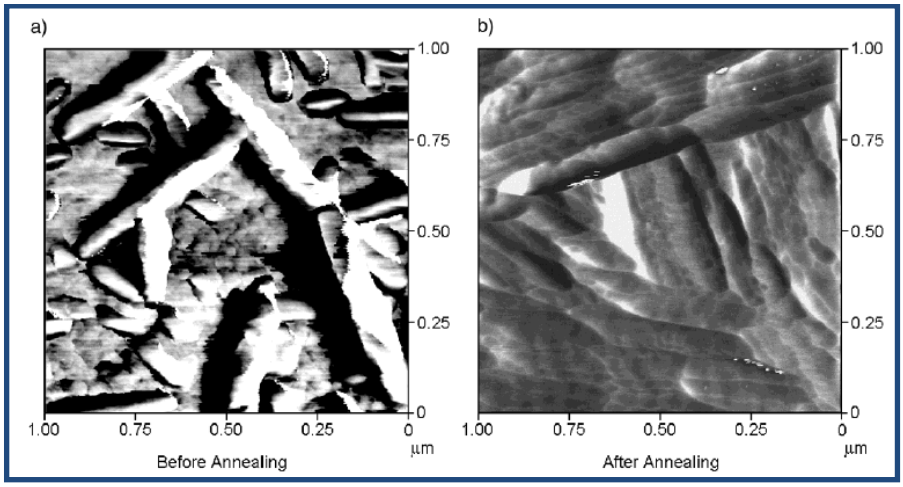

Figure 3.2: Typical AFM-TM images of the 80:20 EP-PTC:P3HT blend film recorded in PDI mode a) before and b) after thermal annealing at 105^{0}C for 1 h. Reproduced with permission from the reference (25).

Howard et al.(27) studied the charge generation and recombination dynamics in perylene tetracarboxydiimide based electron acceptor BHJ using transient absorption spectroscopic measurements. They showed that, when perylenes are finely dispersed in the Poly(9,9-dioctylfluorene-alt-benzothiadiazole) (F8BT) polymer matrix, the very fast bimolecular recombination limits the device efficiency after electron transfer. When the perylenes are coarser in the blend, the perylene excitons are stabilized due to intermolecular relaxation before the charge transfer process. They predicted that the two loss channels always limit the quantum efficiency of perylene based molecules, unless perylenes structures are modified to suppress the rate of intermolecular state formation without compromising charge-transport properties.

Additionally, charge transport in perylene crystals is expected to be anisotropic with high mobility in the π-stacking direction.(28, 29) A recent report from the Brédas, Salleo, and Fréchet groups correlated the J_{sc} to the separation distance between donor and acceptor molecules at the interface.(30) It was shown that small separation distances facilitated the formation of a stable charge-separated state leading to inefficient charge carrier separation. A combination of planar donor and planar acceptor molecules results in small separation distances at the interface. Conversely, a marginal increase in the separation distance between the donor and acceptor can lead to a more loosely bound CT state, resulting in better charge separation and higher short circuit current density.

3.3 Twisted perylene (TP)

A common theme emerging from the previous studies is that the micrometer-scale crystallization (Figure 3.2) of perylenes in blends may have an unfavorable impact on the performance of PDI-based solar cells. This suggests that reducing the co-facial stacking of perylene molecules without adversely impacting their charge-transport properties may be an important design principle. Keeping this in mind, the previously reported PDI (Figure 3.3) has been chosen for the study.(*31-34*)

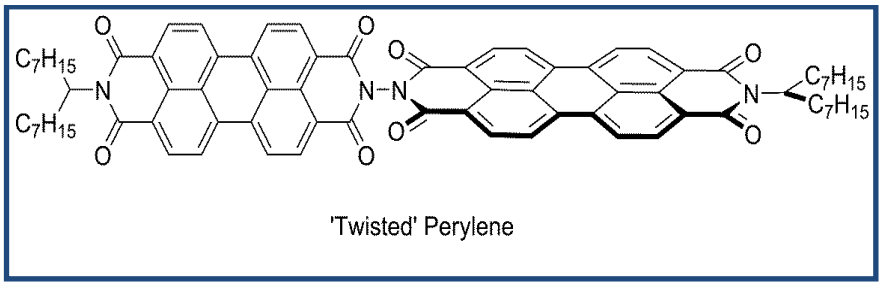

Figure 3.3: Structure of Twisted Perylene (TP).(35) TP was synthesized by attaching two PDI units using hydrazine as a linker. The central N–N single bond is surrounded by four carbonyl groups, wherein negative charge on the oxygens rotates the imide planes and hence the perylene units are oriented perpendicular to each other.

In this molecule, two PDI units are brought together using hydrazine as a linker. The central N–N single bond is surrounded by four carbonyl groups, wherein the oxygens carry a partial negative charge. To minimize the electronic repulsion between the oxygen atoms, the imide planes twist and hence the perylene units get oriented perpendicular to each other.(*35*)

The loss of planarity should result in lower phase segregation, reduce the formation of intermolecular states, and improve charge separation at the interface. In addition, the molecule has a higher extinction coefficient in comparison with $PC_{70}BM$, which should increase the generation of excitons in the acceptor. This is particularly useful when the hole transporting material is a donor–acceptor polymer. Typically these polymers have a bimodal absorption spectrum with very little absorption in the 500 nm to 600 nm range. The intense optical absorption of the non-planar perylenes in this region makes them well-suited for using as electron transporters in blends with donor–acceptor polymers. To evaluate the effect of the loss of planarity, comparative studies were carried out with a planar perylene.(*30*)

3.4 Results and discussions

Steady state photo-physical property of TP film is plotted in the Figure 3.4. The peak of the absorption is ~ 540 nm and the band edge is at 600 nm. The fluorescence spectrum shows red-shift having emission maximum ~ 630 nm. The films were spin coated from anhydrous chlorobenzene solution at 1000 rpm speed on top of the quartz substrates. The electron mobility is measured in bottom-gate FET device structures with TP benzocylcobutene (BCB) as the dielectric layer. The electron mobilities (μe) of ~8×10^{-3} cm^2/V sec are obtained for TP molecule. This value is about an order of magnitude lower than mobilities for various perylenes, which have a larger degree of crystallinity.(*36*) However, the μ_e is comparable to that of $PC_{70}BM$.(*37*)

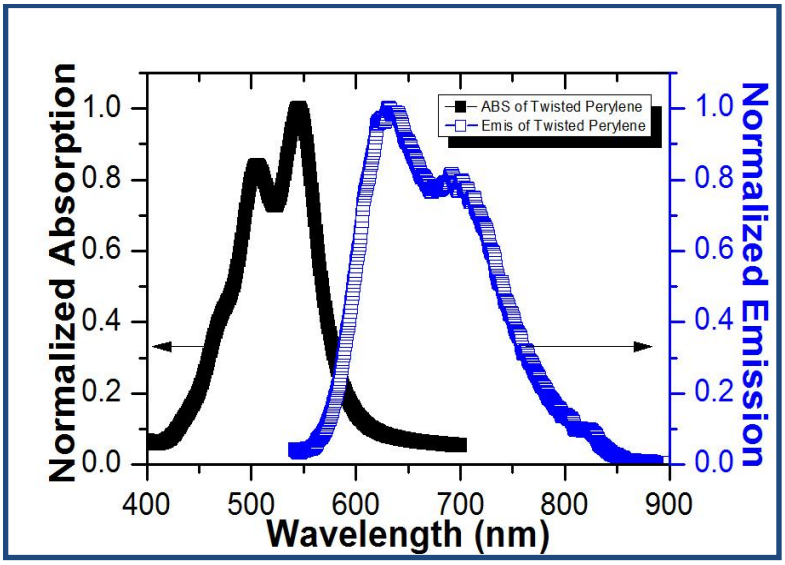

Figure 3.4: Absorption and emission spectra of twisted perylene. The absorption and fluorescence spectra were acquired from films spin coated from TP in anhydrous chlorobenzene solution rotated at 1000 rpm. (Reproduced with permission from the reference (35))

To evaluate TP as an electron acceptor material in solar cells, initially BHJ films using the donor polymer P3HT was studied (Figure 3.5). The devices were fabricated in the both normal and inverted structures. The active layer consists of 1:1 ratio by weight of P3HT and TP. The active layer was spin coated from anhydrous chlorobenzene solvent having solution concentration of 12 mg/mL at a speed of 1000 rpm for 10 s inside the nitrogen filled glove box. The active layer was annealed at 100 ^{0}C for 15 min before coating the top electrodes. In the normal devices, PEDOT:PSS was coated on ITO substrates and used as hole transport layer, Al metal electrode was utilized as top electrode to extract the electrons from the

devices. Most of the normal devices did not show any working devices due to the shorting of the electrodes. In the inverted device geometry, sol-gel based ZnO was coated on top of ITO as electron transport layer and MoOx/Ag was coated as counter electrode to extract the holes. Inverted devices showed better performance compared to normal devices. A power conversion efficiency of 0.28 is achieved with V_{oc} = 0.5 V, J_{sc} = 1.25 mA/cm^2 and *FF* = 56.2 %. The incident photon to current conversion efficiencies (IPCEs) of these devices shows spectal coverage of 400-650 nm with maximum of ~ 5 % at λ ~ 520 nm. The poor performance of these devices compare to P3HT:PC_{61}BM based devices can be attributed to following reasons. P3HT is a crystalline polymer and hence after annealing of BHJ films, the TP molecules are phase separated forming larger domains effecting charge transport. In addition, the absorption of P3HT and TP overlap each other which result in decreased quantum yield of overall exciton creation.

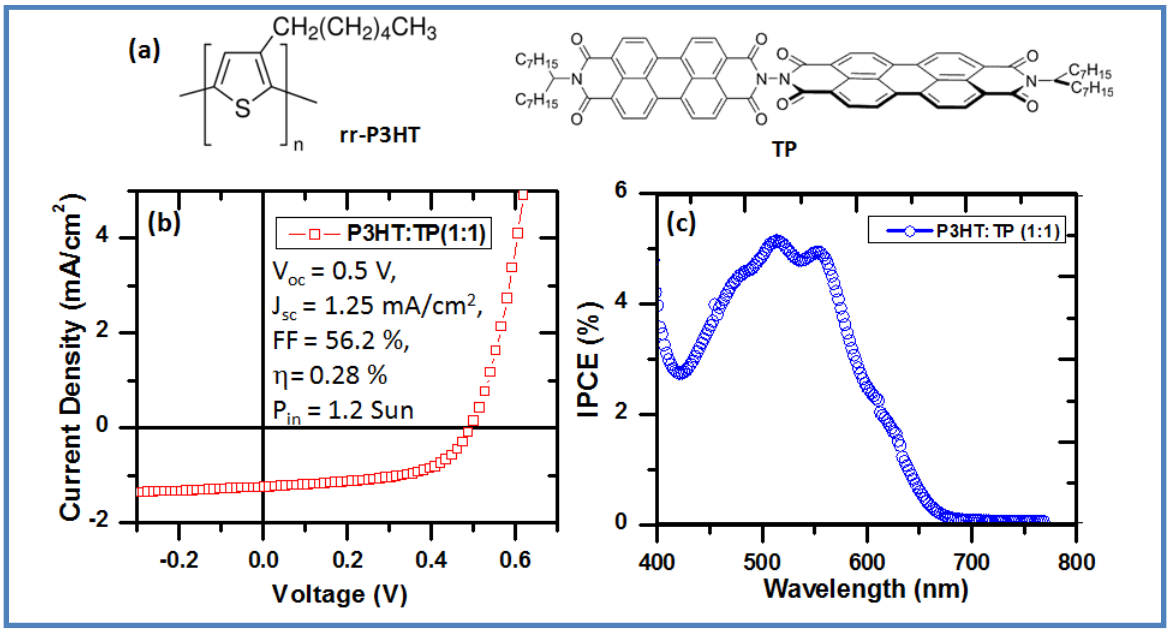

Figure 3.5: (a) structures of P3HT and TP, (b) J-V characteristics of inverted device having heterojunction, ITO/ZnO/P3HT:TP(1:1)/MoOx/Ag, exhibiting η = 0.28 %, V_{oc} = 0.5 V, J_{sc} = 1.25 mA/cm^2, FF = 56.2 %. (c) Incident photons to current conversion efficiency (IPCE) of the devices showing maximum of 5 % at λ ~ 520 nm.

In order to increase the overall absorption of the devices, BHJ films using the low band-gap donor polymer PBDTTT-C-T and TP acceptor are studied. The planar perylene is used as control molecule for TP in the experiments(figure 3.6).([38])

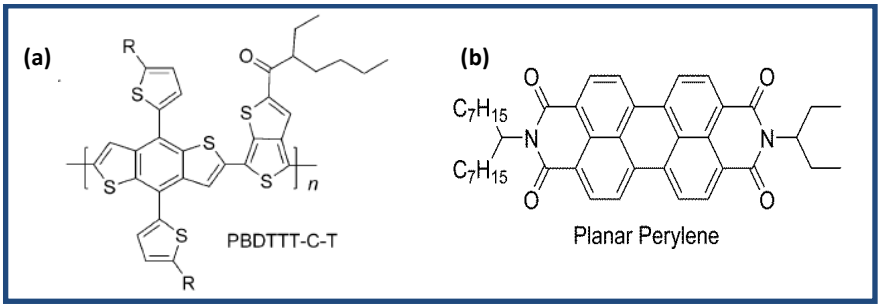

Figure 3.6: Structure of (a) low band-gap donor polymer PBDTTT-CT used in the blend with perylene molecules in fabricating BHJ films and (b) planar perylene (PP) used for comparative study with the twisted non-planar perylene.

Organic BHJ solar cells using this polymer and $PC_{70}BM$ acceptors have exhibited device efficiencies exceeding 7%. The absorption spectrum of PBDTTT-C-T exhibits two bands with minimal absorption between 400 and 550 nm. On the other hand, TP exhibits an absorption maximum at 545 nm along with a lower intensity band at 506 nm (Figure 3.7). Therefore, use of TP could give spectral coverage over a broader wavelength range and lead to good device efficiencies.

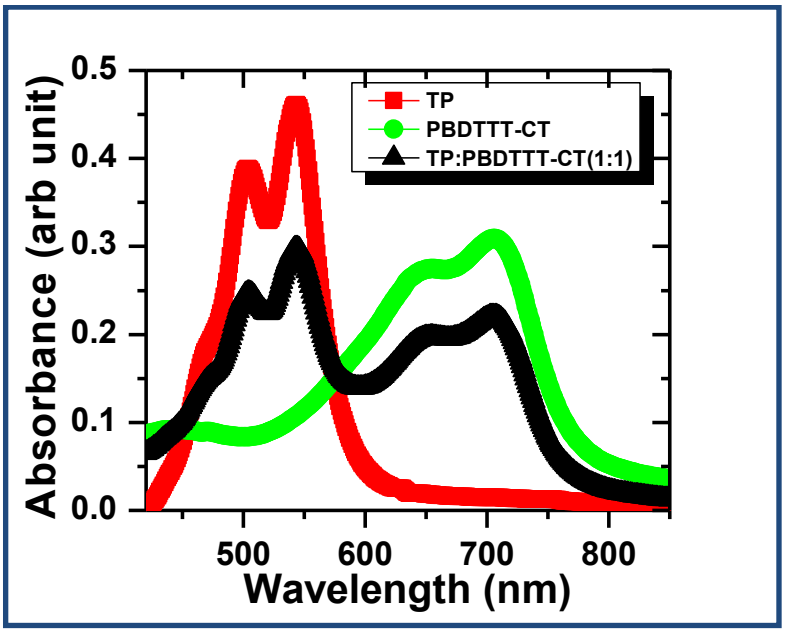

Figure 3.7: Absorption spectra of TP, PBDTTT-CT and blend of PBDTTT-CT:TP (1:1 ratio). All the films were spin coated from the anhydrous chlorobenzene solution at 1000 rpm speed on top of the quartz substrate. (Reproduced with permission from the reference (35))

The HOMO and LUMO levels of perylene were determined by a combination of optical absorption and cyclic voltammetry measurements (Figure 3.8). Cyclic voltammetry is performed on solution containing perylene molecules and supporting electrolyte in the mixture (50:50) of anhydrous acetonitrile/choloroform. IV curve is then recorded at 50 mV/s scan rate. The Figure 3.8 clearly demonstrates the relatively similar electronic levels (LUMO and HOMO) for both TP and PP. Corresponding values for the polymer PBDTTT-CT have

been obtained from the literature. A comparison of these values (Figure 3.9) shows that favorable band offsets exist for transfer of electrons from the polymer PBDTTT-CT to the perylene and for transfer of holes in the reverse direction.

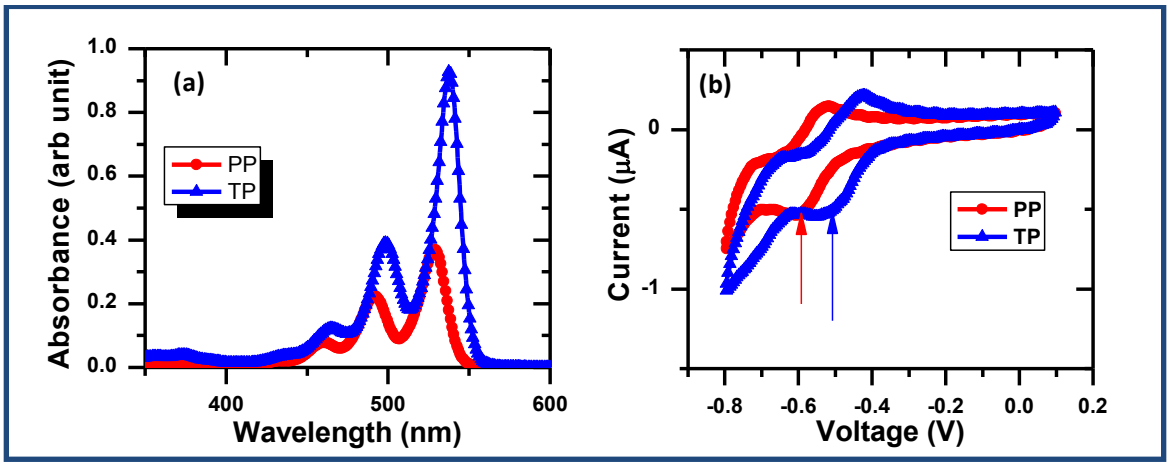

Figure 3.8: (a) Absorption spectra of TP and PP molecule in anhydrous chloroform, and (b) cyclic voltagram of TP and PP molecules obtained against saturated Ag/AgCl electrode. The arrow mark indicate the reduction potential (E_p^{red}) of the molecules. The LUMO level was estimated from the relation, LUMO = - (4.6 + E_p^{red}) eV.

Inverted-structure organic BHJ solar cells were fabricated using a blend of these materials as shown in the figure 3.9a. The sequential layers of heterojunction consist of ITO coated glass substrate, ZnO electron buffer layer, PBDTTT-CT:TP active layer, hole transporting MoO_x and Ag counter electrode. The details of fabrication methods are described in the section 3.8. The band diagram of the heterojunction (Figure 3.9b) shows the optimized energy levels for efficient transport of photogenerated charges.

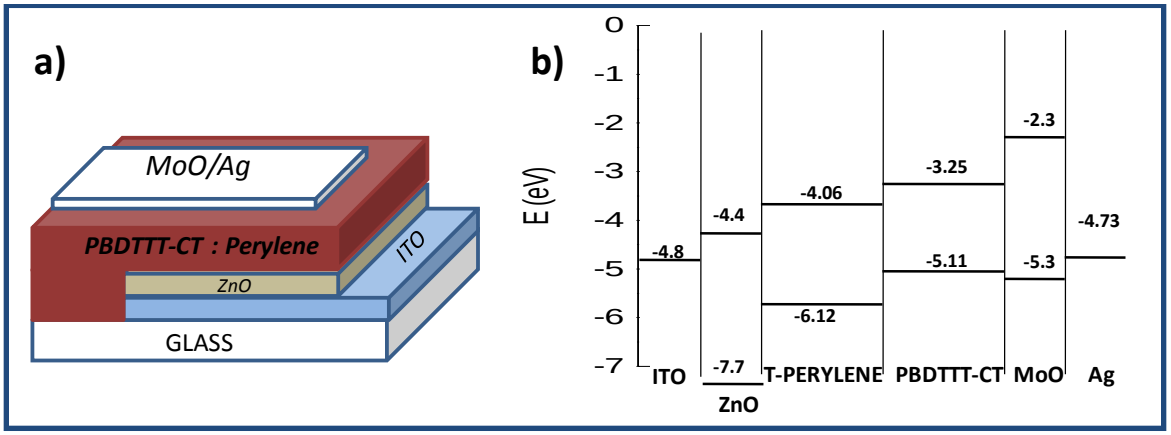

Figure 3.9: (a) Device architecture used in the study. The devices were fabricated in inverted geometry with sol-gel based ZnO as electron buffer layer and MoOx as hole transport layer. Light was illuminated from ZnO side. The thickness of the active layer was estimated to be ~ 100 nm, and (b) energy level of all the materials used in the sandwiched device structure to form hetero-structure solar cells. (Reproduced with permission from the reference (35))

Active layer consisting of 1:1 ratio of PBDTTT-CT and TP were optimized to yield a set of devices with $V_{OC} \approx 0.76$ V, $J_{sc} \approx 9.5$ mA/cm^2, and fill factor ≈ 0.46 under AM 1.5 G,

1.2 sun units illumination (Figure 3.10). The measurements were carried out for a large number of devices, and average power conversion efficiency (PCE) of 2.77% was observed for devices of area ≈ 14 mm^2.

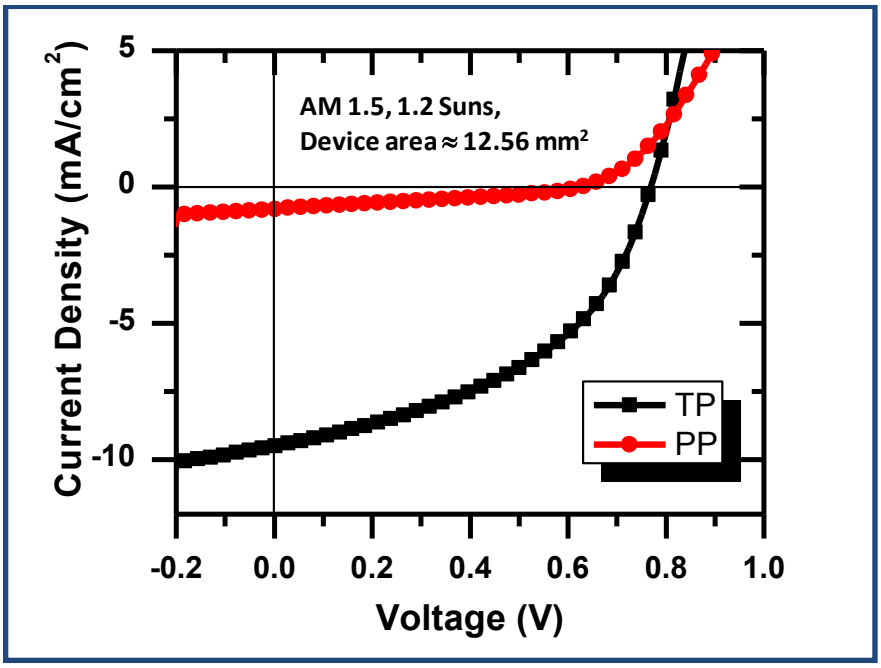

Figure 3.10: J–V characteristics measured under illumination of AM 1.5 G, 1.2 sun units for devices fabricated with polymer PBDTTT-CT and planar perylenes and twisted perylene. Active layer was spun cast from chlorobenzene solution containing a 1:1 ratio by weight of perylene and donor polymer. Blend concentration was 12 mg/mL.

Table 1: J-V characteristics of PBDTTT-CT:TP and PBDTTT-CT:PP BHJ solar cells.

Blend	J_{sc} (mA/cm^2)*	V_{oc} (V)	Fill factor (%)	η (%)
PBDTTT-CT:TP	9.5	0.76	46.5	2.78
PBDTTT-CT:PP	0.8	0.62	30.6	0.13

** the devices were illuminated with AM 1.5, 1.2 Suns unit. (Reproduced with permission from the reference (35))*

It must be noted that this J_{sc} of ~7.9 mA/cm^2 (for 1 Sun) was one of the highest reported to date for solution-processed cells containing PDIs, and the efficiency was one of the highest for a non-fullerene electron transporter till 2012. For comparison, devices were fabricated with PBDTTT-CT: PP under identical conditions. This resulted in devices with a V_{OC} of 0.65 V, J_{sc} of 0.85 mA/cm^2, and fill factor of 0.3 leading to a PCE of 0.13%. Across all parameters, devices fabricated with TP acceptor outperformed the ones fabricated with PP. However, the largest difference was seen in the J_{sc}, wherein the devices with TP are better by an order of magnitude. This supports the hypothesis that use of a non-planar

perylene leads to better short circuit current density. The J-V characteristics for both the blends are tabulated in the table 1.

The reduced J_{sc} for PP based devices can be attributed to the large scale phase separation due to the π-π interaction of the PP molecules. The aggregation of PP molecules is evident from the absorption spectrum acquired in solid state form (films).

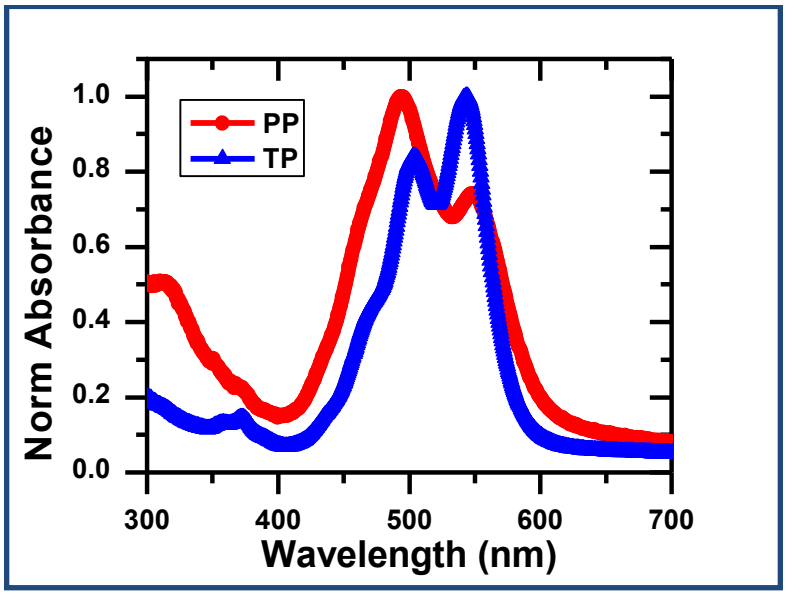

Figure 3.11: Absorption spectra of PP and TP in film form. The films were spin coated from chloroform onto the quartz substrate at 1000 rpm speed.

The PP spectra show the shift in the maximum peak from $S_{0\text{-}0}$ band to $S_{0\text{-}1}$ band. This is a clear indication of the aggregation of PP molecules. Whereas, the TP molecules do not show any change in the maximum of the peaks suggesting less π-π interaction between perylene cores (Figure 3.11).

The IPCEs of devices with TP and PP were measured in the wavelength range of 400 - 850 nm to understand wavelength dependence on photocharge generation (Figure 3.12a). Across all wavelengths, the device with TP acceptor gave higher efficiencies with a maximum close to 40%. A comparison of the absorption spectra of the individual components of the active layer revealed an IPCE of ~35% near the absorption maximum of the non-planar perylene (Figure 3.12b). The hole-transporting polymer has very little optical absorption in this region. This give the possible explanation of hole transfer from TP to PBDTTT-CT and makes a clear case for the use of non-planar perylenes as electron acceptors in solar cells.

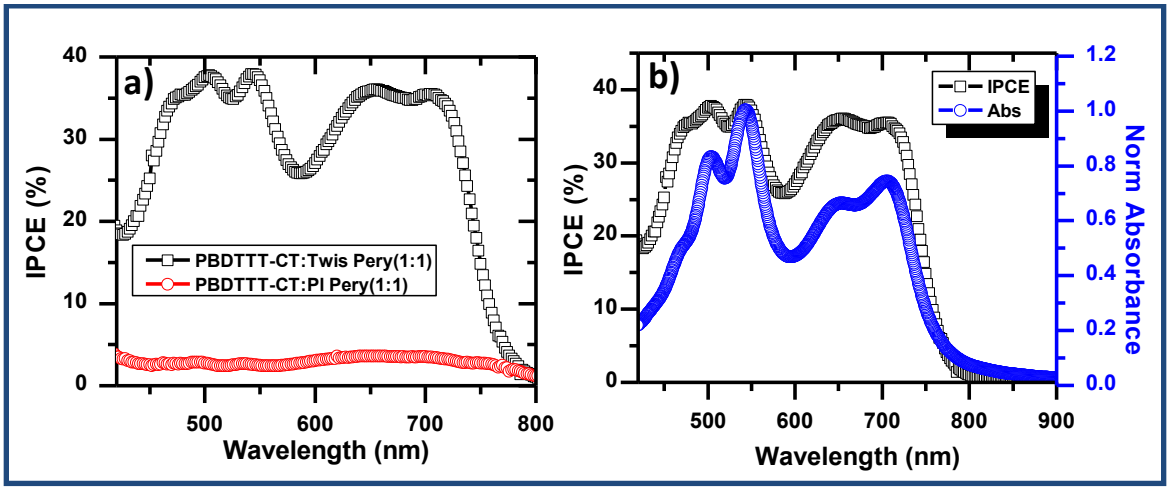

Figure 3.12: (a) IPCE spectra of inverted solar cells containing PBDTTT-CT:TP and PBDTTT-CT:PP. (b) comparison of absorption and IPCE of PBDTTT-CT:TP blend suggests efficient charge generation from both perylene and PBDTTT-CT absorption. (Reproduced with permission from the reference (35))

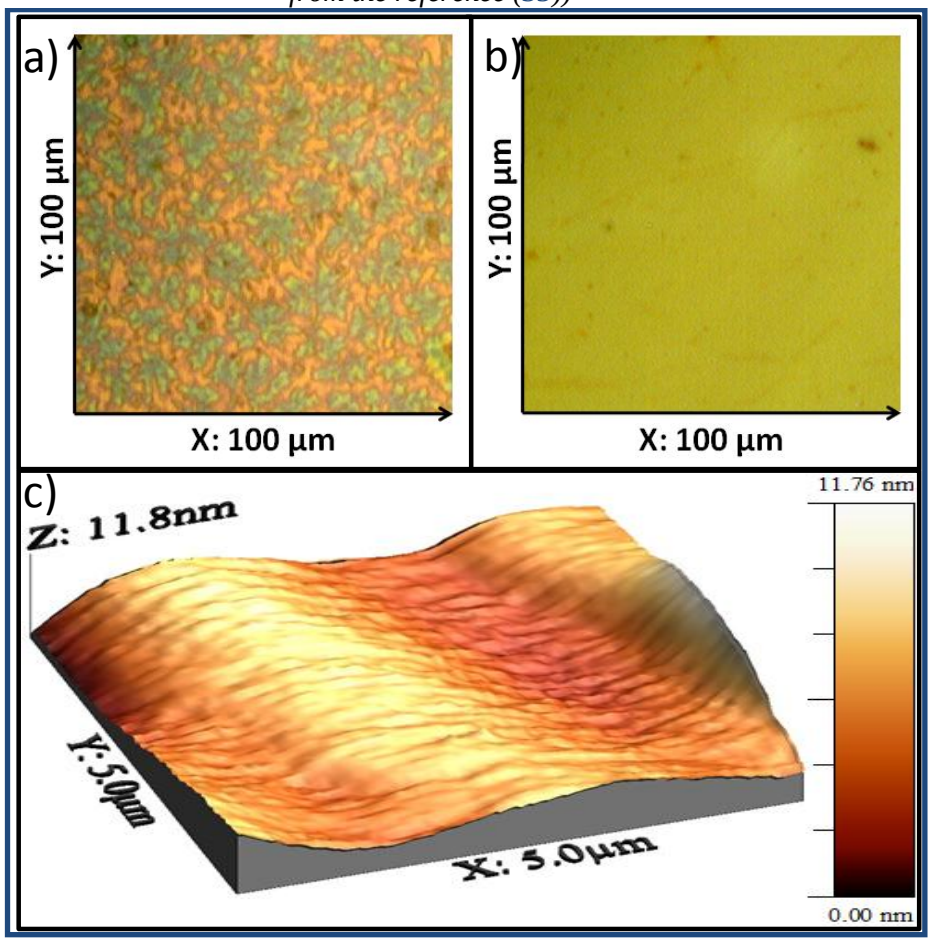

Figure 3.13: (a,b) 100 µm × 100 µm optical images of blend films (1:1 ratio by wt)) of 2 and 1 with PBDTTT-CT, respectively. (c) 5 µm × 5 µm NSOM-transmission contrast image of blend films with 1, obtained from 150 nm glass-aperture tip using a 543 nm light source and scan step-size of 20 nm. The image represents a typical region of the blend film. (Reproduced with permission from the reference (35))

Optical microscopy and near-field scanning optical microscopy (NSOM) were used to study the morphologies of the active layer blends. Optical microscopy images of PP-based blends showed that the perylene underwent phase separation from the polymer, giving rise to micrometer-sized crystals (Figure 3.13a), which was similar to microstructural characteristics found in the previous reports.(*25*, *26*) Similar optical images of blends with TP were featureless (Figure 3.13b). The uniformity and the homogeneity of the TP blends were observed even at a higher resolution of 150 nm length scales, as indicated by NSOM images that are relatively featureless (Figure 3.13c). This indicated that the blends with TP are more intimately mixed and have a larger interfacial area. The disruption of stacking was likely to prevent the crystallization of this perylene. Therefore, large-scale phase separation was not observed. More intimate mixing enhanced the interfacial area. This should lead to a greater percentage of the excitons quenching at the donor–acceptor interface.

Our studies along with previous work indicate three plausible sources for the increase in the short circuit current density. The first is the reduction in the formation of micrometer-size crystals of the acceptor in the active layer blend. Fréchet and coworkers have studied the role of a compatibilizer in reducing the phase segregation of PDIs from blends with poly(3-hexyl thiophene) (P3HT).(*26*) In blends with the compatibilizer, Fréchet and coworkers observed a decrease in the formation of micrometer-sized crystals along with a ~50% increase in the J_{sc}. On the basis of these trends, it appears unlikely that the change in morphology alone can completely account for the sizable (order of magnitude) increase in the J_{sc} seen with TP.

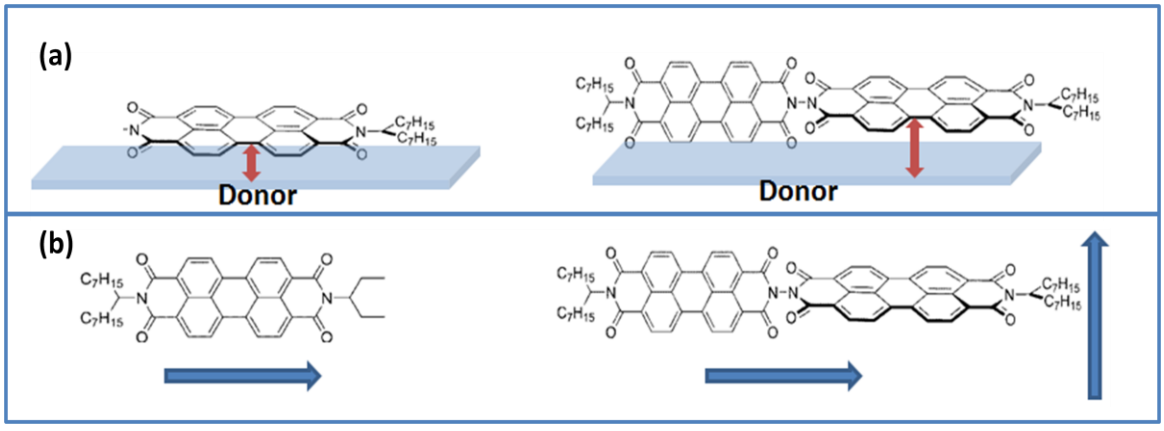

Figure 3.14: Schematic of (a) increased separation distance between the donor and acceptor (TP) at the interface and, (b) increased the dimensionality of the TP from one to two.

Secondly, recent work from the Brédas, Salleo, and Fréchet groups has shown that J_{sc} can be improved by increasing the separation distance between the donor and acceptor molecular planes at the interface. This was accomplished by using a pendant aryl group that would be oriented perpendicular to the polymer backbone. In our study, TP has a similar molecular architecture (Figure 3.14a), and this also potentially contributes toward the observed increase in the J_{sc}. Lastly, by making our perylene nonplanar, we have increased the dimensionality of the perylene from one to two (Figure 3.14b). Recent work from the Gregg(*39*) and Durrant(*6*) groups suggests that this can lead to increased charge separation at the donor–acceptor interface. Overall, a combination of these three effects could account for the order of magnitude increase in the J_{sc}.

3.5 Device fabrication and measurement details

Inverted device structures of the BHJ:PSCs were fabricated on ITO-coated glass substrates using standard protocol. The patterned ITO-coated glass substrates were first cleaned with detergent, sonicated in water and a 1:1:1 mixture of acetone, chloroform, and isopropyl alcohol, and subsequently cleaned with RCA treatment; a mixture of hydrogen peroxide (H_2O_2), ammonium hydroxide (NH_4OH) and water (1:1:5 by volume) at 80 °C for 15 minutes. The ZnO precursor containing zinc acetate dihydrate (314 mg), 2-methoxyethanol (3.14 mL), and ethanolamine (86 µL) was vigorously stirred at 50 °C for 8 h in air. It was then spin coated on to cleaned ITO substrates at 2000 rpm. The substrates were subsequently annealed at 250 °C for 30 min in air to obtain crystalline ZnO films. The ZnO layer thickness was in the ~ 20 - 30 nm range as measured using Dektak thickness profilometer. Inside a glove box, solutions containing a mixture of PBDTTT-CT and Perylene in a 1:1 ratio in anhydrous chlorobenzene with blend concentration of 12 mg/mL were spin-coated on top of ZnO films, at 1200 rpm. The thickness of the active layer was typically ~100nm. The counter electrode MoOx (11 nm) and Ag (100 nm) was deposited by physical vapor deposition through shadow mask at a base pressure of 10^{-6} mbar.

OFETs were fabricated in bottom gated top electrode configuration. Aluminum bottom gate is thermally evaporated on to cleaned glass substrate, on which the dielectric BCB is spin coated at 1000 rpm (100 nm). Annealing the dielectric at 120°C, Perylene 1 in chlorobenzene (20 mg/mL) is spin coated at 1000 rpm (80 nm). After annealing the active region at 150 °C for 15 min, 50 nm top aluminum source-drain electrodes were evaporated by physical vapor deposition using shadow mask technique having a channel width of 60 µm.

The J-V characteristics of PDI BHJs were measured using ORIEL® Sol3A™ CLASS AAA SOLAR SIMULATOR with Oriel PV reference system. The Oriel PV reference system comprised of reference cell Meter and reference Cell. The reference cell consists of a 2 cm x 2 cm Monocrystalline Silicon Photovoltaic Cell and a type K thermocouple assembled in an aluminium housing in accordance with IEC 6090412. Calibration data, notably J_{sc} and the spectral Mismatch Correction Factor, were taken from an accompanying certificate from Newport Corp(Irvine , CA).

The oriel Reference Cell Meter was calibrated to the J_{sc} and the spectral Mismatch Correction Factor of its paired reference cell to read out Irradiance from a solar Simulator in units of "Sun". Solar Simulator output of 1000 W/m^2 at 25^0 C with Air Mass 1.5 Global Spectral filtering is equivalent to one "Sun".

The power input was calculated using this reference cell before each set of measurements. The IV curve presented in the paper was characterized under 1.2 Suns, and not 1.0 Sun . This specification of the simulator was included (η= 2.78 %, V_{oc} = 0.76 V, *FF* = 45.98 %, J_{sc} = 9.5 mA/cm^2 and Pin = 1.2 Sun) . The IPCE measurements were carried out using a homebuilt setup, which comprised of Xenon lamp (Oriel Instruments), Monochromator(Spex) and Keithley 6514 electrometer controlled through Labview. Before each measurement of IPCE on PDI BHJ's, the spectral response of a Si Photodetector (UDT Sensors. Inc.) with the lamp was calculated and calibrated with the responsivity to get the IPCE spectra of the PDI BHJ's. Estimation of J_{sc} from the IPCE data was within the calibration error bar. The 1 Sun estimate was then ~7.9 mA/cm^2. The IPCE spectra for the devices were measured using Spex Monochromator, Keithley 6514 electrometer and calibrated using Si photodetector (UDT Sensors Inc.). FET characteristics were measured using Keithley 42001SCS Semiconductor Characterization System. Absorption and emission spectrum were measured using a Perkin Elmer Spectrometer in the film form.

Cyclic voltammetry was performed using Autolab PG STAT101 with platinum disc as working electrode, platinum wire as counter electrode and aqueous Ag/AgCl as reference electrode. Perylene compound of 0.1 mM and electrolyte solution of 0.1 M tetra-n-butylammonium hexafluorophosphate ($TBAPF_6$) were taken in anhydrous acetonitrile/chloroform (50:50). Ultra-pure nitrogen was used to purge the solution in the cell for ten minutes before experiment, and during the experiment a blanket of nitrogen was maintained. IV curve was recorded at 50 mV/s scan rate.

3.6 Summary

The non-planar perylene derivative was utilized as electron transporter in the organic BHJ solar cells. The limitation of relatively low-optical absorption of fullerene derivatives in the visible range was resolved using high extinction coefficient of non-planar perylene. The disruption of planarity enhanced the short circuit current density leading to better device performance in comparison with planar perylenes. IPCE studies indicated good spectral coverage of the blends and enhanced charge generation from TP excitons. The twisted structure controlled the large scale phase separation of these molecules in the blend. A device efficiency of 2.77% was achieved by blending with PBDTTT-CT donor polymer. The order of magnitude increase in J_{sc} was attributed to three possible reasons: increased donor acceptor interfacial area, increased distance between donor and acceptor plane and increased dimensionality of the molecule. Next chapter discusses the photo-charge carrier generation and recombination dynamics in this system using several spectroscopic techniques.

References:

(1) Søndergaard, R.; Hösel, M.; Angmo, D.; Larsen-Olsen, T.T.; Krebs, F.C., Roll-to-roll fabrication of polymer solar cells. *Materials Today* **2012,** *15*, (1–2), 36-49.

(2) You, J.; Dou, L.; Yoshimura, K.; Kato, T.; Ohya, K.; Moriarty, T.; Emery, K.; Chen, C.-C.; Gao, J.; Li, G., et al., A polymer tandem solar cell with 10.6% power conversion efficiency. *Nat Commun* **2013,** *4*, 1446.

(3) Lizin, S.; Van Passel, S.; De Schepper, E.; Vranken, L., The future of organic photovoltaic solar cells as a direct power source for consumer electronics. *Solar Energy Materials and Solar Cells* **2012,** *103*, (0), 1-10.

(4) Gmbh, H., http://www.heliatek.com.

(5) Hains, A.W.; Liang, Z.; Woodhouse, M.A.; Gregg, B.A., Molecular Semiconductors in Organic Photovoltaic Cells. *Chemical Reviews* **2010,** *110*, (11), 6689-6735.

(6) Clarke, T.M.; Durrant, J.R., Charge Photogeneration in Organic Solar Cells. *Chemical Reviews* **2010,** *110*, (11), 6736-6767.

(7) Brédas, J.-L.; Norton, J.E.; Cornil, J.; Coropceanu, V., Molecular Understanding of Organic Solar Cells: The Challenges. *Accounts of Chemical Research* **2009,** *42*, (11), 1691-1699.

(8) Cheng, Y.-J.; Yang, S.-H.; Hsu, C.-S., Synthesis of Conjugated Polymers for Organic Solar Cell Applications. *Chemical Reviews* **2009,** *109*, (11), 5868-5923.

(9) Liang, Y.; Yu, L., A New Class of Semiconducting Polymers for Bulk Heterojunction Solar Cells with Exceptionally High Performance. *Accounts of Chemical Research* **2010,** *43*, (9), 1227-1236.

(10) Brabec, C.J.; Gowrisanker, S.; Halls, J.J.M.; Laird, D.; Jia, S.; Williams, S.P., Polymer–Fullerene Bulk-Heterojunction Solar Cells. *Advanced Materials* **2010,** *22*, (34), 3839-3856.

(11) Wienk, M.M.; Kroon, J.M.; Verhees, W.J.H.; Knol, J.; Hummelen, J.C.; van Hal, P.A.; Janssen, R.A.J., Efficient Methano[70]fullerene/MDMO-PPV Bulk Heterojunction Photovoltaic Cells. *Angewandte Chemie International Edition* **2003,** *42*, (29), 3371-3375.

(12) Scharber, M.C.; Mühlbacher, D.; Koppe, M.; Denk, P.; Waldauf, C.; Heeger, A.J.; Brabec, C.J., Design Rules for Donors in Bulk-Heterojunction Solar Cells—Towards 10 % Energy-Conversion Efficiency. *Advanced Materials* **2006,** *18*, (6), 789-794.

(13) Anctil, A.; Babbitt, C.W.; Raffaelle, R.P.; Landi, B.J., Material and energy intensity of fullerene production. *Environmental science & technology* **2011,** *45*, (6), 2353-2359.

(14) Anctil, A.; Babbitt, C.W.; Raffaelle, R.P.; Landi, B.J., Cumulative energy demand for small molecule and polymer photovoltaics. *Progress in Photovoltaics: Research and Applications* **2013,** *21*, (7), 1541-1554.

(15) Sonar, P.; Fong Lim, J.P.; Chan, K.L., Organic non-fullerene acceptors for organic photovoltaics. *Energy & Environmental Science* **2011,** *4*, (5), 1558-1574.

(16) Li, C.; Wonneberger, H., Perylene Imides for Organic Photovoltaics: Yesterday, Today, and Tomorrow. *Advanced Materials* **2012,** *24*, (5), 613-636.

(17) Avlasevich, Y.; Li, C.; Mullen, K., Synthesis and applications of core-enlarged perylene dyes. *Journal of Materials Chemistry* **2010,** *20*, (19), 3814-3826.

(18) Herrmann, A.; uuml; llen, K., From Industrial Colorants to Single Photon Sources and Biolabels: The Fascination and Function of Rylene Dyes. *Chemistry Letters* **2006,** *35*, (9), 978-985.

(19) Gunter Buxbaum, G.P., *Industrial Inorganic Pigments, Third Edition*; Editor Ed.^Eds.;Wiley-VCH Verlag GmbH & Co. KGaA: 2005.

(20) Edvinsson, T.; Li, C.; Pschirer, N.; Schöneboom, J.; Eickemeyer, F.; Sens, R.; Boschloo, G.; Herrmann, A.; Müllen, K.; Hagfeldt, A., Intramolecular Charge-Transfer Tuning of Perylenes: Spectroscopic Features and Performance in Dye-Sensitized Solar Cells. *The Journal of Physical Chemistry C* **2007,** *111*, (42), 15137-15140.

(21) R. J. Muller, G.; Meiners, C.; Enkelmann, V.; Geerts, Y.; Mullen, K., Liquid crystalline perylene-3,4-dicarboximide derivatives with high thermal and photochemical stability. *Journal of Materials Chemistry* **1998,** *8*, (1), 61-64.

(22) Horowitz, G.; Kouki, F.; Spearman, P.; Fichou, D.; Nogues, C.; Pan, X.; Garnier, F., Evidence for n-type conduction in a perylene tetracarboxylic diimide derivative. *Advanced Materials* **1996,** *8*, (3), 242-245.

(23) Dittmer, J.J.; Lazzaroni, R.; Leclère, P.; Moretti, P.; Granström, M.; Petritsch, K.; Marseglia, E.A.; Friend, R.H.; Brédas, J.L.; Rost, H., et al., Crystal network formation in organic solar cells. *Solar Energy Materials and Solar Cells* **2000,** *61*, (1), 53-61.

(24) Venkataraman, D.; Yurt, S.; Venkatraman, B.H.; Gavvalapalli, N., Role of Molecular Architecture in Organic Photovoltaic Cells. *The Journal of Physical Chemistry Letters* **2010,** *1*, (6), 947-958.

(25) Dittmer, J.J.; Marseglia, E.A.; Friend, R.H., Electron Trapping in Dye/Polymer Blend Photovoltaic Cells. *Advanced Materials* **2000,** *12*, (17), 1270-1274.

(26) Rajaram, S.; Armstrong, P.B.; Kim, B.J.; Fréchet, J.M.J., Effect of Addition of a Diblock Copolymer on Blend Morphology and Performance of Poly(3-hexylthiophene):Perylene Diimide Solar Cells. *Chemistry of Materials* **2009,** *21*, (9), 1775-1777.

(27) Howard, I.A.; Laquai, F.; Keivanidis, P.E.; Friend, R.H.; Greenham, N.C., Perylene Tetracarboxydiimide as an Electron Acceptor in Organic Solar Cells: A Study of Charge Generation and Recombination. *The Journal of Physical Chemistry C* **2009,** *113*, (50), 21225-21232.

(28) Che, Y.; Datar, A.; Yang, X.; Naddo, T.; Zhao, J.; Zang, L., Enhancing One-Dimensional Charge Transport through Intermolecular π-Electron Delocalization: Conductivity Improvement for Organic Nanobelts. *Journal of the American Chemical Society* **2007,** *129*, (20), 6354-6355.

(29) Grimsdale, A.C.; Müllen, K., The Chemistry of Organic Nanomaterials. *Angewandte Chemie International Edition* **2005,** *44*, (35), 5592-5629.

(30) Holcombe, T.W.; Norton, J.E.; Rivnay, J.; Woo, C.H.; Goris, L.; Piliego, C.; Griffini, G.; Sellinger, A.; Brédas, J.-L.; Salleo, A., et al., Steric Control of the Donor/Acceptor Interface: Implications in Organic Photovoltaic Charge Generation. *Journal of the American Chemical Society* **2011,** *133*, (31), 12106-12114.

(31) Langhals, H.; Jona, W., Intense Dyes through Chromophore–Chromophore Interactions: Bi- and Trichromophoric Perylene-3,4:9,10-bis(dicarboximide)s. *Angewandte Chemie International Edition* **1998,** *37*, (7), 952-955.

(32) Langhals, H.; Saulich, S., Bichromophoric Perylene Derivatives: Energy Transfer from Non-Fluorescent Chromophores. *Chemistry – A European Journal* **2002,** *8*, (24), 5630-5643.

(33) Holman, M.W.; Yan, P.; Adams, D.M.; Westenhoff, S.; Silva, C., Ultrafast Spectroscopy of the Solvent Dependence of Electron Transfer in a Perylenebisimide Dimer. *The Journal of Physical Chemistry A* **2005,** *109*, (38), 8548-8552.

(34) Wilson, T.M.; Tauber, M.J.; Wasielewski, M.R., Toward an n-Type Molecular Wire: Electron Hopping within Linearly Linked Perylenediimide Oligomers. *Journal of the American Chemical Society* **2009,** *131*, (25), 8952-8957.

(35) Rajaram, S.; Shivanna, R.; Kandappa, S.K.; Narayan, K.S., Nonplanar Perylene Diimides as Potential Alternatives to Fullerenes in Organic Solar Cells. *The Journal of Physical Chemistry Letters* **2012,** *3*, (17), 2405-2408.

(36) Huang, C.; Barlow, S.; Marder, S.R., Perylene-3,4,9,10-tetracarboxylic Acid Diimides: Synthesis, Physical Properties, and Use in Organic Electronics. *The Journal of Organic Chemistry* **2011,** *76*, (8), 2386-2407.

(37) Anthopoulos, T.D.; de Leeuw, D.M.; Cantatore, E.; van 't Hof, P.; Alma, J.; Hummelen, J.C., Solution processible organic transistors and circuits based on a C70 methanofullerene. *Journal of Applied Physics* **2005,** *98*, (5), 054503.

(38) Huo, L.; Zhang, S.; Guo, X.; Xu, F.; Li, Y.; Hou, J., Replacing Alkoxy Groups with Alkylthienyl Groups: A Feasible Approach To Improve the Properties of

Photovoltaic Polymers. *Angewandte Chemie International Edition* **2011,** *50*, (41), 9697-9702.

(39) Gregg, B.A., Entropy of Charge Separation in Organic Photovoltaic Cells: The Benefit of Higher Dimensionality. *The Journal of Physical Chemistry Letters* **2011,** *2*, (24), 3013-3015.

Chapter 4

Charge generation and Transport Dynamics

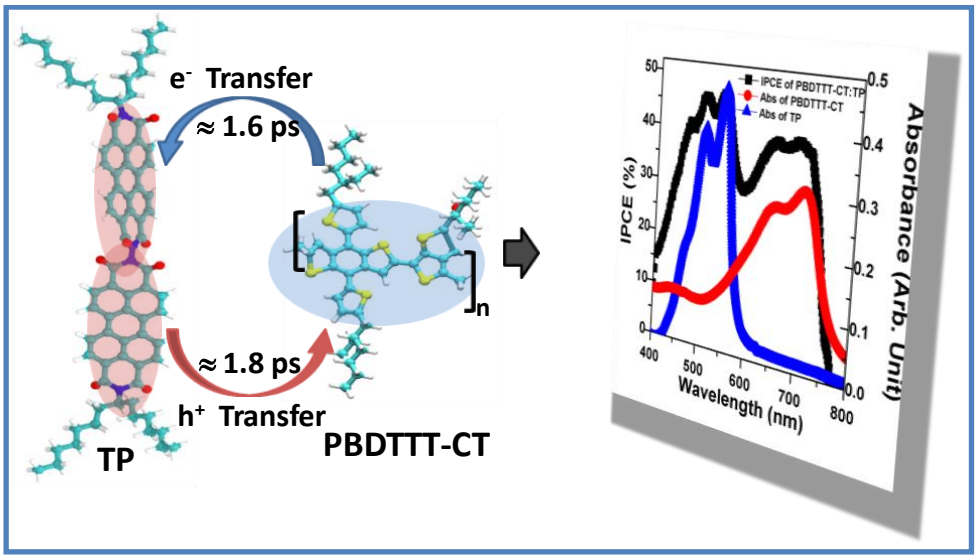

Advanced optical and electrical techniques are employed to investigate the origin of high current density in efficient non-fullerene based BHJ organic solar cells featuring TP as electron acceptor and PBDTTT-CT as electron donor molecules. Complete photoluminescence quenching of both the donor and acceptor excitons indicate the efficient electron and hole transfer processes. The intimate mixing of TP and donor polymer in 1:1 ratio by weight shows incident to current conversion efficiency (IPCE) 45 % in visible region. Power conversion efficiency of 3.2 % is obtained by further optimization blend ratio and device fabrication procedure. Ultrafast transient measurements reveal dissociation of both TP and PBDTTT-CT excitons on similar time scales of a few picoseconds. The magnitude of the polaron yield of PBDTTT-CT:TP blends is observed to be comparable to that in PBDTTT-CT:$PC_{70}BM$ blends and exhibits similar µs-decay dynamics.

4 Charge Generation and Transport Dynamics

Significant insight into the mechanisms of charge generation and recombination in interpenetrating networks of donor polymers and fullerene based acceptors used in BHJ organic solar cells can be gained through optical spectroscopy.(*1-3*) The trend in the structure–function relationships of BHJ has been observed using ultrafast transient absorption spectroscopy to provide valuable guidance for rational materials design and device engineering.(*4-6*) Quantum efficiency of a series of photo-physical processes in BHJ is dictated by the structure-function relationships. Each of the photo-physical processes such as exciton creation, exciton diffusion and charge transfer at the interface, charge dissociation and transport of free charges to the electrodes can be monitored and quantified using transient absorption spectroscopy.(*7-10*) Transient absorption spectroscopy is an optical pump-probe technique in which pump pulse excites the sample and probe pulse monitors the excited species.(*11*, *12*) The delay between pump and probe pulses provides the dynamics of the transient species under consideration. Recent progress in the ultrafast time resolution down to few tens of femtoseconds along with morphological studies of BHJ enhanced the understanding of ultrafast phenomena occur in organic BHJ systems.(*13-22*) However, additional routes other than design of donor polymer and improved nano-morphology of polymer:fullerene BHJ are need to be explore to increase the power conversion efficiency of the devices. One of such routes is the relatively less absorption of fullerene derivative acceptors in the photo-active layer.(*23*, *24*) Hence, despite the recent progress in research and development of novel donor polymers, there is a strong need for photo-physical studies of new electron acceptors likes perylenes with enhanced absorption in the visible in combination with good charge transport properties.

In the previous chapter, the low power conversion efficiencies of perylene derivative based electron acceptor BHJ solar cells corresponding to fullerene devices was addressed by material design and device fabrication techniques.(*25-31*) The low efficiency of these solar cells was mainly attributed to the tendency of crystallization of perylene molecules due to their strong π-π interactions leading to formation of large size crystal domains in the BHJ

films.(25) Previous transient absorption spectroscopic measurements on perylene tetracarboxydiimide based electron acceptor BHJ revealed that,(32) when the perylene molecules are finely dispersed in the polymer matrix, the device efficiency is limited by the very fast bimolecular recombination. When the perylene are coarser in the blend, the perylene singlet excitons are radiatively recombine before the charge transfer process due to their intermolecular relaxation. It was concluded that, the two loss channels always limits the quantum efficiency of perylene based molecules, unless perylenes structures are modified to suppress the rate of intermolecular state formation without compromising charge-transport properties. In the previous chapter, the planarity of the perylene was disrupted by the new design of twisted perylene (TP) which helped to increase the short circuit current density and device efficiency (> 2.75%) (Figure 4.1a).(33) The relatively high performance of the twisted perylene based BHJ device was attributed to a combination of factors including improved morphology, optimal electronic donor-acceptor (D-A) interface which can reduce early-recombination losses and an increase in PDI dimensionality which can lead to a lower barrier for charge separation. In this chapter, the impacts of these factors upon the enhanced device performance are addressed and further suggest strategies to overcome the loss processes in these blend systems. Steady-state absorption and photoluminescence spectroscopy, transient absorption measurements, and nano-morphological probes are used to correlate the device parameters as a function of blend composition and to determine differences in morphology, exciton migration, charge-transfer and charge-recombination dynamics of these polymer/TP blend films at different composition ratios. The results are compared against control data collected from PCBM blend films. The role of morphology in these polymer:TP systems and its correlation with the device performance is highlighted, suggesting routes to higher efficiency device performance for the non-fullerene BHJ solar cells.(34)

4.1 Steady-state photo-physical properties:

The steady state absorption and emission measurements were carried out on the low band-gap electron-donor polymer (PBDTTT-CT)(35-37), electron-acceptor twisted perylene (TP) and blends of different ratios of the molecules. The structures of these molecules are shown in the Figure 4.1a. The UV-visible absorption spectra in the ground state of PBDTTT-CT shows extended absorption till 800 nm with maximum peak λ^{abs}_{max} ~ 720 nm. TP films exhibit strong absorption in ~ 400-600 nm regime with maximum absorbance at ~ 540 nm (Figure 4.1b). The 1:1 ratio of PBDTTT-CT:TP BHJ film shows the additive nature of the

absorption from both the blend components. All the spectra are acquired in the solid state films formed by spin coating 12 mg/mL solution in anhydrous chlorobenzene for 60 s on top of quartz substrate. The thickness of the films is ~ 100 nm as measured from the Dektak profilometer. This shows that the TP has higher extinction co-efficient than the donor polymer in λ ~ 400 - 600 nm. The low-energy absorption corresponds to excitation of the PBDTTT-CT singlet exciton. The blends of different ratios also exhibit the additive nature of absorption of the PBDTTT-CT:TP components.(*34*)

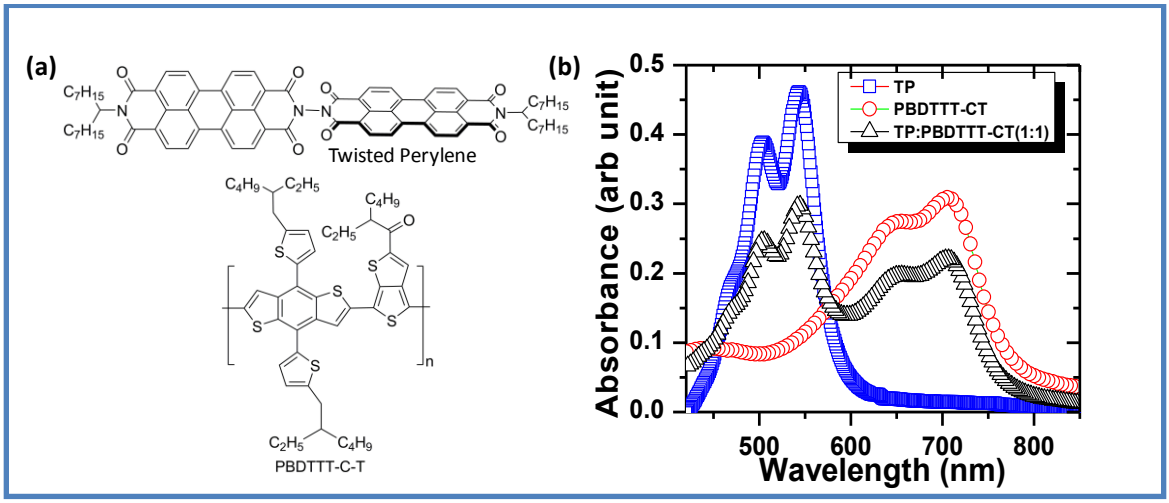

Figure 4.1: (a) Structure of Twisted perylene (TP) and PBDTTT-CT. (b) Absorption spectra of TP, PDBTTT-CT and 1:1 ratio of PBDTTT-CT:TP films; films were spun on glass substrates at 1500 rpm for 60 s from 12 mg/ml concentrated chlorobenzene solution.(Reproduced with permission from the reference(34))

The steady state photoluminescence (PL) spectra of neat PBDTTT-CT and TP films are shown in the Figure 4.2. The spectra indicate emission maxima, λ^{emis}_{max}, at 820 nm and 650 nm for PBDTTT-CT and TP respectively. The emission from the neat TP film is one order of magnitude higher than the PBDTTT-CT film when excited at 543 nm. This corresponds to two reasons: higher extinction coefficient of TP than PBDTTT-CT at 543 nm, and PL quantum yield of TP is higher than PBDTTT-CT. Comparison of the PL of 1:1 blend films with that of neat films indicates complete quenching (> 99 %) of both the PBDTTT-CT and TP emission, and suggests efficient charge transfer between PBDTTT-CT and TP driven by both PBDTTT-CT and TP excitons (Figure 4.2). The insets of the Figure 4.2a and 4.2b represents the possibility of both electron and hole transfer processes. The HOMO and LUMO levels of the PBDTTT-CT and TP align as type II heterojunction systems, and band offsets favors both electron and hole transfer. At higher wavelengths (400 - 600 nm), TP has

larger extinction coefficient over PBDTTT-CT and hence charge generation by efficient hole transfer is expected. Similarly, for lower wavelength regions (600 - 800 nm), only PBDTTT-CT has absorption and expected to have good electron transfer.(1)

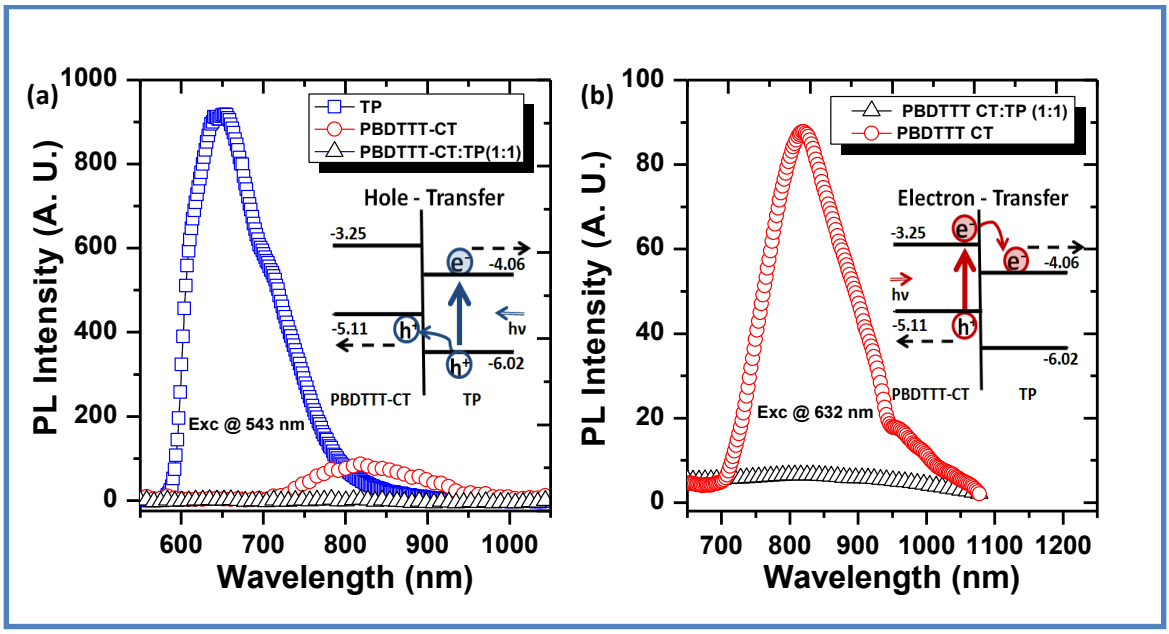

Figure 4.2: Steady state PL spectra of films(a) excited at 543 nm showing emission maxima at 650 nm and 820 nm for pristine TP(blue) and PBDTTT-CT(red) respectively and quenches to >99 %(black) by blending PBDTTT-CT and TP in 1:1weight ratio [inset: schematic of hole transfer mechanism], (b) excited at 632 nm showing emission maxima at 820 nm for pristine PBDTTT-CT(red) which quenches to 99 %(black) by blending PBDTTT-CT and TP in 1:1 weight ratio [inset: schematic of electron transfer]. .(Reproduced with permission from the reference(34))

4.2 Transient absorption spectroscopy

Photoluminescence quenching is an indicator of the efficiency of exciton quenching at the D-A interface; however it is not a reliable measure of the yield of fully dissociated charges. In particular it is insensitive to the non-radiative geminate recombination of the initially generated polaron pairs (or 'charge-transfer(CT)' states) prior to their dissociation into separated charges.(1) As such PL quenching can only provide an indication of an upper limit to the yield of dissociated charges. In order to quantify this yield further, transient absorption spectroscopy (TAS) is employed to monitor the yield of dissociated polarons in such donor:acceptor blend films.(38-40)

4.2.1 *μs*-Transient absorption spectroscopy

The generated free charges in the BHJ films exhibit bimolecular recombination in the timescale of microseconds (μs). To quantify the yield of free charges (polarons),

microsecond transient absorption studies of blend films were carried out with low-intensity (typically 0.8 μJ/cm^2) excitation conditions. The pristine films TP and PBDTTT-CT gave negligible transient signals on the timescales studied. Figure 4.3 represents the transient absorption spectrum, ΔOD(λ,t), of PBDTTT-CT:TP blend film at t ≈ 1μs. The spectrum indicates enhanced broad near infrared absorption in the range 800 nm - 1400 nm assigned to formation of PBDTTT-CT positive polarons. These signals are an order of magnitude in excess of that of neat PBDTTT-CT film measured under same conditions.

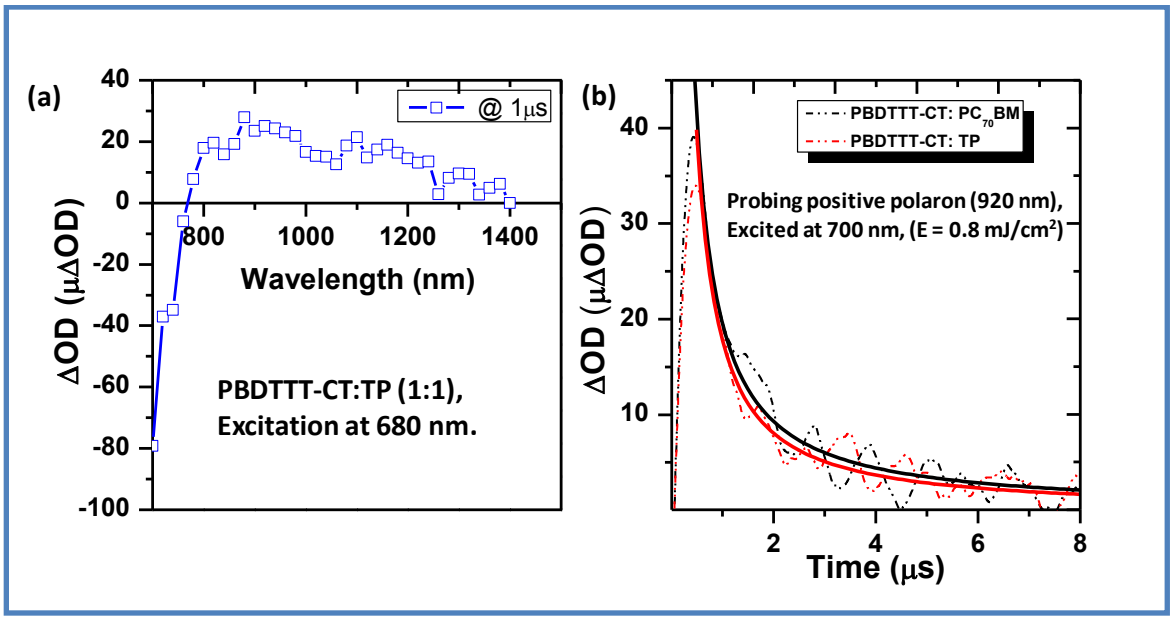

Figure 4.3: (a) μs-Transient absorption spectra of PBDTTT-CT:TP (1:1) film, pumped at 640 nm (and probed at 1 μs showing a broad absorption from 740 nm to 1400 nm having a maximum at 900 nm. (b) compares decay dynamics of positive polaron absorption of PBDTTT-CT at 920 nm by blending with TP and PC70BM acceptors, exhibiting power law decay($\Delta OD(t) = At^{-\alpha}$) (solid lines) with similar amplitudes and decay kinetics.(excitation at 700 nm, 0.8 μJ/cm^2). (Reproduced with permission from the reference (34))

The ΔOD(t) signal for λ < 700 nm exhibits negative magnitude which arises from the ground state photobleaching of the PBDTTT-CT molecules. The signature of negative polarons from TP molecules, expected to be in the region of λ ≈ 600-800 nm, is overlapped by the ground state absorption of PBDTTT-CT. Hence in our study the dynamics of charge generation is correlated using positive polaron of PBDTTT-CT molecules. Further, the transient signals exhibited oxygen-independent decay dynamics, indicative to polaron contribution rather than triplet exciton formation. The Figure 4.3b shows a comparison of this PBDTTT-CT polaron signal between PBDTTT-CT:TP and PBDTTT-CT:PCBM films, employing matched excitation densities (0.8 μJ/cm2) and donor-acceptor concentration ratio

(1:1). It is apparent that both the transients are very similar in amplitude and decay dynamics, indicating similar charge generation and recombination dynamics in these two blend films. In addition, the magnitude of the ΔOD(λ,t) is comparable in both the blends, hence the yield of free charges in TP blend is comparable to $PC_{70}BM$ blend.

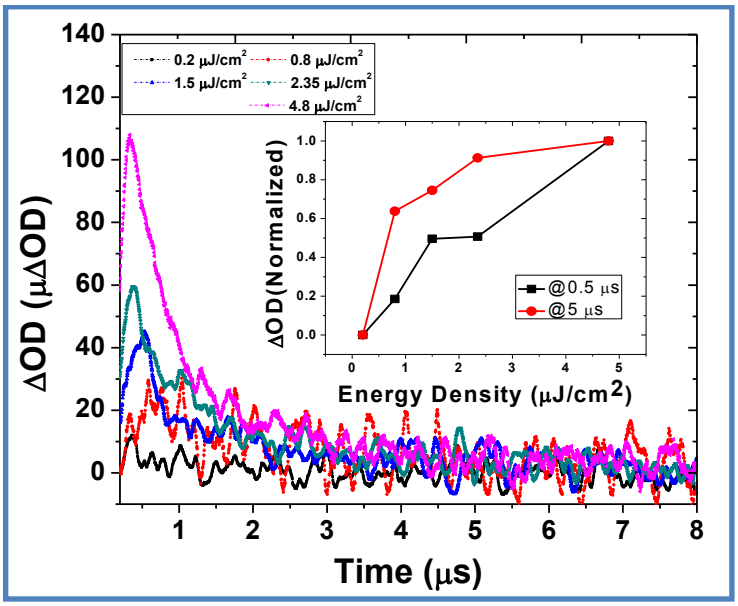

Figure 4.4: Excitation density dependence with ΔOD(t)(all transient are probed at 920 nm excited at 700 nm), Inset shows the normalized ΔOD(t) vs excitation density at 0.5 μs and 5 μs. (Reproduced with permission from the reference (34))

The excitation density dependence on the transient signal prior to 1 μs indicates the extent of geminate recombination in the system. In PBDTTT-CT:TP blends, the amplitudes of the transient signals were observed to vary approximately linearly with excitation density up to 4 μJ/cm2 (Figure 4.4), indicating that neither saturation effects nor non-geminate recombination losses prior to 1 μs distorted this comparison significantly. It should be noted that for other perylene systems, this saturation occurs at much higher intensities.(41) The decay of these absorption transients exhibited power law decays ($\Delta OD(t) = At^{-\alpha}$), consistent with the non-geminate recombination of dissociated charge carriers, as we have discussed previously for other polymer:acceptor blends.(38, 42, 43) This transient absorption signal is therefore assigned to the transient absorption of free PBDTTT-CT positive polarons.

Incident photon to current conversion efficiency (IPCE) measurements are carried out in order to quantify the effect of charge generation and charge collection from both PBDTTT-CT and TP excitons in the blend devices. Different donor-acceptor composition ratios are quantified to correlate the effect of TP content on generation of free charges in the

circuit. In the λ range of 400 - 600 nm, the larger oscillator strength of TP compared to PBDTTT can result in a higher photoinduced hole transfer from TP excitons. Similarly, in the 600 - 800 nm range the higher absorption of PBDTTT-CT should predominantly lead to electron transfer from PBDTTT-CT excitons. The IPCE spectrum follows the trend of the blend absorption and indicates charge generation from both TP and PBDTTT-CT excitons (Figure 4.5a).

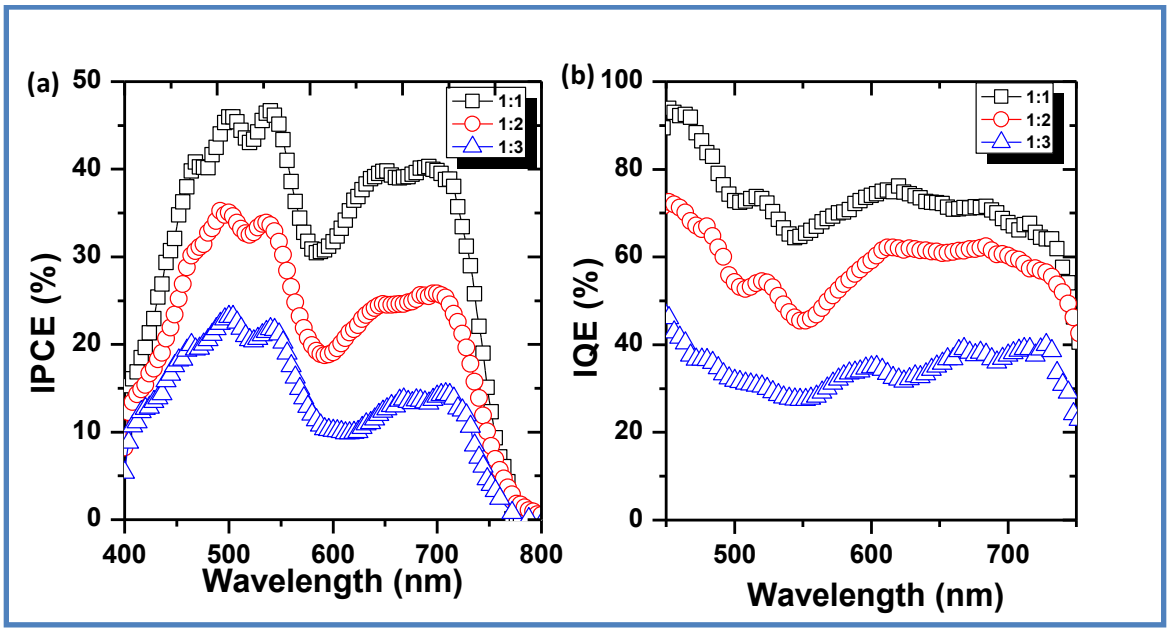

Figure 4.5: (a) IPCE spectra of PBDTTT-CT:TP at different weight ratios 1-1(black), 1-2(red) and 1-3(blue), (b) the corresponding internal quantum efficiencies of these blends. (Reproduced with permission from the reference (34))

A maximum of 46 % IPCE is observed for the 1-1 ratio blend at λ~ 540 nm, showing higher contribution to photocurrent from TP absorption. Increasing the TP ratio in blend, whilst maintaining constant film thickness, decreases the overall IPCE of the device. Also, as the blend composition is increased to TP contents of 66 % and 75 %, the transient absorption amplitude of blend films decreases (Figure 4.6). Internal quantum efficiency (IQE) spectra estimated from optical transmission and IPCE data (without correction for optical interference effects) confirm charge generation from both PBDTTT-CT and TP excitons, with slightly higher quantum efficiencies observed following PBDTTT-CT excitation (Figure 4.5b). At higher TP contents, the IQE is reduced for both PBDTTT-CT and TP excitation. Overall these trends suggest that 50% by wt is near the optimum TP concentration in the blend films for efficient charge generation, which is also evident from the J-V characteristics (Table 2).

The internal quantum efficiency $\eta_{IQE}(\lambda)$ was obtained from the following equation:

$$\eta_{IQE}(\lambda) = \frac{\eta_{EQE}(\lambda)}{abs(\lambda)}$$

Where, $\eta_{EQE}(\lambda)$ is the external quantum efficiency and $abs(\lambda)$ is the percentage absorbance. The overall $abs(\lambda)$ absorbance (%) of the devices is calculated from the transmission mode spectra of the films coated on ZnO-ITO substrates. It was made certain that these films were identical (thickness) to films used for the active devices.

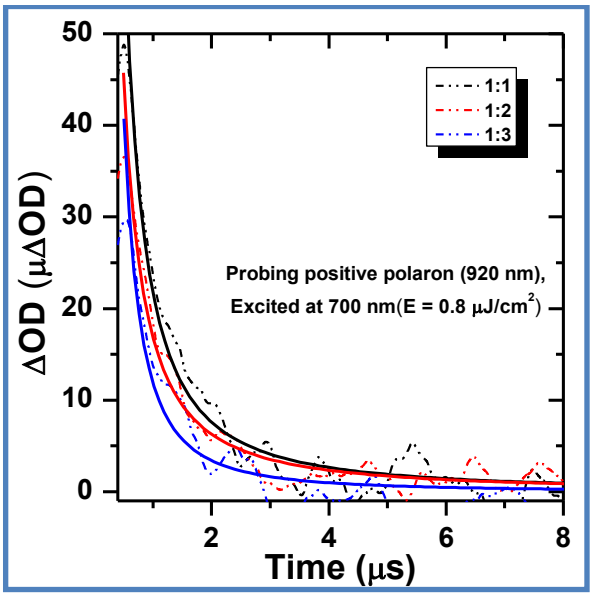

Figure 4.6: Concentration dependence on the TAS. The blend consist of 1:1, 1:2 and 1:3 ratio of PBDTTT-CT:TP films are excited at 700 nm (0.8 μJ/cm^2) and transient signal at 920 nm is monitored. The films containing higher TP molecules exhibit lower magnitude of positive polaron yield. (Reproduced with permission from the reference (34))

4.2.2 *fs*-Transient absorption spectroscopy

The early processes of charge generation like singlet exciton diffusion, quenching and dissociation are monitored using femtosecond transient absorption spectroscopy. The dynamics of the charge separation following generation of both TP and PBDTTT-CT excitons are investigated using this technique.(4, 32, 44-47) Transient absorption spectra of both pristine film and the blend film are measured from 200 fs to 6 ns in the visible and near IR region (Figure 4.7a – 4.7c).

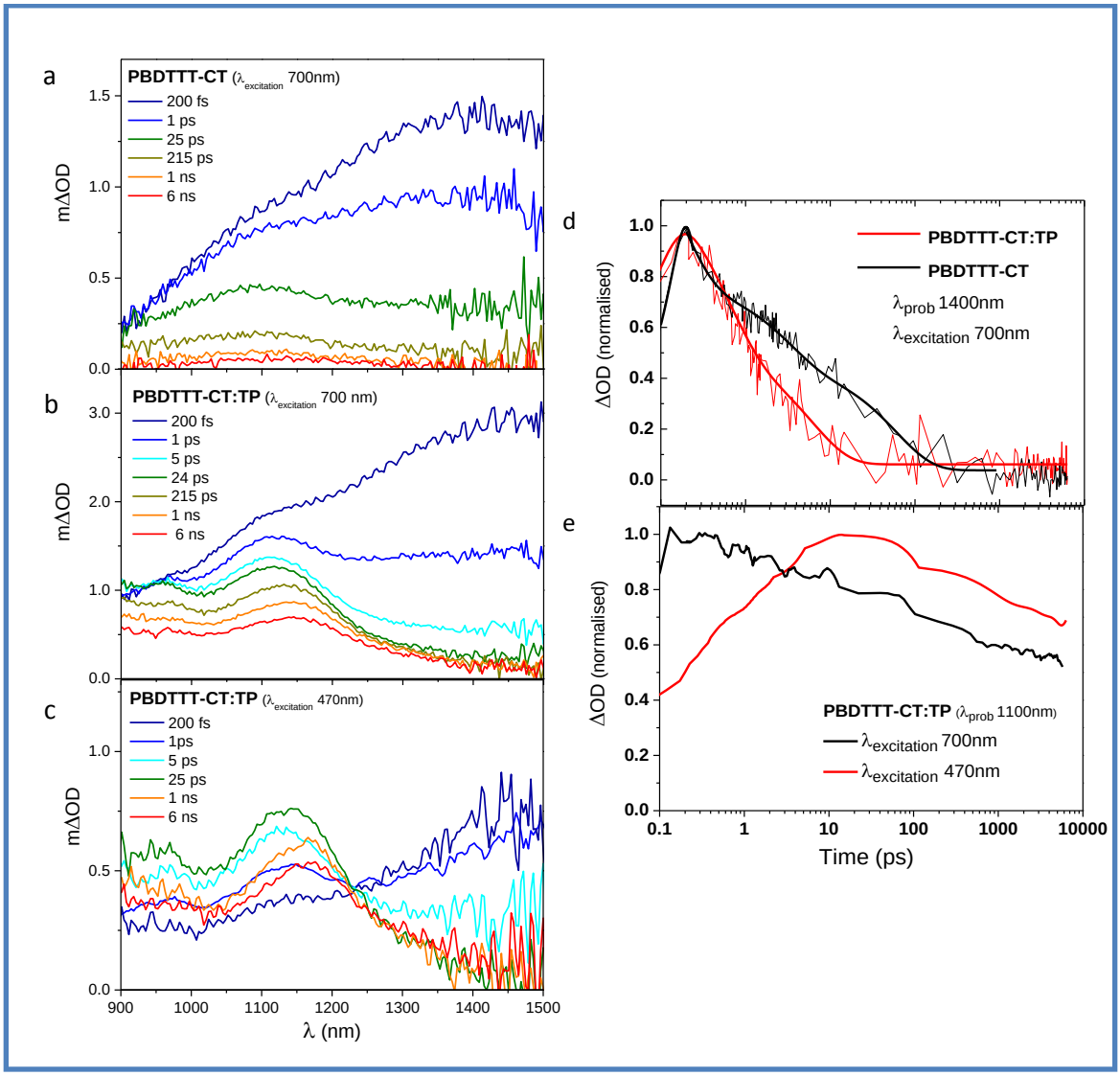

Figure 4.7: fs- Transient absorption spectra of (a) neat PBDTTT-CT excited at 700 nm, (b) blend of PBDTTT-CT:TP excited at 700 nm and (c) excited at 470 nm. (d) Transient absorption decay dynamics for neat PBDTTT-CT (black) and PBDTTT-CT:TP blend (red) excited at 700nm and probed at 1400 nm(black). (e) Transient absorption decay dynamics of PBDTTT-CT:TP blend probed at 1100 nm and excited at 700 nm (black) and 470 nm (red). (Reproduced with permission from the reference(34))

The pristine and blend films are excited at an excitation intensity of 2 μJ/cm^2 at 470 and 700 nm. Data as a function of excitation density show the absence of non-linear processes (e.g. exciton-exciton annihilation) at this excitation density. For an excitation wavelength of 470 nm, the primary excitation is of TP excitons while polymer excitation is insignificant. At 700 nm excitation, only polymer is excited.

The transient absorption spectra (ΔOD) of neat PBDTTT-CT polymer film (excited at 700 nm) as a function of time delay are shown in the Figure 4.7a. These ΔOD spectra exhibit a photoinduced band peaking at around 1400 nm, which is assigned to PBDTTT-CT exciton

absorption. The decay of this photoinduced absorption exhibits rather dispersive, biphasic dynamics, with a half time of 10 ± 2 ps, assigned to the decay of photogenerated singlet excitons. A small residual, long lived signal is also observed and assigned to polaron/triplet states generated in the neat film. Analogous data for neat TP films showed no measurable signals over this spectral range, indicating TP excitons do not absorb significantly over this spectral range.

The transient spectra of blend films selectively exciting polymer excitons and monitoring the decay dynamics are shown in the figure 4.7b. ΔOD spectra of PBDTTT-CT:TP blends at early timescale (200 fs) have spectra similar to that of neat polymer film (Figure 4.7a), indicating that in the blend, polymer excitons are also initially photogenerated. However, this initial spectrum rapidly evolves to new spectra with absorption maxima at ~ 1100 nm and < 900 nm, assigned, by comparison with the microsecond data, to PBDTTT-CT positive polarons. This evolution can be monitored most easily from the decay dynamics of the 1350-1400 nm singlet exciton absorption band (Figure 4.7d, black line). It is apparent that in the blend film, this exciton absorption band decays with a 1.6 ± 0.4 ps half-time, assigned to photoinduced electron transfer from the PBDTTT-CT exciton into the TP acceptor. This electron transfer is approximately an order of magnitude faster than the singlet exciton lifetime in the neat film (10 ± 2 ps), consistent with the high efficiency of this photoinduced electron transfer process.

Considering the transient data collected following 470 nm pumping of the blend film, corresponding to primarily TP excitation. Again at early times, the transient spectrum resembles that of the neat PBDTTT-CT film, although with a relatively small amplitude, consistent with the low PBDTTT-CT absorption at 470 nm (the low amplitude and instrument response limited rise of this PBDTTT-CT singlet exciton absorption indicates this signal does not originate from energy transfer, i.e, from TP excitons to PBDTTT-CT). As for 700 nm excitation, the long time delay spectrum is indicative of PBDTTT-CT polarons. However it is striking to observe that when probing at 1100 nm, the peak of PBDTTT-CT polaron absorption, a pronounced rise time is observed with a half-time of 1.8 ± 0.4 ps (Figure 4.7e). This rise cannot be assigned to spectral evolution from PBDTTT-CT excitons (which absorb more strongly than polarons at this wavelength) and is therefore assigned to hole transfer from TP excitons to PBDTTT-CT. We thus conclude that photoinduced charge separation from TP excitons proceeds with a half-time of 1.8 ± 0.4 ps, on a similar timescale to charge separation from PBDTTT-CT excitons. It is possible that the half-times for these

photoinduced charge separation processes may be limited, at least in part, by exciton migration to the polymer:TP interface. Nevertheless, in terms of charge separation efficiency, both charge separation half-times are fast relative to excite state decay to ground, consistent with relatively intimate mixing of the blend on a length scale much less than the material exciton diffusion lengths, consistent with our PL quenching and structural analyses.

4.2.3 Förster Resonance Energy Transfer (FRET):

The photoluminescence (PL) from the TP molecule overlaps very well with the PBDTTT-CT polymer. This gives us a possibility of energy transfer process from TP to PBDTTT-CT polymer. Hence, TP acts as FRET-donor and PBDTTT-CT acts a FRET-acceptor. The simple experiment to identify the energy transfer process is to monitor the emission from FRET-acceptor by exciting FRET-donor (TP). However, the blend exhibits > 99 % of PL quenching for both PBDTTT-CT and TP in the blend. Hence steady state measurements were not able to identify the mechanism of FRET in this system.

The efficient PL quenching of TP gives two possible path ways: 1) energy transfer to PBDTTT-CT or 2) hole transfer to PBDTTT-CT. At this point we can analyze the transient absorption spectra of blend films excited at 470 nm (TP excitation). In Figure 4.7c, the 1400 nm band corresponding to singlet exciton of PBDTTT-CT decays monotonically without any increase in the ΔOD, whereas the 1100 nm band corresponding to polymer cation (hole) exhibits increased ΔOD upto few tens of picoseconds followed by decay in the magnitude. This suggests that the TP excitation prominently increased the population of polymer cation (holes) when compared to polymer singlet exciton. Hence in this system, charge transfer from TP to PBDTTT-CT is more prominent than energy transfer.

All the transient absorption measurements were carried out on the solid state films of BHJ consisting of PBDTTT-CT and TP at different weight ratios (1:1. 1:2 and 1:3 of PBDTTT-CT:TP). All the active layers were spin coated onto cleaned quartz substrates at 1000 rpm from blend concentration of 12 mg/mL for 60 s. All the blends were dissolved in anhydrous chlorobenzene and spin coated inside nitrogen filled glove box. During TAS measurements, the films were places in a custom made chamber consisting of continuous flow of nitrogen. For triplet quenching measurements, intentionally oxygen was allowed in order to monitor the sensitization of triplet states with the oxygen molecules. As mentioned in the before, in *μs*-TAS excitation density was ~ 0.8 μJ/cm^2 while for *fs*-TAS it was ~ 2 μJ/cm^2.

4.3 Charge transport studies

Efficient photo-induced charge generation should be followed by efficient charge extraction processes in ideal situation. The comparable charge carrier yield accompanied by lower efficiency compared to fullerene based BHJ indicates the limiting factors posed by the transport processes.

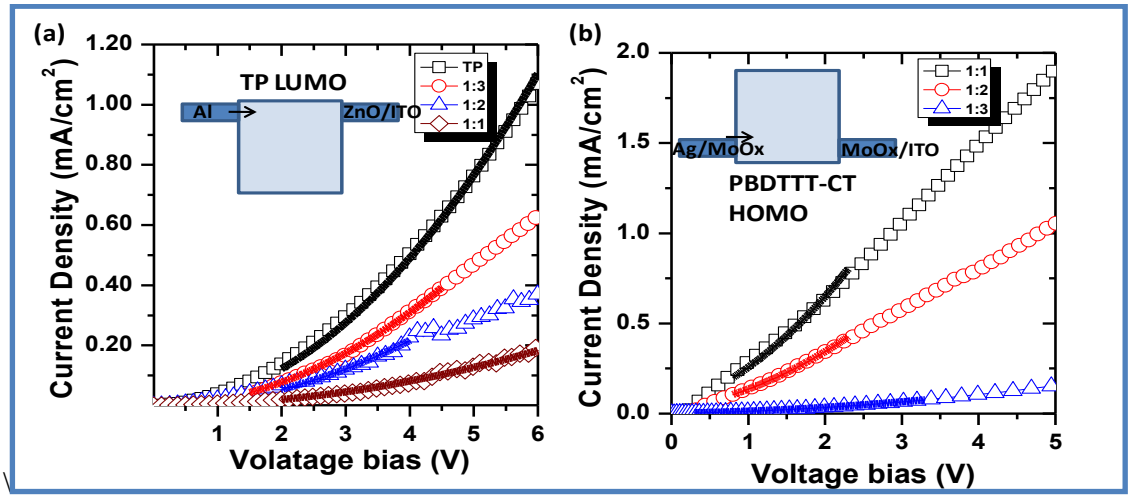

Figure 4.8: SCLC measurement showing the J- V curves for electron-only (a) and hole-only (b) devices consisting of different TP compositional ratio in the blend. The applied bias is corrected for the built-in potential (V_{bi}) so that $V=V_{applied}-V_{bi}$. (Reproduced with permission from the reference(34))

SCLC measurements on the TP blends highlight the difference in carrier mobility brought out by compositional variations.(48-51) The electron and hole mobilities were measured separately in electron only and hole only devices (Figure 4.8).The electron only devices are fabricated by coating 1:1 ratio active layer onto ZnO coated ITO substrate working as electron extracting and Al as electron injecting electrode. The hole only device were fabricated on to MoO_x coated ITO substrate working as hole injecting and MoO_x/Ag as hole extracting electrode. All the films were coated at 1000 rpm with blend concentration of 12 mg/ml for 60 s. The thicknesses of active layer were measured using Dektak profilometer exhibiting thickness in the range of 1.5 - 2.5 µm.

Dark *J-V* curves of devices are fitted to SCLC model at low voltages using Mott–Gurney equation(50),

$$J = 9\varepsilon_o\varepsilon_r\mu V^2/8L^3$$

Where, J is space charge limited current, ε_o is the permittivity of free space, ε_r is the permittivity of the polymer, μ is the carrier mobility, and L is the device thickness. The mobilities are summarized in Table 1.

PBDTTT-CT:TP (wt:wt)	μ_e (cm^2/Vs) x 10^{-4}	μ_h (cm^2/Vs) x 10^{-4}
1-1	1.47 ± 0.29	2.74 ± 0.38
1-2	3.08 ± 0.51	0.98 ± 0.45
1-3	4.47 ± 0.69	0.72 ± 0.53

Table 1: *Charge mobilities in the blend films of different compositional ratio in electron only and hole only devices. (Reproduced with permission from the reference (34))*

A key aspect of the results is that 1:1 ratio blend reveals a more balanced charge transport similar to fullerene based BHJs.(50) The interesting point to be noted is that, the hole mobility is higher than the electron mobility for optimized 1:1 ratio.

4.4 Device optimization:

The device characterization of blends of different compositional ratio was carried out in inverted BHJ device geometry (ITO/ZnO/PBDTTT-CT:TP/MoO_x/Ag). Current density-voltage (J-V) characteristics of the devices measured under AM 1.5G irradiation are shown in Figure 4.9. The resulting J_{sc}, V_{oc}, *FF*, and *PCE* values, as determined from the *J-V* curves, are summarized in Table 2.

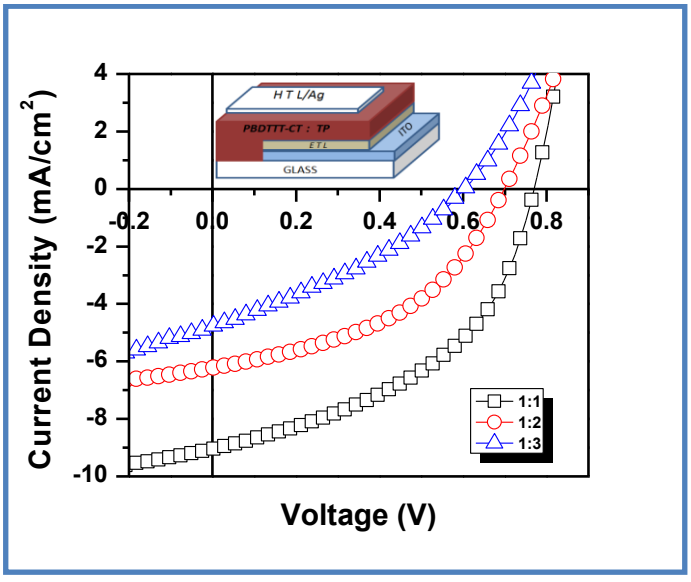

Figure 4.9: J-V characteristics of PBDTTT-CT:TP devices with different compositional ratio of 1:1(black), 1:2(red) and 1:3(blue) under illumination of an AM 1.5G solar simulator (100 mW/cm^2). Inset shows the schematic of inverted device structure fabricated for testing BHJ-OSC's.(Reproduced with permission from the reference(34))

Increasing the composition of acceptor in the blend from 50 % to 75 % decreased all the device parameters and their efficiency. Maximum device efficiency of 3.2 % was achieved for 50 % composition of TP. As evident from the table the J_{sc}, V_{oc} and *FF* decrease drastically for 75 % acceptor composition, indicating of a threshold composition ratio for efficient charge transport and collection.

PBDTTT-CT:TP (wt:wt)	**J_{sc} (mA/cm^2)**	**V_{oc} (V)**	**Fill factor (%)**	**η (%)**	**ΔOD (μΔOD)**
1:1	9.0	0.77	46.5	3.20	25.0
1:2	6.2	0.70	44.4	1.93	20.1
1:3	4.8	0.60	32.3	0.94	18.6

Table 2: *Device performance of PBDTTT-CT:TP BHJ solar cell at different acceptor ratio under AM 1.5, 1 sun unit illumination. Final column represents corresponding ΔOD at 1μs of blends when pumped at 700 nm with E=0.8 μJ/cm^2 and probed at 920 nm.(Reproduced with permission from the reference (34))*

Inverted devices were fabricated on patterned ITO-coated glass substrate. The ITO substrates were cleaned with RCA treatment (a mixture of hydrogen peroxide (H2O2), ammonium hydroxide (NH4OH) and water (1:1:5 by volume) at 80 °C for 15 minutes) to make substrate hydrophilic. The zinc acetate dihydrate (314 mg), 2-methoxyethanol (3.14 mL), and ethanolamine (86 μL) was mixed and stirred vigorously for 2 h at 60 °C in air. The precursor is now spin coated at 2000 rpm on to cleaned ITO substrates to get a smooth ZnO films. Crystalline ZnO films were obtained by subsequent annealing of substrate at 250 °C for 30 min in air. The blends of different weight ratio of PBDTTT-CT:TP is mixed in anhydrous chlorobenzene with blend concentration of 12 mg/mL. These blend solutions were spin coated on to ZnO substrate inside the glove box at 1000 rpm. The Hole transport layer MoOx (≈11 nm) and Ag (≈100 nm) was deposited by shadow mask method through physical vapor deposition at a base pressure of 10^{-6} mbar.

4.5 Morphological studies

Atomic force microscopy (AFM) scans were carried out for 1-1 ratio blend films spun coated on the ITO substrate with similar fabrication condition as that of devices (Figure 4.10).

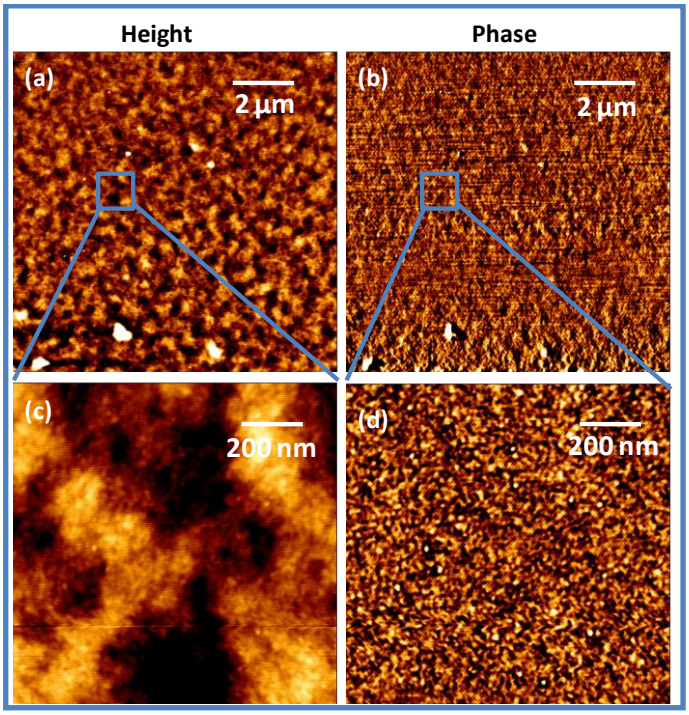

Figure 4.10: AFM images of PBDTTT-CT:TP of 1:1 weight ratio blend film in intermittent contact mode. (a) topography, (b) phase image of 10 x 10 µm^2 area scan and (c) topography, (d) phase image of 1 x 1 µm^2 area scan. (Reproduced with permission from the reference(34))

The large area scans of 10 x 10 µm^2 show a smooth surface morphology with average root mean square roughness of 8 nm, and the corresponding phase image exhibits features smaller than instrument resolution. Scanning on the smaller area of 1 x 1 µm^2, the phase image displays domains of average size about 10 nm. This implies the system achieves mixing of both TP and PBDTTT-CT in the blend on the 10 nm or less length scale, consistent with high PL quenching. Maximum donor-acceptor interfacial area with optimum domain sizes is required not just for efficient charge generation but also charge transport.(52, 53)

In the previous observations, the planar perylene blend films typically exhibit larger domains, sometimes extending upto micron size.(33) From this study we conclude that, though the intermittent mixing of blend is efficient in charge generation, and has improved device performance, however, the device efficiencies are still limited by optimized transport through the donor –acceptor percolation network. Fine tuning the morphology during fabrication processes have indicated that the performance of the device can be further enhanced. The efficiency of the devices is further optimized by engineering active-layer: buffer-layer interface which will be discussed in the subsequent chapters.

4.6 Summary:

The origin of high current density in efficient non-fullerene based bulk heterojunction (BHJ) organic solar cells employing a non-planar perylene dimer (TP) as an electron acceptor and a thiophene based donor polymer PBDTTT-CT are investigated using electrical and optical techniques. The optimized device composition of TP based BHJs exhibit one of the highest reported power conversion efficiencies for non-fullerene acceptor based organic solar cells ($\eta \approx 3.2$ %). The prerequisite condition (high J_{sc}) of sizable charge generation yields in TP based BHJ is verified by a combination of transient and steady-state photophysical measurements. Strong PL quenching of both the donor and acceptor emission indicates efficient electron and hole transfer processes at the PBDTTT-CT:TP interface. The near-IR pump-probe experiments and IPCE measurements demonstrate that polarons are generated from both the polymer and TP excitons. It was observed that in these blends, electron and hole transfer processes occur on a similar time scale of a few picoseconds. In the microsecond timescale, the magnitude of polaron yield of PBDTTT-CT:TP blends is comparable to that of fullerene blends and exhibits similar decay dynamics. Efficient charge generation and transport is observed in devices with 50% by weight composition of TP acceptor. Based, on the charge generation yield and decay dynamics it is reasonable to expect efficiencies comparable to fullerene systems. The molecular, interfacial and morphology aspects of BHJ's with TP as an acceptor suggests its role as a promising model system for efficient hole transferring system and paves a route to efficient, fullerene-free BHJ solar cells.

References:

(1) Clarke, T.M.; Durrant, J.R., Charge Photogeneration in Organic Solar Cells. *Chemical Reviews* **2010,** *110*, (11), 6736-6767.

(2) Howard, I.A.; Hodgkiss, J.M.; Zhang, X.; Kirov, K.R.; Bronstein, H.A.; Williams, C.K.; Friend, R.H.; Westenhoff, S.; Greenham, N.C., Charge Recombination and Exciton Annihilation Reactions in Conjugated Polymer Blends. *Journal of the American Chemical Society* **2010,** *132*, (1), 328-335.

(3) Howard, I.A.; Laquai, F., Optical Probes of Charge Generation and Recombination in Bulk Heterojunction Organic Solar Cells. *Macromolecular Chemistry and Physics* **2010,** *211*, (19), 2063-2070.

(4) Etzold, F.; Howard, I.A.; Forler, N.; Cho, D.M.; Meister, M.; Mangold, H.; Shu, J.; Hansen, M.R.; Müllen, K.; Laquai, F., The Effect of Solvent Additives on Morphology and Excited-State Dynamics in PCPDTBT:PCBM Photovoltaic Blends. *Journal of the American Chemical Society* **2012,** *134*, (25), 10569-10583.

(5) Etzold, F.; Howard, I.A.; Mauer, R.; Meister, M.; Kim, T.-D.; Lee, K.-S.; Baek, N.S.; Laquai, F., Ultrafast Exciton Dissociation Followed by Nongeminate Charge Recombination in PCDTBT:PCBM Photovoltaic Blends. *Journal of the American Chemical Society* **2011,** *133*, (24), 9469-9479.

(6) Howard, I.A.; Mauer, R.; Meister, M.; Laquai, F., Effect of Morphology on Ultrafast Free Carrier Generation in Polythiophene:Fullerene Organic Solar Cells. *Journal of the American Chemical Society* **2010,** *132*, (42), 14866-14876.

(7) Kraabel, B.; Lee, C.H.; McBranch, D.; Moses, D.; Sariciftci, N.S.; Heeger, A.J., Ultrafast photoinduced electron transfer in conducting polymer—buckminsterfullerene composites. *Chemical Physics Letters* **1993,** *213*, (3–4), 389-394.

(8) Brabec, C.J.; Zerza, G.; Cerullo, G.; De Silvestri, S.; Luzzati, S.; Hummelen, J.C.; Sariciftci, S., Tracing photoinduced electron transfer process in conjugated polymer/fullerene bulk heterojunctions in real time. *Chemical Physics Letters* **2001,** *340*, (3–4), 232-236.

(9) Hwang, I.-W.; Moses, D.; Heeger, A.J., Photoinduced Carrier Generation in P3HT/PCBM Bulk Heterojunction Materials. *The Journal of Physical Chemistry C* **2008,** *112*, (11), 4350-4354.

(10) Zhang, F.; Jespersen, K.G.; Björström, C.; Svensson, M.; Andersson, M.R.; Sundström, V.; Magnusson, K.; Moons, E.; Yartsev, A.; Inganäs, O., Influence of Solvent Mixing on the Morphology and Performance of Solar Cells Based on Polyfluorene Copolymer/Fullerene Blends. *Advanced Functional Materials* **2006,** *16*, (5), 667-674.

(11) Megerle, U.; Pugliesi, I.; Schriever, C.; Sailer, C.F.; Riedle, E., Sub-50 fs broadband absorption spectroscopy with tunable excitation: putting the analysis of ultrafast molecular dynamics on solid ground. *Applied Physics B* **2009,** *96*, (2-3), 215-231.

(12) Brida, D.; Manzoni, C.; Cirmi, G.; Marangoni, M.; Bonora, S.; Villoresi, P.; Silvestri, S.D.; Cerullo, G., Few-optical-cycle pulses tunable from the visible to the mid-infrared by optical parametric amplifiers. *Journal of Optics* **2010,** *12*, (1), 013001.

(13) Mukhopadhyay, S.; Das, A.J.; Narayan, K., High Resolution Photocurrent Imaging of Bulk Heterojunction Solar Cells. *The Journal of Physical Chemistry Letters* **2013,** *4*, 161-169.

(14) Grancini, G.; Maiuri, M.; Fazzi, D.; Petrozza, A.; Egelhaaf, H.J.; Brida, D.; Cerullo, G.; Lanzani, G., Hot exciton dissociation in polymer solar cells. *Nat Mater* **2013,** *12*, (1), 29-33.

(15) Bakulin, A.A.; Rao, A.; Pavelyev, V.G.; van Loosdrecht, P.H.; Pshenichnikov, M.S.; Niedzialek, D.; Cornil, J.; Beljonne, D.; Friend, R.H., The Role of Driving Energy and Delocalized States for Charge Separation in Organic Semiconductors. *Science* **2012**.

(16) Gélinas, S.; Rao, A.; Kumar, A.; Smith, S.L.; Chin, A.W.; Clark, J.; van der Poll, T.S.; Bazan, G.C.; Friend, R.H., Ultrafast Long-Range Charge Separation in Organic Semiconductor Photovoltaic Diodes. *Science* **2014,** *343*, (6170), 512-516.

(17) Rao, A.; Wilson, M.W.; Hodgkiss, J.M.; Albert-Seifried, S.; Bässler, H.; Friend, R.H., Exciton fission and charge generation via triplet excitons in pentacene/C60 bilayers. *Journal of the American Chemical Society* **2010**.

(18) Wilson, M.W.; Rao, A.; Clark, J.; Kumar, R.S.S.; Brida, D.; Cerullo, G.; Friend, R.H., Ultrafast Dynamics of Exciton Fission in Polycrystalline Pentacene. *Journal of the American Chemical Society* **2011**.

(19) Rao, A.; Chow, P.C.; Gélinas, S.; Schlenker, C.W.; Li, C.-Z.; Yip, H.-L.; Jen, A.K.-Y.; Ginger, D.S.; Friend, R.H., The role of spin in the kinetic control of recombination in organic photovoltaics. *Nature* **2013,** *500*, (7463), 435-439.

(20) Bakulin, A.A.; Dimitrov, S.D.; Rao, A.; Chow, P.C.; Nielsen, C.B.; Schroeder, B.C.; McCulloch, I.; Bakker, H.J.; Durrant, J.R.; Friend, R.H., Charge-Transfer State Dynamics Following Hole and Electron Transfer in Organic Photovoltaic Devices. *The Journal of Physical Chemistry Letters* **2012,** *4*, (1), 209-215.

(21) Hodgkiss, J.M.; Albert-Seifried, S.; Rao, A.; Barker, A.J.; Campbell, A.R.; Marsh, R.A.; Friend, R.H., Exciton-Charge Annihilation in Organic Semiconductor Films. *Advanced Functional Materials* **2012**.

(22) Savoie, B.M.; Rao, A.; Bakulin, A.A.; Gelinas, S.; Movaghar, B.; Friend, R.H.; Marks, T.J.; Ratner, M.A., Unequal Partnership: Asymmetric Roles of Polymeric Donor and Fullerene Acceptor in Generating Free Charge. *Journal of the American Chemical Society* **2014,** *136*, (7), 2876-2884.

(23) Wienk, M.M.; Kroon, J.M.; Verhees, W.J.H.; Knol, J.; Hummelen, J.C.; van Hal, P.A.; Janssen, R.A.J., Efficient Methano[70]fullerene/MDMO-PPV Bulk Heterojunction Photovoltaic Cells. *Angewandte Chemie International Edition* **2003,** *42*, (29), 3371-3375.

(24) Hummelen, J.C.; Knight, B.W.; LePeq, F.; Wudl, F.; Yao, J.; Wilkins, C.L., Preparation and Characterization of Fulleroid and Methanofullerene Derivatives. *The Journal of Organic Chemistry* **1995,** *60*, (3), 532-538.

(25) Dittmer, J.J.; Marseglia, E.A.; Friend, R.H., Electron Trapping in Dye/Polymer Blend Photovoltaic Cells. *Advanced Materials* **2000,** *12*, (17), 1270-1274.

(26) Shin, W.S.; Jeong, H.-H.; Kim, M.-K.; Jin, S.-H.; Kim, M.-R.; Lee, J.-K.; Lee, J.W.; Gal, Y.-S., Effects of functional groups at perylene diimide derivatives on organic photovoltaic device application. *Journal of Materials Chemistry* **2006,** *16*, (4), 384-390.

(27) Mikroyannidis, J.A.; Stylianakis, M.M.; Suresh, P.; Sharma, G.D., Efficient hybrid bulk heterojunction solar cells based on phenylenevinylene copolymer, perylene bisimide and TiO2. *Solar Energy Materials and Solar Cells* **2009,** *93*, (10), 1792-1800.

(28) Sharma, G.D.; Suresh, P.; Mikroyannidis, J.A.; Stylianakis, M.M., Efficient bulk heterojunction devices based on phenylenevinylene small molecule and perylene-pyrene bisimide. *Journal of Materials Chemistry* **2010,** *20*, (3), 561-567.

(29) Zhan, X.; Tan, Z.a.; Zhou, E.; Li, Y.; Misra, R.; Grant, A.; Domercq, B.; Zhang, X.-H.; An, Z.; Zhang, X., et al., Copolymers of perylene diimide with dithienothiophene and dithienopyrrole as electron-transport materials for all-polymer solar cells and field-effect transistors. *Journal of Materials Chemistry* **2009,** *19*, (32), 5794-5803.

(30) Sommer, M.; Lindner, S.M.; Thelakkat, M., Microphase-Separated Donor–Acceptor Diblock Copolymers: Influence of HOMO Energy Levels and Morphology on Polymer Solar Cells. *Advanced Functional Materials* **2007,** *17*, (9), 1493-1500.

(31) Rajaram, S.; Armstrong, P.B.; Kim, B.J.; Fréchet, J.M.J., Effect of Addition of a Diblock Copolymer on Blend Morphology and Performance of Poly(3-

hexylthiophene):Perylene Diimide Solar Cells. *Chemistry of Materials* **2009,** *21*, (9), 1775-1777.

(32) Howard, I.A.; Laquai, F.; Keivanidis, P.E.; Friend, R.H.; Greenham, N.C., Perylene Tetracarboxydiimide as an Electron Acceptor in Organic Solar Cells: A Study of Charge Generation and Recombination. *The Journal of Physical Chemistry C* **2009,** *113*, (50), 21225-21232.

(33) Rajaram, S.; Shivanna, R.; Kandappa, S.K.; Narayan, K.S., Nonplanar Perylene Diimides as Potential Alternatives to Fullerenes in Organic Solar Cells. *The Journal of Physical Chemistry Letters* **2012,** *3*, (17), 2405-2408.

(34) Shivanna, R.; Shoaee, S.; Dimitrov, S.; Kandappa, S.K.; Rajaram, S.; Durrant, J.R.; Narayan, K.S., Charge generation and transport in efficient organic bulk heterojunction solar cells with a perylene acceptor. *Energy & Environmental Science* **2014,** *7*, (1), 435-441.

(35) Huo, L.; Zhang, S.; Guo, X.; Xu, F.; Li, Y.; Hou, J., Replacing Alkoxy Groups with Alkylthienyl Groups: A Feasible Approach To Improve the Properties of Photovoltaic Polymers. *Angewandte Chemie International Edition* **2011,** *50*, (41), 9697-9702.

(36) Adhikary, P.; Venkatesan, S.; Adhikari, N.; Maharjan, P.P.; Adebanjo, O.; Chen, J.; Qiao, Q., Enhanced charge transport and photovoltaic performance of PBDTTT-C-T/PC70BM solar cells via UV-ozone treatment. *Nanoscale* **2013,** *5*, (20), 10007-10013.

(37) Xi, F.; Guojia, F.; Fei, C.; Pingli, Q.; Huihui, H.; Yongfang, L., Enhanced performance and stability in PBDTTT-C-T : PC 70 BM polymer solar cells by optimizing thickness of NiO x buffer layers. *Journal of Physics D: Applied Physics* **2013,** *46*, (30), 305106.

(38) Ohkita, H.; Cook, S.; Astuti, Y.; Duffy, W.; Tierney, S.; Zhang, W.; Heeney, M.; McCulloch, I.; Nelson, J.; Bradley, D.D.C., et al., Charge Carrier Formation in Polythiophene/Fullerene Blend Films Studied by Transient Absorption Spectroscopy. *Journal of the American Chemical Society* **2008,** *130*, (10), 3030-3042.

(39) Nelson, J., Diffusion-limited recombination in polymer-fullerene blends and its influence on photocurrent collection. *Physical Review B* **2003,** *67*, (15), 155209.

(40) Clarke, T.M.; Ballantyne, A.; Shoaee, S.; Soon, Y.W.; Duffy, W.; Heeney, M.; McCulloch, I.; Nelson, J.; Durrant, J.R., Analysis of Charge Photogeneration as a Key Determinant of Photocurrent Density in Polymer: Fullerene Solar Cells. *Advanced Materials* **2010,** *22*, (46), 5287-5291.

(41) Shoaee, S.; Clarke, T.M.; Huang, C.; Barlow, S.; Marder, S.R.; Heeney, M.; McCulloch, I.; Durrant, J.R., Acceptor Energy Level Control of Charge Photogeneration in Organic Donor/Acceptor Blends. *Journal of the American Chemical Society* **2010,** *132*, (37), 12919-12926.

(42) Nogueira, A.F.; Montanari, I.; Nelson, J.; Durrant, J.R.; Winder, C.; Sariciftci, N.S.; Brabec, C., Charge Recombination in Conjugated Polymer/Fullerene Blended Films Studied by Transient Absorption Spectroscopy. *The Journal of Physical Chemistry B* **2003,** *107*, (7), 1567-1573.

(43) Shoaee, S.; Eng, M.P.; Espildora, E.; Delgado, J.L.; Campo, B.; Martin, N.; Vanderzande, D.; Durrant, J.R., Influence of nanoscale phase separation on geminate versus

bimolecular recombination in P3HT:fullerene blend films. *Energy & Environmental Science* **2010,** *3*, (7), 971-976.

(44) Westenhoff, S.; Howard, I.A.; Hodgkiss, J.M.; Kirov, K.R.; Bronstein, H.A.; Williams, C.K.; Greenham, N.C.; Friend, R.H., Charge Recombination in Organic Photovoltaic Devices with High Open-Circuit Voltages. *Journal of the American Chemical Society* **2008,** *130*, (41), 13653-13658.

(45) Guo, J.; Ohkita, H.; Benten, H.; Ito, S., Near-IR Femtosecond Transient Absorption Spectroscopy of Ultrafast Polaron and Triplet Exciton Formation in Polythiophene Films with Different Regioregularities. *Journal of the American Chemical Society* **2009,** *131*, (46), 16869-16880.

(46) Guo, J.; Ohkita, H.; Benten, H.; Ito, S., Charge Generation and Recombination Dynamics in Poly(3-hexylthiophene)/Fullerene Blend Films with Different Regioregularities and Morphologies. *Journal of the American Chemical Society* **2010,** *132*, (17), 6154-6164.

(47) Mickley Conron, S.M.; Shoer, L.E.; Smeigh, A.L.; Ricks, A.B.; Wasielewski, M.R., Photoinitiated Electron Transfer in Zinc Porphyrin–Perylenediimide Cruciforms and Their Self-Assembled Oligomers. *The Journal of Physical Chemistry B* **2013,** *117*, (7), 2195-2204.

(48) Melzer, C.; Koop, E.J.; Mihailetchi, V.D.; Blom, P.W.M., Hole Transport in Poly(phenylene vinylene)/Methanofullerene Bulk-Heterojunction Solar Cells. *Advanced Functional Materials* **2004,** *14*, (9), 865-870.

(49) Mihailetchi, V.D.; Koster, L.J.A.; Blom, P.W.M.; Melzer, C.; de Boer, B.; van Duren, J.K.J.; Janssen, R.A.J., Compositional Dependence of the Performance of Poly(p-phenylene vinylene):Methanofullerene Bulk-Heterojunction Solar Cells. *Advanced Functional Materials* **2005,** *15*, (5), 795-801.

(50) Mihailetchi, V.D.; Xie, H.X.; de Boer, B.; Koster, L.J.A.; Blom, P.W.M., Charge Transport and Photocurrent Generation in Poly(3-hexylthiophene): Methanofullerene Bulk-Heterojunction Solar Cells. *Advanced Functional Materials* **2006,** *16*, (5), 699-708.

(51) Andersson, L.M.; Inganas, O., Acceptor influence on hole mobility in fullerene blends with alternating copolymers of fluorene. *Applied Physics Letters* **2006,** *88*, (8), 082103-082103.

(52) Yang, X.; Loos, J.; Veenstra, S.C.; Verhees, W.J.H.; Wienk, M.M.; Kroon, J.M.; Michels, M.A.J.; Janssen, R.A.J., Nanoscale Morphology of High-Performance Polymer Solar Cells. *Nano Letters* **2005,** *5*, (4), 579-583.

(53) Mukhopadhyay, S.; Das, A.J.; Narayan, K.S., High-Resolution Photocurrent Imaging of Bulk Heterojunction Solar Cells. *The Journal of Physical Chemistry Letters* **2012,** *4*, (1), 161-169.

Chapter 5:

Charge Generation from Relaxed Charge Transfer States

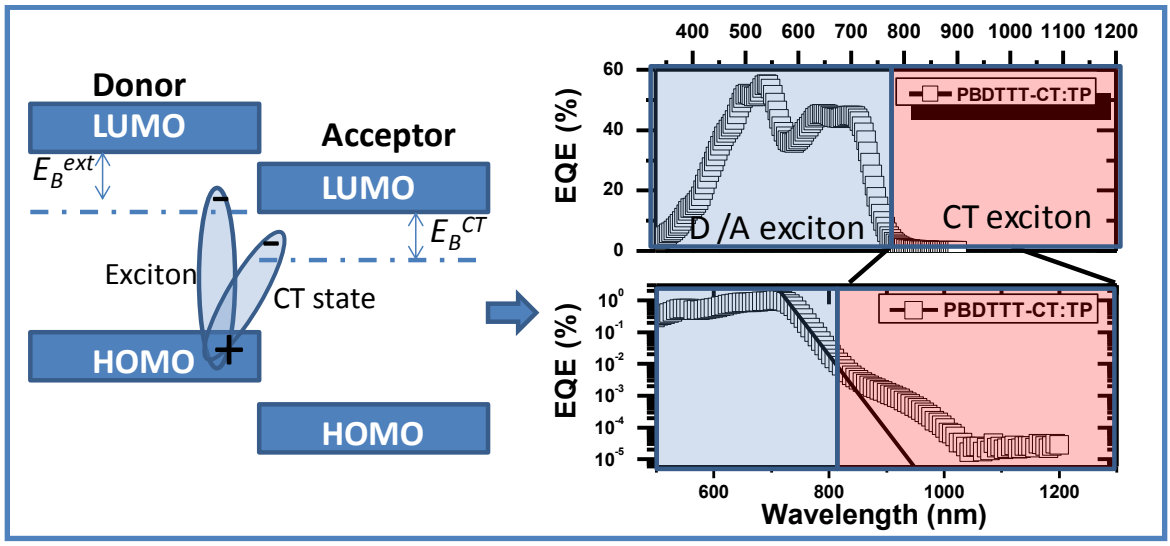

Charge-transfer (CT) states in bulk heterojunction (BHJ) solar cells play a decisive role in determining the characteristics and performance of the devices. The comparison of nature of photophysical processes and C-T states in non-fullerene based BHJs to that of fullerene based BHJs is closely investigated. Striking similarity and differences in the band-tail photocurrent, PL/EL and morphology of twisted perylene (TP) acceptor based BHJs with that of PCBM systems reveal the role of molecular structure-order correlation on charge generation processes. The inference drawn from these results points to lower recombination losses at the TP-donor interface and possibility of higher efficiencies in such non-fullerene systems compared to PCBM based systems.

5 Charge Generation from Relaxed Charge Transfer States

The material interface between donor and acceptor molecules in organic bulk-heterojunction solar cells is crucial for an efficient conversion of photons to free charges.(1) A decisive role for the efficient generation of charges is played by the charge transfer (CT) complexes, which are interfacial charge pairs residing at sub gap energies at the donor-acceptor interface.(1-6) During charge photogeneration, this CT state represents the intermediate step between exciton dissociation and charge extraction. Theoretical and experimental studies show that open circuit voltage (V_{oc}) and short circuit current density (J_{sc}) directly depends on the CT states.(7-11) The maximum achievable V_{oc} is determined by the energy associated with the CT state, and the overall current generation is determined by the recombination losses of these CT states. In order to increase the V_{oc} of the devices, the energy of the CT state is increased by decreasing the driving energy associated with the electron transfer process (exciton dissociation). This trading of excess kinetic energy of the CT state reduces the efficiency of exciton dissociation. Hence, in order to simultaneously increase V_{oc} *and* J_{sc}, it is imperative to have a detailed understanding of fundamental processes associated with CT-state formation and dissociation.

As discussed earlier in the thesis, the photogeneration of charges in fullerene based BHJ involves creation of singlet exciton upon photo absorption in the donor domain which diffuses to the donor:acceptor interface and dissociates by transferring the electron to the acceptor LUMO level.(1) The energetic offset between the donor and acceptor LUMOs (ΔG_{ET}) drives the dissociation of exciton.(12, 13) The electron on the acceptor molecule and the hole on the donor molecule are coulombically bound forming the interfacial charge transfer (CT) states.(13) Spectroscopic measurements showed that the binding energy of the CT state (E_B^{CT}) is in well excess of thermal energy (~25 meV) and is in the range of 0.1-0.5 eV.(14-16) Both static and dynamic factors play an important role in enhancing the yield of CT dissociation. Static factors include dipolar lowering of binding energy at the interface, entropy effects, and electric fields (built-in and external field). The dissociation of CT-state

into free charges is explained in two possible ways: hot CT-state dissociation and relaxed CT-state dissociation.

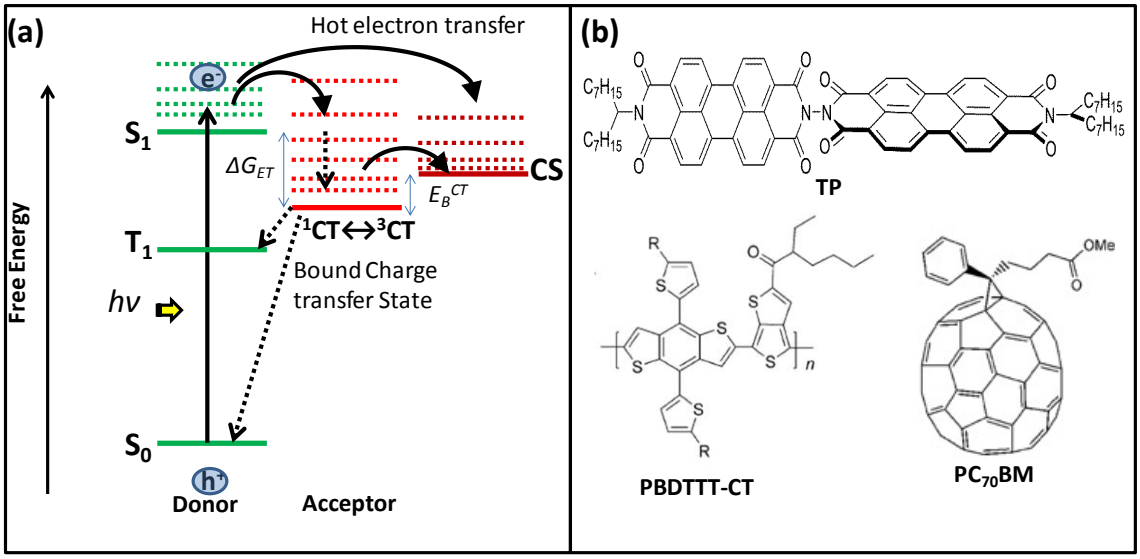

Figure 5.1: Schematic of generation of photocharges in BHJ system. (a) Depicts the possible routes for the formation of free charges (CS) from the singlet exciton in the donor. ΔG_{ET} is the electron driving energy

In the hot CT-state dissociation framework, the free charges are generated utilizing the excess thermal energy caused due to energetic offset ΔG_{ET} between the donor and acceptor LUMO level.([17-19]) This model is substantiated by ultrafast spectroscopic measurements where the generation of free charges are observed within 100 fs,([17]) suggesting the transfer of hot electron before thermally relaxing to its ground state. In this model, the excess energy should asses in dissociation of hot–CT states into free charges (increase in dissociation efficiency) ([20-23]) and hence it is expected to have wavelength dependent internal quantum efficiency (IQE). However, many of the efficient blend systems exhibit wavelength independent IQE suggesting a more appropriate framework. In the relaxed CT-state dissociation framework, the thermally relaxed CT-state acts as a precursor in the generation of free charges. Sub-band gap photocurrent measurements were utilized by Vandewal et al.([11]) to show wavelength independent IQE spectra extending to relaxed ground state CT absorption.([24], [25]) This confirmed that the relaxed CT-states were the exclusive precursor for charge dissociation. However, this model failed to explain the driving force for dissociation of these relaxed CT state and hence further insights to this framework are needed. Although both the models explain substantial experimental results, a general consensus for free charge generation is needed for designing new high efficient donor and acceptor molecules.

The properties of CT states are highly dependent on the choice of donor and acceptor materials. Most of the understanding of CT states is based on the BHJ formed by polymer donors and fullerene derivative based acceptors. As mentioned in the earlier chapters, fullerenes are limited by their tunability of energy levels and the low lying LUMO level of the fullerene derivatives restrict further optimization of the V_{oc} in the devices. Hence alternative acceptors with tunable LUMO levels are preferred in order to increase the overall power conversion efficiency. In this regard, perylene derivatives offer a viable alternative due to their flexibility in tuning their energy levels. In this endeavor, the design principle of twisted perylene (TP) was introduced in the previous chapter, where the co-facial stacking of perylene units was disrupted by twisting the two perylenes perpendicular to each other. This aided in improved bulk morphology resulting in increased short circuit current density (J_{sc}) and hence power conversion efficiency of the cells.(*26*) Further studies using transient absorption spectroscopy revealed that the charge generation process in TP and PCBM blends follows similar dynamics.(*27*) In addition the magnitude of polaron generation is similar in both the blend systems.(*27*) These studies provide a rationale to pursue and strengthen the understanding of these systems. Particularly, it is important to understand and quantify the fundamental processes involved in charge generation via CT states in these systems.

Since the basic morphology and microstructure of these blends are different from that of PCBM blends, the rules and strategies for obtaining high performance can be reasonably different. One of the important aspects needs to consider in designing new acceptors is the entropic factor at the donor-acceptor interface. It was shown through simulation that the charge separation is entropically favored in a disordered BHJ system.(*28*, *29*) This chapter discusses the comprehensive study on formation and dissociation of charge transfer state in TP acceptor based BHJ systems. Existence of CT state is observed in BHJs featuring TP acceptor with different donor polymers and quantified using photo-thermal deflection spectroscopy (PDS) and sensitive lock-in based EQE measurements. Electroluminescence (EL) of BHJ in the forward bias conditions is used to monitor the radiative recombination of CT state. The correlation between V_{oc} of the device and the effective band gap of BHJs ($HOMO_{donor} - LUMO_{acceptor}$) are explored in these systems. Considering that the electron affinities of TP and $PC_{71}BM$ are similar, a comparative study on energetics of CT state formation and dissociation is addressed in the BHJ consisting of donor polymer PBDTTT-CT.

5.1 Results and discussions:

5.1.1 Absorption of CT state:

The formation and dissociation of CT states is characterized in the efficient fullerene-free BHJ system consisting of donor polymer PBDTTT-CT and acceptor small molecule TP (figure 5.1b) molecules. The ground state CT of BHJ is formed by molecular orbital hybridization of donor HOMO and acceptor LUMO by overlap of their wavefunctions.(29) Since the hybridization of orbitals occurs only at the donor: acceptor interface, the absorption cross section of CT state is low in BHJ films. The conventional approach to follow the signature of the CT states is using high sensitive EQE and PDS methods.(30, 31) Both EQE and PDS measurements have been previously reported for PCBM based BHJs to identify the CT state in the form of red shifted sub band-gap states in the blends.(7, 8, 11) This procedure is repeated and reproduced for observing sub-gap states in high-efficiency PCBM blends and is used as a reference.

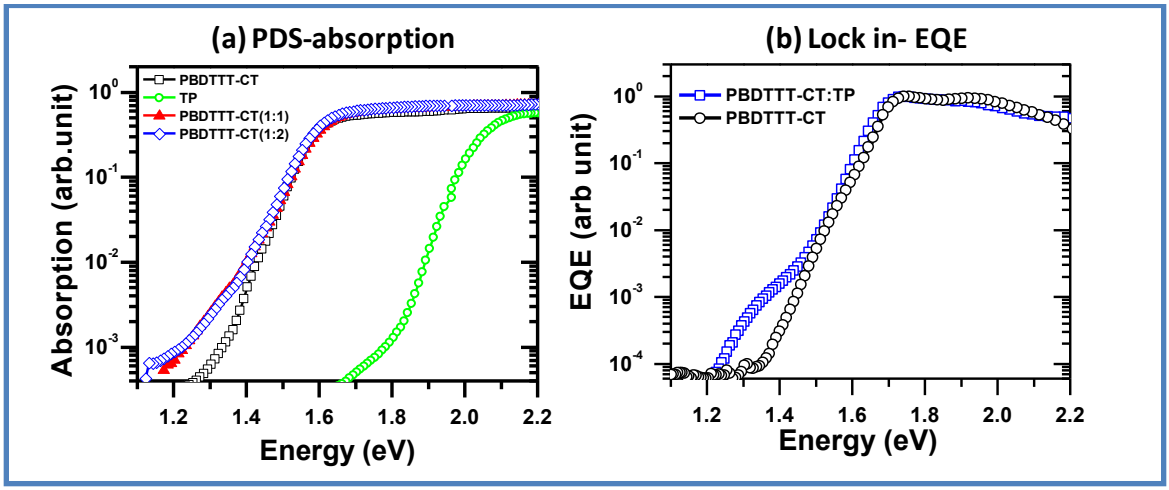

Figure 5.2: (a) Photothermal deflection spectroscopy (PDS) of TP, PBDTTT-CT and 1:1 ratio of PBDTTTT-CT:TP films on quartz substrates. (b) External quantum efficiency of devices (normalized with respect to 1.77 eV) consisting of pristine PBDTTT-CT and PBDTTT-CT:TP blend as active layer. The extended tail states, both in absorption and EQE measurements are assigned to charge transfer state.

PDS measurements were carried out on BHJ films coated on top of quartz substrates. Figure 5.2a represents the PDS spectra of neat TP, neat PBDTTT-CT and PBDTTTT-CT:TP blend films. A clear red-shifted tail state absorption can be seen in the blends compared to pristine films in the range of 1.1 – 1.3 eV. This enhanced sub gap absorption corresponds to ground state CT formed between the PBDTTT-CT and TP molecules. Figure 5.2b shows the EQE spectra of pristine PBDTTT-CT and 1:1 ratio PBDTTT-CT:TP blend devices in the

inverted geometry with ITO/ZnO and MoOx/Ag electrodes. The onset of photoresponse response, $I_{ph}(\lambda)$, of PBDTTT-CT:TP device at ~ 1.1 eV as compared to ~1.34 eV observed for pristine PBDTTT-CT clearly highlights the enhanced tail state photoresponse in blends. This red shifted $I_{ph}(\lambda)$ can be directly attributed to the photocurrent generation from the ground state CT formed at PBDTTT-CT:TP interface. The Gaussian fit of the tail state indicates a local maximum at ~1.39 eV corresponding to peak of the CT-state band.

The experimental setup used for EQE measurement consisted of a tungsten-Halogen light source coupled with a monochromator (Zolix Instruments). The modulated monochrome light was concentrated on to the device area using a convex lens. The photogenerated current from the devices was measured using Stanford Research System (SRS 830) lock-in amplifier. For CT-state photocurrent response, the intensity of illuminated monochrome light was increased by an order of magnitude. The current to voltage converting transimpedence pre-amplifier, Femto DLPCA 200, was connected prior to SRS 830 lock-in amplifier in series for low current measurements.

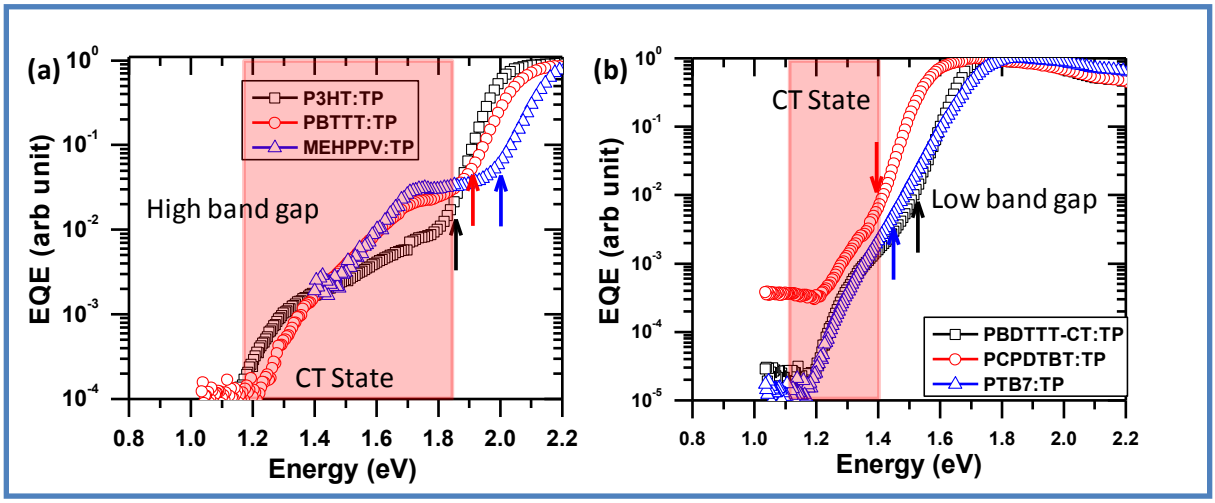

Figure 5.3: Tail state EQE measurements (normalized w.r.t individual maximum) on different blend system consisting of TP as electron acceptor. (a) for relatively high band gap semiconducting donor polymers such as P3HT, PBTTT and MEHPPV (b) for relatively low band gap semiconducting donor polymers such as PBDTTT-CT, PCPDTBT and PTB7.(Arrow mark indicates the absorption edge of the pristine donor molecules)

Different donor polymers were used to study the influence of HOMO level on the formation of CT state with TP acceptor blend systems. Blends based on a set of relatively high band gap donor polymers such as P3HT, PBTTT and MEHPPV and relatively low band gap donor polymers such as PBDTTT-CT, PCPDTBT and PTB7 were studied. A table

containing HOMO level, LUMO level and electron transfer driving energy for all the blend donors with respect to TP acceptor is shown below (Table 1).

Material	HOMO (eV)	LUMO (eV)	ΔG_{ET} (eV) with respect to $TP_{LUMO= -4.1\ eV}$
P3HT (*32*)	- 5.0	- 3.0	~0.9
PBTTT (*33*)	- 5.1	-3.1	~1.0
MEHPPV (*34*)	- 5.02	- 2.7	~0.92
PBDTTT-CT (*35*)	- 5.11	- 3.25	~1.01
PTB7 (*36*)	- 5.15	- 3.31	~1.05
PCPDTBT (*37*)	- 4.9	- 3.5	~0.8

Table 2: HOMO level, LUMO level and electron transfer driving energy for all the blend donors with respect to TP acceptor.

The devices with 1:1 donor to acceptor ratio were fabricated in the inverted BHJ solar cell structure geometry with ZnO and MoOx as electron and hole transporting buffer layers respectively with similar fabrication procedures. The EQE measurements on these devices are shown in the figure 5.3. A distinct formation of CT state is observed in all the devices by blending with TP acceptor in the form of a red-shifted short-circuit photoresponse in the band-tail superimposed by a Gaussian feature. For comparison, the EQE spectrum of each device is normalized with respect to its maximum value. It should be noted that to observe a true correlation between V_{oc} and I_{ph}-onset, efficient devices were needed which were not feasible across the entire set of the donor polymers. The C-T states in these systems is offset by the variability in crystallinity, morphology, non-optimum D:A ratio, quantum yield for transfer process and mobility which exist in these different donor systems.

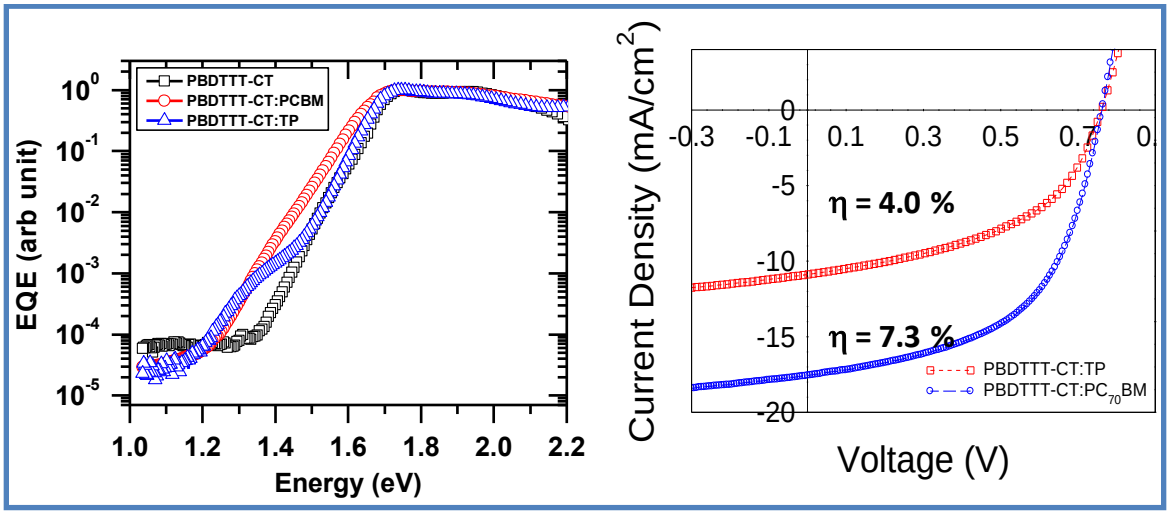

Figure 5.4: (a) EQE measurement of pristine PBDTTT-CT and blend of PBDTTT-CT:TP and

PBDTTT-CT:PC70BM acceptor in 1:1 ratio extending to absorption tail (normalized w.r.t to 1.77 eV). (b) J-V characteristics of PBDTTT-CT:TP and PBDTTT-CT:PCBM films at AM 1.5, 1 Sun illumination.

Molecular structure-order correlation on charge generation in the BHJ is compared between TP and $PC_{70}BM$ acceptors. The similar electron affinity of TP and PCBM molecules, as measured from cyclic voltammetry in similar conditions,(*38*) suggest that these systems are ideal to do a comparative study of the effect of acceptor structural-disorder at the charge transfer interface. $PC_{70}BM$ is a spherically symmetric 3D molecule, whereas, TP is a combination of two planar perylene units in the twisted structure. Due to the higher symmetry, after photoinduced charge transfer, electron delocalization is expected to be higher for $PC_{70}BM$ aggregates as compared to TP aggregates. Although, TP and PCBM have similar LUMO levels, the interface geometry, domain sizes and organization can be vastly different. Figure 5.4a represents the normalized EQE spectra of PBDTTT-CT:TP and PBDTTT-CT:PC70BM blends. The graph clearly demonstrates the formation of CT state in both the blend systems by comparing with the EQE of pristine PBDTTT-CT. The onset of short circuit photocurrent is at ~ 1.1 eV for TP and ~ 1.08 eV for PCBM blend. The similar onset in photoresponse corresponds to similar electron affinity of TP and PCBM molecules (TP_{LUMO} ~ 4.02 eV, $PCBM_{LUMO}$ ~ 4.1 eV). However, the Gaussian fit for the CT state absorption exhibits broader band for PCBM compared to the TP blend. This can be attributed to 3D isotropic electron transfer and spherical symmetry of fullerene molecules leading to higher degree of electron-phonon coupling. The device *J-V* characteristics for both the blends illuminated under AM 1.5 1 Sun illumination is shown in the figure 5.4b. The J-V characteristics are tabulated in the table 2.

Blend	**J_{sc} (mA/cm^2)**	**V_{oc} (V)**	**FF (%)**	**η (%)**
PBDTTT-CT:TP	10.9 ± 0.1	0.765 ± 0.005	48.4 ± 0.2	4.0 ± 0.03
PBDTTT-CT:$PC_{70}BM$	17.5 ± 0.4	0.761 ± 0.006	54.8 ± 0.3	7.3 ± 0.06

Table 2: J-V characteristics of PBDTTT-CT:TP and PBDTTT-CT:$PC_{70}BM$ blends.

The devices were fabricated in the inverted geometry on cleaned patterned ITO substrates. Sol-gel based ZnO layer was used as electron transport layer. ZnO sol was spin coated at 2000 rpm for 60 s and annealed at 250 0C for 30 min in air. For PCBM based cells, the active layer was spin coated from 25 mg/mL solution (1:1 ratio) in anhydrous

chlorobenzene at 900 rpm for 60 s. For TP based cells, the active layer concentration of 12 mg/mL (1:1 ratio) in anhydrous chlorobenzene was spin coated at 1000 rpm for 60 s. All the active layers were spin coated inside a nitrogen filled glove box. The hole transport layer MoOx (≈10 nm) and Ag (≈100 nm) were subsequently deposited by physical vapor deposition at a base pressure of 10-6 mbar.

The optimized blends of PBDTTT-CT:PCBM exhibit a power conversion efficiency (η) of 7.3 %, whereas the PBDTTT-CT:TP blend exhibits 4 %. The higher efficiency of PCBM blend is due to varied reasons, namely higher transport dimensionality, phase purity and aggregate organization leading to a higher effective electron mobility in the BHJ.(27) Lack of these attributes is reflected in the decreased J_{sc} and *FF* for the TP blend system. It is to be noted that the V_{oc} of both the systems is ~ 0.76 V, which is consistent with similar electron affinities and onset of photocharge generation.

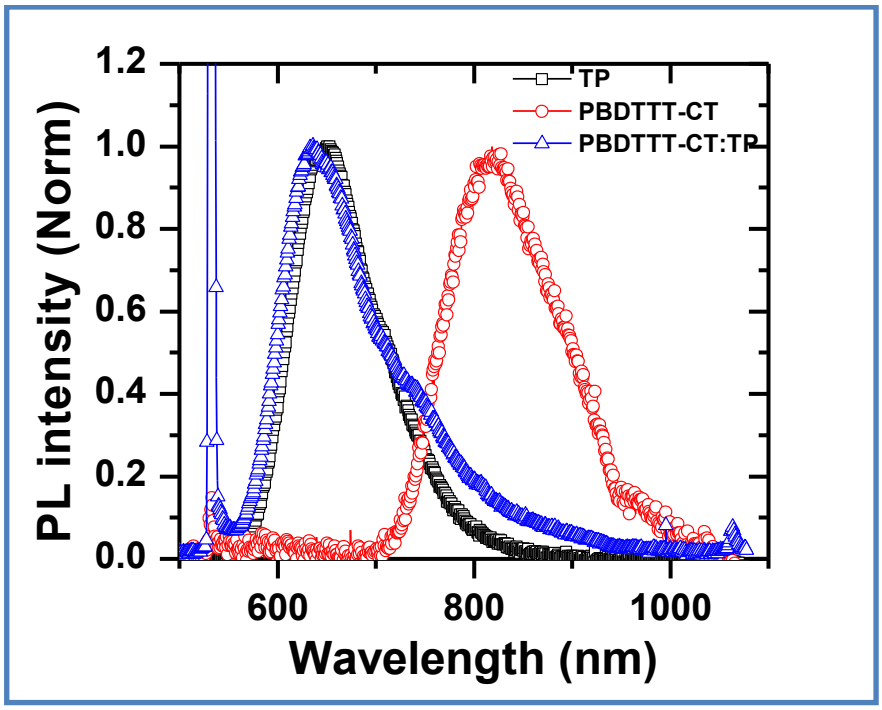

Figure 5.5: Photoluminescence spectra of pristine TP, pristine PBDTTT-CT and 1:1 ratio blend of PBDTTT-CT:TP. A higher excitation intensity was used for blend films.(Excitation density for neat PBDTTT-CT and PBDTTT-CT:TP blends were 10x and 1000x compare to TP excitation)

5.1.2 Emission from CT state:

Photo and electro- luminescence from these CT states are studied in the next section. In a well mixed blend exhibiting good efficiency, the photoluminescence (PL) of both donor and an acceptor molecule is almost completely quenched. However, a red shifted weak PL

can be observed in many BHJ systems.(*39*, *40*) These emissions are attributed to radiative recombination of bound CT state at the donor: acceptor interface. In order to identify the CT emission from TP based BHJ, we carried out PL measurement on the BHJ blends at higher intensities. Figure 5.5 represents the normalized PL spectra from neat TP, neat PBDTTT-CT and 1:1 ratio PBDTTT-CT:TP blend. Both TP and PBDTTT-CT singlet excitons exhibited > 99 % quenching upon blending in 1:1 ratio.(*27*) However the C-T emission from the BHJ is not observed, even at high excitation intensity, and can be reasoned out by the fact that the higher emission from the (unquenched) acceptor molecules generated by the high level of pumping masks the C-T emission with associated broadening factors.

Hence, the option of using EL methods to examine the C-T states is more feasible. The PL is primarily due to the geminate radiative recombination via the CT state while EL is a consequence of recombination (non-geminate) of the injected carriers via the interface states. It is known in PCBM systems that the forced bimolecular recombination occurs via a lower energy state vis-à-vis the geminate radiative transition in PL.(*40-43*) Figure 5.6 shows the EL spectra of PBDTTT-CT:TP and PBDTTT-CT:$PC_{70}BM$ BHJ in forward bias condition. The BHJ solar cells were forward biased using Kiethley 2400 source meter. EL spectrum was acquired from a fiber coupled Hamamatsu mini spectrometer (Model: TM-VIS/NIR C10083CA) equipped with back-thinned CCD image sensor of 2048 pixels. The spectral response range is 320 nm – 1000 nm with spectral resolution of 8 nm (FWHM). The data was collected using SpecEvaluation^{TM} software.

The highlight of the EL response for TP and PCBM blends are the following: (i) No observable emission is recorded from pristine donor and acceptor components of the blends even at higher forward bias condition. (ii) The observed EL spectra in the blends corresponds to the region of absorption tail (CT state) with the TP devices clearly blue-shifted (λ^{max} ≈850 nm) compared to the PCBM devices (λ^{max} ≈880 nm) (Figure 5.6). (iii) The onset of EL for the TP blend is at a higher threshold voltage (a factor of 2 to 3) than PCBM-BHJs with the emission intensity increasing with respect to the current density in both the blends (iv) For a similar injected current density, EL of TP blend showed lower emission yield compared to the $PC_{71}BM$ blend and (v) The spectral emission profile parameter of both the blends (λ^{max} and line width) are fairly constant with respect to bias/current-density (Figure 5.7).

Absence of pristine component emission from the blend confirms that the detected EL is solely from the CT state formed at the donor-acceptor interface. The red shifted EL for PCBM blend compared to TP blend can be attributed to radiative recombination from highly

ordered regions of PCBM having lower interfacial energy (870 nm), which is consistent with the reported observations for other PCBM blends.(*43*)

The PCBM systems are expected to be more isotropic with a tendency to form a relatively uniform aggregate which result in an ordered interface with the donor polymers. Recent studies of TP dispersed in the semicrystalline ferroelectric matrix revealed the effects of symmetry and geometry of the molecule and the tendency of TP to form clusters even at low-levels of concentration along with the inability to form larger size domains.(*44*)

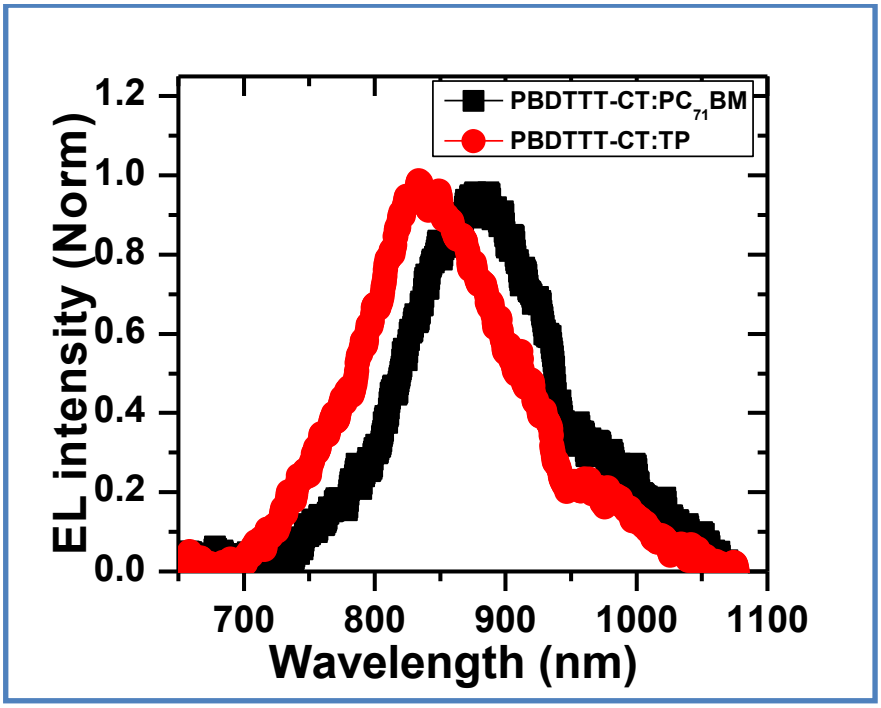

Figure 5.6: Electroluminescence spectra of PBDTTT-CT:TP and PBDTTT-CT:$PC_{70}BM$ blends in forward bias conditions. 2.5 V forward bias is applied for both the blends. The spectrum is normalized for visualization.

The non-planar TP molecules forms a lose cluster (not a uniform aggregate) and can result in a disordered interface. The accompanied increased injection current density (or higher threshold voltage) in TP based devices required for radiative recombination can be attributed to transport barriers in the bulk which is expected since the electron mobilities in TP films are lower than that in PCBM films. The reduced radiative recombination yield in TP blend is then principally due to a combination of two factors: reduced access for the electrons upon injection to the TP interfacial sites arising from lower electron mobility, and higher interfacial disorder/entropy at the D-A heterojunctions.

5.2 Comparison of TP and $PC_{71}BM$ based BHJ:

In spite of different structural order of TP and PCBM molecules in the BHJ films, the similarity in the V_{oc} obtained from the optimized devices can be explained by the following arguments: The V_{oc} of the solar cells depends on effective band gap of the BHJ and can be quantified as,

$$eV_{oc} = E_g - E_{loss}$$

where, $E_g = LUMO_A - HOMO_D$ is the effective band gap of the BHJ, 'E_{loss}' is the energy loss factors associated with photo-charge generation. Generally, 'E_{loss}' can be explained as,

$$E_{loss} = E_{ED} + E_{TC} + E_{CE}$$

Where, 'E_{ED}' is the energy loss during exciton dissociation into free charges. 'E_{ED}' involves both the energy loss associated in exciton quenching to form CT states and dissociation of bound CT state to free charges at the donor-acceptor interface. 'E_{TC}' is the energy loss during bulk transport of dissociated charges from the donor-acceptor interface to respective electrodes. 'E_{TC}' depends on the bulk mobilities of the charges. 'E_{CE}' is the energy loss associated with extraction of charges at the active layer and electrode interface. 'E_{CE}' depends on the work function matching between electrode and active layer.

Due to comparatively high interfacial disorder in TP molecules, geminate recombination is suppressed in the TP blend compared to PCBM. Hence, it is expected that 'E_{ED}' is relatively less in TP blends than PCBM. However, the electron mobility is an order of magnitude less in TP blends, suggesting energy loss associated with transport is high for TP than in PCBM blends. Since the devices are fabricated in similar conditions having similar buffer layers and electrodes, the 'E_{CE}' is assumed to be similar in these systems. Hence the similar V_{oc} in both the blends can be explained on the basis of competition between 'E_{ED}' and 'E_{TC}' factors. This analysis suggests that optimization of charge transport properties of TP molecules in the BHJ can further increase the V_{oc} of the devices. In addition, the absence of PL corresponding to the C-T state in these devices and the presence of EL (albeit higher flux), simultaneously indicates the significance of bimolecular reconbination losses prevailing in these systems.

5.3 Field and charge density dependence on EL spectra

Figure 5.7 (a) and (b) represents the EL spectra of PBDTTT-CT:TP and PBDTTT-CT:PCBM blends at different forward bias. It is interesting to note that the λ_{max} in EL

spectral profile is unchanged even at higher current injection flux rates. Previous reports on polymer:fullerene blends exhibited considerable changes in the EL spectra at different forward bias.(*41*) It was explained that, at higher current densities, the electron and hole can tunnel trough the interface and recombine in the pure donor or acceptor domains of the BHJ, resulting in emission from the pristine components.(*41*) Hence the EL spectrum from the BHJ usually consists of a combination of donor, acceptor and CT emissions.(*41*) The extent of donor/acceptor EL depends on the ambipolarity of the individual component. For our high efficient low band gap polymer system, the field dependence is negligible as shown in the Figure 5.7.

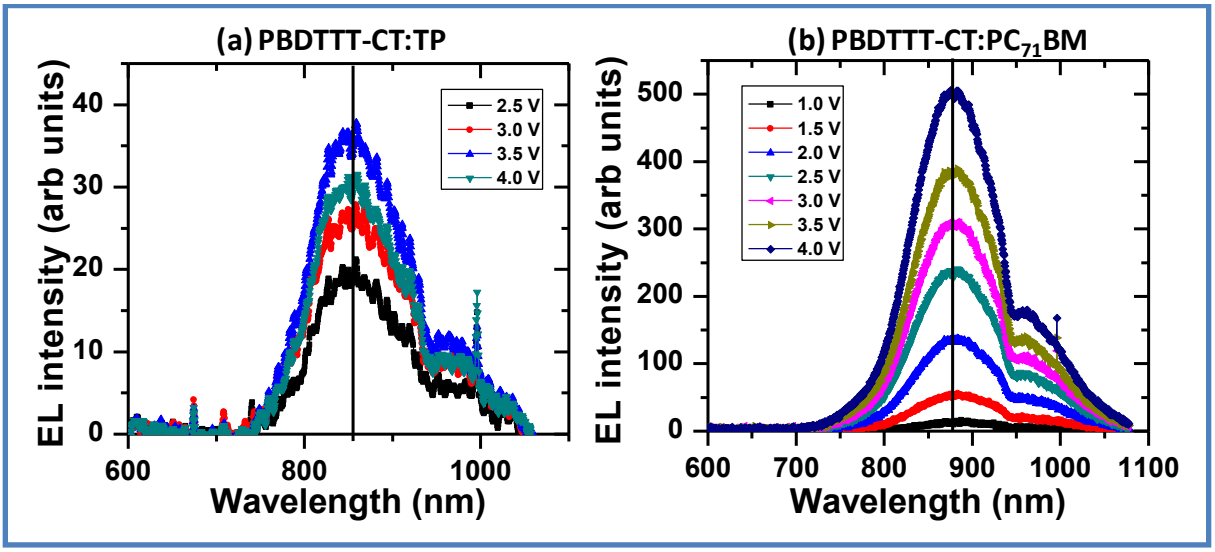

Figure 5.7: Electroluminescence spectra of PBDTTT-CT :TP (a) and PBDTTT-CT:PC_{70}BM at different forward bias. The vertical line guides for any change in the peak position.

This reveals significant homogenous mixing of D-A phases in the active layer which is consistent with efficient charge generation in both the blends. Preliminary temperature dependent studies also reveal this constant nature of λ^{max} with respect to over a wide range. An essence of the outcome from these results points to the possibility of higher PCE in TP systems. A significant yield of charge transfer efficiency which is comparable to PCBM systems accompanied by lower radiative losses upon formation of C-T states can be exploited. Any improvement in the electron mobility by different processing strategies should enable high PCE.

5.4 Summary:

The presence of C-T states is identified and quantified in efficient TP acceptor based devices using a variety of sensitive techniques. The red shifted weak absorbing band in PDS

and EQE measurements clearly demonstrates the formation of ground state CT in different polymer donors and TP acceptor BHJ systems. Electroluminescence in forward bias is observed in BHJs featuring TP as well as PCBM acceptors. Higher threshold voltage for onset of EL in TP blend suggests the charge transport limitation in TP compared to PCBM blends. The J-V characteristics of PBDTTT-CT:TP and PBDTTT-CT:PCBM blends exhibits similar V_{oc}, which is consistent with similar electron affinities and onset of photocurrent. The comparative study of TP and PCBM devices emphasizes the molecular basis of the structure-order correlation on charge generation by dissociation of CT state. Homogenous mixture of donor and acceptor molecules in both BHJs is indicated from field independent EL spectra of the blend. The trend in the CT state characteristics indicates the possibility of sizable efficiencies which can be achieved in these non-fullerene devices, which may surpass PCE exhibited by PCBM based devices.

References:

(1) Clarke, T.M.; Durrant, J.R., Charge Photogeneration in Organic Solar Cells. *Chemical Reviews* **2010,** *110*, (11), 6736-6767.

(2) Gao, F.; Inganas, O., Charge generation in polymer-fullerene bulk-heterojunction solar cells. *Physical Chemistry Chemical Physics* **2014,** *16*, (38), 20291-20304.

(3) Deibel, C.; Strobel, T.; Dyakonov, V., Role of the Charge Transfer State in Organic Donor–Acceptor Solar Cells. *Advanced Materials* **2010,** *22*, (37), 4097-4111.

(4) Piliego, C.; Loi, M.A., Charge transfer state in highly efficient polymer-fullerene bulk heterojunction solar cells. *Journal of Materials Chemistry* **2012,** *22*, (10), 4141-4150.

(5) Albrecht, S.; Vandewal, K.; Tumbleston, J.R.; Fischer, F.S.U.; Douglas, J.D.; Fréchet, J.M.J.; Ludwigs, S.; Ade, H.; Salleo, A.; Neher, D., On the Efficiency of Charge Transfer State Splitting in Polymer:Fullerene Solar Cells. *Advanced Materials* **2014,** *26*, (16), 2533-2539.

(6) Ran, N.A.; Kuik, M.; Love, J.A.; Proctor, C.M.; Nagao, I.; Bazan, G.C.; Nguyen, T.-Q., Understanding the Charge-Transfer State and Singlet Exciton Emission from Solution-Processed Small-Molecule Organic Solar Cells. *Advanced Materials* **2014,** *26*, (43), 7405-7412.

(7) Vandewal, K.; Gadisa, A.; Oosterbaan, W.D.; Bertho, S.; Banishoeib, F.; Van Severen, I.; Lutsen, L.; Cleij, T.J.; Vanderzande, D.; Manca, J.V., The Relation Between Open-Circuit Voltage and the Onset of Photocurrent Generation by Charge-Transfer Absorption in Polymer : Fullerene Bulk Heterojunction Solar Cells. *Advanced Functional Materials* **2008,** *18*, (14), 2064-2070.

(8) Vandewal, K.; Tvingstedt, K.; Gadisa, A.; Inganas, O.; Manca, J.V., On the origin of the open-circuit voltage of polymer-fullerene solar cells. *Nat Mater* **2009,** *8*, (11), 904-909.

(9) Rau, U., Reciprocity relation between photovoltaic quantum efficiency and electroluminescent emission of solar cells. *Physical Review B* **2007,** *76*, (8), 085303.

(10) Kirchartz, T.; Rau, U., Detailed balance and reciprocity in solar cells. *physica status solidi (a)* **2008,** *205*, (12), 2737-2751.

(11) Vandewal, K.; Albrecht, S.; Hoke, E.T.; Graham, K.R.; Widmer, J.; Douglas, J.D.; Schubert, M.; Mateker, W.R.; Bloking, J.T.; Burkhard, G.F., et al., Efficient charge generation by relaxed charge-transfer states at organic interfaces. *Nat Mater* **2014,** *13*, (1), 63-68.

(12) Sariciftci, N.S.; Smilowitz, L.; Heeger, A.J.; Wudl, F., Photoinduced Electron Transfer from a Conducting Polymer to Buckminsterfullerene. *Science* **1992,** *258*, (5087), 1474-1476.

(13) Veldman, D.; Meskers, S.C.J.; Janssen, R.A.J., The Energy of Charge-Transfer States in Electron Donor–Acceptor Blends: Insight into the Energy Losses in Organic Solar Cells. *Advanced Functional Materials* **2009,** *19*, (12), 1939-1948.

(14) Zhu, X.Y.; Yang, Q.; Muntwiler, M., Charge-Transfer Excitons at Organic Semiconductor Surfaces and Interfaces. *Accounts of Chemical Research* **2009,** *42*, (11), 1779-1787.

(15) Drori, T.; Sheng, C.X.; Ndobe, A.; Singh, S.; Holt, J.; Vardeny, Z.V., Below-Gap Excitation of $$\pi${}$-Conjugated Polymer-Fullerene Blends: Implications for Bulk Organic Heterojunction Solar Cells. *Physical Review Letters* **2008,** *101*, (3), 037401.

(16) Hallermann, M.; Haneder, S.; Da Como, E., Charge-transfer states in conjugated polymer/fullerene blends: Below-gap weakly bound excitons for polymer photovoltaics. *Applied Physics Letters* **2008,** *93*, (5), 053307.

(17) Grancini, G.; Maiuri, M.; Fazzi, D.; Petrozza, A.; Egelhaaf, H.J.; Brida, D.; Cerullo, G.; Lanzani, G., Hot exciton dissociation in polymer solar cells. *Nat Mater* **2013,** *12*, (1), 29-33.

(18) Ohkita, H.; Cook, S.; Astuti, Y.; Duffy, W.; Tierney, S.; Zhang, W.; Heeney, M.; McCulloch, I.; Nelson, J.; Bradley, D.D.C., et al., Charge Carrier Formation in Polythiophene/Fullerene Blend Films Studied by Transient Absorption Spectroscopy. *Journal of the American Chemical Society* **2008,** *130*, (10), 3030-3042.

(19) Virgili, T.; Marinotto, D.; Manzoni, C.; Cerullo, G.; Lanzani, G., Ultrafast Intrachain Photoexcitation of Polymeric Semiconductors. *Physical Review Letters* **2005,** *94*, (11), 117402.

(20) Clarke, T.M.; Ballantyne, A.M.; Nelson, J.; Bradley, D.D.C.; Durrant, J.R., Free Energy Control of Charge Photogeneration in Polythiophene/Fullerene Solar Cells: The Influence of Thermal Annealing on P3HT/PCBM Blends. *Advanced Functional Materials* **2008,** *18*, (24), 4029-4035.

(21) Shoaee, S.; An, Z.; Zhang, X.; Barlow, S.; Marder, S.R.; Duffy, W.; Heeney, M.; McCulloch, I.; Durrant, J.R., Charge photogeneration in polythiophene-perylene diimide blend films. *Chemical Communications* **2009**, (36), 5445-5447.

(22) Clarke, T.M.; Ballantyne, A.M.; Tierney, S.; Heeney, M.; Duffy, W.; McCulloch, I.; Nelson, J.; Durrant, J.R., Charge Photogeneration in Low Band Gap Polyselenophene/Fullerene Blend Films. *The Journal of Physical Chemistry C* **2010,** *114*, (17), 8068-8075.

(23) Dimitrov, S.D.; Durrant, J.R., Materials Design Considerations for Charge Generation in Organic Solar Cells. *Chemistry of Materials* **2014,** *26*, (1), 616-630.

(24) Lee, J.; Vandewal, K.; Yost, S.R.; Bahlke, M.E.; Goris, L.; Baldo, M.A.; Manca, J.V.; Voorhis, T.V., Charge Transfer State Versus Hot Exciton Dissociation in Polymer−Fullerene Blended Solar Cells. *Journal of the American Chemical Society* **2010,** *132*, (34), 11878-11880.

(25) van der Hofstad, T.G.J.; Di Nuzzo, D.; van den Berg, M.; Janssen, R.A.J.; Meskers, S.C.J., Influence of Photon Excess Energy on Charge Carrier Dynamics in a Polymer-Fullerene Solar Cell. *Advanced Energy Materials* **2012,** *2*, (9), 1095-1099.

(26) Rajaram, S.; Shivanna, R.; Kandappa, S.K.; Narayan, K., Nonplanar perylene diimides as potential alternatives to fullerenes in organic solar cells. *The Journal of Physical Chemistry Letters* **2012,** *3*, (17), 2405-2408.

(27) Shivanna, R.; Shoaee, S.; Dimitrov, S.; Kandappa, S.K.; Rajaram, S.; Durrant, J.R.; Narayan, K., Charge generation and transport in efficient organic bulk heterojunction solar cells with a perylene acceptor. *Energy & Environmental Science* **2014,** *7*, (1), 435-441.

(28) D'Avino, G.; Mothy, S.; Muccioli, L.; Zannoni, C.; Wang, L.; Cornil, J.; Beljonne, D.; Castet, F., Energetics of Electron–Hole Separation at P3HT/PCBM Heterojunctions. *The Journal of Physical Chemistry C* **2013,** *117*, (25), 12981-12990.

(29) McMahon, D.P.; Cheung, D.L.; Troisi, A., Why Holes and Electrons Separate So Well in Polymer/Fullerene Photovoltaic Cells. *The Journal of Physical Chemistry Letters* **2011,** *2*, (21), 2737-2741.

(30) Benson-Smith, J.J.; Goris, L.; Vandewal, K.; Haenen, K.; Manca, J.V.; Vanderzande, D.; Bradley, D.D.C.; Nelson, J., Formation of a Ground-State Charge-Transfer Complex in Polyfluorene//[6,6]-Phenyl-C61 Butyric Acid Methyl Ester (PCBM) Blend Films and Its Role in the Function of Polymer/PCBM Solar Cells. *Advanced Functional Materials* **2007,** *17*, (3), 451-457.

(31) Goris, L.; Poruba, A.; Hod'ákova, L.; Vaněček, M.; Haenen, K.; Nesládek, M.; Wagner, P.; Vanderzande, D.; De Schepper, L.; Manca, J.V., Observation of the subgap optical absorption in polymer-fullerene blend solar cells. *Applied Physics Letters* **2006,** *88*, (5), 052113.

(32) http://www.sigmaaldrich.com/catalog/product/aldrich/698997?lang=en&region=IN.

(33) http://www.sigmaaldrich.com/catalog/product/aldrich/l753971?lang=en&region=IN.

(34) Wu, C.-S.; Chen, Y., Copolyfluorenes containing pendant bipolar groups: Synthesis, optoelectronic properties and applications. *Journal of Materials Chemistry* **2010,** *20*, (36), 7700-7709.

(35) Huo, L.; Zhang, S.; Guo, X.; Xu, F.; Li, Y.; Hou, J., Replacing Alkoxy Groups with Alkylthienyl Groups: A Feasible Approach To Improve the Properties of Photovoltaic Polymers. *Angewandte Chemie* **2011,** *123*, (41), 9871-9876.

(36) Lu, L.; Yu, L., Understanding Low Bandgap Polymer PTB7 and Optimizing Polymer Solar Cells Based on It. *Advanced Materials* **2014,** *26*, (26), 4413-4430.

(37) Peet, J.; Kim, J.Y.; Coates, N.E.; Ma, W.L.; Moses, D.; Heeger, A.J.; Bazan, G.C., Efficiency enhancement in low-bandgap polymer solar cells by processing with alkane dithiols. *Nat Mater* **2007,** *6*, (7), 497-500.

(38) Shoaee, S.; Deledalle, F.; Shakya Tuladhar, P.; Shivanna, R.; Narayan, K.; Rajaram, S.; Durrant, J.R., A Comparison of Charge Separation Dynamics in Organic Blend Films Employing Fullerene and Perylene Diimide Electron Acceptors. *The Journal of Physical Chemistry Letters* **2014**.

(39) Loi, M.A.; Toffanin, S.; Muccini, M.; Forster, M.; Scherf, U.; Scharber, M., Charge Transfer Excitons in Bulk Heterojunctions of a Polyfluorene Copolymer and a Fullerene Derivative. *Advanced Functional Materials* **2007,** *17*, (13), 2111-2116.

(40) Zhou, Y.; Tvingstedt, K.; Zhang, F.; Du, C.; Ni, W.-X.; Andersson, M.R.; Inganäs, O., Observation of a Charge Transfer State in Low-Bandgap Polymer/Fullerene Blend Systems by Photoluminescence and Electroluminescence Studies. *Advanced Functional Materials* **2009,** *19*, (20), 3293-3299.

(41) Tvingstedt, K.; Vandewal, K.; Gadisa, A.; Zhang, F.; Manca, J.; Inganäs, O., Electroluminescence from Charge Transfer States in Polymer Solar Cells. *Journal of the American Chemical Society* **2009,** *131*, (33), 11819-11824.

(42) Faist, M.A.; Kirchartz, T.; Gong, W.; Ashraf, R.S.; McCulloch, I.; de Mello, J.C.; Ekins-Daukes, N.J.; Bradley, D.D.C.; Nelson, J., Competition between the Charge Transfer State and the Singlet States of Donor or Acceptor Limiting the Efficiency in Polymer:Fullerene Solar Cells. *Journal of the American Chemical Society* **2012,** *134*, (1), 685-692.

(43) Tvingstedt, K.; Vandewal, K.; Zhang, F.; Inganäs, O., On the Dissociation Efficiency of Charge Transfer Excitons and Frenkel Excitons in Organic Solar Cells: A Luminescence Quenching Study. *The Journal of Physical Chemistry C* **2010,** *114*, (49), 21824-21832.

(44) Chellappan, K.V.; Kandappa, S.K.; Rajaram, S.; Narayan, K.S., Ferroelectric Polymer Matrix for Probing Molecular Organization in Perylene Diimides. *The Journal of Physical Chemistry Letters* **2015,** *6*, (2), 224-229.

Chapter 6

Interface engineering for efficient charge extraction

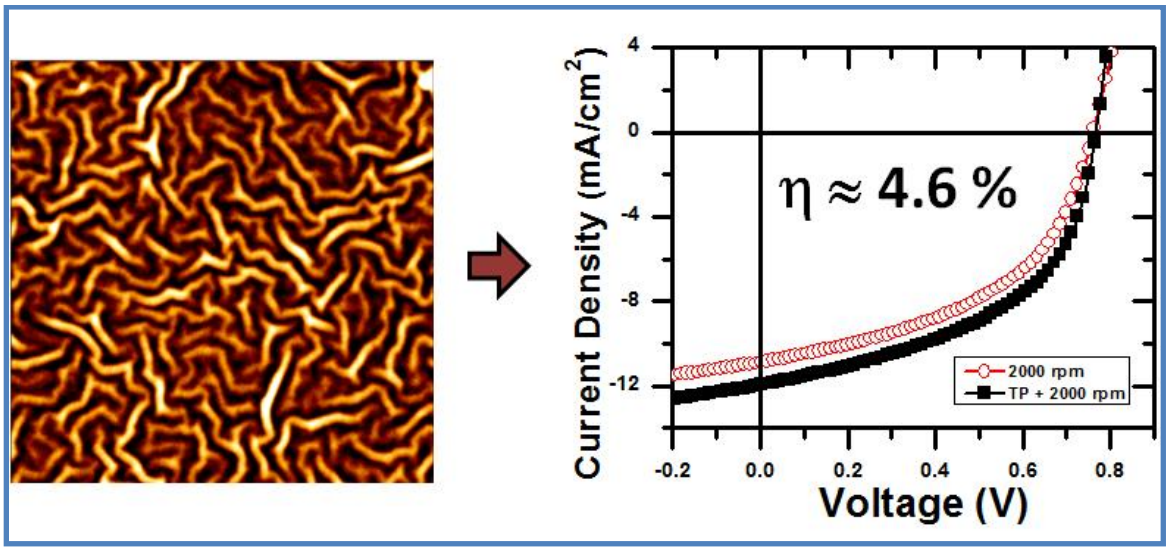

The nano-structured ZnO buffer layer and an additional TP interlayer are utilized to enhance the performance of fullerene-free bulk heterojunction inverted organic solar cells. An overall increase of 40 % in power conversion efficiency is demonstrated in these devices. The insertion of a twisted perylene (TP) acceptor layer planarizes and decreases the electron extraction barrier. Along with the reduced work function difference, selective transport of electrons prevents the accumulation of charges and decreases the electron-hole recombination at the interface. A combination of all these factors enhances the overall efficiency to 4.6 % which is significantly high and makes this system of the highest efficient fullerene-free solution-processed organic solar cells.

6 Interface engineering for efficient charge extraction

The drastic improvements in the device engineering and controlled fabrication methods have facilitated the realization of highly efficient BHJ organic solar cells.(*1-3*) Greater attention is given towards fabrication of large area modules using roll-to-roll fabrication techniques.(*4-6*) Despite the reports on high efficiency of solar cells in the laboratory scales (typical area of 10 mm^2), this technology is still challenged by stability, competitively lower efficiency and mass production of large area modules. To address the stability issue, the inverted geometry was proposed as an alternative to the conventional device architecture.(*1*, *7*) In the normal or conventional architecture, low work function metals such as Ca or Al are used as an electron collecting top electrode, which is prone to oxidation in the presence of moisture and oxygen. In addition to the top electrode degradation, the hole transporting buffer layer PEDOT:PSS is inherently hygroscopic and acidic which further accelerates the degradation of devices.(*8*) To overcome these problems, an inverted geometry of device is proposed wherein; the polarity of charge collection is reversed and stable electrodes are used. In the inverted geometry, high work function metals like Ag and Au are used as hole collecting top electrode. On the transparent conducting electrode side, PEDOT:PSS layer is replaced by a stable electron collecting metal oxide buffer layers.(*8*) The inverted device architecture has gained considerable attention in the research community particularly because of improved device stability.(*9-14*) Several metal oxides are effectively demonstrated as efficient buffer layer for electron collection (TiO_2, ZnO, SnO_x) and hole collection (MoO_x, NiO_x, V_2O_5) in organic BHJ solar cells.

Most of the device engineering and fabrication techniques are directed towards developing efficient solar cells containing a fullerene acceptor based photoactive layer. The strategies implemented for fullerene solar cell may not be directly applicable to the non-fullerene acceptor systems. In this regard, a new approach is required to increase the efficiency of organic solar cells featuring a non-fullerene acceptor. In this chapter, it is demonstrated that the efficiency of twisted perylene (TP) based solar cells can be further improved by utilizing nano-structured ZnO buffer layer and additional TP interlayer at the

electrode:photoactive interface. This effort is a direct consequence of the understanding and evaluation of the magnitude of the charge generation process which were discussed in earlier chapters. The order of magnitude increase in the J_{sc} is attributed to improved nano-morphology of the blend films.(*15*) Transient absorption spectroscopic measurements concluded that the charge generation magnitude in the TP acceptor blend system is comparable to that of fullerene blends.(*16*) However, the overall efficiency of the devices is limited by the charge transport properties. The challenges of charge transport and extraction in TP blends needs further optimization to achieve a high PCE. Since the TP molecules are fundamentally different from fullerene based acceptors in terms of bulk organization, phase distribution and electrode-interface formation, conventional approaches which are utilized for PCBM blends may not be directly applicable. This chapter addresses these issues and presents a combination of strategies involving a patterned ZnO layer and an acceptor interlayer to enhance the PCE of the TP based solar cell devices.(*16 b*)

6.1 Zinc oxide as electron collecting layer:

Zinc oxide is perhaps the most widely used electron transporting metal oxide buffer layer because of its high electron mobility, high transparency, low cost, stability and band level matching with LUMO of the acceptor molecules.(*17*) The band-gap of ZnO is ~ 3.3 eV which helps to block the UV-component of light and reduces the photo-degradation of active molecules.(*18*) Solution processed ZnO layer is an attractive option due to its low cost and compatibility for roll-to-roll fabrication of large area modules.(*19*) The key challenge in the roll-to-roll fabrication of solar cell is the processing temperature of each layer. Since the modules are fabricated on plastic substrates like ITO coated PET substrate, the maximum processing temperature of any coating layer should be less than 150 ^{0}C (temperature PET substrate can withstand). Therefore it is imperative to use low processing temperatures for all the layers, including the metal oxide buffer layer.(*20*) The early reports of sol-gel based ZnO layer used processing temperatures > 300 ^{0}C and this showed an effective increase in the electron collection efficiency of the solar cells.(*21-25*) Hence, a solution of ZnO nanoparticles dispersed in low boiling point solvent was used as an alternative in roll-to-roll fabrication. However, the metal oxide nanoparticle films are inclined to form a porous structure which further limits the device efficiency.(*26-31*) However, recent strategies in low temperature processed ZnO layer have yielded well connected amorphous layer with

improved electron extraction efficiency.(*32*, *33*) Further, surface modification of the ZnO buffer layer demonstrates efficient extraction of electrons at the interface.(*34-39*)

In addition, the spontaneous formation of nano-structures in solution deposited electron-extracting metal oxide layer enhances optical absorption due to scattering at the active layer:buffer layer interface in inverted organic solar cells.(*36*, *38*, *39*) The sol-gel based ZnO films of controlled thickness exhibits spontaneous formation of wrinkles upon annealing.(*23*) Along with the functionality of selectively extracting electrons, ZnO wrinkles provided appropriate texturing and effectively increase the optical path length. However, the wrinkling also engenders current inhomogeneity. This was compensated by surface modification.(*34*, *37*, *38*) In this chapter, the wrinkled ZnO surface is modified by inserting an ultrathin electron conducting TP layer prior to depositing the active layer. This procedure leads to reduced bimolecular recombination at the electron extracting interface which is evident from conducting and surface potential mapping measurements.(*16 b*)

6.2 Evolution of zinc oxide wrinkles:

Atomic force microscopy (AFM) images obtained from a high-resolution AFM (JPK Instruments Inc., Germany) system of ZnO sol-gel films spin coated on top of ITO coated glass substrate before thermal annealing is shown in the Fig. 1(a),(b). The height and phase image clearly demonstrates the nucleation of wrinkles in the ZnO film The wrinkle formation in a thin film is attributed to the deformation introduced from factors leading to surface instability.(*40*) For sol-gel based thin films, the compressive stress is generated during the evaporation of solvent due to difference in the thermal expansion coefficient between the film and substrate.(*41*) The phase image shows the evaporation of solvent from the sol-gel leading to compressive stress. This compressive stress induces a volumetric strain in the film leading to nucleation of wrinkles. The line profile of height and phase image along the ridge of the nucleated wrinkle is shown in the Figure 6.1c and 6.1d. The line profile clearly demonstrates the increased height and is devoid of solvent along the ridge. A schematic of the above mentioned phenomenon of wrinkling is presented in the Figure 6.1e.

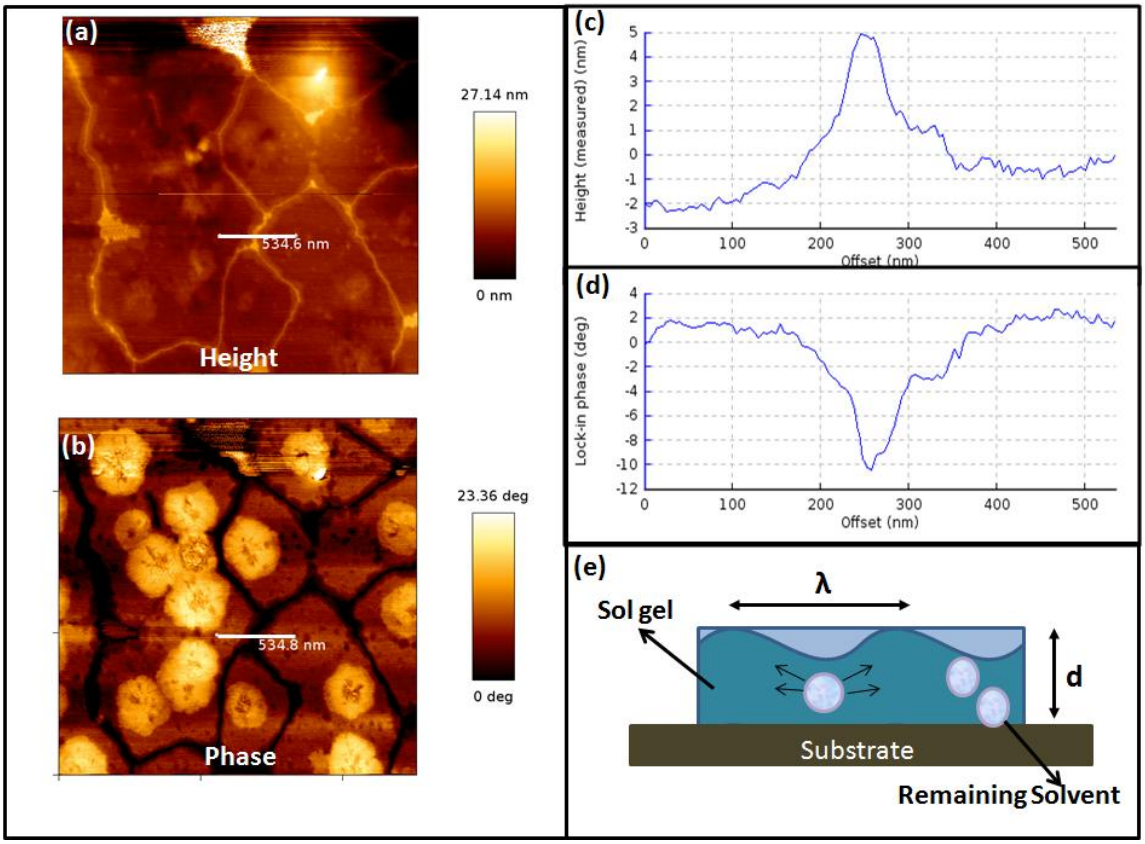

Figure 6.1: Evolution of ZnO wrinkles, the AFM height and its corresponding phase image (a, b) of the ZnO thin film before annealing exhibits the nucleation of wrinkles (scale ≈ 10 µm x 10 µm area). The phase image clearly shows the evaporation of solvent from the sol-gel leading to spatial instability. The instability due to volumetric stress manifested as bending of thin film is evident in the line profiles(c,d). (e) Represents the schematic of wrinkling of sol gel film with characteristic spacing 'λ' and thickness 'd'.(Reproduced with permission from the reference (16 b))

Further increase in the temperature above the boiling point of the solvent increases the volumetric strain in the film. This process leads to bending of the gelated film and finally results in the formation of a network of wrinkles. Figure 6.2 compares the AFM height and phase images of ZnO films before and after annealing. The ZnO film after annealing shows formation of the wrinkled network (Figure 6.2c) and corresponding phase image (Figure 6.2d) exhibits decreased phase difference due to complete evaporation of solvent.

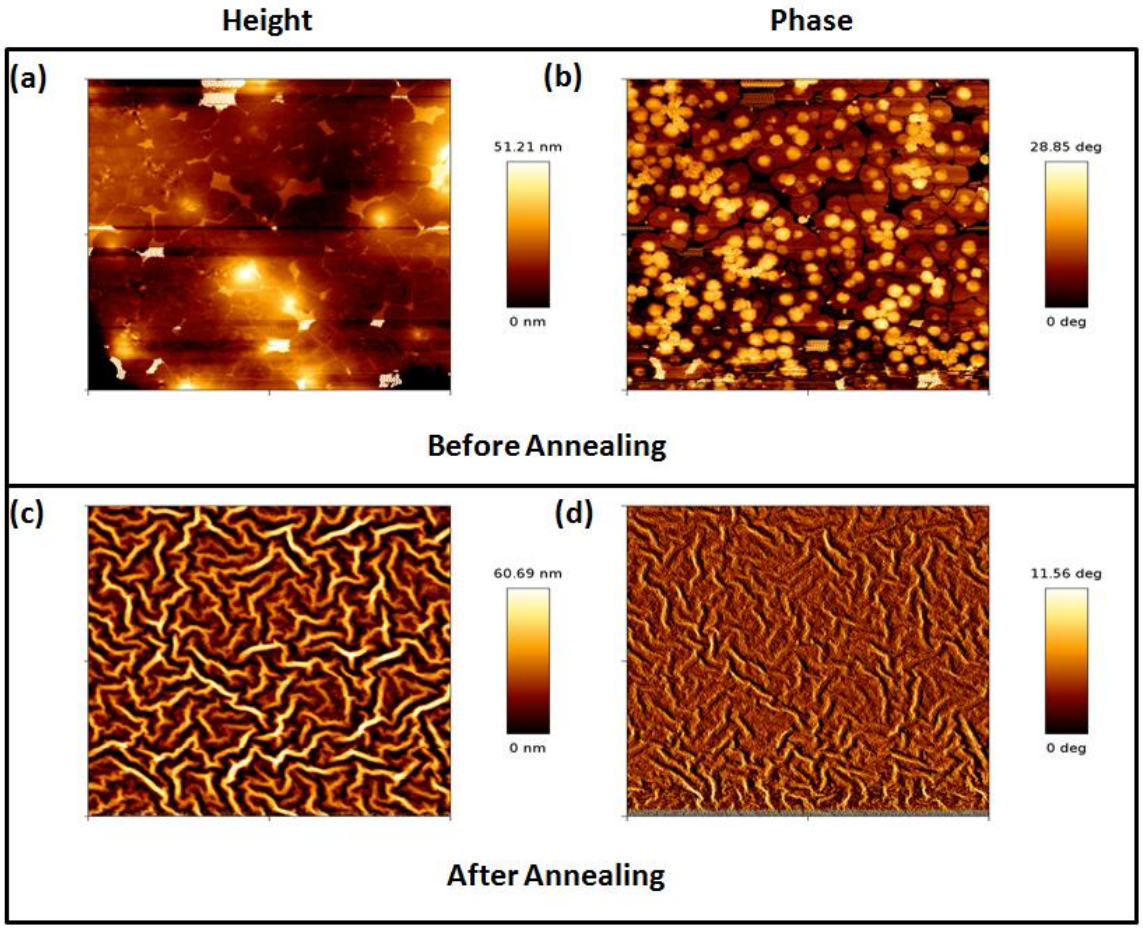

Figure 6.2: The AFM height and corresponding phase image of 10 µm x 10 µm area of ZnO sol-gel thin film on ITO substrate. (a) and (b) represents the ZnO film before annealing exhibiting nucleation of wrinkles during removal of solvent in the sol-gel. (c,d) represents the ZnO film after annealing with the characteristic spontaneous wrinkle formation. (scale ≈10 µm x 10 µm area). (Reproduced with permission from the reference (16 b))

6.3 Characteristics of zinc oxide wrinkles:

AFM images of ZnO sol-gel films spin coated at different speed is illustrated in Fig. 3(a-e). The top and bottom row represent the height and corresponding phase image respectively. The height images exhibit isotropic wrinkle patterns with characteristic spacing (λ), fractal length (L_f) and root mean squared (RMS) surface roughness (σ_{rms}). Corresponding phase images show more uniform distribution exhibiting complete formation of ZnO.

The characteristics of wrinkles are strongly dependent on film thickness [$\lambda \approx (d)^{0.75}$] and annealing conditions.(41) The wrinkle density and surface roughness of the film also increases with annealing time while maintaining the characteristic 'λ'. In our procedure, ZnO sol-gel precursor was prepared by dissolving Zinc acetate dihydrate [$Zn(CH_3COO)_2.2H_2O$] in 2-methoxyethanol and ethanolamine as stabilizer (see device fabrication and details section).

The solution was stirred for 1 hr at 65^0 C and left for 3 hr to form a gel. The sol-gel precursor was spin coated at different speeds, annealed with ramp rate of 5^0 C/min till 150^0 C and kept at 150^0 C for 2 hr in air.

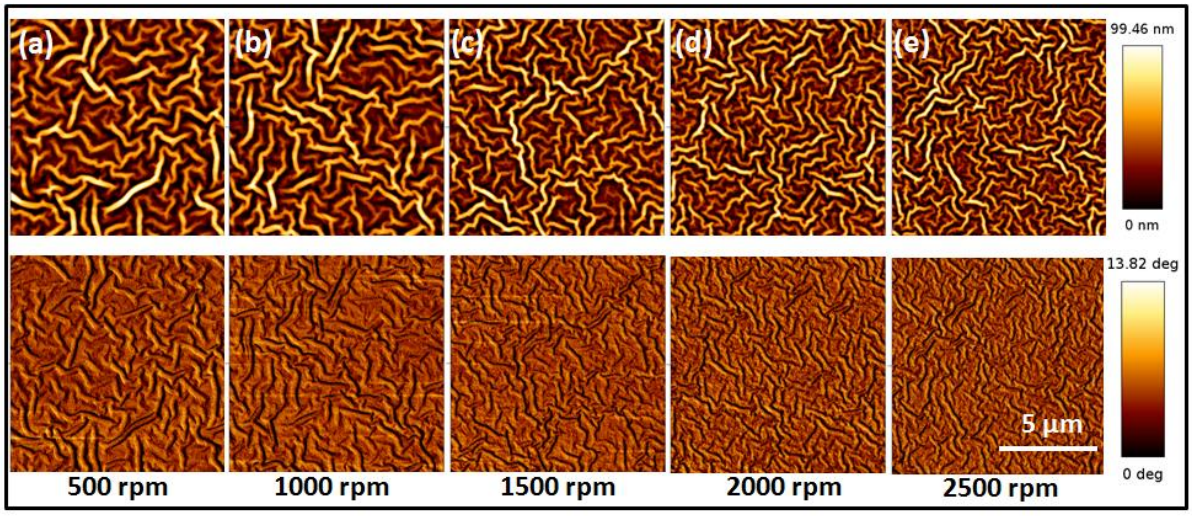

Figure 6.3: Wrinkling of ZnO Sol gel films upon annealing. Change in the wavelength and fractal length of the wrinkles for different film thickness varied by spin coating at different speed (a-e). Top row is the AFM height image and bottom row shows the corresponding phase image. (Reproduced with permission from the reference (16 b))

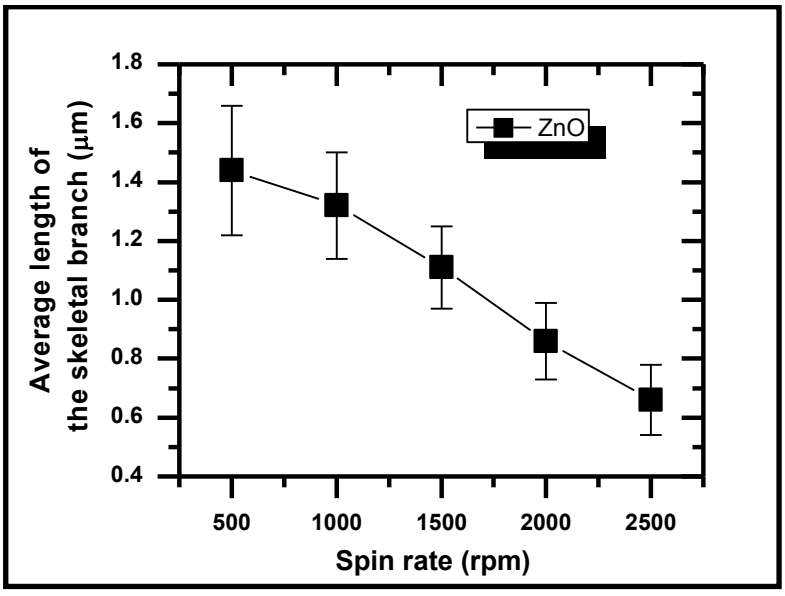

Figure 6.4: The average length of the skeletal branch or the fractal length changes with different thickness of the ZnO film. The graph shows the fractal lengths of ZnO wrinkles obtained in our experiments by spin coating at different rpms. Error bar corresponds to an average over an 10 µm x 10µ m area image. (Reproduced with permission from the reference (16 b))

Fig. 3 represents the formation of wrinkles of ZnO films with different λ, L_f and σ_{rms} spun at different speed from the same precursor annealed at similar conditions. The L_f

decreases from ~1.4 µm to ~0.6 µm (Figure 6.4) and λ decreases from ~ 800 nm to ~ 200 nm for the films coated at 500 rpm and 2500 rpm respectively.

6.4 Nano-structured zinc oxide buffer layer:

Blend films consisting of PBDTTT-CT electron donor and TP electron acceptor (Figure 6.5 (c) inset) in a 1:1 ratio by weight were spin coated (12 mg/ml solution concentration in anhydrous chlorobenzene inside a nitrogen filled glovebox at 1000 rpm) on the nanostructured ZnO layer. This procedure of spin coating resulted in an active layer of ~ 100 nm film thickness on a planar surface, which was optimum for efficient charge generation in BHJ systems.(*16*) Two important factors that have to be considered in depositing the active layer on nano-structured films are surface wettability and pinhole-free surface coverage of active layer.(*42*) Increased surface roughness generally leads to pinholes and hence increases leakage current through electrical shorting. This pinhole effects results in overall reduction of PCE, open circuit voltage and fill factor

.

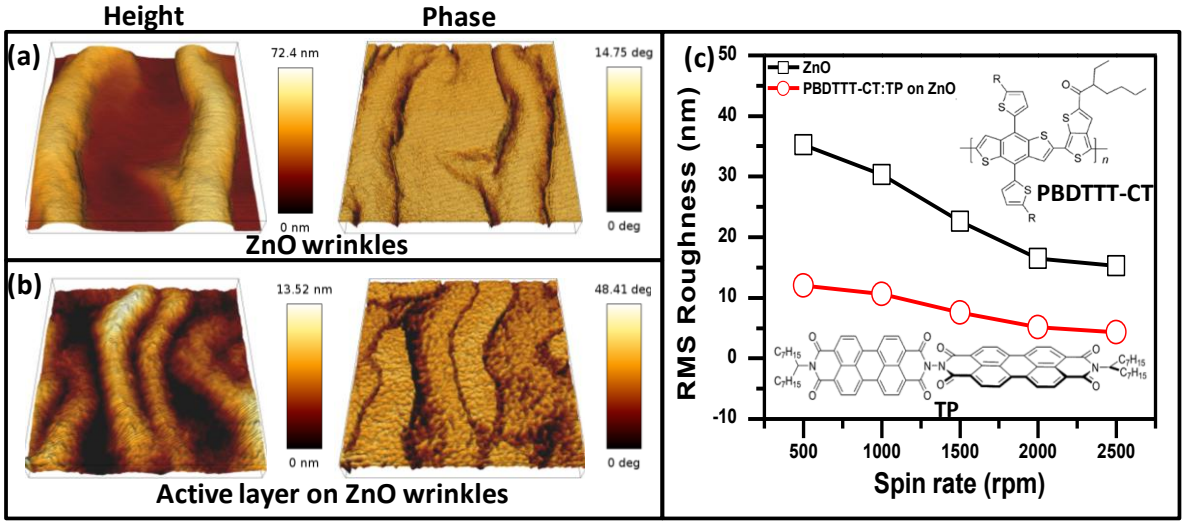

Figure 6.5: Wetting of ZnO wrinkles with PBDTTT-CT:TP active layer. (a) AFM height and phase image showing the features of bare wrinkles, (b) AFM Height and phase image exhibiting complete wetting of ZnO surface with PBDTTT-CT:TP BHJ, and (c) RMS roughness of the surface with and without PBDTTT-CT:TP on ZnO at different rpm films. Area of the 3D images is 1 µm x 1 µm. Inset of (c) shows the chemical structure of PBDTTT-CT and TP. (Reproduced with permission from the reference (16 b))

The surface morphology of ZnO and PBDTTT-CT:TP/ZnO films is represented in Fig. 5 (a) and (b). Comparison of height and phase images between the films clearly demonstrates the decrease in peak-to-valley roughness and areal coverage. This trend is established

throughout the surface as shown in the large area scan (Figure 6.6). Phase image exhibits increased phase difference on the PBDTTT-CT:TP/ZnO surface due to the donor-acceptor components in the BHJ. σ_{rms} reduces from ~35 nm to ~12 nm for the ZnO film coated at 500 rpm without and with active layer respectively. Fig. 5 (c) represents the monotonic decrease of σ_{rms} with increase in spin rate for both the films.

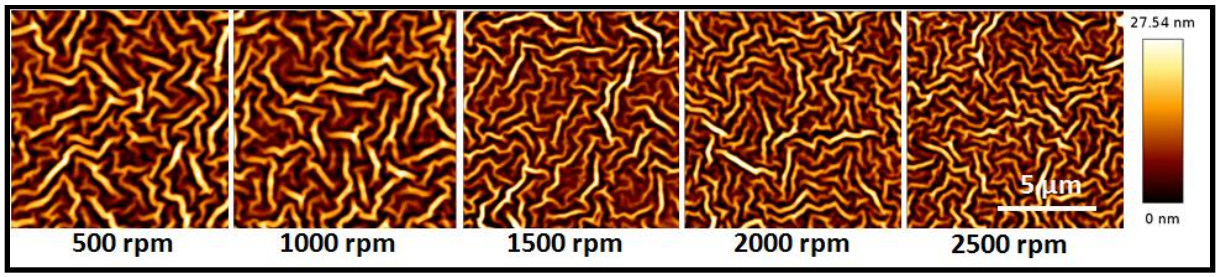

Figure 6.6: AFM height image of photoactive blend coated on top of ZnO wrinkle suface formed at different rotation speed. The image exhibits full coverage of the ZnO surface without any pinholes. (Reproduced with permission from the reference (16 b)).

The fabrication of inverted solar cells was completed by thermal evaporation of hole transport layer MoOx (~11 nm) followed by deposition of Ag (~100nm) using a shadow mask at a base pressure of 10^{-6} mbar. The current density(J)-voltage(V) characteristics of solar cells fabricated by spin coating ZnO films at different rate are represented in Figure 6.7 (a). The results are tabulated in table 1.

When the spin speed for depositing ZnO was increased from 500 to 2000 rpm, the J_{sc} increased from 8.15 to 10.02 mA/cm^2 and the V_{oc} increased from 0.32 to 0.73 V. The maximum power conversion efficiency (PCE) of 4.02 %, J_{sc} = 10.9 mA/cm^2, V_{oc} = 0.76 and fill factor (*FF*) = 48.4 % was achieved for ZnO layer coated at 2000 rpm. In comparison to the planar ZnO layer, the nanostructured ZnO layer offers a higher interfacial area which enables a more efficient charge extraction process.(16) Figure 6.7 (b) shows the incident photon to current conversion efficiency (IPCE) of these devices. The bimodal absorption of blend components leads to efficient generation of charges over the entire visible spectrum (400-800 nm) with maxima at 540 nm for all the devices. Maximum IPCE of ~50 % at 540 nm was obtained for the device with 2000 rpm ZnO layer. The calculated J_{sc} from the IPCE curve correlates with the measured device J_{sc} for all the films. The inset of Fig. 7 (b) shows the schematic of a complete device consisting of Glass/ITO/ZnO/PBDTTT-CT:TP/MoOx/Ag heterojunction.

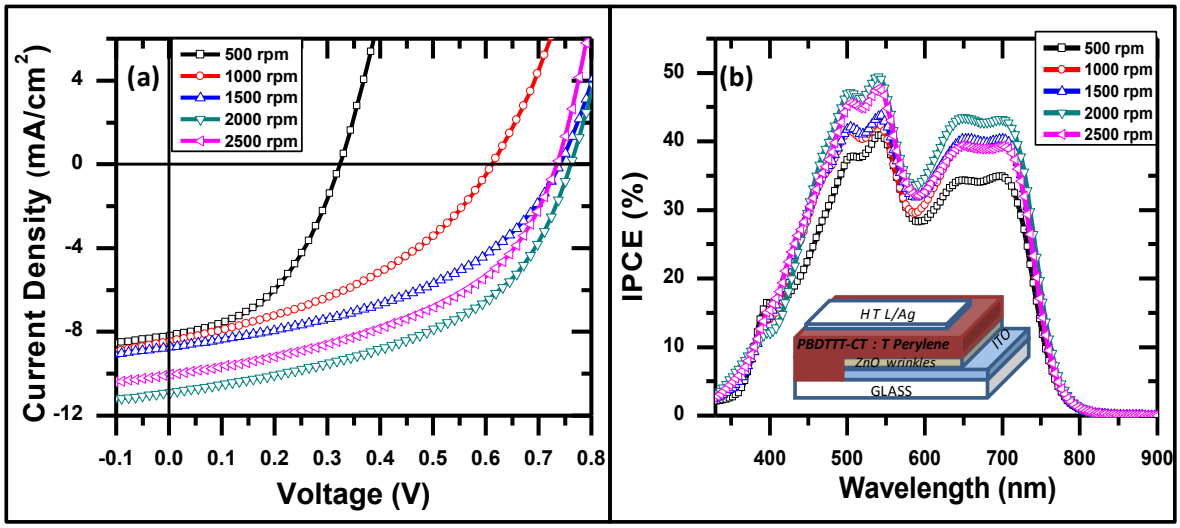

Figure 6.7: (a) J-V curves of solar cells of 1:1 ratio PBDTTT-CT:TP BHJ on ZnO wrinkle surface formed by spin coating at different rpms. (b) Corresponding IPCE of solar cells. Inset of Fig. 3(b) shows the device architecture. (Reproduced with permission from the reference (16 b))

Table I: J-V characteristics of solar cells on ZnO wrinkle of different thickness.

Speed (rpm)	J_{sc} (mA/cm^2)	V_{oc} (V)	FF (%)	η (%)[a]
500	8.15 ± 0.2	0.322 ± 0.010	45.62 ± 0.7	1.20 ± 0.12 (1.34)
1000	8.45 ± 0.4	0.615 ± 0.015	40.24 ± 1.0	2.07 ± 0.18 (2.12)
1500	8.69 ± 0.3	0.739 ± 0.009	44.30 ± 0.6	2.84 ± 0.07 (2.93)
2000	10.85± 0.1	0.760 ± 0.005	48.41 ± 0.2	3.99 ± 0.03 (4.02)
2500	10.02± 0.1	0.733 ± 0.006	46.56 ± 0.3	3.42 ± 0.06 (3.53)

[a] number in the brackets show highest efficiency devices.

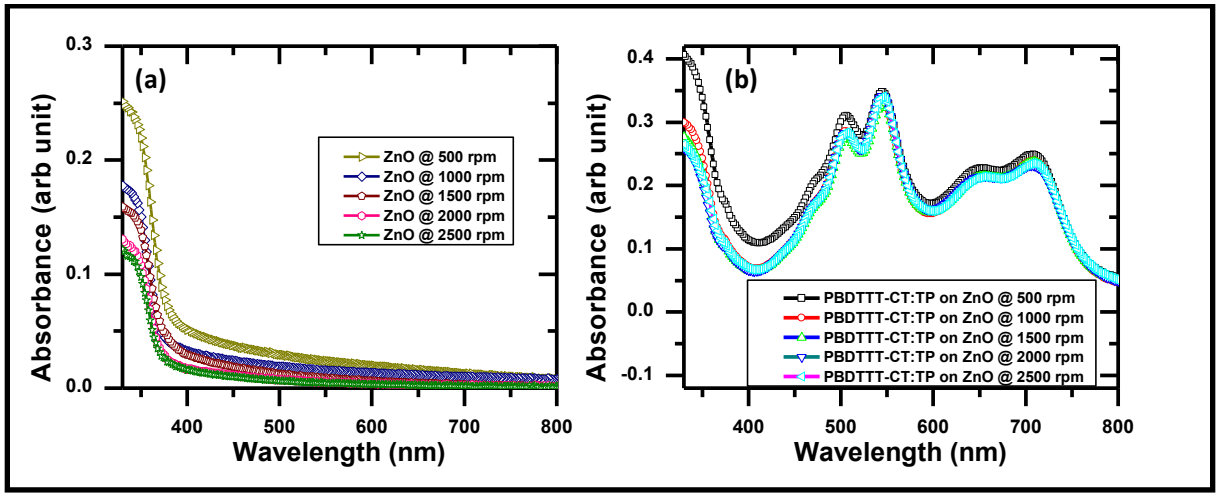

Figure 6.8: (a) The absorption spectra of nanostructured ZnO films spin coated at different rpms. (b) The absorption spectra of PBDTTT-CT:TP 1:1 ratio donor acceptor blend spin coated at 1000 rpm(12mg/ml in chlorobenzene) on top of nanostructured ZnO films spin coated at different rpms. (Reproduced with permission from the reference (16 b))

The absorption of ZnO/PBDTTT-CT:TP films with different ZnO rpm rates exhibit increased contribution of ZnO absorption below 400 nm (Figure 6.8a). However, the IPCE does not show significant photocurrent below 400 nm in the device. This clearly indicates that ZnO has minimal contribution to carrier photogeneration. Increased PCE is mainly assisted by efficient electron extraction at the ZnO/PBDTTT-CT:TP interface (Figure 6.8b). Further, variation of ZnO thickness varies the optical field profile inside the BHJ. This is evident from the normalized IPCE spectra (Figure 6.9).

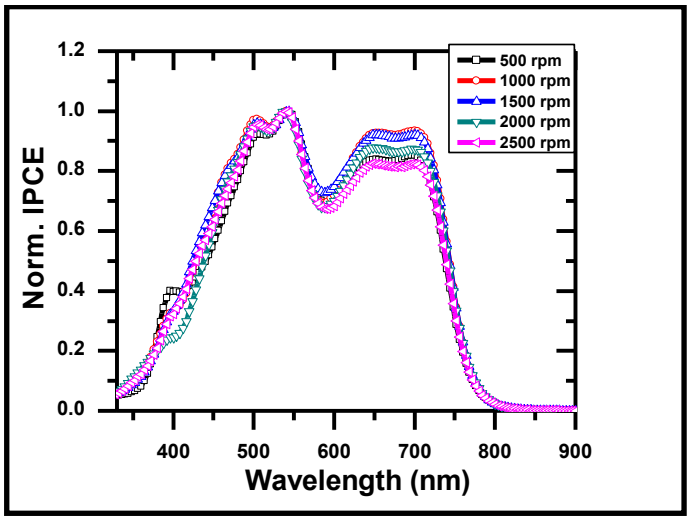

Figure 6.9: Normalized incident photon to current conversion efficiency of PBDTTT-CT:TP device fabricated on nanopatterned ZnO buffer layer spin coated at different rpm in inverted solar cell geometry. The difference arises due to varied field profile due to different thickness of the buffer layer. (Reproduced with permission from the reference (16 b))

6.5 Additional TP interlayer:

To further optimize the cells, a thin layer of electron acceptor was introduced between the ZnO wrinkle surface and the photo-active layer. Cho et al.(*34*) have reported 16 % increase in PCE by adding $PC_{61}BM$ interlayer between ZnO and BHJ. The insertion of additional $PC_{61}BM$ interlayer enhanced current homogeneity and lowered charge accumulation at the interface. In the present study, we utilize the ultrathin layer of TP as electron extractor between ZnO wrinkle surface and PBDTTT-CT:TP active layer. TP solution of 1 mg/ml concentration in anhydrous chlorobenzene was spin coated at 1000 rpm for 60 s on top of ZnO wrinkles. The films were annealed at 100^0 C for 5 mins. Just before coating the active blend layer, an orthogonal-solvent (ethanol) was spin coated at 1000 rpm for 5 s to avoid the re-dispersal of the thin TP layer upon introduction of the blend solution.

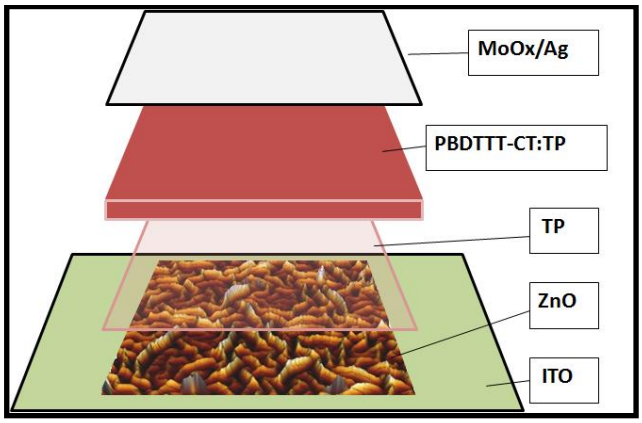

Figure 6.10: Schematic showing insertion of additional TP electron extracting layer in between ZnO wrinkles and PBDTTT-CT:TP active layer.

Conducting AFM imaging was used to follow the electron extracting homogeneity of TP interlayer on the ZnO wrinkle surface as shown in Figure 6.11 (a) and (b) with a bias between ITO and Pt/Cr coated CAFM tip. Wrinkled ZnO surface without TP interlayer shows inhomogeneous current mapping. The current values exhibit maxima in the trenches and minima at the ridges. Under similar bias conditions, the ZnO surface with TP interlayer displays more homogenous current mapping. In effect, the additional TP layer increases the uniformity of electron extraction at the electrode:active-layer interface.

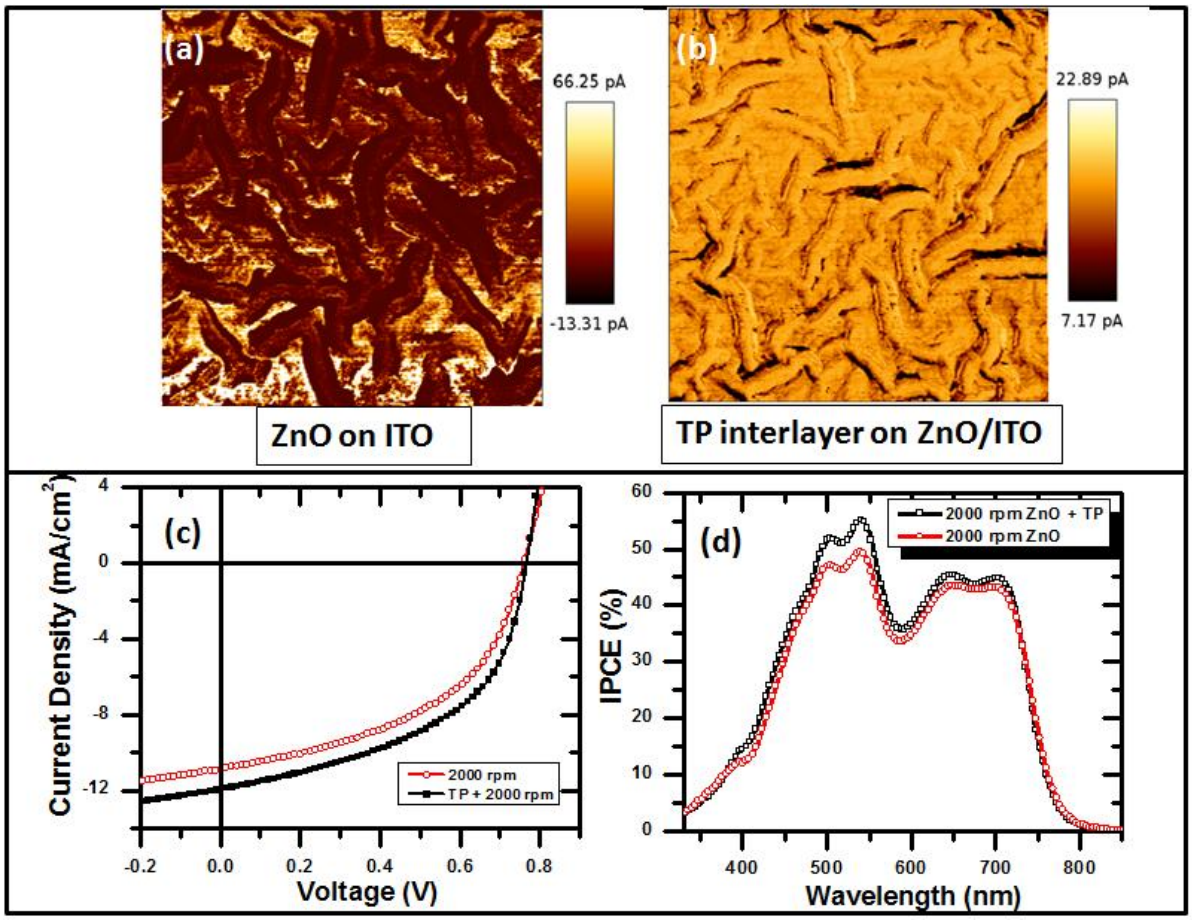

Figure 6.11: (a) CAFM of bare ZnO surface and (b) Zno surface coated with TP interlayer. (c) J-V curves of solar cells of 1:1 ratio PBDTTT-CT:TP BHJ on ZnO surface with and without TP interlayer. (c) Corresponding IPCE of solar cells showing maximum of 55 % at λ ≈540 nm. Scale bar represents the relative current value for an applied 8 V bias w.r.t Pt/Cr coated tip. (Reproduced with permission from the reference (16 b))

Further, the solar cell fabrication was completed by evaporating MoO_x and Ag on top of the active layer. Fig. 11 (c) represents the J-V characteristics of devices with and without the TP interlayer. The cell with TP interlayer shows an enhanced PCE of 4.6 %, with J_{sc} = 11.9 mA/cm^2, V_{oc} = 0.76 V and *FF* = 50.3 %. Adequate number of devices were fabricated and measured to arrive at a statistics, necessary to affirm the trend. This trend represents a 15 % increase in PCE when compared to devices without TP interlayer. This high PCE places the device among the group of highly efficient fullerene-free organic BHJ solar cells. The J-V curve clearly indicates that the enhanced PCE with additional TP layer is due to the increase in J_{sc} when compared to devices without TP interlayer. Increased J_{sc} is attributed to increased current homogeneity at the ZnO and active layer interface.(43) Reduced bimolecular recombination of photogenerated electrons and holes at the charge extracting interface assists in increasing overall charge extraction efficiency. Fig. 11 (d) shows the

IPCE spectra of devices with and without TP interlayer. Devices with TP interlayer exhibit overall increase in the IPCE spectrum with maximum of ~55 % at ~540 nm. This is further evident from the increased J_{sc} in the J-V characteristics. Additionally, J_{sc} estimated from IPCE correlates with the measured J_{sc} from the J-V curve. In addition, Kelvin probe force microscopy (KPFM) was carried out to map the surface potential of ZnO with and without TP interlayer (Figure 6.12). Surface potential with respect to Pt/Cr coated AFM tip shows reduced potential between ZnO and ZnO+TP layers. This implies ZnO with TP interlayer effectively reduces the work function of the electrode leading to efficient extraction of electrons. The overall increase in IPCE spectrum and reduced work function from KPFM data suggests that the additional TP interlayer essentially contributes to the charge extraction process along with relatively increased photocharge generation from the TP absorption.

All the AFM images were acquired using high resolution AFM system (JPK Instruments Inc., Germany). Conducting-AFM measurements were carried out using Pt/Cr tip biased at 8 V with respect to AFM tip. Kelvin Probe measurements were carried out to map the surface potential on Zno and ZnO+TP layer with respect to Pt/Cr coated conducting tip.

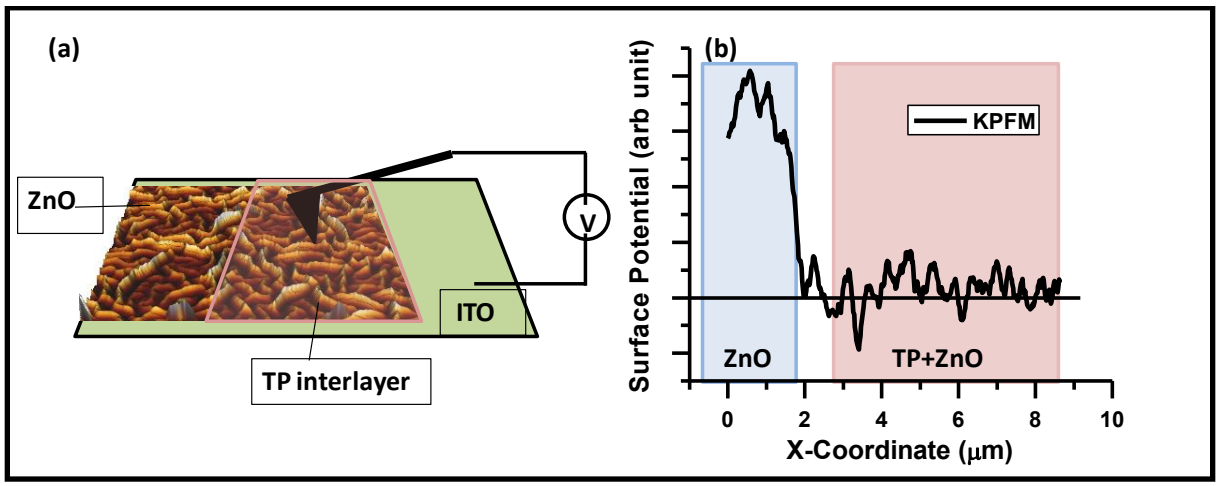

Figure 6.12: (a) schematic of executing Kelvin probe force microscopy (KPFM) on ZnO wrinkle surface partially coated with additional TP interlayer. (b) Surface potential line scan using Pt/Cr coated conducting tip exhibiting reduced surface potential by additional TP interlayer. (Reproduced with permission from the reference (16 b))

In previous studies,(16) it was shown that the charge generation efficiency of TP blends is comparable with $PC_{70}BM$ blends. However, the device efficiency was limited by the charge transport through the bulk. In the present study the charge extraction efficiency is

improved by utilizing an additional TP layer between ZnO and active layer. A 15 % improvement in PCE is observed compared to devices without the additional TP layer. This improvement follows the trend observed in fullerene based cells, where an additional $PC_{60}BM$ layer was introduced to improve the charge extraction (*34*) and PCE by 16 %. These set of observations indicate that in general, the additional pristine acceptor layer can enhance PCE by improving electron extraction.

6.6 Summary:

The device engineering utilizing nanostructured ZnO wrinkles and insertion of a TP electron acceptor interlayer yielded an overall increase of > 40 % in PCE in TP based BHJs. The morphology of the ZnO wrinkles was controlled by spin coating the sol-gel at different speeds. The wrinkles enhanced the light-harvesting efficiency of the active layer by acting as light scattering centers along with increased surface area. Good surface coverage was obtained by spin coating active layer on top of ZnO wrinkles. The devices with PBDTTT-CT:TP photoactive layer exhibited enhanced performance with PCE as high as 4 %. IPCE spectra of these devices concluded that the ZnO wrinkles contribute more towards the charge extraction property than photogeneration of charge carriers. The cells with additional TP interlayer introduced between the ZnO wrinkles and active layer exhibited superior performance. The devices exhibited a PCE of 4.6 %, which is among the high efficient fullerene free-organic BHJ solar cells. IPCE reached a maximum of 55 % at 540 nm. The 15 % increase in PCE was attributed to increased current homogeneity at the ZnO wrinkle and photoactive layer interface as measured by CAFM. In addition, KPFM showed a decrease in work function of the ZnO surface containing TP interlayer. We attribute the enhanced performance of the device to efficient extraction by reduced bimolecular recombination of photogenerated electrons and holes at the ZnO wrinkles and photo active layer interface. Further refinements in the present approach can possibly lead to device performances comparable to fullerene based BHJs.

References:

(1) Nelson, J., Polymer:fullerene bulk heterojunction solar cells. *Materials Today* **2011,** *14*, (10), 462-470.

(2) Koster, L.J.A.; Shaheen, S.E.; Hummelen, J.C., Pathways to a New Efficiency Regime for Organic Solar Cells. *Advanced Energy Materials* **2012,** *2*, (10), 1246-1253.

(3) He, Z.; Zhong, C.; Su, S.; Xu, M.; Wu, H.; Cao, Y., Enhanced power-conversion efficiency in polymer solar cells using an inverted device structure. *Nat Photon* **2012,** *6*, (9), 591-595.

(4) Søndergaard, R.; Hösel, M.; Angmo, D.; Larsen-Olsen, T.T.; Krebs, F.C., Roll-to-roll fabrication of polymer solar cells. *Materials Today* **2012,** *15*, (1–2), 36-49.

(5) Krebs, F.C., All solution roll-to-roll processed polymer solar cells free from indium-tin-oxide and vacuum coating steps. *Organic Electronics* **2009,** *10*, (5), 761-768.

(6) Krebs, F.C.; Fyenbo, J.; Jorgensen, M., Product integration of compact roll-to-roll processed polymer solar cell modules: methods and manufacture using flexographic printing, slot-die coating and rotary screen printing. *Journal of Materials Chemistry* **2010,** *20*, (41), 8994-9001.

(7) Schumann, S.; Da Campo, R.; Illy, B.; Cruickshank, A.C.; McLachlan, M.A.; Ryan, M.P.; Riley, D.J.; McComb, D.W.; Jones, T.S., Inverted organic photovoltaic devices with high efficiency and stability based on metal oxide charge extraction layers. *Journal of Materials Chemistry* **2011,** *21*, (7), 2381-2386.

(8) Chen, L.-M.; Hong, Z.; Li, G.; Yang, Y., Recent Progress in Polymer Solar Cells: Manipulation of Polymer:Fullerene Morphology and the Formation of Efficient Inverted Polymer Solar Cells. *Advanced Materials* **2009,** *21*, (14-15), 1434-1449.

(9) Liao, H.-H.; Chen, L.-M.; Xu, Z.; Li, G.; Yang, Y., Highly efficient inverted polymer solar cell by low temperature annealing of Cs2CO3 interlayer. *Applied Physics Letters* **2008,** *92*, (17), 173303.

(10) White, M.S.; Olson, D.C.; Shaheen, S.E.; Kopidakis, N.; Ginley, D.S., Inverted bulk-heterojunction organic photovoltaic device using a solution-derived ZnO underlayer. *Applied Physics Letters* **2006,** *89*, (14), 143517.

(11) Waldauf, C.; Morana, M.; Denk, P.; Schilinsky, P.; Coakley, K.; Choulis, S.A.; Brabec, C.J., Highly efficient inverted organic photovoltaics using solution based titanium oxide as electron selective contact. *Applied Physics Letters* **2006,** *89*, (23), 233517.

(12) Shim, W.H.; Park, S.-Y.; Park, M.Y.; Seo, H.O.; Kim, K.-D.; Kim, Y.T.; Kim, Y.D.; Kang, J.-W.; Lee, K.H.; Jeong, Y., et al., Multifunctional SWCNT-ZnO Nanocomposites for Enhancing Performance and Stability of Organic Solar Cells. *Advanced Materials* **2011,** *23*, (4), 519-522.

(13) Savva, A.; Petraki, F.; Elefteriou, P.; Sygellou, L.; Voigt, M.; Giannouli, M.; Kennou, S.; Nelson, J.; Bradley, D.D.C.; Brabec, C.J., et al., The Effect of Organic and Metal Oxide Interfacial layers on the Performance of Inverted Organic Photovoltaics. *Advanced Energy Materials* **2013,** *3*, (3), 391-398.

(14) Jørgensen, M.; Norrman, K.; Gevorgyan, S.A.; Tromholt, T.; Andreasen, B.; Krebs, F.C., Stability of Polymer Solar Cells. *Advanced Materials* **2012,** *24*, (5), 580-612.

(15) Rajaram, S.; Shivanna, R.; Kandappa, S.K.; Narayan, K.S., Nonplanar Perylene Diimides as Potential Alternatives to Fullerenes in Organic Solar Cells. *The Journal of Physical Chemistry Letters* **2012,** *3*, (17), 2405-2408.

(16 a) Shivanna, R.; Shoaee, S.; Dimitrov, S.; Kandappa, S.K.; Rajaram, S.; Durrant, J.R.; Narayan, K.S., Charge generation and transport in efficient organic bulk heterojunction solar cells with a perylene acceptor. *Energy & Environmental Science* **2014,** *7*, (1), 435-441.

(16 b) Shivanna, R.; Rajaram, S.; Narayan, K., Interface engineering for efficient fullerene-free organic solar cells. *Applied Physics Letters* **2015,** *106*, (12), 123301.

(17) Meyer, J.; Hamwi, S.; Kröger, M.; Kowalsky, W.; Riedl, T.; Kahn, A., Transition Metal Oxides for Organic Electronics: Energetics, Device Physics and Applications. *Advanced Materials* **2012,** *24*, (40), 5408-5427.

(18) Gao, Y.; Gereige, I.; El Labban, A.; Cha, D.; Isimjan, T.T.; Beaujuge, P.M., Highly Transparent and UV-Resistant Superhydrophobic SiO2-Coated ZnO Nanorod Arrays. *ACS Applied Materials & Interfaces* **2014,** *6*, (4), 2219-2223.

(19) Znaidi, L., Sol–gel-deposited ZnO thin films: A review. *Materials Science and Engineering: B* **2010,** *174*, (1–3), 18-30.

(20) Lakatos, A.I., Introduction. *Journal of the Society for Information Display* **2000,** *8*, (1), 1-1.

(21) Chunfu, Z.; Hailong, Y.; Zhenhua, L.; Yue, H., Inverted Organic Photovoltaic Cells with Solution-Processed Zinc Oxide as Electron Collecting Layer. *Japanese Journal of Applied Physics* **2011,** *50*, (8R), 082302.

(22) Liang, Z.; Zhang, Q.; Wiranwetchayan, O.; Xi, J.; Yang, Z.; Park, K.; Li, C.; Cao, G., Effects of the Morphology of a ZnO Buffer Layer on the Photovoltaic Performance of Inverted Polymer Solar Cells. *Advanced Functional Materials* **2012,** *22*, (10), 2194-2201.

(23) Lim, S.Y.; Macdonald, D., Measuring dopant concentrations in p-type silicon using iron-acceptor pairing monitored by band-to-band photoluminescence. *Solar Energy Materials and Solar Cells* **2011,** *95*, (8), 2485-2489.

(24) Sekine, N.; Chou, C.-H.; Kwan, W.L.; Yang, Y., ZnO nano-ridge structure and its application in inverted polymer solar cell. *Organic Electronics* **2009,** *10*, (8), 1473-1477.

(25) Kang, Y.-J.; Lim, K.; Jung, S.; Kim, D.-G.; Kim, J.-K.; Kim, C.-S.; Kim, S.H.; Kang, J.-W., Spray-coated ZnO electron transport layer for air-stable inverted organic solar cells. *Solar Energy Materials and Solar Cells* **2012,** *96*, (0), 137-140.

(26) Mbule, P.S.; Kim, T.H.; Kim, B.S.; Swart, H.C.; Ntwaeaborwa, O.M., Effects of particle morphology of ZnO buffer layer on the performance of organic solar cell devices. *Solar Energy Materials and Solar Cells* **2013,** *112*, (0), 6-12.

(27) Ibrahem, M.A.; Wei, H.-Y.; Tsai, M.-H.; Ho, K.-C.; Shyue, J.-J.; Chu, C.W., Solution-processed zinc oxide nanoparticles as interlayer materials for inverted organic solar cells. *Solar Energy Materials and Solar Cells* **2013,** *108*, (0), 156-163.

(28) Beek, W.J.E.; Wienk, M.M.; Kemerink, M.; Yang, X.; Janssen, R.A.J., Hybrid Zinc Oxide Conjugated Polymer Bulk Heterojunction Solar Cells. *The Journal of Physical Chemistry B* **2005,** *109*, (19), 9505-9516.

(29) Pacholski, C.; Kornowski, A.; Weller, H., Self-Assembly of ZnO: From Nanodots to Nanorods. *Angewandte Chemie International Edition* **2002,** *41*, (7), 1188-1191.

(30) Frederik, C.K.; Yi, T.; Ralf, T.; Jens, W.A., A simple nanostructured polymer/ZnO hybrid solar cell—preparation and operation in air. *Nanotechnology* **2008,** *19*, (42), 424013.

(31) Jeong, S.; Moon, J., Low-temperature, solution-processed metal oxide thin film transistors. *Journal of Materials Chemistry* **2012,** *22*, (4), 1243-1250.

(32) Ka, Y.; Lee, E.; Park, S.Y.; Seo, J.; Kwon, D.-G.; Lee, H.H.; Park, Y.; Kim, Y.S.; Kim, C., Effects of annealing temperature of aqueous solution-processed ZnO electron-selective layers on inverted polymer solar cells. *Organic Electronics* **2013,** *14*, (1), 100-104.

(33) Park, H.-Y.; Lim, D.; Kim, K.-D.; Jang, S.-Y., Performance optimization of low-temperature-annealed solution-processable ZnO buffer layers for inverted polymer solar cells. *Journal of Materials Chemistry A* **2013,** *1*, (21), 6327-6334.

(34) Cho, S.; Kim, K.-D.; Heo, J.; Lee, J.Y.; Cha, G.; Seo, B.Y.; Kim, Y.D.; Kim, Y.S.; Choi, S.-y.; Lim, D.C., Role of additional PCBM layer between ZnO and photoactive layers in inverted bulk-heterojunction solar cells. *Sci. Rep.* **2014,** *4*.

(35) Bai, S.; Jin, Y.; Liang, X.; Ye, Z.; Wu, Z.; Sun, B.; Ma, Z.; Tang, Z.; Wang, J.; Würfel, U., et al., Ethanedithiol Treatment of Solution-Processed ZnO Thin Films: Controlling the Intragap States of Electron Transporting Interlayers for Efficient and Stable Inverted Organic Photovoltaics. *Advanced Energy Materials* **2015,** *5*, (5), n/a-n/a.

(36) Lim, D.C.; Kim, K.-D.; Park, S.-Y.; Hong, E.M.; Seo, H.O.; Lim, J.H.; Lee, K.H.; Jeong, Y.; Song, C.; Lee, E., et al., Towards fabrication of high-performing organic photovoltaics: new donor-polymer, atomic layer deposited thin buffer layer and plasmonic effects. *Energy & Environmental Science* **2012,** *5*, (12), 9803-9807.

(37) Kim, K.-D.; Lim, D.C.; Hu, J.; Kwon, J.-D.; Jeong, M.-G.; Seo, H.O.; Lee, J.Y.; Jang, K.-Y.; Lim, J.-H.; Lee, K.H., et al., Surface Modification of a ZnO Electron-Collecting Layer Using Atomic Layer Deposition to Fabricate High-Performing Inverted Organic Photovoltaics. *ACS Applied Materials & Interfaces* **2013,** *5*, (17), 8718-8723.

(38) Hsieh, C.-H.; Cheng, Y.-J.; Li, P.-J.; Chen, C.-H.; Dubosc, M.; Liang, R.-M.; Hsu, C.-S., Highly Efficient and Stable Inverted Polymer Solar Cells Integrated with a Cross-Linked Fullerene Material as an Interlayer. *Journal of the American Chemical Society* **2010,** *132*, (13), 4887-4893.

(39) Cheng, Y.-J.; Hsieh, C.-H.; He, Y.; Hsu, C.-S.; Li, Y., Combination of Indene-C60 Bis-Adduct and Cross-Linked Fullerene Interlayer Leading to Highly Efficient Inverted Polymer Solar Cells. *Journal of the American Chemical Society* **2010,** *132*, (49), 17381-17383.

(40) Bowden, N.; Brittain, S.; Evans, A.G.; Hutchinson, J.W.; Whitesides, G.M., Spontaneous formation of ordered structures in thin films of metals supported on an elastomeric polymer. *Nature* **1998,** *393*, (6681), 146-149.

(41) Kwon, S.J.; Park, J.-H.; Park, J.-G., Wrinkling of a sol-gel-derived thin film. *Physical Review E* **2005,** *71*, (1), 011604.

(42) Mukhopadhyay, S.; Das, A.J.; Narayan, K.S., High-Resolution Photocurrent Imaging of Bulk Heterojunction Solar Cells. *The Journal of Physical Chemistry Letters* **2012,** *4*, (1), 161-169.

(43) Gupta, D.; Bag, M.; Narayan, K.S., Correlating reduced fill factor in polymer solar cells to contact effects. *Applied Physics Letters* **2008,** *92*, (9), -.

Chapter 7

Summary and Future Directions

7 Summary and Future directions

This thesis reports the realization of high efficient fullerene-free bulk heterojunction polymer solar cells. The combinatorial strategies of rational material design and device engineering enabled increased device performance. The first part of the thesis specifically deals with perylene based electron acceptors as potential alternatives to fullerene derivatives in BHJ organic solar cells. The rationale design of twisted structure between two perylene units was utilized to reduce the large scale phase separation in the BHJ blends. In combination with a low band-gap polymer PBDTTT-CT and Twisted Perylene (TP), a device efficiency of 2.77% has been achieved. The disruption of planarity in twisted perylene enhanced the short circuit current density by order of magnitude when compared to planar perylene blends.

The second part of the thesis investigated the origin of high current density in TP system using electrical and optical techniques. Photoluminescence measurements revealed almost complete quenching of both the donor and acceptor excitons, indicating efficient electron and hole transfer processes at the interface. Incident photons to current conversion efficiency (IPCE) measurements further confirmed the charge generation form both donor and acceptor excitons. The dynamics of charge generation was probed using near-IR transient absorption spectroscopy in the timescale of femtosecond to millisecond range. At the donor–acceptor interface, both polymer and TP excitons undergo fast dissociation with similar time scales of a few picoseconds. The magnitude of the polaron yield of PBDTTT-CT:TP blends was observed to be comparable to that of PBDTTT-CT:$PC_{71}BM$ blends and exhibits similar μs-decay dynamics. The blend ratio were optimized to obtain power conversion efficiency of devices > 3.2 %. However, the less current density of TP blends was attributed to lower bulk electron transport mobility compare to $PC_{71}BM$ blends.

In the next part of the thesis, the relaxed charge transfer (CT) states were probed using sensitive techniques. Both absorption and emission measurements proved the existence of red shifted CT band for several combinations of donor molecules with TP acceptors. Particularly, in comparing the nature of photophysical processes and CT states in TP based BHJs to that of $PC_{71}BM$ based BHJs is closely investigated. The role of molecular structure-order correlation on charge generation processes was revealed from this study.

In the final part, the role of zinc oxide (ZnO) morphology and the addition of an acceptor interlayer were utilized to achieve high efficiency fullerene-free BHJ inverted organic solar cells. The features of the ZnO wrinkles were controlled by spin coating the sol-gel at different speeds. The nano-structured wrinkles enhanced the light-harvesting efficiency of the active layer by acting as light scattering centers along with increased surface area. Additional TP interlayer reduced the work function difference and increased the current homogeneity at the interface between active layer and ZnO wrinkles. This resulted in decreased electron-hole recombination at the interface and enabled an overall increase of efficiency to 4.6%, which is one of the highest efficiencies for devices featuring a non-fullerene as the electron transporter.

In summary, this thesis is a step forward towards realizing fullerene-free organic BHJ solar cells. The molecular, interfacial and morphology aspects of BHJ's with TP as an acceptor suggest their role as a promising model system and pave the way for efficient, fullerene-free BHJ solar cells. It is envisioned that the inference and conclusions drawn from this study provides strategies for rational design of new electron acceptors, which may surpass overall efficiencies exhibited by fullerene based devices.

Future Directions:

A set of studies on charge transfer states revealed a possibility for further optimization of V_{oc} by suppressing the bimolecular recombination in TP systems. This can be achieved by optimization of material design and blend morphology to improve the overall electron mobility in the BHJs. Pump-push-probe measurements on these systems may give further insights to fundamental process of charge transfer dynamics between donor polymers and twisted perylene acceptors. These studies would culminate in realizing a general theory for charge transfer and dissociation in organic BHJ films.

Synthetically, more options of non-fullerene based electrons acceptors with twisted structures can be explored. Increasing the dimensionality of the acceptor by attaching multiple chromophores in non-planar geometry should increase charge generation and transport. Implementing these strategies may lead to fullerene-free devices with increased efficiency overcoming the limitations of fullerene molecules.

Careful optimization of annealing temperature, additive processing and controllable self-assembly morphology may be helpful to improve further the efficiency of solar cells based on fullerene –free acceptors. Different donors with suitable bandgaps, appropriate HOMO and LUMO energy levels and high charge carrier mobilities can be explored with

twisted perylene acceptors. Protection from ambient condition using suitable encapsulants may lead to longevity of these cells. Detailed study and understanding of degradation phenomena in these systems are a prerequisite for successful implementation in outdoor performance.

Chapter 8

Confinement induced aggregation of chromophores salts

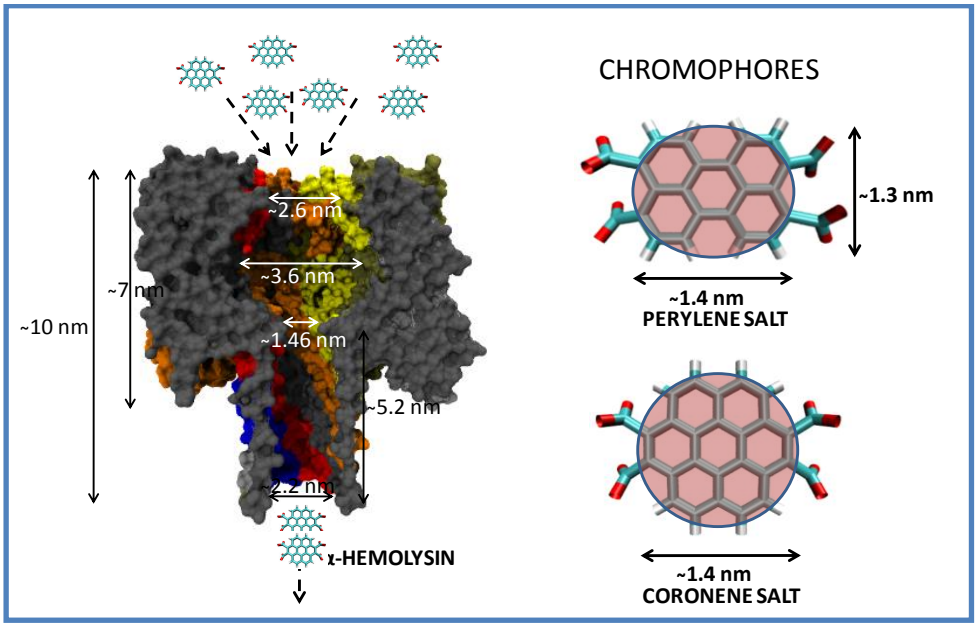

It should be mentioned that this chapter deviates from the central theme of the thesis. However, the implications of the observations described in this chapter are in general relevant to the microstructure and morphology required for designing efficient OPVs. The results demonstrate the possibility of tracking molecules which have the propensity to organize and assemble. A set of coronene and perylene based charged molecules is utilized to demonstrate the utility of protein-nanopores. Nanopores of dimension comparable to the chromophore provides optimum nano-confined regime to study early aggregation kinetics. Probing early stages of nucleation can enable understanding of supramolecular assembly and biocrystallization processes. In this chapter, early aggregation dynamics of coronene and perylene based salts is studied using translocation dynamics through the α-hemolysin (α-HL) protein nanopore. The confinement induced aggregations of polyaromatic chromophores during the different stages of translocation are correlated to the spatial symmetry and charge distribution of the molecules.

8 Confinement induced aggregation of chromophores

Confinement of tailored molecules offers valuable insight into the aggregation dynamics and stochastic sensing prospects. (*1*, *2*) The possibility of monitoring minute changes in ionic current as discrete units of the molecules translocate across a channel is a valuable tool for molecular engineering and sensing applications. In addition, for cases where the molecules are accompanied by a fluorescence signature, the high degree of sensitivity and information offered by nanopore translocation signals surpasses traditional optical methods. In this chapter, the transmembrane protein α-hemolysin (α-HL) nanopore is utilized to investigate molecular aggregation of polyaromatic chromophore salts (Figure 8.1a, 8.1b); namely coronene salt (CS) and perylene salt (PS) in the nano-confined regime.(*3*) The choice of these molecules stems from their ability to have π-π interactions, accompanied by coulombic and solvophobic interactions.(*4*) In aqueous solutions, due to strong hydrophobic interactions these polyaromatic molecules tend to form aggregates via π-π interactions.(*5*) However in dilute solutions, these π-π stacking interactions are strongly opposed by coulombic repulsion arising due to ionic carboxylate groups.(*6*, *7*) We explore the possibility of supramolecular organization of these anionic molecules driven by confinement. The basis and the mechanism of such processes in a macroscopically dilute solution in the vicinity and confines of the nanopore are interesting and relevant to aggregation kinetics.

The coronene and perylene series of molecules offer a model system to systematically follow the correlation between size-symmetry-charge and their translocation dynamics. The coronene and perylene molecules used in this study consist of rigid aromatic cores functionalized with negatively charged carboxylate groups. These carboxylate groups impart high solubility to these molecules in water and the rigid aromatic core prevents the molecular geometry from conformational distortions in solution. The confinement of the molecules in the pore and its vicinity induces assembly of the molecules resulting in a definite blockade in the passage of ionic current through the nanopore. We emphasize these results

experimentally and obtain additional insight into the transport process via fully atomistic molecular dynamics simulations.

The structure of α-HL nanopore consists of relatively spherical alpha helix vestibule with a diameter of ≈ 3.6 nm, which resides outside the lipid membrane, and a β-barrel channel, which is cylindrical shape with ≈2 nm average internal diameter and resides inside the lipid membrane.(*8*) The vestibule and β-barrel are separated by a ≈1.4 nm physical constriction. The internal volume of the pore is ≈18 nm^3 and the β-barrel can hold ≈600 water molecules.(*9*) Blocking events, if observed is correspond to aggregation of the molecules in specific regions driven by a variety of factors. We report clear blocking events of these molecular system in our experiment.

The experimental details are as follows: The main procedure involved in growing a lipid bilayer film and introducing the bacterial protein to form the nanpore. The lipid 1,2-diphytanoyl-*sn*-glycero-3-phosphocholine (DPhPC) was procured from Avanti polar lipids(USA), Protein alpha-hemolysin(99% pure) from Sigma Aldrich. The electrolytes (KCl, HEPES and EDTA) were obtained from Sigma Aldrich and used in the experiment without further purification.

The lipid DPhPC was formed on a 100 μm orifice in a 25 μm-thick Teflon septum (Eastern Scientific LLC, USA) that separates the cis and trans compartments (1 ml each) of a planar bilayer apparatus using Montal and Mueller method.(*12*) As convention, the cis compartment was connected to ground and trans was held at different potentials. Both the chambers were filled with electrolyte consisting of 10 mM of HEPES buffer at pH 8, 1M KCl and 1 mM of EDTA. 1- 2 ng/mL^{-1} wild type α-hl protein monomers were added to the cis compartment and held at a positive potential of 100 mV till single pore oligomerase in the lipid membrane. The solution in the cis chamber was purged with fresh electrolyte as soon as the fist pore was formed.

Single channel currents were recorded with a patch clamp amplifier (Picoamp 300B, along with HS-2A headstage, Eastern Scientific LLC, Rockville, USA). The signal was low-pass filtered with a built-in 4-pole Bessel filter at 1- 5 kHz, and sampled at 10 kHz with a Digital oscilloscope (Lecroy Waverunner 6100A). Data was analyzed and prepared for presentation by using pClamp 9.0 software (Axon Instruments), EasyPlot 4 and Origin 8 (Microcal,Northampton, MA).

H-NMR spectra of CS and PS of different concentrations in D_2O was taken from Bruker AVANCE 400(400 MHz) Fourier transform NMR spectrometer with chemical shifts reported in parts per million (ppm).

8.1 Experimental Results:

Introducing choromophore salts (CS and PS) at an appropriate concentration in the buffer medium in the cis-side of the nanopore modifies the time-series pattern of the ionic current *I(t)* through the nanopore. Clear blocking events are evident in the time trace of *I(t)* (Figure 8.1c, 8.1d). Blockades can be classified in two categories: (i) shallow - where the ionic current decreases less than half of initial value and is associated with large temporal distribution (ii) deep – where the ionic current decreases more than half of its initial value and is associated with small temporal distribution. Unlike the signature of polymers with well defined multiple step blockade events,(*10*) these small molecule blockades are single step events (rectangular blockades). Both the types of blockades have specific current peak amplitudes for two salts for same applied voltage bias.

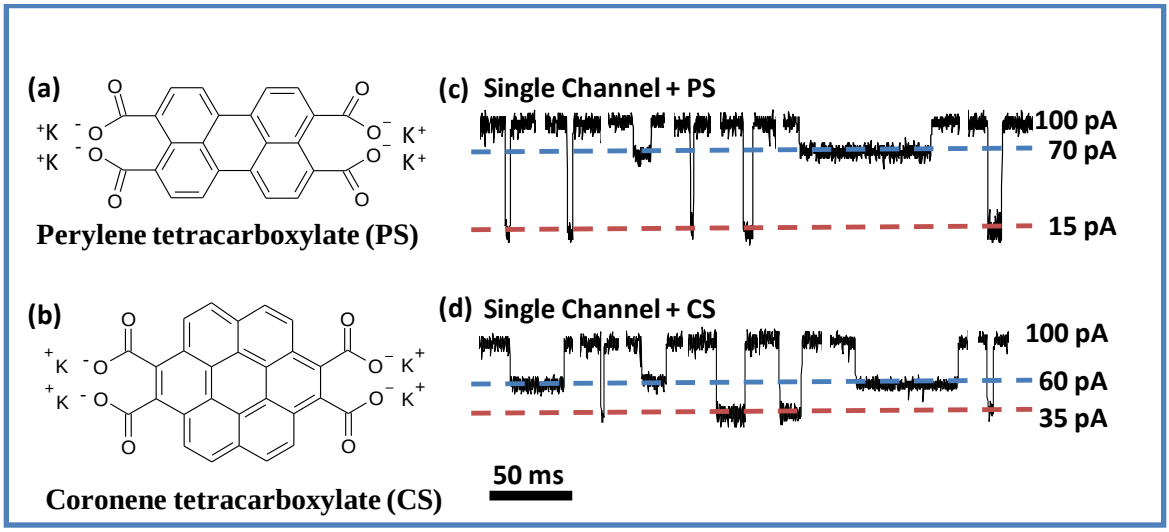

Figure 8.1: (a), (b) Structures of potassium salts of Perylene tetracarboxylate (PS) and coronene tetracarboxylate (CS), I(t) for Single α–hl protein channel biased at 100 mV for 1 M KCl buffer solution having baseline of≈100 pA with 10 mM of (c) PS and (d) CS in cis-compartment showing two different current blockades for both PS and CS. (time scale bar refers to 50 ms)(reproduced with permission from reference (3))

The event diagram for CS at 2 mg/ml and PS at 7 mg/ml concentration for 100 mV applied bias across the nanopore (Figure 8.2). Each point in the event diagram corresponds to a single translocation event. The plot shows a bimodal distribution of points for both salts, representing two completely distinguishable translocation events.

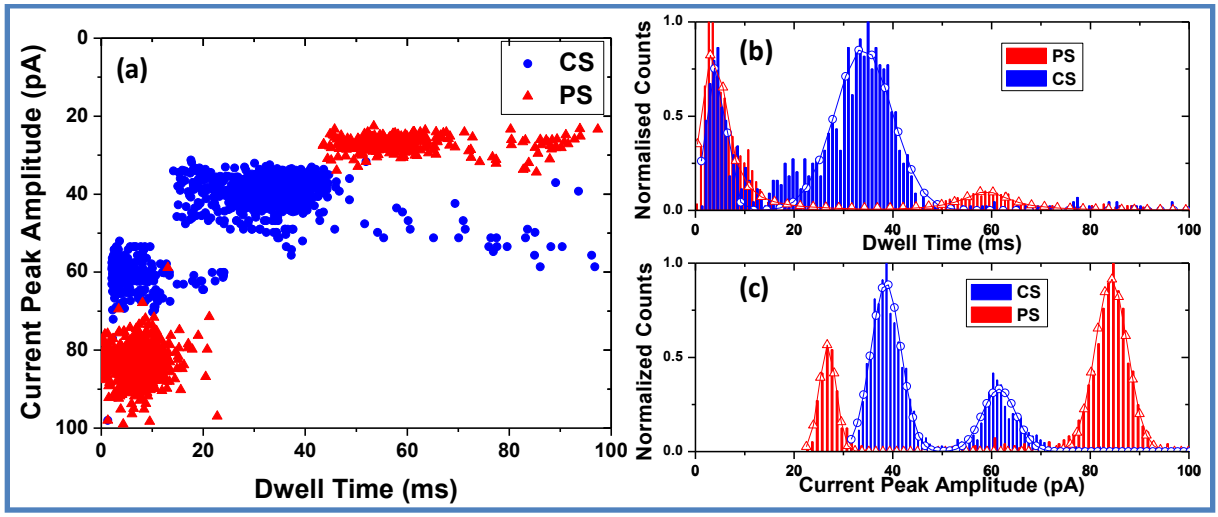

Figure 8.2: (a) Event diagram of 3000 points for CS and PS at 2 mM and 7mM concentration respectively at 100 mV applied bias, showing bimodal distribution of points for both CS and PS. (b) and (c) corresponding histogram of dwell time and current peak amplitude respectively. (reproduced with permission from reference (3))

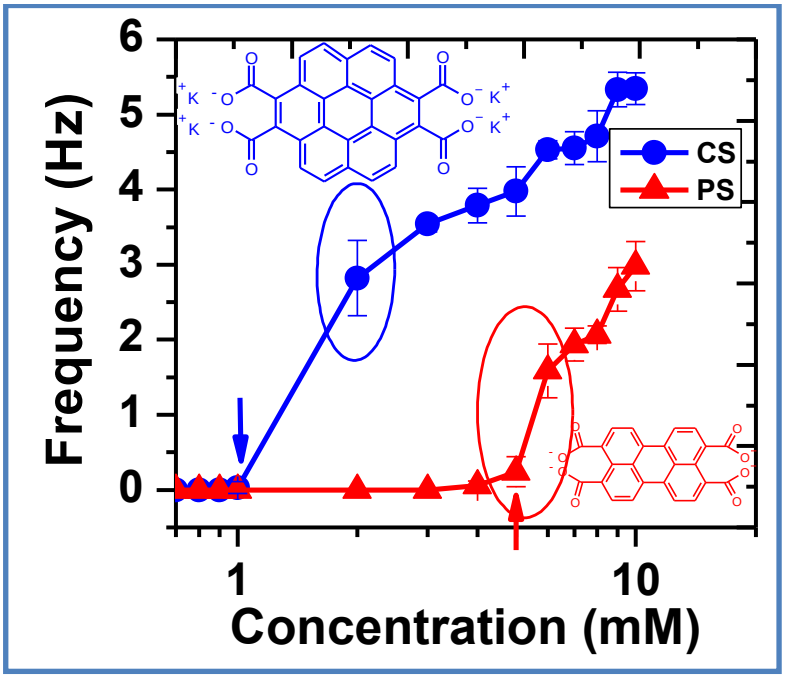

Figure 8.3: Frequency of blockades showing concentration dependent translocation events for both chromophores. The arrows indicate threshold concentration for CS and PS for 100 mV applied bias across the pore, which are at 1 mM and 5 mM respectively. (Error bars indicates standard deviation). (reproduced with permission from reference (3))

8.2 Concentration dependence:

The chromophore salts are observed to exhibit concentration(C) dependent translocation events. Both salts show the presence of a threshold concentration (C_{cr}) beyond

which the electrical blockades are observed. Frequency of blockades increases drastically for CS, when compared to PS. The threshold concentration is ≈1 mM for CS and ≈5 mM for PS at 100 mV bias across the protein (Figure 8.3). Frequency of blockades increases linearly with applied bias across the single nanopore in the lipid membrane.

8.3 Noise Analysis:

Noise studies of the signal can provide further insight into the microscopic processes. In the present studies, the power spectral density (PSD) of ionic-current time series was analyzed for both analytes. The PSD evaluated from the time series revealed characteristic noise features in the form of *1/f* behavior. The introduction of polyaromatic salts in the cis chamber increases the amplitude of low frequency noise and manifests as pink noise (*1/f*). The fluctuations associated with the translocation of individual and aggregates of ionic molecules can also contribute to the noise spectra. Main evidence is that the charged dye-molecule translocation events are accompanied by a distinct noise signature. The introduction of CS or PS changes the PSD from white (frequency-independent noise) to pink (*1/f*) response (Figure 8.4). The *1/f* feature arises upon the mere presence of analytes, well below C_{cr} required for blocking. The time-series at different bias indicates $1/f^{\alpha}$ behavior, where α scales from 0.5 - 2 with bias. Hence, these low frequency fluctuations can be attributed to the fluctuation of ionic current due to translocation of monomers through the nanopore.

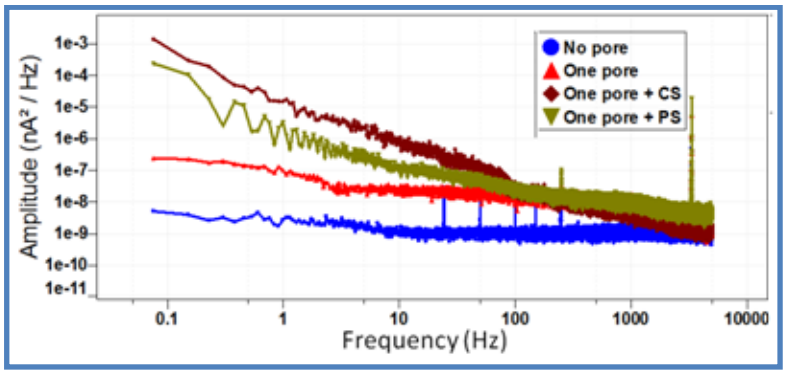

Figure 8.4: Comparison of power spectral density of I(t) of single pore and single pore with PS (2 mM) and CS (0.8 mM). Data was acquired with 1 kHz low-pass analog filter and digitized at 10 kHz sampling rate over a range of 400 s. (reproduced with permission from reference (3))

8.4 Interpretation and Discussion:

A clear understanding of the translocation processes can be arrived at after taking into account the following: (i) non-existence of blocking events below the threshold concentration

(ii) presence of two distinctive blocking signatures for the same salt beyond a critical concentration (iii) molecular dynamics simulation of the polyaromatic molecules translocating through the nanopore.

Since these molecules are highly photoresponsive, the photophysical measurements were also employed to detect the molecules which are translocated to trans chamber. The absorption spectra from the trans-chamber acquire the typical attributes of the translocated CS species. The trend of increasing aromatic-salt emission with the number of translocation events in the trans chamber clearly provides a direct evidence of molecular translocation.

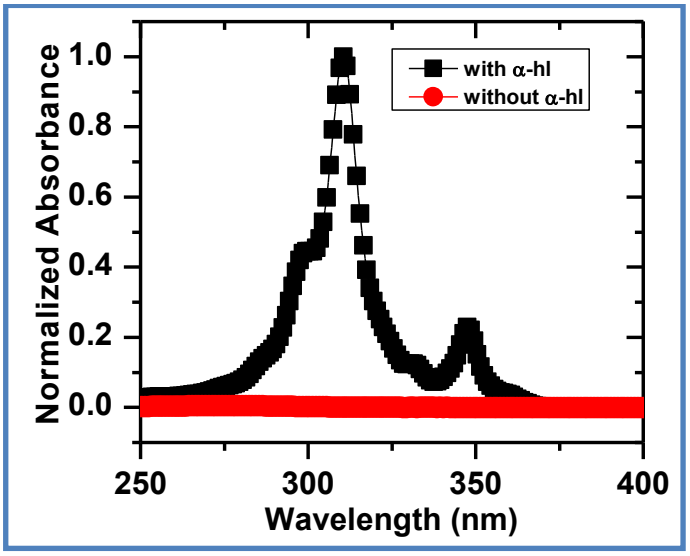

Figure 8.5: Absorption of solution from the trans chamber (CS was added in cis chamber). The black curve with square symbols correspond to normalized absorbance of collected solution from set of experiment with multiple pore running for more than 10,000 s. The red curve with circle symbols correspond to normalized absorbance of collected solution from measurement chamber running with only BLM without protein pore. (reproduced with permission from reference (3))

In the dilute solution ($C < C_{cr}$), the translocating-entity is in isolated monomer form. The existence of monomers in the low concentration regime is indicated by NMR and PL studies. During the translocation process($C < C_{cr}$), the monomers can be expected to enter the pore with a preferred orientation which permits a facile passage. We have argued in the noise analysis section that even at concentration ($C < C_{cr}$), the *1/f* feature is observed in PSD and we attributed this feature to monomers translocation.

The appearance of finite number of blocking events beyond a threshold concentration($C > C_{cr}$) and bias, suggests the formation of charged aggregates within/in the vicinity of the nanopore contributing to the blocking events. The H-NMR spectra of CS and PS shows characteristic monomer peaks even at bulk concentration higher than the threshold

concentration ($C > C_{cr}$) used in these studies. Hence we rule out the possibility of aggregation in the bulk for the concentration range used in these studies. The magnitude of the dwell time of these blockade events are large compared to the typical polyelectrolyte translocation due to the loss of the conformational entropic factor.(*10*) It should be noted that the conditions for aggregation in the translocation set-up, where nano-confinement effects come into play are different from the standard kinetics prevalent in a bulk solution. The two different sets of blocking; shallow and deep can be attributed to aggregation and transit in different spatial zones. In case of CS, as the blocking events commence for $C \approx C_{cr}$, they are largely the shallow-type and as the blocking frequency increases with concentration or bias, the deeper blockade events commence and grow in frequency and this event appearance is a stronger function of bias. The applied electric field increases the flux of molecules entering the vestibule of the α-HL pore. This increased flux increases the concentration of chromophores inside the vestibule and facilitates π- π stacking or agglomeration of the polyaromatic chromophore. These agglomerated molecules are restricted by the ≈1.5 nm constriction before entering the β-barrel of the α-HL nano-channel.

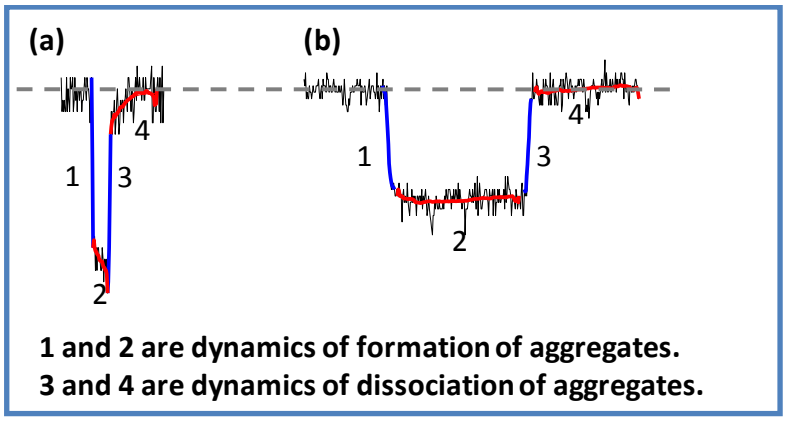

Figure 8.6: Aggregation and dissociation dynamics of chromophores inside the nanochannel. (reproduced with permission from reference (3))

The interpretation and assigning of locations associated with the characteristic blocking events can be arrived based on the combination of experimental observation. The deeper blockades are attributed to an agglomeration or aggregation of molecules at the vestibule. The dwell time of these blockades are smaller compared to shallow blockades. The kinetics of formation and dissociation of deeper blockades exhibit two different time scales. During the formation of aggregates, the ionic current drops to ≈ 80 % of current peak amplitude instantaneously (≈ 200 μs, path 1 of Figure 8.6(a)). From ≈ 80 % to reach peak (minima)

amplitude, the ionic current exhibit slower decay with statistical mean dwell time of 3.8 ms. Similarly, in the reverse process, the dissociation of aggregate follows a fast-instantaneous initial step, altering the magnitude by 80 % (path 3 of figure 8.6(a)), and then exhibits an exponential type increase with time constant of ≈ 1.4 ms to reach the base-line value as shown in the Figure 8.6(a). This mono-exponential increase of ionic current can be attributed to the dissociation process of bigger aggregate at the vestibule to monomers and dimer fragments. The Shallow blockades are due to agglomeration or aggregation of molecules at the ≈ 1.46 nm constriction. Both formation and dissociation kinetics of shallow blockades are instantaneous without having any tailing ends (Figure 8.6(b)). The MD simulation shows that only monomer and dimer can enter the ≈ 1.46 nm constriction. During crossing at the ≈ 1.46 nm constriction, the monomer and dimer orient their plane of the molecule along the direction of the force field. As soon as it crosses ≈ 1.46 nm constriction and enter the β-barrel, these molecules translocates rapidly. Hence the long dwell time for the shallow blockades is associated to the time taken by the molecules to orient itself before entering the ≈ 1.46 nm constriction.

8.5 Conclusion:

The aggregation dynamics of anionic polyaromatic molecules are monitored and studied using characteristic blocking events during the translocation through the α-HL nanopore. The main features include: a large duration of blocking (several ms), two discrete types of blocking (shallow and deep), and a correlation of the frequency and magnitude of blocking to the molecular parameters and concentration. The results indicate the specific region where the aggregation occurs. This possibility of controlling aggregation and monitoring the kinetics at nanoscale by external parameters such as concentration gradient and bias, can be used as a tool to study dynamic processes in bio-crystallization and supramolecular assembly.

References:

(1) Bayley, H.; Cremer, P.S., Stochastic sensors inspired by biology. *Nature* **2001,** *413*, (6852), 226-230.

(2) Kumar, H.; Lansac, Y.; Glaser, M.A.; Maiti, P.K., Biopolymers in nanopores: challenges and opportunities. *Soft Matter* **2011,** *7*, (13), 5898-5907.

(3) Shivanna, R.; Pramanik, D.; Kumar, H.; Rao, K.V.; George, S.J.; Maiti, P.K.; Narayan, K., Confinement induced stochastic sensing of charged coronene and perylene aggregates in α-hemolysin nanochannels. *Soft Matter* **2013,** *9*, (42), 10196-10202.

(4) Rao, K.V.; Jayaramulu, K.; Maji, T.K.; George, S.J., Supramolecular Hydrogels and High-Aspect-Ratio Nanofibers through Charge-Transfer-Induced Alternate Coassembly. *Angewandte Chemie International Edition* **2010,** *49*, (25), 4218-4222.

(5) Huang, M.; Schilde, U.; Kumke, M.; Antonietti, M.; Cölfen, H., Polymer-Induced Self-Assembly of Small Organic Molecules into Ultralong Microbelts with Electronic Conductivity. *Journal of the American Chemical Society* **2010,** *132*, (11), 3700-3707.

(6) Tanford, C., The Hydrophobic Effect: Formation of Micelles and Biological Membranes, Wiley-Interscience **1980,** 2nd edn, (New York).

(7) Wennerström, D.F.E.H., The Colloidal Domain: Where Physics, Chemistry, Biology, and Technology Meet. *The Colloidal Domain: Where Physics, Chemistry, Biology, and Technology Meet, VCH Publishers, New York* **1994**.

(8) Song, L.; Hobaugh, M.R.; Shustak, C.; Cheley, S.; Bayley, H.; Gouaux, J.E., Structure of Staphylococcal α-Hemolysin, a Heptameric Transmembrane Pore. *Science* **1996,** *274*, (5294), 1859-1865.

(9) Deamer, D.W.; Branton, D., Characterization of Nucleic Acids by Nanopore Analysis. *Accounts of Chemical Research* **2002,** *35*, (10), 817-825.

(10) Wong, C.T.A.; Muthukumar, M., Polymer translocation through alpha-hemolysin pore with tunable polymer-pore electrostatic interaction. *The Journal of Chemical Physics* **2010,** *133*, (4), 045101-045112.

(11) Wang, W.; Bando, Y.; Zhi, C.; Fu, W.; Wang, E.; Golberg, D., Aqueous Noncovalent Functionalization and Controlled Near-Surface Carbon Doping of Multiwalled Boron Nitride Nanotubes. *Journal of the American Chemical Society* **2008,** *130*, (26), 8144-8145.

(12) Montal, M.; Mueller, P., Formation of Bimolecular Membranes from Lipid Monolayers and a Study of Their Electrical Properties. *Proceedings of the National Academy of Sciences* **1972,** *69*, (12), 3561-3566.

Appendix

9 Appendix

9.1 Appendix 1:

9.1.1 µs-TAS study on P3HT:TP BHJ films

Ground state absorption spectra of P3HT, TP and P3HT:TP blend are represented in the Figure A-1.1. Both molecules exhibit visible absorption in the range ≈ 400- 650 nm. Absorption edge of P3HT and TP is at 650 nm and 620 nm respectively. The films of 1:1 ratio by weight of P3HT:TP show additive absorption spectra of both the blend components. µs-TAS studies were employed on P3HT:TP blends in order to probe the decay dynamics of photogenerated charges.

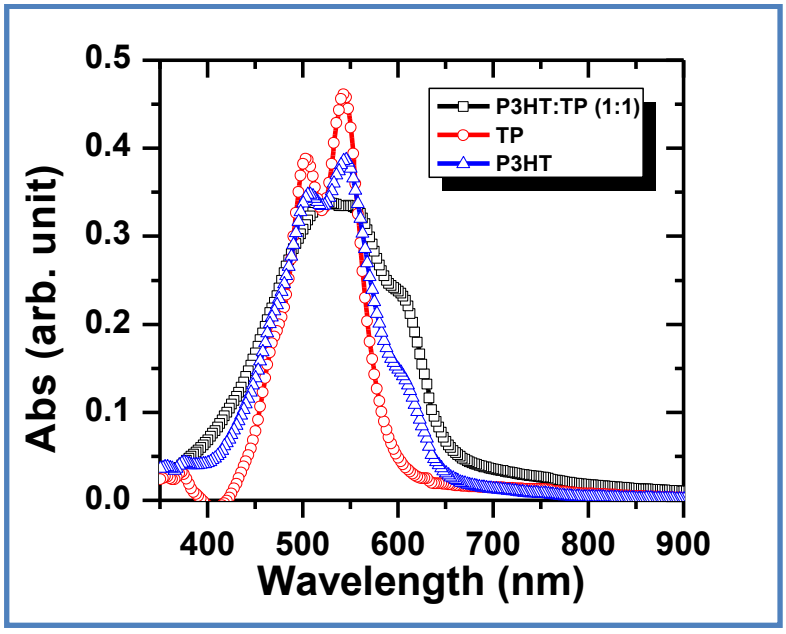

Figure A-1.1: Absorption spectra of P3HT, TP and P3HT:TP(1:1) blend films.

Transient Recombination Dynamics:

Figure A-1.2 shows typical micro to millisecond time scale transient decay kinetics observed for blends of PBDTTT-CT:TP and P3HT:TP in 1:1 ratio by weight. The transient dynamics of PBDTTT-CT blend is probed at 920 nm by exciting the singlet excitons at 700 nm (Figure A-1.2a). Similarly, the transient dynamics of P3HT blend is probed at 980 nm by exciting the singlet excitons at 540 nm (Figure A-1.2b). Both blends were excited using similar excitation density of 4.8 µJ/cm^2 per pulse at room temperature.

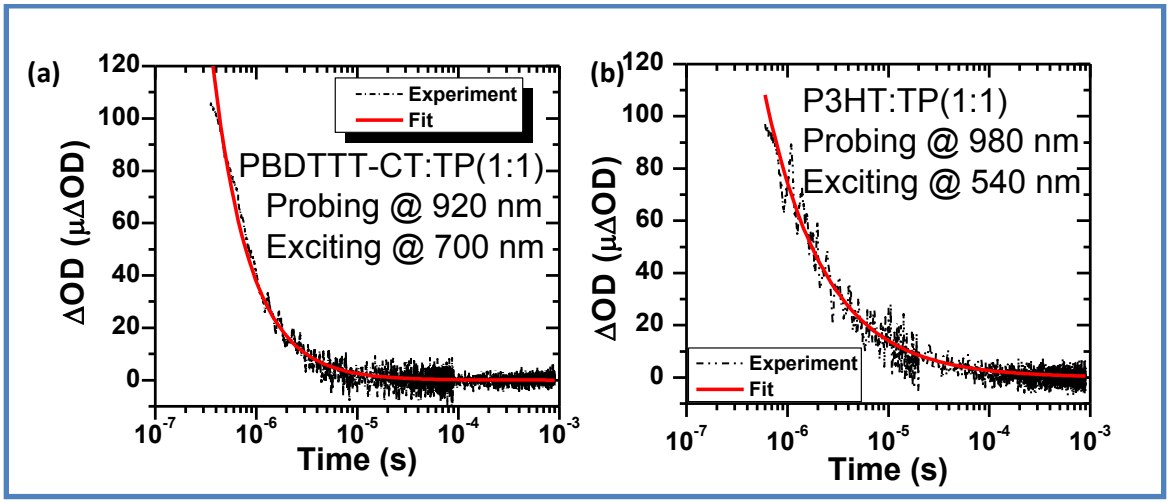

Figure A-1.2: Transient decay dynamics of positive polarons of PBDTTT-CT (a) and P3HT (b).

PBDTTT-CT blend films shows fast decay dynamics (few μs) when compared to P3HT:TP films. In both cases, the transients exhibited micro- to millisecond power law decay ($\Delta OD \ \alpha \ t^{-\alpha}$), and oxygen-independent decay dynamics, consistent with their assignment to polaron rather than triplet absorption. As discussed previously, and confirmed by numerical modeling, such power law kinetics on the micro- to millisecond timescales are characteristic of bimolecular recombination of dissociated charge carriers. Such bimolecular recombination kinetics can be readily distinguished from the geminate recombination in such blend films, which exhibit exponential decay dynamics characteristic of such monomolecular processes on the nanosecond (and faster) timescales. We therefore assign these absorption transients to the bimolecular recombination of dissociated polarons. It should be noted that, the initial magnitude of ΔOD, which corresponds to magnitude of dissociated charges, is similar in both the blends. The power law fitting of decay dynamics is tabulated in the table 1.

Blend	A	α
PBDTTT-CT:TP(1:1)	3.68407E-12	1.16846
P3HT:TP(1:1)	3.36269E-9	0.72449

Table A1.1: Power law decay fittings of transient signal.

The magnitudes of the power law decay for PBDTTT-CT:TP and P3HT :TP are $\alpha \approx 1.16$ and $\alpha \approx 0.72$ respectively. The slower decay dynamics of P3HT polarons is consistent with the previous studies on P3HT: PCBM blends ($\alpha \approx 0.4$). This suggests that the bimolecular recombination rates in P3HT blends are slower compare to PBDTTT-CT blends.

It is imperative to expect higher performance of P3HT blends. However, the devices of P3HT:TP active layer exhibited lower performance as discussed in the chapter 3. This might be due to the high crystallinity of P3HT polymer which may phase segregates to form larger domains of TP. Hence further insights into morphological aspects of crystalline polymer and TP blends are needed in order to increase the efficiency of these cells.

9.2 Appendix 2:

9.2.1 Capacitance-Voltage measurements on BHJ

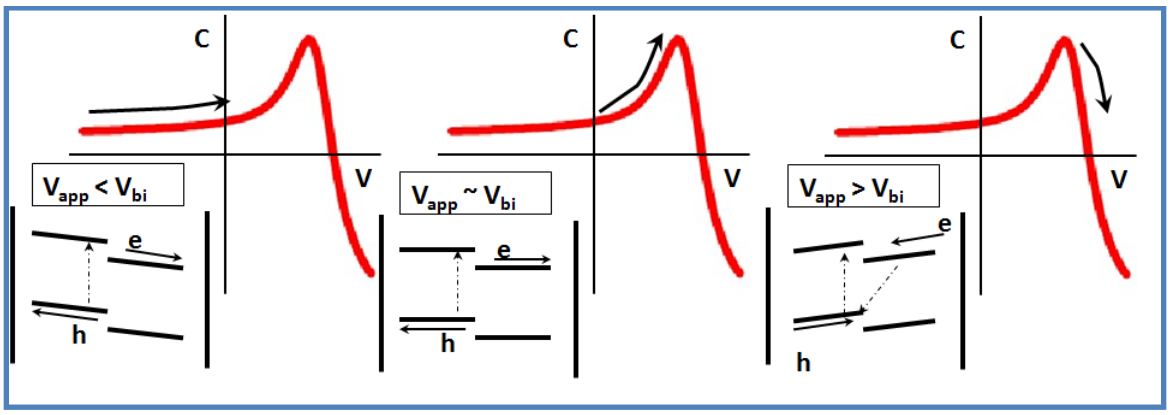

Figure A-2.1: Schematic of capacitance-voltage characteristics in organic BHJ solar cells.

Photoexcitation-assisted capacitance voltage (CV) spectroscopy is utilized to probe the charge trapping and accumulation effects at the active layer-electrode interface. This section contains the key initial observation of the high efficiency device described in Chapter 6. The mechanism of photo-assisted capacitance is represented schematically in the Figure A-2.1.

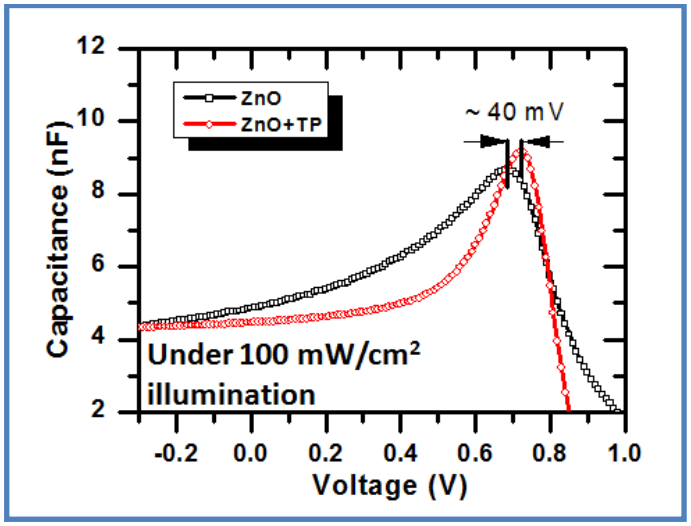

Figure A-2.2: CV characteristics of BHJ solar cells with and without TP interlayer.

The results from capacitance measurements in dark and illuminated conditions of the high efficiency TP based devices along with the additional interlayers between ZnO and active layer are shown in Figure A-2.1. The C-V characterizations were carried using Keithley 4200 semiconductor parameter analyser. The devices of thickness ~ 100 nm and electrode area of ~ 13mm^2 is utilized for this study. These devices were appropriately masked when measured under illumination to avoid the overflow of current through the circuit. The C-V characteristics curves measured at 50 kHz frequency are shown in the Figure A-2.1. When the external bias is less than the built-in potential of the BHJ ($V_{app}<V_{bi}$), the constant capacitance value is exhibited. When the $V_{app}<V_{bi}$, capacitance reaches the maximum value followed by sharp decrease due to injection of charges. It was shown previously that, the voltage value at maximum capacitance ($V_{C\text{-}max}$) shift upon illumination. This corresponds to the voltage at which the charge carrier starts injecting from the electrodes and hence neutralizes the generated photo-charges and thereby decreases the capacitance value. For PCBM BHJ systems, the degree of $V_{C\text{-}max}$ shift between dark and 1 Sun illumination is utilized to estimate the amount of accumulated charges. For the present study on TP based BJH system, the $V_{C\text{-}max}$ does not show function of light intensity. However, $V_{c\text{-}max}$ observed to be marginally higher (40 mV) for devices with additional TP layer. This suggests that, under illumination, the accumulation of charges at the interface is suppressed in the devices by addition of TP interlayer. However, in the present case it was realized after a set of initial measurements on the TP based BHJ devices, that these studies requires a rigorous approach with detailed measurements as a function of many different device parameters (buffer layers and acceptor layer) and appropriate models to understand the results.